

Réactive and polymer blending process : controlled synthesis of polystyrene and polyamide graft copolymers and compatibilizing efficiency of these copolymers

Cai-Liang Zhang

▶ **To cite this version:**

Cai-Liang Zhang. Réactive and polymer blending process : controlled synthesis of polystyrene and polyamide graft copolymers and compatibilizing efficiency of these copolymers. Other. Institut National Polytechnique de Lorraine, 2008. English. NNT : 2008INPL067N . tel-01753063

HAL Id: tel-01753063
https://hal.univ-lorraine.fr/tel-01753063

Submitted on 29 Mar 2018

HAL is a multi-disciplinary open access archive for the deposit and dissemination of scientific research documents, whether they are published or not. The documents may come from teaching and research institutions in France or abroad, or from public or private research centers.

L'archive ouverte pluridisciplinaire **HAL**, est destinée au dépôt et à la diffusion de documents scientifiques de niveau recherche, publiés ou non, émanant des établissements d'enseignement et de recherche français ou étrangers, des laboratoires publics ou privés.

AVERTISSEMENT

Ce document est le fruit d'un long travail approuvé par le jury de soutenance et mis à disposition de l'ensemble de la communauté universitaire élargie.

Il est soumis à la propriété intellectuelle de l'auteur. Ceci implique une obligation de citation et de référencement lors de l'utilisation de ce document.

D'autre part, toute contrefaçon, plagiat, reproduction illicite encourt une poursuite pénale.

Contact : ddoc-theses-contact@univ-lorraine.fr

LIENS

Code de la Propriété Intellectuelle. articles L 122. 4
Code de la Propriété Intellectuelle. articles L 335.2- L 335.10
http://www.cfcopies.com/V2/leg/leg_droi.php
http://www.culture.gouv.fr/culture/infos-pratiques/droits/protection.htm

Nancy-Université INPL

en co-tutelle avec Zhejiang University

Ecole Doctorale
Ressources **P**rocédés **P**roduits **E**nvironnement
(RP2E)

Ecole **N**ationale **S**upérieure des
Industries **C**himiques
(ENSIC)

Laboratoire des **S**ciences
du **G**énie **C**himique
(LSGC-CNRS UPR 6811)

Procédés d'extrusion réactive et de mélange de polymères : Synthèse contrôlée de copolymères greffés à base de polystyrène et de polyamide ; et étude de l'efficacité de compatibilisation de ces copolymères

THESE

présentée en vue de l'obtention du

DOCTORAT DE L'INSTITUT NATIONAL POLYTECHNIQUE DE LORRAINE

Spécialité : Génie des Procédés et des Produits

par

Cai-Liang ZHANG
Master en Génie des Procédés
Zhejiang Université, Hangzhou, Chine

Soutenance prévue le 10 novembre 2008 à 9h

Composition du jury :

Rapporteurs :	M. Luc AVEROUS	Professeur (Université de Strasbourg)
	M. Ming-Qiang ZHONG	Professeur (Zhejiang University of Technology, Chine)
Examinateurs :	M. Guo-Hua HU	Professeur (Nancy-Université, INPL) et membre de l'IUF
	M. Lian-Fang FENG	Professeur (Zhejiang University, Chine)

Acknowledgments

First and foremost I would like to express my gratitude to my advisors Dr. Guo-Hua HU and Dr. Lian-Fang FENG. Besides their creactive ideas of research, continuous guidance and inspiring discussion, their consistently encouraging and supporting to my study and research have been the key to the success of my Ph.D. I am thankful to them for providing me with a great research environment, resources, advice, and flexibility in my work. From them I have also learnt more than just how to do good research. Special thanks are given Dr. Sandrine HOPPE, Xue-Ping GU and Dr. Jia-Jun WANG for providing helps and suggestions for this study.

I am thankful to my mates both in Chinese and French research group — Guang-Zan LI, Xian-Ming ZHANG, Yu-Hua XUE, Jing CHANG, Jian ZHAO, Feng-Yong LI, Wen-Feng ZHANG, Xiao-Bo SONG, Sha-Sha CUI, Jin-Xia Li, Chao ZHAO, Yan-Fei TANG, Zheng-Hui LI, Fang SHAO, Guo-Long JI, Shan-Shan DAI, Jing-Gang GAI, Christian PENU, Jean-Marie BOISSIERE, Marina MAGATON, Ahmed BHRAN, Jonathan LEBLANC who helped in varying ways to understand some of the fascinating science of polymers. Of all these names, Jian ZHAO deserves a special mention, who has participated in the research work about the efficiency of graft copolymer at stabilizing the co-continuous phase. I would like to express my great appreciation to Tao-Tao FU, Dong AN, Yuan FANG who have contributed to my wonderful life in France.

This research would not have been possible finished without the generous financial support of the National Natural Science Foundation of China (grant numbers 50390097 and 20310285), the Ministry of Science and Technology of China through an international cooperation program (grant number: 2001CB711203), and the Association Franco-Chinoise pour la Recherche Scientifique et Technique-AFCRST (grant number: PRA Mx02-07). I would like to thank China Scholarship Council for supporting my study in France.

The completion of this thesis would not have been possible without the support of my family. I owe a debt of gratitude to my parents for their patience and understanding. I will give my final note of thanks to my wife, Ling-Li HU. Her love, constant understanding and encouraging and sharing every feeling are the ultimate support to the success of this thesis.

Abstract

Polymer blending offers an important route to new materials with combinations of properties not available in constituent polymers. Most polymer pairs are immiscible, leading to phase separation at equilibrium and yield a material with poor properties. To address this challenge, block or graft copolymers pre-made or generated in-situ by reactive blending are often used as compatibilizers. Most studies are focused on the compatibilizing efficiency of block copolymers and few studies address that of graft copolymers, partly because of difficulties of controlling their molecular structures.

This thesis is devoted to the study of the emulsification efficiency of graft copolymers. It is composed of three parts: (1) development of a novel reactive extrusion process for synthesizing graft copolymers with polystyrene (PS) as backbone and polyamide 6 (PA6) as grafts; (2) emulsification efficiency of PS-g-PA6 graft copolymers for PS/PA6 blends; and (3) concept of tracer-emulsifier.

The underlying chemistry for the synthesis of PS-g-PA6 graft copolymers was based on the use of a copolymer of styrene (St) and 3-isopropenyl-α, α-dimethylbenzene isocyanate (TMI), PS-co-TMI, to activate/e the polymerization of ε-caprolactam (CL) in the presence of sodium ε-caprolactam (NaCL) as an anionic catalyst. The structure of a graft copolymer is mainly determined by the following three parameters: backbone length, graft density, and graft chain length. The backbone length of the PS-g-PA6 depended only on the molar mass of the initial PS-co-TMI and the PA6 graft density was dictated by the TMI content in PS-co-TMI.

The efficiency of graft copolymers at compatibilizing the dispersed phase/matrix morphology of PS and PA6 blends and stabilizing the co-continuous morphology of the blends during quiescent annealing were studied. Results showed that for graft copolymers with similar backbone and graft density, the longer the grafts, the higher their efficiency. For a given backbone/graft composition, graft copolymers having fewer and longer grafts were more efficient at comaptibilizing and stabilizing the morphology.

Feeding mode had a very significant effect on the size of the dispersed phase domains at short mixing time and its effect decreased or became negligible at long mixing time. This indicates that feeding mode affected mostly the time necessary for the PS-g-PA6 compatibilizer to reach and emulsify the interfaces between PS and PA6. A good feeding mode should meet the following two requirements: first, the matrix should melt faster than the dispersed phase in order to avoid the phase inversion;

second, the compatibilizer should be present as soon as the blending process starts, namely, the dispersed phase begins to melt.

Building up an emulsification curve may not always be practical because of limited amounts of copolymers available. This is especially true for an industrial polymer blending process. A so-called concept of emulsifier-tracer was developed to solve the problem. Very small amounts of fluorecent moities such as anthracene were incorporated in PS-co-TMI. When the latter was used to activate the polymerization of CL, the resulting PS-g-PA6 graft copolymer contained fluorescent moities. An original method for constructing the emulsification curve of a polymer blend in a continuous mixer such as a twin-screw extruder was developed based on the tracer-emulsifier concentration distribution (i.e. the residence time distribution) and the corresponding dispersed phase domain size distribution of the blend system. The resulting emulsification curves exhibited unique features that would open a new research field for polymer blending.

Keywords: Reactive extrusion process; polymer blends; compatibisation.

Résumé

Les mélanges de polymères ouvrent une importante voie à l'obtention de nouveaux matériaux dont les propriétés peuvent être très différentes de celles de chacun des constituants des mélanges. La plupart des polymères sont immiscibles. Ainsi leurs mélanges constituent des phases distinctes et les propriétés de ces mélanges sont souvent médiocres. Afin de relever ce défi, copolymères à bloc ou greffés synthétisés séparément ou générés in-situ lors du procédé de mélanges sont souvent utilisés en tant que agents compatibilisants. Beaucoup d'études ont porté sur l'efficacité de compatibilisation de copolymères à bloc et peu d'études sur celle de copolymères greffés, en partie en raison des difficultés dans le contrôle de leurs structures moléculaires.

Cette thèse porte sur l'étude de l'efficacité d'émulsification de copolymères greffés. Elle est composée de trois parties : (1) développement d'un nouveau procédé d'extrusion réactive pour la synthèse de copolymères greffés avec polystyrène (PS) comme squelette et polyamide 6 (PA6) comme greffons ; (2) efficacité d'émulsification du copolymère greffé, PS-g-PA6 pour les mélanges à base de PS et PA6 ; et (3) développement d'un nouveau concept dit d'agent émulsifiant – traceur.

La chimie de synthèse mise en jeu de copolymères greffés de PS-g-PA6 était basée sur l'utilisation d'un copolymère de styrène (St) et d'isocyanate de 3-isopropenyl-α, α-dimethylbenzène (TMI), PS-co-TMI, pour activer la polymérisation de l'ε-caprolactame (CL) en présence d'ε-caprolactame de sodium (NaCL) en tant que catalyseur anionique. La structure du copolymère greffé ainsi formé est caractérisée par les trois paramètres suivants : longueur du squelette, densité des greffons et longueur des greffons.

Au niveau de l'efficacité de copolymères greffés PS-g-PA6 pour compatibiliser les mélanges PS/PA6 de type morphologie phase dispersée /matrice lors du procédé de mélange ou stabiliser ces mélanges de type morphologie co-continue en état statique, il a été montré que pour des copolymères greffés ayant le même squelette et le même nombre de greffons par squelette, plus les greffons sont longs, meilleure l'efficacité. D'autre part, pour une composition massique squelette/greffons donnée, les copolymères greffés ayant moins de greffons par squelette mais avec des greffons plus longs ont une plus grande efficacité de compatibilisation ou stabilisation.

Le mode d'alimentation du copolymère greffé a eu un impact significatif sur la taille des domaines de la phase dispersée pour des temps de mélange courts et cet

impact devient négligeable à temps de mélange longs. Ceci montre que le mode d'alimentation de l'agent compatibilisant influe sur le temps nécessaire pour qu'il atteigne et émulsifie les interfaces entre le PS et le PA6. Il est préconisé qu'un bon mode d'alimentation satisfasse les deux conditions suivantes : tout d'abord, la matrice doit fondre plus rapidement que la phase disperse afin d'éviter l'inversion de phases ; en deuxième lieu, l'agent compatibilisant doit être présent dans le système de mélange dès que le procédé de mélange est mis en route, autrement dit, dès que la phase dispersée commence à fondre.

Il n'est pas toujours possible de construire une courbe d'émulsification en raison des quantités de copolymères disponibles. Ceci est d'autant plus vrai pour un procédé de mélange industriel. Un concept d'compatibilisant – traceur a donc été proposé. De très faibles quantités d'entités fluorescents tells qu'anthracène sont incorporés dans le PS-co-TMI. Lorsque ce dernier est utilisé pour activer la polymérisation du CL, le copolymère greffé PS-g-PA6 obtenu contient des entités fluorescentes. Une technique originale a donc été développée permettant de construire une courbe d'émulsification pour des mélanges de polymères élaborés dans un mélangeur continu de type extrudeuse bi-vis. Elle est basée sur la la distribution de la concentration en compatibilisant-traceur (c'est-à-dire, la distribution des temps de séjour) et celle de la taille des domaines de la phase dispersée du mélange de polymères correspondante. La courbe d'émulsification ainsi obtenue présente des caractéristiques très intéressantes ouvrant un nouveau champ d'étude dans le domaine des mélanges de polymères.

Mots clés : Procédé d'extrusion réactive ; copolymère greffé ; mélange de polymères ; compatibilisation.

Table of contents

Acknowledgments ..... **I**

Abstract ..... **II**

Résumé ..... **IV**

Chapter 1 Introduction **1**

1.1 Motivation and objectives *1*

1.2 Overview of thesis *2*

Chapter 2 A novel reactive extrusion process for the synthesis of PS-g-PA6 graft copolymers **4**

2.1 Introduction *4*

2.1.1 Synthesis methods of graft copolymer 4

2.1.2 Graft copolymer formation by reactive blending 7

2.2 Study object and strategy *11*

2.3 Mechanism of the graft copolymer PS-g-PA6 formation *12*

2.4 Experimental *14*

2.4.1 Material 14

2.4.2 Synthesis of PS-co-TMI 14

2.4.3 Synthesis of PS-g-PA6 graft copolymer and homopolymer PA6 15

2.4.4 Methods used for the determination of the CL conversion 16

2.4.5 Purification and fractionation of polymerized products 18

2.4.6 Determination of the characterization of Homo-PA6 and PS-g-PA6 by SEC 19

2.4.7 FTIR analysis 20

2.4.8 NMR spectroscopy 20

2.4.9 DSC measurements 20

2.5 Comparison of various methods of measuring the conversion of CL to PA6 ..... *21*

2.5.1 Effect of the pre-drying of polymerized product films 21

2.5.2 Performances of the various methods of measuring the CL conversion for grafting polymerization system 23

2.5.3 Suitability of the above methods for the anionic homopolymerization system 30

2.5.4 Summary 32

2.6 Characterization of PS-g-PA6 by SEC at room temperature *33*

2.6.1 Choice of co-solvents for the *N*-trifluoracetylation reaction 34

2.6.2 Characterization of the *N*-trifluoroacetylation reaction 37

2.6.3 Measurement of the molar mass of PS-g-PA6 by SEC 40

2.6.4 SEC measurement of the composition of PS-g-PA6 43

2.6.5 Summary 48

2.7 PS-co-TMI characterization *48*

2.7.1 Molar mass 48

2.7.2 TMI content and distribution in PS-co-TMI 49

2.8 Evaluation of as-synthesized graft copolymer *51*
2.8.1 Composition of as-polymerized products 51
2.8.2 Composition of pure PS-g-PA6 56
2.8.3 Melting and recrystallization behavior of pure PS-g-PA6 59

2.9 Kinetics of the anionic polymerization of CL from PS-co-TMI *60*
2.9.1 Relationship between conversion and torque 60
2.9.2 Effect of the set temperature on the polymerization 61
2.9.3 Effect of NaCL/CL 63
2.9.4 Effect of the NCO/CL molar ratio 65
2.9.5 Effect of feeding mode 69

2.10 Conclusions *71*

Chapter 3 Degradation of PS-g-PA6 graft copolymer 74

3.1 Introduction *74*

3.2 Experimental *75*
3.2.1 Treatment in formic acid 75
3.2.2 Static annealing and mixing 75
3.2.3 TEM microscopy 75

3.3 Results and discussion *75*
3.3.1 Degradation in the process of formic acid extraction 75
3.3.2 Degradation in high temperature and high shear 84

3.4 Conclusions *92*

Chapter 4 Compatibilization efficiency of graft copolymers for immiscible polymer blends 94

4.1 Introduction *94*

4.2 Experimental *97*
4.2.1 Blending process 97
4.2.2 Rheological characterization 97
4.2.3 Characterization of blend morphologies 97

4.3 Results and discussion *98*
4.3.1 Rheology 98
4.3.2 Effect of PS-g-PA6 graft copolymer for PS/PA6 (20/80) blend system 98
4.3.3 Effect of PS-g-PA6 graft copolymer for PS/PA6 (80/20) blend system 101
4.3.4 Comparison of two blend systems 103

4.4 Conclusions *107*

Chapter 5 Efficiency of graft copolymers at stabilizing co-continuous polymer blends during quiescent annealing 109

5.1 Introduction *109*

5.2 Experimental *111*
5.2.1 Blend preparation 111
5.2.2 Quiescent annealing 111

5.2.3 Solvent extraction 111
5.2.4 Mercury intrusion porosimetry 111

5.3 Results and Discussion 112
5.3.1 Rheology 112
5.3.2 Annealing of blend systems without PS-g-PA6 112
5.3.3 Annealing of polymer blends with PS-g-PA6 115

5.4 Conclusions 120

Chapter 6 Effect of feeding mode on the morphologies of immiscible polymer blends 122

6.1 Introduction 122

6.2 Experimental 123
6.2.1 Blending process 123

6.3 Results and discussion 124

6.4 Conclusions 129

Chapter 7 Preparation of tracer-emulsifier and comparison of RTD and DSD in TSE 130

7.1 Introduction 130

7.2 Basic principles of the preparation of tracer-emulsifier 132

7.3 Experimental 133
7.3.1 Synthesis of the tracer-emulsifier 133
7.3.2 Extruder, screw configurations and instrumentation 133
7.3.3 Measurement Procedure 134
7.3.4 SEC measurements 135

7.4 Results and discussion 135
7.4.1 PS-co-TMI-MAMA 135
7.4.2 Tracer-emulsifier 136
7.4.3 Mass of tracer-emulsifier for one experiment in twin screw extruder 139
7.4.4 Comparability of RTD and DSD in different conditions 141
7.4.5 DSD in different time domains 147

7.5 Conclusions 149

Chapter 8 General conclusion and future work 151

8.1 General conclusion 151

8.2 Future work 154

Appendix 156

References 158

List of Figures

Figure 2.1 Scheme of three methods for the synthesis of graft copolymers: (a) "grafting through", (b) "grafting onto" (X and Y are the pendant functional groups of the backbone and the end-functional groups of grafts, respectively), (c) "grafting from" (* is an initiating group).....5

Figure 2.2 Schematic description of the in-situ polymerization and in-situ compatibilization. A* denotes polymer A chains bore initiating sites either at the chain end(s) or along the chain backbones. 10

Figure 2.3 Synthesis of PS-co-TMI and anionic polymerisation of CL from PS-co-TMI in the presence of NaCL as a catalyst. 13

Figure 2.4 TGA diagrams of a typical product obtained by the anionic grafting polymerization of CL onto PS-co-TMI. (a) Accumulated mass loss as a function of temperature increase; (b) Instantaneous mass loss as a function of temperature increase. 18

Figure 2.5 Procedure used for the purification and fractionation of polymerized products. 19

Figure 2.6 Effect of the pre-drying in a vacuum oven at 50 °C for 12 h on the TGA diagrams of the polymerised product of the experiment E14. (a) Accumulated mass loss as a function of temperature increase; (b) Instantaneous mass loss as a function of temperature increase. 22

Figure 2.7 FTIR spectra of PS-co-TMI4, PS-co-TMI4-CL and residue D from the polymerized product of E5. 24

Figure 2.8 ^{13}C NMR spectra of PS-co-TMI, PS-co-TMI4-CL and residue D from the as-polymerized product of E5. 24

Figure 2.9 UV spectra of (a) PS-co-TMI in THF and (b) solution C from the as-polymerized product of E5. 25

Figure 2.10 Procedure used for evaluating the performance of water and methanol as solvent for extraction. 26

Figure 2.11 UV spectra of (a) the solution of CL, (b) solution A and (c) solution L. 26

Figure 2.12 TGA traces of the polymerized product E5 subjected to one of the following treatments: (1) methanol extraction then vacuum drying at 140 ºC for 24 h; (2) methanol extraction then vacuum drying at 80 °C for 24 h and (3) vacuum drying at 140 ºC for 24 h. (a) remaining mass percentage; (b) instantaneous loss in the mass percentage. 28

Figure 2.13 TGA traces of the polymerized product E5 subjected to: (1) no treatment; (2) THF extraction and then vacuum drying at 80 °C for 24 h; (3) water extraction and then vacuum drying at 80 °C for 24 h and (4) vacuum drying at 140 °C for 24 h. (a) remaining mass percentage; (b) instantaneous loss in the mass percentage. 30

Figure 2.14 TGA traces of the polymerized product E19 subjected to one of the following treatments: (1) without any treatment; (2) water extraction then vacuum drying at 80 ºC for 24 h; (3) methanol extraction then vacuum

drying at 80 ºC for 24 h; (4) THF extraction then vacuum drying at 80 ºC for 24 h and (5) acetone extraction then vacuum drying at 80 ºC for 24 h. (a) accumulated mass loss; (b) instantaneous mass loss. 32
Figure 2.15 Schematic of the *N*-trifluoroacetylation reaction of polyamides with TFAA. 34
Figure 2.16 FTIR spectrum of the residual liquid compounds of a mixture of toluene/TFAA (8 ml/4 ml) after 30 min of rotary evaporation at 30 ºC. That of toluene is shown for comparison. 36
Figure 2.17 FTIR spectrum of the residual liquid compounds of a mixture of THF/TFAA (8 ml/4 ml) after 30 min of rotary evaporation at 30 ºC. Those of THF and TFAA alone are shown for comparison. 37
Figure 2.18 FTIR spectra of the homo-PA6 and the *N*-trifluoroacetylated homo-PA6 (PA6-TFAA) before and after the vacuum drying at 80 °C for 2 h.....38
Figure 2.19 FTIR spectra of the PS-g-PA6 and the *N*-trifluoroacetylated PS-g-PA6 before and after the vacuum drying at 80 °C for 2 h.....38
Figure 2.20 Mass fraction of the PS backbone and that of PA6 grafts and PS-g-PA6 from E5 after 15 or 24 h of *N*-trifluoroacetylation reaction using chloroform as a co-solvent as a function of the molar mass of PS-g-PA6b. Experimental and calculation methods will be given in the subsequent sections.....39
Figure 2.21 SEC traces of the homo-PA6 and PS-g-PA6 from E12 from the RI detector after *N*-trifluoroacetylation reaction using chloroform as a co-solvent. 40
Figure 2.22 UV spectra of the PS-co-TMI, PA6-TFAA, PS-g-PA6-TFAA solutions in THF. The mass concentrations are 0.2, 0.05 and 0.04 mg/ml in the PS-co-TMI, homo-PA6 and PS-g-PA6, respectively.....41
Figure 2.23 SEC traces of the *N*-trifluoroacetylated homo-PA6 and PS-g-PA6 from E12 from UV detection at 238 and 260 nm. 42
Figure 2.24 SEC traces of the *N*-trifluoroacetylated PS-g-PA6 from E5 detected by RI and UV-254 detectors. The *N*-trifluoroacetylation reaction was carried out with the use of THF as a co-solvent.....43
Figure 2.25 SEC trace of the *N*-trifluoroacetylated PS-g-PA6 from E11 corresponding to the UV detection at 238 nm. The shaded area represents the integrated UV absorbance. 44
Figure 2.26 Integrated areas of the SEC traces of the PS-co-TMI or the N-trifluoroacetylated PA6 as a function of the polymer (PS-co-TMI or homo-PA6) concentration for the UV detection at two different wavelengths: 238 and 260 nm.....44
Figure 2.27 Mass fractions of PS-g-PA6 from E11 and E12 (a), those of the PS backbone and PA6 grafts (b) and PS backbone/PA6 grafts mass ratios (c) as a function of the molar masses of PS-g-PA6. 47
Figure 2.28 FTIR spectra of PS-co-TMI1, PS-co-TMI2, PS-co-TMI4, PS-co-TMI6 and PS-co-TMI8. 50

Figure 2.29 Schematic of the reaction of PS-co-TMI with MAMA. 50
Figure 2.30 SEC traces of the PS-co-TMI-MAMA using a dual UV detector at 254 and 367 nm as a function of its molar mass. 51
Figure 2.31 FTIR spectra of PS-co-TMI4, residue H and solute F. The latter two are from the polymerized product of E5. 52
Figure 2.32 FTIR spectra of PS-co-TMI4 (a), the insoluble product of PS-co-TMI4 after extraction in methanol under reflux for 1 h (b) and the as-polymerized product from E5 without any extraction (c). 53
Figure 2.33 FTIR spectra of the insoluble material from Ex.4 and Ex.5 by methanol extraction and homo-PA6. 55
Figure 2.34 DSC thermograms of the insoluble material in methanol from EX.4 and EX.5 by methanol extraction. They were heated from 50 to 250 ºC at 10 ºC/min and maintained at 250 ºC for 2 min to erase their previous thermal history, and then cooled to 50 ºC at 10 ºC/min (recrystallization), finally heated up again to 250 ºC at 10 ºC/min (melting). 55
Figure 2.35 Mass percentages of the PS backbone and PA6 grafts of the four pure PS-g-PA6 graft copolymers from E7, E11, E5 and E12 (a) and the mass ratios between the PS backbone and PA6 grafts (b) as a function of their molar masses. 59
Figure 2.36 Melting and recrystallization DSC traces of PS-co-TMI4, PA6 and three pure PS-g-PA6 graft copolymers from the experiments E11, E5 and E12. (a) Melting at 10 ºC/min, (b) Recrystallization at -10 ºC/min. 60
Figure 2.37 Conversion of CL to PA6 as a function of time for experiments E14 and E5. 61
Figure 2.38 Torque values and melting temperature as a function of time for experiments E14 and E5. 61
Figure 2.39 Effect of set temperature on the torque versus time of the PS-co-TMI4/CL/Cat (50/50/5 by mass) polymerization system corresponding to E1 to E6. 63
Figure 2.40 Effect of the NaCL/CL molar ratio on the polymerization rate characterised by the torque of the PS-co-TMI4/CL/Cat (50/50/Cat by mass) polymerization system. The percentage of the Cat was 1.7, 5.0 and 8.4 wt.%, corresponding to E14, E5 and E16, respectively. 63
Figure 2.41 Effect of the NaCL/CL molar ratio on the polymerization torques of PS-co-TMI2/CL/Cat and PS-co-TMI4/CL/Cat (50/50/Cat by mass) polymerization systems with Cat being 1.7 and 5.0 wt.%, corresponding to E8, E13, E9 and E15. 64
Figure 2.42 Effect of the NaCL/CL molar ratio on the mass percentages of the PS backbone and PA6 grafts (a) and PS backbone/PA6 grafts mass ratios (b) of various PS-g-PA6 obtained from E14, E5 and E16 as a function of the respective molar masses of these pure graft copolymers. PS-co-TMI4/CL = 50/50 by mass. 65
Figure 2.43 Effect of the TMI content in PS-co-TMI on the polymerization torque of the PS-co-TMI/CL/Cat (50/50/5 by mass) polymerization system

with PS-co-TMI being PS-co-TMI1, PS-co-TMI2, PS-co-TMI4, PS-co-TMI6 and PS-co-TMI8, corresponding to E7, E8, E5, E9 and E10, respectively. 66

Figure 2.44 Mass percentages of the PS backbone and PA6 grafts (a) and PS backbone/PA6 grafts mass ratios (b) of various PS-g-PA6 from E7, E8, E5 and E10 as a function of the respective molar masses of these pure graft copolymers. 67

Figure 2.45 Effect of the NCO/CL molar ratio on the torque evolution as a function of time for the PS-g-TMI4/CL/Cat polymerization system corresponding to E12, E5 and E11, respectively. 68

Figure 2.46 Effect of the NCO/CL molar ratio on the mass percentages of the PS backbone and PA6 grafts (a) and PS backbone/PA6 grafts mass ratio (b) of various PS-g-PA6 obtained from E11, E5 and E12 as a function of the their molar masses. 69

Figure 2.47 Comparison between the one-step and two-step feeding modes in terms of the torque evolution as a function of mixing time for the polymerising system: (a) PS-co-TMI4/CL/Cat=50/50/1.7 (E14 one-step versus E17 two-step); (b) PS-co-TMI4/CL/Cat=50/50/5.0 (E5 one-step versus E18 two-step). 70

Figure 2.48 Mass percentages of the PS backbone and PA6 grafts (a) and PS backbone/PA6 grafts mass ratios (b) of various PS-g-PA6 graft copolymers obtained from one-step (E5) and two-step (E18) feeding modes as a function of the respective molar masses. 71

Figure 3.1 Mass percentage of the soluble residue after PS-g-PA6 dipped in formic acid at 30 ºC as a function of dipping time. 76

Figure 3.2 FTIR spectra of PS-co-TMI, Homo-PA6, PS-g-PA6 and the soluble residue M after PS-g-PA6 dipped in formic acid at 30 °C for 12 h. 77

Figure 3.3 PA6 contents in PS-g-PA6 copolymers by dipped in formic acid at 30 °C for different times (0, 3, 6, 12 and 24 h). The PA6 content obtained by two methods: (1) Weighting; (2) SEC. 78

Figure 3.4 M_n (a) and M_w/M_n (b) of residue soluble in formic acid as a function of time for the extraction in formic acid at 30 °C. 79

Figure 3.5 Mass percentages of the PS backbone and PA6 grafts of the PS-g-PA6 graft copolymers after dipped in formic acid for different times at 30 ºC (a) and the PA6 grafts contents in PS-g-PA6 (b) as a function of their molar masses. 80

Figure 3.6 Percentage of the soluble residue after PS-g-PA6 being dipped in formic acid for 12 h as a function of temperature. 81

Figure 3.7 PA6 graft chain content of PS-g-PA6 copolymers after being by dipped in formic acid for 12 h at different temperature (30, 60 or 90 ºC). The PA6 graft chain content obtained by two methods: (1) Weighting; (2) SEC. 81

Figure 3.8 M_n (a) and M_w/M_n (b) of residue soluble in formic acid as a function of temperature for the extraction in formic acid for 12 h. 83

Figure 3.9 Mass percentages of the PS backbone and PA6 grafts of the PS-g-PA6 graft copolymers after dipped in formic acid for 12 h at different temperature (30, 60 and 90 ºC) (a) and the PA6 grafts content in PS-g-PA6 (b) as a function of their molar masses. 83
Figure 3.10 Torque and melting temperature versus time of PS-g-TMI/CL/Cat (30/70/5) polymerisation system. Rotate speed of screw: 65 rpm, temperature: 230 ºC. 84
Figure 3.11 Torque and melting temperature versus time of the CL/Cat/TDI (100/6/3.6) polymerisation system. Rotate speed of screw: 65 rpm, temperature: 230 ºC. 85
Figure 3.12 TEM micrographs of the phase morphology of various PS-g-PA6 by different treatment. A: Pure PS-g-PA6; B: Formic acid treatment 12 h at 30 ºC; C: Static annealing for 2 h at 230 ºC； D: Formic acid treatment 12 h at 30 ºC after static annealing for 2 h at 230 ºC; E: Haake mixing for 10 min at 230 ºC; F: Formic acid treatment 12 at 30 ºC after Haake mixing for 10 min at 230 ºC. 86
Figure 3.13 Percentage of soluble residue after PS-g-PA6 extracted in formic acid for static annealing and Haake mixing for different time at 230 ºC..... 87
Figure 3.14 M_n of soluble residue after PS-g-PA6 extracted in formic acid for static annealing and Haake mixing for different time at 230 ºC. 87
Figure 3.15 PA6 graft chain contents of PS-g-PA6 copolymers that were treated by static annealing and Haake mixing for different time at 230 ºC and then extracted in formic acid for 12 h at 30 ºC. The PA6 graft chain content obtained by two method: (1) Weight method; (2) SEC method. 88
Figure 3.16 FTIR spectra of the soluble residue after PS-g-PA6 dipped in formic acid for 12 h at 30 °C. Residue M, N and O came from the PS-g-PA6 without treatment, by static annealing for 2 h at 230 ºC and Haake mixing for 10 min at 230 ºC, respectively. 89
Figure 3.17 Degradation mechanism of the PA6 graft in Haake mixing or static annealing. 90
Figure 3.18 Mass percentages of the PS backbone and PA6 grafts of the PS-g-PA6 graft copolymers after dipped in formic acid for different time at 30 ºC (a) static annealing at 230 ºC for different time (0, 5, 10, 30, 60 and 120 min); (b) Haake mixing at 230 ºC for different time (0, 2, 5, 10 and 20 min) 91
Figure 3.19 PA6 graft chain content in PS-g-PA6 graft copolymers after dipped in formic acid for different time at 30 ºC. (a) static annealing at 230 ºC for different time (0, 5, 10, 30, 60 and 120 min); (b) Haake mixing at 230 ºC for different time (0, 2, 5, 10 and 20 min) 92
Figure 4.1 Complex viscosity vs. frequency for the PS, PA6 and PS/PA6 blends (80/20, 20/80) blend at 230 ºC. 98
Figure 4.2 SEM micrographs of microtomed surface for the various PS/PA6 (20/80) blends: (A) without PS-g-PA6, (B) PS-g-PA6a (5%), (C) PS-g-PA6a (10%), (D) PS-g-PA6a (15%), (E) PS-g-PA6b (5%), (F) PS-g-PA6b (10%),

(G) PS-g-PA6b (15%), (H) PS-g-PA6c (5%), (I) PS-g-PA6c (10%), (J) PS-g-PA6c (15%), (K) PS-g-PA6d (5%), (L) PS-g-PA6d (10%) and (M) PS-g-PA6d (15%). The compatibilizer concentration was based on the dispersed phase concentration. Mixing temperature: 230 ºC; mixing time: 8 min and rotation speed: 65 rpm. 100

Figure 4.3 Effect of PS-g-PA6 structure and composition as the compatibilizer on emulsification curves of the PS/PA6 (20/80) blend. The PS-g-PA6 concentration bases on the mass of the dispersed phase. Mixing temperature: 230 ºC, mixing time: 8 min; rotation speed: 65 rpm. Symbols: experimental data; lines: trend line. 101

Figure 4.4 SEM micrographs of microtomed surface for the various PS/PA6 (80/20) blends: (A) without PS-g-PA6, (B) PS-g-PA6a (5%), (C) PS-g-PA6a (10%), (D) PS-g-PA6a (15%), (E) PS-g-PA6b (5%), (F) PS-g-PA6b (10%), (G) PS-g-PA6b (15%), (H) PS-g-PA6c (5%), (I) PS-g-PA6c (10%), (J) PS-g-PA6c (15%), (K) PS-g-PA6d (5%), (L) PS-g-PA6d (10%) and (M) PS-g-PA6d (15%). The compatibilizer concentration was based on the dispersed phase concentration. Mixing temperature: 230 ºC; mixing time: 8 min and rotation speed: 65 rpm. 102

Figure 4.5 Effect of PS-g-PA6 structure and composition as the compatibilizer on emulsification curves of the PS/PA6 (80/20) blend. The PS-g-PA6 concentration bases on the mass of the dispersed phase. Mixing temperature: 230 ºC, mixing time: 8 min; rotation speed: 65 rpm. Symbols: experimental data; lines: trend line. 103

Figure 4.6 Schematic diagrams of the morphology formation process for PS/PA6 (80/20) and (20/80) blend systems with PS-g-PA6 as the compatibilizer. . 106

Figure 5.1 Complex viscosity vs. frequency for the PS, PA6 and PS/PA6 blends (50/50) at 230 ºC. 112

Figure 5.2 Effect of the quiescent annealing on the morphology of the PS/PA6 (50/50) blend obtained after mixing at 100 rpm at 230 ºC for 10 min. Without annealing (a); annealing at 230 ºC for 5 min (b), 10 min (c) and 15 min (d); annealing at 235 ºC for 5 min (e); 10 min (f) and 15 min (g); annealing at 240 ºC for 5 min (h), 10 min (i) and 15 min (j). 114

Figure 5.3 Pore diameter (*d*) vs. annealing time for the PS/PA6 (50/50) blend at different annealing temperatures (230, 235 and 240 ºC). 115

Figure 5.4 SEM micrographs of PS/PA6/PS-g-PA6 (50/50/1) blends after mixing at 100 rpm for 10 min at 230 ºC followed by annealing at 240 ºC. The blend with PS-g-PA6e as the compatibilizer was annealed for 0 (a), 5 (b), 10 (c) and 20 min (d), respectively; the blend with PS-g-PA6f as the compatibilizer was annealed for 0 (e), 5 (f), 10 (g) and 20 min (h), respectively; the blend with PS-g-PA6g as the compatibilizer was annealed for 0 (i), 5 (j), 10 (k) and 20 min (l), respectively. 116

Figure 5.5 Effect of adding 1 wt.% of PS-g-PA6 graft copolymer on the morphology of the PS/PA6 (60/40) blend after mixing at 100 rpm for 10 min at 230 ºC followed by annealing at 240 ºC. Without PS-g-PA6 and

annealing for 0 (a), 5 (b) and 15 min (c), respectively; with PS-g-PA6e and annealing for 0 (d), 5 (e) and 15 min (f), respectively; with PS-g-PA6f and annealing for 0 (g), 5 (h) and 15 min (i), respectively; with PS-g-PA6g and annealing for 0 (j), 5 (k) and 15 min (l), respectively; with PS-g-PA6h and annealing for 0 (m), 5 (n) and 15 min (o). 117

Figure 5.6 Pore diameters of the PS/PA6/PS-g-PA6 (60/40/1) blends versus annealing time at 240 ºC. The compatibilizer was PS-g-PA6e, PS-g-PA6f, PS-g-PA6g and PS-g-PA6h, respectively. 118

Figure 5.7 Schematic of the molecular architectures and molar masses of the four PS-g-PA6 graft copolymers used in this work. 118

Figure 6.1 Emulsification curves of the PS/PA6 (80/20) blend for four different feeding modes. The PS-g-PA6f concentration was based on the mass of the dispersed phase. (a) rotation speed at 65 rpm, (b) rotation speed at 130 rpm. Mixing time: 8 min for the one-step feeding and 4 min for the two-step feeding after the last component of the blend was charged; temperature = 230 ºC. Symbols: experimental data; lines: trend lines. 125

Figure 6.2 SEM micrographs of microtomed surface of the PS/PA6/PS-g-PA6f (80/20/20.6) blend for four different feeding modes. (A) Feeding mode 1, (B) Feeding mode 2, (C) Feeding mode 3 and (D) Feeding mode 4. Mixing time: 8 min for the one-step feeding and 4 min for the two-step feeding after the last component of the blend was charged; temperature = 230 ºC. 126

Figure 6.3 SEM micrographs of microtomed surface of the PS/PA6/PS-g-PA6f (80/20/13.7) blend change with mixing time for feeding mode 1. Mixing temperature = 230ºC and rotation speed = 65 rpm. Mixing time: (A) 2 min, (B) 4 min, (C) 6 min, (D) 10 min. 128

Figure 6.4 Change in the size of the dispersed phase of the PS/PA6/PS-g-PA6f (80/20/13.7) blend with mixing time for different feeding modes. Mixing temperature = 230ºC and rotation speed = 65 rpm. For feeding mode 1 time "0" corresponds to the moment when all the components were fed to the mixer. In the other feeding modes it corresponds to the moment when the last component was fed to the mixer, i.e., 4 min after the first two components were fed to the mixer. Symbols: experimental data; lines: trend lines. 128

Figure 7.1 Underlying chemistry used for the preparation of tracer-emulsifier 133

Figure 7.2 Screw configurations of the twin screw extruder 134

Figure 7.3 Infrared spectra of PS-co-TMI before and after reaction with MAMA. 136

Figure 7.4 Linear relationships between the intensity of UV absorption of MAMA and its concentration in THF at room temperature. The UV wavelength is located at 367 nm. 136

Figure 7.5 Torque value as a function of time for the polymerization system of PS-co-TMI-MAMA/CL/Cat: (a) 30/70/5; (b) 70/30/5. Temperature: 230 ºC; screw speed: 65 rpm. 137

Figure 7.6 UV spectra of the solutions of PS-co-TMI and PS-g-PA6-TFAA in

THF. The mass concentrations of polymers are 0.2 and 0.04 mg/ml (excluding the mass of TFAA in PA6-TFAA and PS-g-PA6-TFAA), respectively. 137

Figure 7.7 Mass percentages of the PA6 grafts, PS backbone and MAMA of the tracer-emulsifier A and tracer-emulsifier B as a function of their molar mass..... 139

Figure 7.8 A typical residence time distribution curve. Screw speed: 100 rpm; Feed rate: 13 kg/h..... 140

Figure 7.9 Mass distribution of tracer-emulsifier corresponding to the RTD curve in Figure 7.8. 140

Figure 7.10 Comparison of the RTD and DSD curves obtained using two different tracer-emulsifiers and PS-tracer (only RTD). Their masses are 4.8, 4.8 and 0.16 g, respectively. Feed rate: 13 kg/mol; Screw speed: 100 rpm. 142

Figure 7.11 Effect of the mass of the tracer-emulsifier A for an experiment on the RTD and DSD curves. Feed rate: 13 kg/h; screw speed: 100 rpm..... 143

Figure 7.12 Effect of the mass of the tracer-emulsifier B for an experiment on the RTD curves. Feed rate: 13 kg/h; screw speed: 100 rpm. 143

Figure 7.13 SEM micrographs of microtomed surface for PS/PA6 (80/20) blends collected at different extruder die exit at different times. In the extrusion process, the tracer-emulsifier A was injected to the hopper as a pulse at zero time. The mass of tracer-emulsifier A for an experiment is 1.6 g (A), 3.2 g (B) and 4.8 (C). 144

Figure 7.14 Comparison of DSD curves and mass distribution of tracer-emulsifier of PS/PA6 (80/20) blend systems extruded in TSE with different amounts of tracer-emulsifier A for an experiment. The mass distribution of tracer-emulsifier obtained from the data in Figure 11. The mass indicated in the figures corresponds to the amounts of tracer-emulsifier A injected to the extruder. 145

Figure 7.15 Effect of the screw speed on the RTD and DSD curves. The mass of tracer-emulsifier A injected to the extruder is 3.2 g; feed rate is 13 kg/h. . 146

Figure 7.16 Effect of the PS/PA6 ratio on RTD and DSD curves. PS/PA6 mass ratio is 90/10 (a) and 80/20 (b); the mass of tracer-emulsifier A injected to the extruder is 1.6 g; feed rate is 13 kg/h; screw speed is 100 rpm. 146

Figure 7.17 Effects of the amount of the tracer-emulsifier (a), the screw speed (b) and the PS/PA6 mass ratio (c) on the emulsification curve of the PS/PA6 blend. The emulsification curve from a Haake torque rheometer (a batch mixer) is shown in c. The structure of the emulsifier used is similar to that of the tracer-emulsifier. The PA6 content and the number of the PA6 grafts per PS backbone of the emulsifier were 30.3% and 6.6, respectively. 149

List of Tables

Table 2.1 Compositions of St, TMI, BPO and toluene, polymerization temperature and time used for the synthesis of PS-co-TMI. 14
Table 2.2 Selected information on the experimental trials carried out in this work 15
Table 2.3 Mass losses of various polymerized products subjected to different pre-drying times in a vacuum oven at 50 ºC. 22
Table 2.4 Comparison of the CL conversions measured by extraction in various solvents. 23
Table 2.5 Times necessary for complete solvent removal under vacuum drying at 80 °C. 27
Table 2.6 CL conversions measured by vacuum drying at 140 ºC for 24 h 27
Table 2.7 CL conversions obtained by the nitrogen analysis 30
Table 2.8 CL conversions measured by extraction in various solvents 31
Table 2.9 CL conversions of E19 obtained by vacuum drying at 140 ºC and TGA 32
Table 2.10 Molar masses of *N*-trifluoroacetylated homo-PA6 and PS-g-PA6 from E12 by SEC using a RI detector and based on the PS standards. 40
Table 2.11 Molar masses of the *N*-trifluoroacetylated homo-PA6 and PS-g-PA6 from E12 calculated from the UV detection at 238 and 260 nm and based on the PS standards. 42
Table 2.12 Mass fractions of the PS backbone and PA6 grafts of PS-g-PA6 graft copolymers obtained by SEC and selective extraction. 45
Table 2.13 The molar mass and TMI content of as-synthesized PS-co-TMI. 49
Table 2.14 Mass percentages of the various fractions of four as-polymerized products obtained according to the procedure in Figure 2.5 52
Table 2.15 Selected information on the experimental trials for CL/Cat mixing and the CL conversion 54
Table 2.16 Mass percentages and the molar masses of the PS backbone and a single PA6 graft of four pure PS-g-PA6 graft copolymers obtained by successive extraction. 57
Table 2.17 Composition and relative molar mass of pure PS-g-PA6 obtained by SEC. 57
Table 2.18 Heating behavior of the PA6 grafts of three PS-g-PA6 graft copolymers and homo-PA6 60
Table 4.1 Literature results on the emulsification efficiency of copolymers. 94
Table 4.2 Normalized interfacial coverage (Σ/Σ_{max}) for PS/PA6/PS-g-PA6 blends. 104
Table 4.3 Asymmetry index obtained from the PS/PA6 blends without and with PS-g-PA6. 107
Table 5.1 Literature results on the efficiency of copolymers to stabilize co-continuous morphology. 110
Table 5.2 Apparent interfacial coverage (Σ) and normalized interfacial coverage

(Σ /Σ_{max}) for PS/PA6/PS-g-PA6 (60/40/1) blends before and after the annealing at 240 ºC. 119
Table 6.1 Literature results on the effects of feeding mode on the morphology of reactive blends. 122
Table 6.2 Description of four feeding modes for the PS/PA6/PS-g-PA6f blends. 124
Table 7.1 Molar mass, the PA6 content and the MAMA content of two tracer-emulsifiers 138

Chapter 1 Introduction

1.1 Motivation and objectives

Polymeric alloys or polymer blends hold considerable research interest. Just as metal alloys have long been used because they have properties unattainable in any one metal alone, blending existing polymers can also used as a means of creating new materials with combination of properties superior to the components at relatively low cost. However, the actual fabrication of polymer blends poses significant challenges. Most polymer pairs are immiscible and thermodynamically unstable, which leads to the phase separation into macroscopic domain and may yield a material with poor properties. To address this challenge, immiscible polymer blends must be compatibilized. A common method of compatibilization is the introduction of another component known as a compatibilizer (also called interfacial modifier or emulsifier), which is made up of segments that are chemically identical to or have affinity with each of the polymer components. Thus the compatibilizer molecule can be convenient to locate between the two polymer phases, which results in promotion of the interfacial adhesion, reduction of interfacial surface tension, promote the dispersion of one phase in another and stabilize resulting blends [1-3]. Therefore, it is very important to find an additive that act as an effective compatibilizer.

Block or graft copolymers are commonly used as compatibilizers in immiscible polymer blends. The efficiencies of block or graft copolymers as compatibilizers are believed to depend on their molecular architectures [4-10], molecular weights [11-15], compositions [15-18], the interaction parameter balance between the homopolymers and the copolymer blocks [19-22]. Therefore, there are, at least, four important factors to be kept in mind when selecting a block copolymer for a specific application: choice of monomers, molecular architecture, composition, and molecular weight. Choice of monomers controls the enthalpy of the system, while the molecular architecture, composition and molecular weight control their aggregation and processing characteristics. The former is determined by the blend systems and the copolymer is composed of the same or similar monomers that are used in the polymers making up the blends. Therefore, the choice of copolymer focuses mainly on the latter.

In order to choose the suitable compatiblizer for an immiscible polymer blend, we first have to know how copolymer architecture and composition affect the compatibilization of a polymer blend. Most of the experimental reports in this field

are related to the effect of the molecular architecture of the block copolymers on the compatibilization of immiscible polymer blends. This is because their molecular parameters are easy to control using anionic polymerization process. More importantly, there are a few commercially available block copolymers (mainly those based on styrene-butadiene or –isoprene block copolymers) that can be used as compatiblizers.

However, many important polymer blends are constituted by components, whose corresponding block copolymers are difficult to prepare. In addition, the prevailing method of in-situ compatibilization results mainly from the formation of graft copolymer by the coupling reaction between two functional polymers [23,24]. Currently, there are very few studies about how changes in the graft copolymer architecture such as graft chain length and density will impact its ability to compatibilize an interface. The objective of the work presented in this thesis is to develop a novel method to synthesize the graft copolymers with controllable architecture and to investigate the compatibilized efficiency of the resulting graft copolymers with different molecular architectures and/or molecular weights.

1.2 Overview of thesis

An important challenge in the study of compatibilizing efficiency of graft copolymer in polymer blends lies in the development of controllable synthesis of the graft copolymer. The first part of this thesis focuses on addressing this challenge. The second part of this thesis is to investigate the compatibilizing efficiency of the synthesized graft copolymers as compatibilizers. A brief overview of the organization of this thesis is as follows.

In chapter 2, a novel method for the controllable synthesis of graft copolymer was developed. The grafting of polyamide 6 (PA6) onto polystyrene (PS) is achieved by the use of a copolymer of styrene (St) and 3-isopropenyl-α,α-dimethylbenzene isocyanate (TMI), PS-co-TMI, to activate the polymerization of ε-caprolactam (CL) in the presence of sodium ε-caprolactam (NaCL) as an anionic catalyst. The control and analysis method of the structure of graft copolymer is addressed in detail.

Chapter 3 deals with the study of the degradation of the graft copolymer (PS-g-PA6) with PS as backbone and PA6 grafts in the formic acid extraction and at the high temperature and high shear. The latter was investigated at 230 ºC by two methods: one is annealing treatment, static press at a pressure of 10 MPa; the other is haake mixing, mix in haake torque rheometer.

Chapter 4 studies the compatibilizing efficiencies of the four as-synthesized graft copolymers in PS/PA6 blend systems with dispersed phase/matrix structure. The PS/PA6 composition is either 20/80 or 80/20. The role of the length and density of graft chains in compatibilizing PS/PA6 blend is discussed.

Chapter 5 evaluates the efficiency of the as-synthesized graft copolymers in stabilizing the morphology of PS/PA6 co-continuous phase in the process of quiescent annealing.

Chapter 6 investigates the effect of feeding mode on the morphology development of PS/PA6 (80/20) blend with PS-g-PA6 as compatiblizer.

Chapter 7 reports on a concept of tracer-emulsifier and its applications in continous polymer blending processes.

Finally, the mainly conclusion of this thesis are summarized and futher research directions are proposed in Chapter 8.

Chapter 2 A novel reactive extrusion process for the synthesis of PS-g-PA6 graft copolymers

2.1 Introduction

2.1.1 Synthesis methods of graft copolymer

A graft copolymer is composed of a polymer backbone to which one or more graft chains are connected through covalent bonds. Graft copolymers represent a valuable class of polymeric materials due to the availability of many structural variables which in turn can reveal a broad range of new materials with new properties [25-27]. These structural variables include: main and side chain polymer type; degree of polymerization and polydispersities of main and side chain; graft density (average spacing in-between the side chains) and so on.

Therefore, it is important to develop an easy and effective method to synthesize controlled graft copolymers with a view to obtain impact-resistant plastics by combining a hard polymer backbone with soft polymer graft chains, thermoplastic elastomers by grafting a hard polymer segments onto a soft polymer backbone, or amphiphilic copolymer used as the additive, dispersant and compatibilizer in polymer blend, etc [27-30]. Generally, useful synthetic approaches to the preparation of graft copolymers include[25,27]: (I) “grafting through”, which is the homo-polymerization of a macromonomer or the copolymerization of a macromonomer with a monomer, (II) “grafting onto”, where the grafting of side chains onto a backbone is carried out via a coupling reaction between the pendant functional groups of the backbone and the end-functional group of grafts; and (III) “grafting from”, in this case the graft chains are grown from a polymer with multiple initiating sites located throughout its main chain. The above three strategies for the synthesis of graft copolymers are shown in Figure 2.1. In addition, noncovalent interactions, such as hydrogen bonding [31], ionic interaction [32], and so on, have also been used to graft surfactants onto linear polymer chains to form polymer graft architectures.

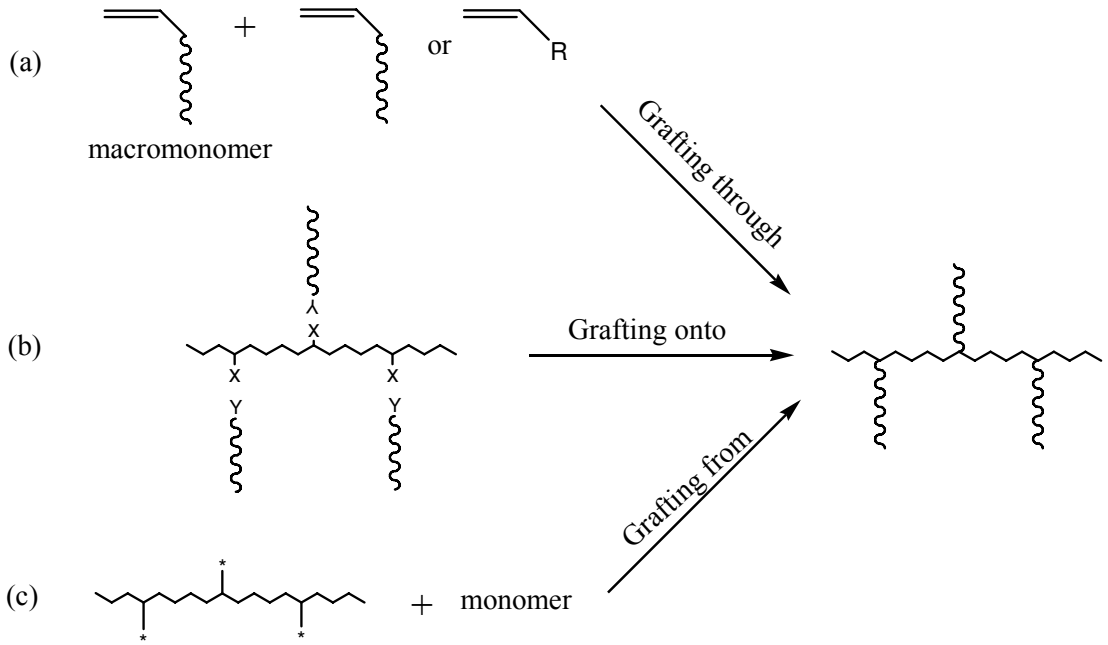


Figure 2.1 Scheme of three methods for the synthesis of graft copolymers: (a) "grafting through", (b) "grafting onto" (X and Y are the pendant functional groups of the backbone and the end-functional groups of grafts, respectively), (c) "grafting from" (* is an initiating group).

2.1.1.1 Grafting through

The "graft through" approach has been applied for the synthesis of graft copolymer for about twenty years. The approach is via random or systematic chemical attachment of initiating groups onto the molecular substrate, which in turn can enable the synthesis of branches. An example is the introduction of terminal vinylic group (double bond) in a macromonomer, which in turn can be polymerized by the radical polymerization [33- 36].

For the preparation of the controlled structural graft copolymer, a living or controlled polymerization should be involved [28,37]. In general, the macromonomers can be synthesized by a living or controlled polymerization technique and thus be well defined the graft chain parameter [36,38]; the backbone parameters of graft copolymer also can be controlled by a living or controlled copolymerization of the macromonomers with a low molecular weight comonomer [39,40]. For example, Rieger and Dubois et al. [39] obtained the biodegradable and biocompatible poy(ε-caprolactone)-graft-poly(ethylene oxide) copolymers, by ring-opening copolymerization of ε-caprolactone and poly(ethylene oxide) (PEO) macromonomer, i.e., PEO end-capped by an ε-caprolactone unit. The control is effective on the composition and length of both the hydrophobic polyester backbone and the hydrophilic PEO grafts. However, the "grafting through" method still has been

deficient in controlling the spacing distribution of the graft chains because the reactivity ratios of macromonomer and comonomer influence the spacing distribution of the graft chains, which were influenced by many factors, such as the diffusion differences of macromonomer in comparison to the low molecular weight comonomer, the inherent reactivity of macromonomer and comonomer and the potential incompatibility of the propagating comonomer chain and the macromonomer [28,41].

2.1.1.2 Grafting onto

In the "graft onto" method, the graft architecture is formed via a coupling reaction between the pendant functional groups (X) of the backbone and the end-functional group (Y) of grafts (see Figure 2.1b). This method provides the advantage that both the backbone and graft chain can be characterized separately, that is, the backbone and graft chain can be prepared via different living polymerization techniques independently so that the resulting graft copolymer is defined with respect to their backbone and grafts [25, 27]. A characteristic example is the functionalization of polybutadiene with chlorosilane groups, via the hydrosilylation reaction, followed by the coupling reaction with living polystyrene chains [42].

You and Hong et. al. [41] report a novel "graft onto" procedure to prepare graft copolymers with controlled backbone length, grafting sites and grafting density: firstly, reversible addition-fragmentation transfer (RAFT) polymerization of styrene (St) was performed by using polytrithiocarbonate as chain transfer agent to produce trithiocarbonate-containing polystyrene (PS) with controlled distance between sequentially spaced trithiocarbonate functional group; Secondly, "graft points" maleic anhydride (MAH) were inserted into the backbone chain between St and trithiocarbonate; finally, Poly(ethylene glycol methylether) (PEGM) or poly(tetrahydrofuran) (PTHF) chains were linked onto the main chain by esterification reaction of maleic anhydride with PEGM or PTHF to from graft copolymer with well-controlled backbone length, graft sites and graft density.

However, the grafting density of graft copolymer synthesized with the "grafting onto" method is often limited for both kinetic and thermodynamic reasons [29]. First, with increasing grafting density, the diffusion of unreacted grafts to the reactive sites on the backbone slows down because of increasing steric hindrance. Second, the attachment of grafts to the backbone with a high grafting density becomes entropically unfavorable because the graft must change from a random coil conformation to a more stretched conformation once it is attached to the backbone. Thus, it is difficult to achieve the complete coupling reaction, which results in low

grafting efficiency and fail in controlling the graft sites and graft density. In addition, an incomplete coupling reaction often produces impure products and cause difficulty in purification.

2.1.1.3 Grafting from

The "grafting from" method, is based on the growth of side chains from the active sites contained in the main polymer chain, has received much attention recently as a new path way for the preparation of well defined graft copolymer [25,27]. This technique procedure requires the generation of active sites on the main polymer chain, macroinitiator, which are capable of initiating the graft polymerization of an appropriately chosen monomer.

The "grafting from" method is most effective to control the structure of graft copolymers by living or controlled polymerization techniques. Generally, these well-defined macroinitiators can be obtained directly via various living or controlled polymerization techniques (atom transfer radical polymerization (ATRP) [43], anionic polymerization [44] and RAFT [45]), which allow the control of the main chain parameters as well as the sites and distribution of active that can determine the graft sites and the graft density. The grow of the graft chains by the active groups well-distributed along main chain initiating the polymerization of chosen monomer also can be well controlled by living or controlled polymerization techniques (ATRP [29, 30,46- 50] and anionic polymerization [51,52]). Therefore, the graft copolymer with high graft density and well-defined backbones and graft chains can be prepared. In particular, the purification of the resulting copolymer is much simper in comparison with the other two methods.

2.1.2 Graft copolymer formation by reactive blending

The process of blending existing polymers holds considerable promise as a means of creating new materials with combination of properties superior to the components at relatively low cost. However, since most polymer pairs are immiscible, polymer blends often need to be compatibilized using block or graft copolymers [1]. The one that has been frequently practiced is the so-called in-situ (or reactive) compatibilization. In the in-situ compatibilization process, the graft copolymer can be formed directly by two techniques: one is the interfacial coupling reactions between two premade polymers bearing functional groups [53- 61], which is the most important application of the "grafting onto" method; the other is the in-situ polymerization of the chosen monomer from the macroinitiator [62- 65], which is a typical application of the "graft from" method.

2.1.2.1 Interfacial coupling reactions

Generally, interfacial coupling reactions require two functional polymers: one polymer is synthesized via a stepwise mechanism, which leaves functional groups at the chain ends such as polyamides, polyesters and polycarbonates; the other polymer has a few functional groups placed randomly along the chain, either by copolymerization (for example: the copolymer SMA of styrene (St) and maleic anhydride (MAH)) or by grafting onto the premade polymer (for example: the MAH grafting polyolefin) [61]. Thus the graft copolymers are formed by coupling reaction between the functional groups. Copolymer formation must occur during reactive extrusion process whose mean residence time is typically short and less than a few minutes. Therefore, coupling reaction should be fast to form an amount of copolymers sufficient to cover the phase interface and compatibilize a blend and/or to increase adhesion within the processing time. The most common reactive pair is amine/anhydride which has been used for most commercial reactively compatibilized blends, for example, polyamide/SMA [59] and amine terminal polystyrene (PS-NH_2) and anhydride terminal poly (methyl methacrylate) (PMMA-An). Many other reactive pairs such as carboxylic acid/epoxy [66] and hydroxyl and carbonyl [31] have been considered as a reactive pair for reactive compatibilization.

It is difficult to determine reactivity between two functional polymer chains. The concentration of functional groups is very low, so standard techniques like nuclear magnetic resonance (NMR) and fourier transform infrared spectroscopy (FTIR) do not have sufficient sensitivity [67]. Most blends have been developed based on property improvement and changes in morphology. It is inferred that coupling must be occurring if the morphology becomes finer and more stable. Some previous researchers have used solvent extraction to determine the amount of copolymer formed during processing by measuring the mass directly or aided by NMR or FTIR analysis [68-70]. The blend is broken into a fine powder, then extracted first with a solvent for the matrix and then with one for the dispersed phase. By repeating this extraction sequence several times the mass of reactively formed graft copolymer can be estimated. However, this method can yield falsely high values due to the difficulty in complete removal of unreacted polymer.

If a mutual solvent can be found for both polymers, reaction conversion to copolymer can be measured with size exclusion chromatography (SEC) by using narrow distribution end functional polymers [67]. The sensitivity of the technique can be increased by 100-fold by incorporation of a fluorescent group on a polymer [71,72].

For example, Jeon and Feist et al. [59] used fluorescent pyrene to label SMA allowed the detection of small amounts of reactively formed block (SMA-g-PA66) in the PS/PA66/SMA blends via SEC with a fluorescence detector and found an extremely fast reactions giving > 60% conversion in 0.5 min mixing.

This approach is technically very attractive and economically appealing for preparing immiscible blends. However, it does not allow obtaining pure graft copolymers when the functional polymers are immiscible, unless the molar mass of at least one of the reactive polymer components is smaller than its critical entanglement molar mass, or once formed at the interfaces the copolymer chains walk away. Limited amounts of copolymer formed by interfacial reactions can be explained as follows [73,74]. First, the interfacial volume available for reaction between two immiscible polymers is often very small, even under intense mixing; second, the intrinsic reactivity of two mutually reactive groups attached to polymer backbones can be much smaller than their small-molecule analogues because of steric hindrance effects.

2.1.2.2 In-situ polymerization

Hu et al. [62-64] have developed a novel reactive extrusion process to obtain compatilibilzed A/B immiscible polymer blends. It consisted of polymerizing a monomer of polymer B in the presence of polymer A. A fraction of polymer A chains bore initiating sites either at the chain end(s) or along the chain backbones, from which polymer B chains could grow, which is an application of “grafting from” method in bulk copolymerization. In the process, polymer B and a graft or block copolymer of A and B were formed simultaneously leading to in situ polymerized and in situ compatibilized A/B polymer blends. In fact, four phenomena are involved in the process: polymerization of MB which produces polymer B and causes phase separation and eventually phase inversion; formation of an A-B copolymer that stabilizes the system. For this reason, the method is called in situ polymerization and in situ compatibilization of polymer blends. Schematic description of this process is shown in Figure 2.2.

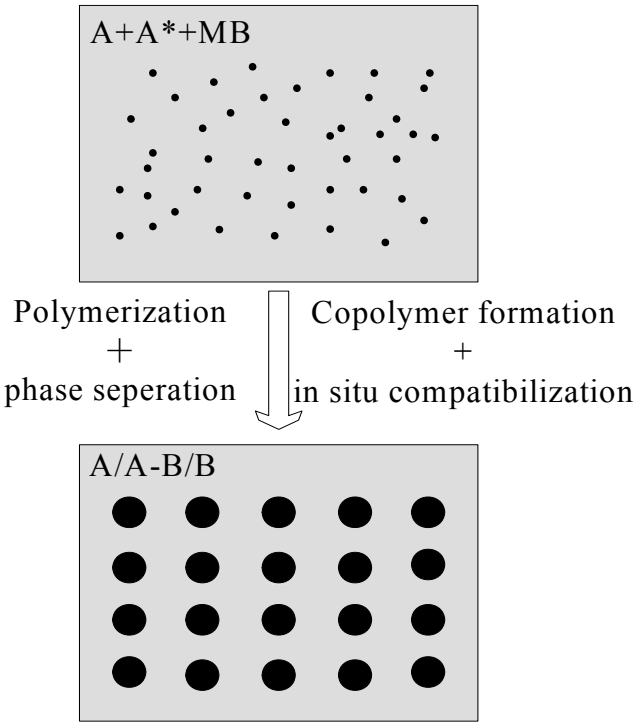


Figure 2.2 Schematic description of the in-situ polymerization and in-situ compatibilization. A* denotes polymer A chains bore initiating sites either at the chain end(s) or along the chain backbones.

The above chemical process can be explored for two interesting applications. One is to obtain polymer blends with a variety of morphology including nanodisperspersion of one polymer in the other upon controlling the kinetics of polymerization, phase separation and copolymer formation. For example, nanoblends were obtained by polymerizing lactam like CL in the presence of polypropylene (PP) homopolymer and 3- isopropenyl-α,α-dimethylbenzene isocyanate (TMI) grafted PP (PP-g-TMI) [62-64], PP homopolymer and maleic anhydride (MAH) grafted PP (PP-g-MAH) [65] and poly(2,6-dimethyl-1,4-phenylene oxide) (PPO) and 4-methoxyphenylacrylate (MPAA) grafted PPO [75]. The other is to polymerize a chosen monomer onto a polymer backbone via initiating sites by reactive extrusion. The grafting polymerization route is expected to generate graft copolymers with very high purity. This is because, unlike interfacial coupling reactions, both the interfacial area limitation and steric hindrance effects are much reduced or totally absent.

Lactams such as CL is suitable as the monomer of the above graft polymerization because it can be polymerized anionically in the prescence of a catalyst like NaCL. Some 35 years ago, Matzner et al. [76] used the acrylic esters incorporated PS or PE as activators from which the polymerization of CL could grow in the presence of an anionic catalyst such as NaCL, leading to the formation of PA6 grafts. Ester and

bischloroformate bearing polymers were also used to activate the polymerization of CL to form graft copolymers [77,78]. However, the overall polymerization rate is often very slow because of the slow initiation rate and is thus incompatible with reactive extrusion process. The latter have residence times typically less than 5 min. An activator is thus required to accelerate the initiation rate and consequently the polymerization rate. Hu et al. [73,74,79] used an isocyanate-bearing polypropylene (PP-g-TMI) as an activator and obtained high purity graft copolymers of PP and PA6 in about a minute in a batch mixer. TMI not only shows much higher activation performance and but also sufficiently stable under extrusion conditions (high temperatures and exposure to moisture).

Hu et al. [74] had studied on the effects of temperature and the concentrations of NaCL and the isocyanate group in the form of PP-g-TMI on the polymerization rate. The torque as a function of time could be used as rapid and convenient measures for evaluating and controlling the effects of chemical and operating conditions on the polymerization rate [79]. For example, a high polymerization rate will necessarily lead to a fast increase in the viscosity of the polymerization system and consequently a rapid increase in the polymerization temperature and torque, and vice versa. Results suggested that if the polymerization is to be carried out by a reactive extrusion process whose mean residence time is less than a few minutes, it is recommended that the polymerization temperature be higher than 220 ºC. Moreover, the molar ratio between NaCL and CL should be higher than 0.5 and at the same time that between the isocyanate group in the form of PP-g-TMI and NaCL, should be smaller than 4.

2.2 Study object and strategy

The previous studies of Hu et al. have obtained pure graft copolymer PP-g-PA6 by the anionic polymerization of CL from PP-g-TMI. However, they did not answer the following two important questions. First, did all the isocyanate moieties in the PP-g-TMI participate in the activation of the polymerization of CL? If yes, the number of the PA6 grafts per PP chain was then equal to that of the isocyanate moieties per PP-g-TMI chain. Second, the anionic polymerization scheme of CL is known to be complex [80,81]. For the PP-g-TMI/CL/NaCL graft polymerization system, what were the composition of the resulting polymer product and the structure of the resulting graft copolymer? This work is aimed at addressing those two questions upon using a random copolymer of styrene (St) and TMI (PS-co-TMI) as the activator. The resulting copolymer is expected to be a graft copolymer with the PS as backbone and

PA6 as grafts. It will be denoted as PS-g-PA6. The reason for choosing the PS-co-TMI/CL/NaCL polymerization system is that unlike the PP-g-TMI/CL/NaCL polymerization system and its corresponding polymerized product which can be soluble only in exotic solvents and at very high temperature, the PS-co-TMI/CL/NaCL polymerization system and its corresponding polymerized product can be soluble in several classical solvents at room temperature. As such, it is much easier to characterize them.

In addition, the PS-co-TMI/CL/NaCL polymerization system differed from the PP-g-TMI/CL/NaCL one in that prior to polymerization the former was miscible and the latter was not. Another goal of this work was to answer to what extent would the conclusions obtained from the PP-g-TMI/CL/NaCL polymerization system be valid for other immiscible or miscible ones?

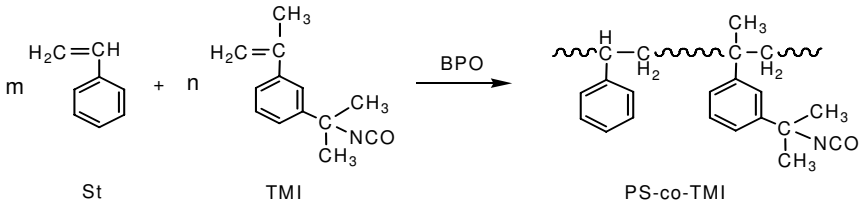
2.3 Mechanism of the graft copolymer PS-g-PA6 formation

The anionic polymerization of CL has been studied very extensively [80- 86]. For example, CL can be polymerized anionically above 100 ºC in the presence of a catalyst like NaCL. However, the rate of polymerization is low because of the slow initiation and is thus incompatible with the mean residence time of a typical reactive extrusion process. An activator is thus required to accelerate the initiation rate and consequently the polymerization rate. It can be an isocyanate, an ester, etc. The polymerization of lactams such as CL in the presence of a catalyst and an activator is called activated anionic polymerization. The above chemical mechanism can be used to advantage for the synthesis of polyamide bearing copolymers. For example, if the activator moieties are attached to a polymer chain, a graft copolymer will be formed. Therefore, the first step was to incorporate an isocynanate bearing vinyl monomer such as TMI in a polymer chain by copolymerization [87- 90]or free radical grafting [91]. The latter technique is most useful for polymers like polyolefins whose monomers can not be copolymerized easily with TMI. Hu et al. [73,79,91] have attached TMI onto PP backbone by free radical grafting and used St as comonomer to control the grafting yield and the molar mass of PP-g-TMI. For the studied system PS/PA6 in this work, TMI can be incorporated easily in PS substrates by free radical solution copolymerization of TMI and St, as shown in Figure 2.3.

Figure 2.3 also depicts the anionic polymerization of CL from PS-co-TMI in the presence of NaCL as a catalyst. It is composed of activation, initiation and propagation steps [63,73,74]. Basically, polymerization starts with the formation of an

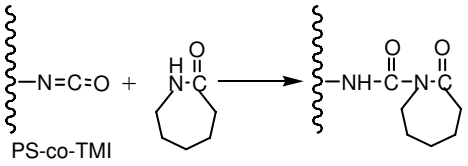
acyl caprolactam as a result of the reaction between R-N=C=O and CL. This acyl caprolactam then reacts readily with NaCL forming a new reactive sodium salt. This latter initiates the polymerization of CL; meanwhile the catalyst (NaCL) is restored. Finally polymerization leads to high molecular weight PA6 grafts. It is obviously highly simplified because in practice many side reactions may occur especially at elevated temperatures.

1. Preparation of PS-co-TMI by free radical polymerization of St and TMI

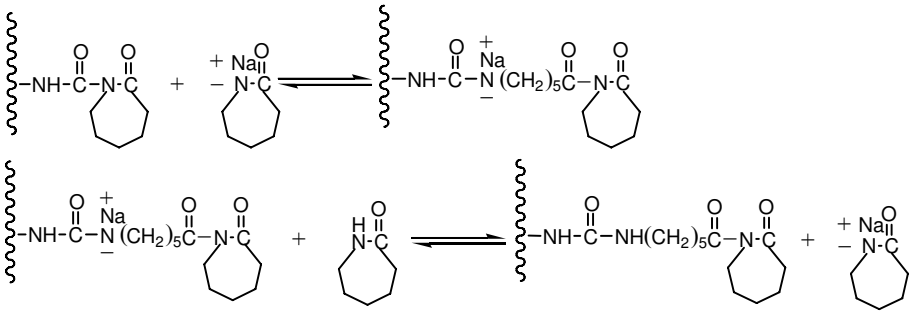


2. Preparation of the graft copolymer of PS and PA6 via the anionic polymerisation of CL from PS-co-TMI

(a) Activation:



(b) Initiation:



(c) Propagation:

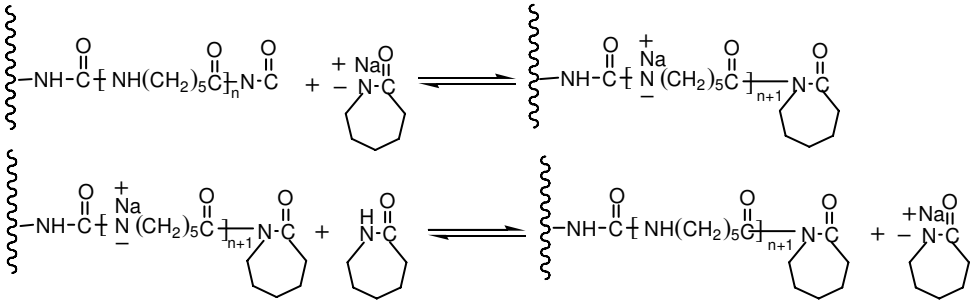


Figure 2.3 Synthesis of PS-co-TMI and anionic polymerisation of CL from PS-co-TMI in the presence of NaCL as a catalyst.

2.4 Experimental

2.4.1 Material

There were two types of materials: one for the free radical copolymerization of St and TMI to obtain PS-co-TMI and the other one for the synthesis of PS-g-PA6 by anionic polymerization of CL from PS-co-TMI. The two monomers used for the free radical copolymerization, St and TMI, were purchased from Aldrich. The formula mass and the boiling temperature of TMI are 201 g/mol and 270 ºC/760 mmHg, respectively. Prior to the copolymerization, St was purified over an aluminum oxide column while TMI was not purified. Benzoyl peroxide (BPO) was used as the free radical initiator. It was purified by dissolution in methanol, precipitation in chloroform and then dried in a vacuum oven at room temperature. Toluene was used as the solvent for the copolymerization of TMI and St and was purified by boiling in the presence of anhydrous calcium oxide. CL was purified by rectification under vacuum at about 100 mmHg. Its melting temperature is 69~71 ºC and its boiling temperature is 268.5 ºC/760 mmHg and 139 ºC/12 mmHg. The catalyst used for the anionic polymerization was supplied by DSM in the form of a mixture of NaCL and CL containing 1.4 mol NaCL/kg CL. It will be denoted as Cat. The micro-activator used to initiate the homopolymerization of CL, was 2, 4-tolunene diisocyanate (TDI) with a formula mass of 174.16 g/mol.

2.4.2 Synthesis of PS-co-TMI

The free radical copolymerization of St and TMI was carried out in a one-liter glass reactor equipped with a mechanical agitator. The reactor was purged by nitrogen and its temperature was controlled at set temperature by circulating water.

Table 2.1 Compositions of St, TMI, BPO and toluene, polymerization temperature and time used for the synthesis of PS-co-TMI.

PS-co-TMI	St/TMI/BPO/toluene	Temperature (ºC)	Time (h)
PS-co-TMI1	40ml/0.4ml/0.2g/60ml	80	24
PS-co-TMI2	40ml/0.8ml/0.2g/60ml	80	24
PS-co-TMI4	40ml/1.6ml/0.2g/60ml	80	24
PS-co-TMI6	40ml/2.4ml/0.2g/60ml	80	24
PS-co-TMI8	40ml/3.2ml/0.2g/60ml	80	24
PS-co-TMI4L	40ml/1.6ml/0.4g/60ml	90	24
PS-co-TMI4H	40ml/1.6ml/0.1g/60ml	80	24

Toluene was first charged to the reactor, followed by St, TMI and BPO. At the end of the polymerization, the product was precipitated twice in methanol, filtered and then dried in a vacuum at 80 ºC for 24 h. Table 2.1 shows some of the information for the synthesis of PS-co-TMI.

2.4.3 Synthesis of PS-g-PA6 graft copolymer and homopolymer PA6

A batch mixer of type Haake torque rheometer (HBI systems 90) was used for the anionic polymerization of CL in the presence of NaCL as catalyst. The mixing chamber had a volume capacity of about 60 ml and was equipped with two rotors. During the polymerization, those two screws rotated in the opposite directions with a rotation speed of 65 revolutions per minute to ensure mixing. CL, Cat and PS-co-TMI macro-activator (or micro-activator) were fed to the mixer in a one-step or two-step feeding mode. In the one-step feeding mode, all the ingredients were charged to the mixer together while in the two-step feeding, first all PS-co-TMI and 80% of CL were added to the mixer and then the remaining CL and all Cat were added later. Samples were taken out from the mixing chamber after a prescribed mixing time. Table 2.2 gathers some of the information on the experimental trials carried out in this work.

Table 2.2 Selected information on the experimental trials carried out in this work

Exp. No.	Mass composition PS-co-TMI/CL/Cat	PS-co-TMI	NCO/CL mol/mol	NaCL/CL mol/mol	T_{set} (ºC)	Feeding mode
E1	50/50/5.0	PS-co-TMI4	2.08/100	1.23/100	170	one-step
E2	50/50/5.0	PS-co-TMI4	2.08/100	1.23/100	180	one-step
E3	50/50/5.0	PS-co-TMI4	2.08/100	1.23/100	200	one-step
E4	50/50/5.0	PS-co-TMI4	2.08/100	1.23/100	220	one-step
E5	50/50/5.0	PS-co-TMI4	2.08/100	1.23/100	230	one-step
E6	50/50/5.0	PS-co-TMI4	2.08/100	1.23/100	240	one-step
E7	50/50/5.0	PS-co-TMI1	0.52/100	1.23/100	230	one-step
E8	50/50/5.0	PS-co-TMI2	1.04/100	1.23/100	230	one-step
E9	50/50/5.0	PS-co-TMI6	3.11/100	1.23/100	230	one-step
E10	50/50/5.0	PS-co-TMI8	4.15/100	1.23/100	230	one-step
E11	70/30/5.0	PS-co-TMI4	4.60/100	1.94/100	230	one-step
E12	30/70/5.0	PS-co-TMI4	0.91/100	0.90/100	230	one-step
E13	50/50/1.7	PS-co-TMI2	1.04/100	0.43/100	230	one-step
E14	50/50/1.7	PS-co-TMI4	2.19/100	0.43/100	230	one-step

E15	50/50/1.7	PS-co-TMI6	3.11/100	0.43/100	230	one-step
E16	50/50/8.3	PS-co-TMI4	1.97/100	1.94/100	230	one-step
E17	50/50/1.7	PS-co-TMI4	2.19/100	0.43/100	230	two-step
E18	50/50/5.0	PS-co-TMI4	2.08/100	1.23/100	230	two-step
E19	3.6/100/6	TDI	2.34/100	0.74/100	230	one-step

2.4.4 Methods used for the determination of the CL conversion

Prior to the determination of the conversion of CL to the PS-g-PA6 graft copolymer or PA6 homopolymer (Homo-PA6), samples were all subjected to the following pretreatment. They were pressed with a hot press at 200 ºC and 30 MPa to films of about 200 μm thick. The whole process took about 3 min. The films were then dried under vacuum at 50 ºC for 12 h in order to remove traces of water. The importance of this pre-drying procedure will be discussed later. The amounts of the CL remained in the films were subsequently measured by the following methods.

2.4.4.1 Method 1: Gravimetry by solvent extraction

Known amounts (about 0.5g) of pre-dried films were placed in one of the following solvents under reflux (water, methanol, THF or acetone) for 1 h to extract the residual monomer from the films. This duration was found to be largely enough for water or methanol. The extracted films were then vacuum-dried at 80 ºC for 12 to 48 h. Finally their masses were weighted. The CL conversion was calculated using the following equation:

$$CL\% = \left[1 - \frac{W_1 - W_2}{W_1 * (W_{CL,0} + W_{cat,0} * 97.4\%) / W} \right] * 100\% \qquad (2.1)$$

where W_1 and W_2 are the masses of the polymerized product before and after extraction, respectively; W is the initial total mass of the polymerizing system. $W_{CL,0}$ and $W_{cat,0}$ are the initial masses of CL and Cat; and 97.4% is the mass percentage of the equivalent CL in the Cat [74].

2.4.4.2 Method 2: Vacuum drying at 140 °C

Known amounts (about 0.5g) of pre-dried films were placed in a vacuum oven at 140 °C for 12 or 24 h. The mass losses were considered to be the amounts of CL that remained in the films before the vacuum drying. The CL conversion was calculated using the following equation:

$$CL\% = \left[1 - \frac{W_3 - W_4}{W_3 * (W_{CL,0} + W_{cat,0} * 97.4\%)/W}\right] * 100\% \qquad (2.2)$$

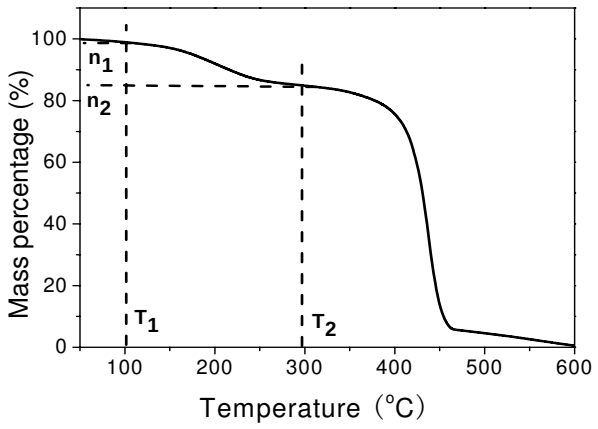
where W_3 and W_4 are the masses of the polymerized product before and after vacuum drying at 140 °C, respectively.

2.4.4.3 Method 3: TGA

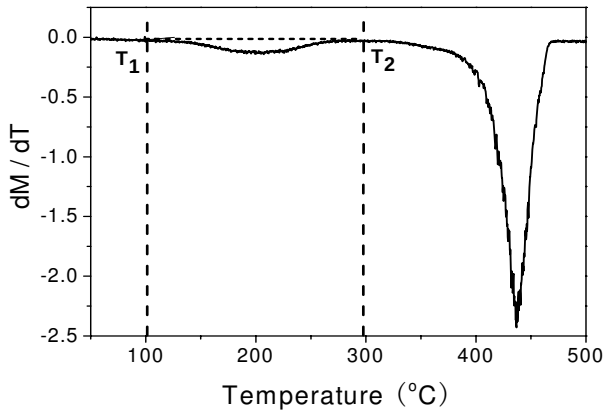
A thermogravimetric analysis (TGA) of type Perkin Elmer, Pyris 1, was used. Its accuracy was within 0.1 μg. Pre-dried films (about 2 mg) were heated from 25 to 600 ºC at 10 ºC /min under nitrogen. A typical TGA diagram is shown in Figure 2.4a. Its differential form is shown in Figure 2.4b. It is seen that the mass loss took place most significantly in two different temperature ranges. The first one was between 100 and 300 °C and was a result of small molecule evaporation. The second one was located between 350 and 465 °C and corresponded to the thermal degradation of the polymer product. The first mass loss was actually due to the evaporation of CL since its melting and boiling temperatures were 69~71 and 268.5 ºC/760 mmHg, respectively. Figure 2.4b shows that the CL started to evaporate at about 100 °C (T_1) and the evaporation was complete at about 300 °C (T_2). The CL conversion was calculated according to the following equation:

$$CL\% = \left[1 - \frac{n_1 - n_2}{(W_{CL,0} + W_{cat,0} * 97.4\%)/W}\right] * 100\% \qquad (2.3)$$

where n_1 and n_2 are the mass percentages of the product at the beginning and at the end of the evaporation of CL.



(a)



(b)

Figure 2.4 TGA diagrams of a typical product obtained by the anionic grafting polymerization of CL onto PS-co-TMI. (a) Accumulated mass loss as a function of temperature increase; (b) Instantaneous mass loss as a function of temperature increase.

2.4.4.4 Method 4: Elemental analysis

Pre-dried films were first put in boiling methanol for 1 h in order to extract the residual CL from them and then dried in a vacuum oven at 80 ºC for 12 h. The nitrogen contents of the films before and after extraction in boiling methanol were measured by element analysis. The CL conversion was calculated by the following equation:

$$CL\% = \frac{N_2 - N_3 * 7\%}{N_1 - N_3 * 7\%} * 100\% \qquad (2.4)$$

where N_1 and N_2 (%) are the nitrogen content in the polymerized product before and after extraction in methanol, respectively; N_3 (%) is the TMI mass content in PS-co-TMI; 7% is the nitrogen content in TMI.

2.4.5 Purification and fractionation of polymerized products

Figure 2.5 shows the procedure used for the purification and fractionation of as-polymerized products. Typically, a polymerized product was pressed to a film of about 200 μm thick at 200 ºC and under 30 MPa. About 1.5 g of the film was extracted in methanol under reflux for 1 h. The solution in methanol contained the un-reacted CL and possibly low molar mass derivatives of CL (solution A). The product that was insoluble in methanol was referred to as solute B. It was then extracted in tetrahydrofuran (THF) under reflux for 1 h. The THF soluble and insoluble products were referred to as solution C and solute E, respectively. Residue

D was obtained from solution C by rotatory evaporation and then vacuum drying at 80 ºC for 24 h. Subsequently, solute E was subjected to extraction in formic acid at room temperature for 12 h. The formic acid insoluble product was dried in a vacuum oven at 80 ºC for 24 h and was referred to as solute F. Residue H was obtained from the formic acid solution (solution G) by rotatory evaporation and vacuum drying at 80 ºC for 24 h.

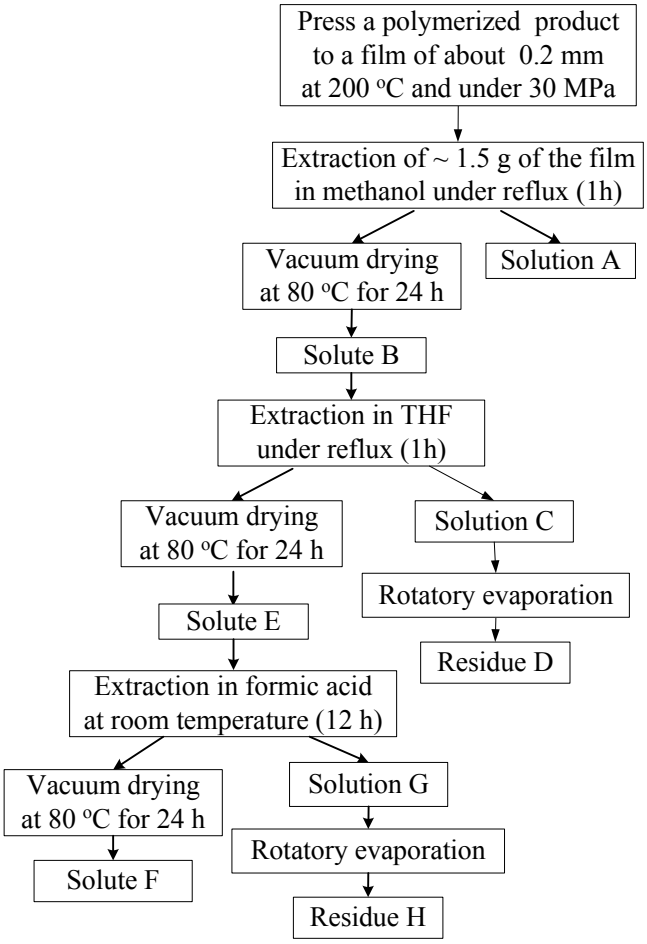


Figure 2.5 Procedure used for the purification and fractionation of polymerized products.

2.4.6 Determination of the characterization of Homo-PA6 and PS-g-PA6 by SEC

2.4.6.1 *N*-trifluoroacetylation of homo-PA6 and PS-g-PA6

Prior to the *N*-trifluoroacetylation reaction, homo-PA6 or PS-g-PA6 was dried in a vacuum oven at 80 ºC for 24 h. A given amount of homo-PA6 or PS-g-PA6 was added to a two-neck flask of about 10 ml capped with a rubber septum. One of the necks was connected to a vacuum pump to remove air and the other one to nitrogen to purge the flask. Then, dry CH_2Cl_2 (2 to 3 ml), trifluoroacetic anhydride (TFAA) (2 ml) and a co-solvent (a co-solvent was used only in the case of PS-g-PA6) were

successively added to the flask. The molar ratio between TFAA and the amide group of the homo-PA6 or PS-g-PA6 was approximately 1.5:1. A few minutes to a few hours were needed for the homo-PA6 or PS-g-PA6 to be completely dissolved at room temperature. After 24 h of reaction, the *N*-trifluoroacetylated homo-PA6 (PA6-TFAA) or PS-g-PA6 (PS-g-PA6-TFAA) was isolated using a rotary evaporator at 30 ºC.

2.4.6.2 ***Measurement by SEC***

THF was added to the flask with *N*-trifluoroacetylated and rotary evaporated homo-PA6 or PS-g-PA6 to form a concentration of 3 mg/ml in equivalent homo-PA6 or PS-g-PA6. After filtration, the solution was injected into the SEC apparatus (Waters 1525/2414, injection volume: 50 µl) equipped with a refractometer and a UV-detector. Ideally, the above solution should be freshly prepared prior to the SEC measurement. Otherwise it could form gel in a few hours.

2.4.7 FTIR analysis

A FTIR of type Nicolet 5700 was used to characterize some products. For that purpose, the polymer products were ground with KBr powder and then pressed to form films of 200 µm thick or were pressed to films of 40 to 100 µm thick using a hot press at 220 ºC and under 30 MPa for 4 min; liquid products were cast to thin films on a KBr disc. FTIR spectra were then recorded on those films with 32 scans and a resolution of 4 cm^{-1}.

2.4.8 NMR spectroscopy

NMR could not characterize pure PS-g-PA6 graft copolymers because of a lack of appropriate solvents capable of dissolving them. However, it could characterize some of the components such as residue D involved in as-polymerized products. ^{13}C-NMR spectra were recorded on a NMR of type Bruker Avance 400/500 DMX and $CDCl_3$ was used as the solvent.

2.4.9 DSC measurements

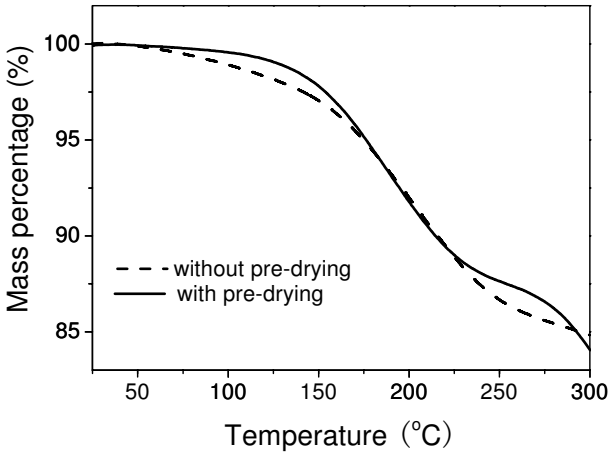
The melting and recrystallization behaviors of purified PS-g-PA6 graft copolymers were studied using a differential scanning calorimetry (DSC) of type DSC7 Perkin-Elmer under nitrogen atmosphere. Samples were subjected to the following thermal cycle. They were heated from 50 to 260 ºC at 10 ºC/min and maintained at 260 ºC for 2 min to erase their previous thermal history. They were then cooled down to 50 ºC at 10 ºC/min (recrystallization). Finally, they were heated up again to 260 ºC at 10 ºC/min (melting).

2.5 Comparison of various methods of measuring the conversion of CL to PA6

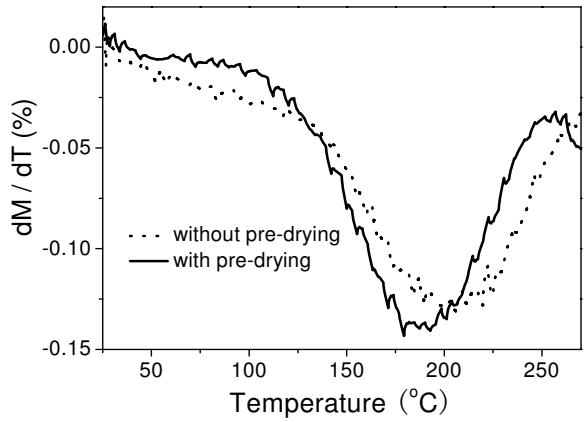
Various methods have been proposed to determine the conversion of CL. They include gravimetry [73,74,81, 92 - 94], gas chromatography [95, 96], enthalpy of polymerization [84, 97] and in-line infrared spectroscopy [98]. Among them, the gravimetry is used the most. It is based on the ratio of the mass of the polymerized product whose residue monomer is removed over its initial mass. The performance of this type of method depends very much on how easy and the extent to which the residual monomer is removed. In order to determine the conversion of CL to PA6, a few analytical methods were compared. These analytical methods were gravimetry by solvent extraction, vacuum drying at 140 ºC, TGA and elemental analysis based on nitrogen.

2.5.1 Effect of the pre-drying of polymerized product films

Polymerized products were expected to contain PS-g-PA6 graft copolymer (or Homo-PA6) and CL residue. They were all prone to water absorption, especially the latter. Thus removal of the absorbed water seemed to be necessary for the subsequent determination of the CL conversion. This was confirmed by the TGA traces (Figure 2.6) of the polymerized product E14 with and without pre-drying in a vacuum oven at 50 ºC for 12 h. Without pre-drying, the films started to loss mass at about 50 °C. With the pre-drying, the mass loss was noticeable only at about 100 °C. These results confirmed that water started to evaporate at a much lower temperature than CL, as expected. When the temperature reached about 260 °C, the rate of the mass loss was significantly reduced. This implies that at that temperature both water and CL residue were completely removed. It is interesting to note that the difference in mass between the two films (one with the pre-drying and the other one without pre-drying) at 100 °C was the same as that at 260 ºC. Moreover, that mass difference was also very similar to that obtained by the pre-drying procedure. Those results confirmed that that mass difference was indeed related to the amount of water absorbed in the films. Table 2.3 shows the mass losses of various polymerized products after different pre-drying times. It is seen that 12 h was long enough to remove the absorbed water. Moreover, the higher the CL mass percentage in the polymerizing system, the higher the water content in the film, as expected.



(a)



(b)

Figure 2.6 Effect of the pre-drying in a vacuum oven at 50 °C for 12 h on the TGA diagrams of the polymerised product of the experiment E14. (a) Accumulated mass loss as a function of temperature increase; (b) Instantaneous mass loss as a function of temperature increase.

Table 2.3 Mass losses of various polymerized products subjected to different pre-drying times in a vacuum oven at 50 ºC.

The product of experiment	CL content in the polymerizing system (%)	Masses at different pre-drying times (g)			Mass loss percentage (%)[a]
		0 h	12 h	24 h	
E12	69.7	0.5378	0.5250	0.5243	2.38
E5	51.6	0.5108	0.5020	0.5016	1.80
E14	50.6	0.5245	0.5147	0.5147	1.87
E11	32.6	0.5358	0.5301	0.5301	1.06

(a) Calculated based on the masses after 12 h pre-drying.

2.5.2 Performances of the various methods of measuring the CL conversion for grafting polymerization system

2.5.2.1 Method 1: Gravimetry by solvent extraction

Table 2.4 shows the CL conversions obtained by extraction in different solvents followed by vacuum drying at 80 °C for 24 h. It is noted that while the measured CL conversions followed the order: THF < acetone < methanol < water for the experiments E5 and E11, those for the experiment E12 almost followed the opposite order: THF > acetone > water > methanol.

Table 2.4 Comparison of the CL conversions measured by extraction in various solvents.

The product of experiment	CL conversion obtained by extraction (%)			
	Water	Methanol	Acetone	THF
E12	93.7	87.7	95.5	95.8
E5	95.8	90.9	86.0	71.0
E11	95.9	93.2	82.3	79.9

This might be explained by two different scenarios. The first one is that the PS-g-PA6 graft copolymer might contain molecules with very short PA6 grafts. Their solubility characteristics could be very similar to those of the PS-co-TMI. The second one is that all PS-co-TMI chains might not have been able to participate in the anionic grafting polymerization. Unlike water or methanol, when acetone or THF was used as a solvent, those two types of chains could be extracted from the polymerized products. As a result, the measured CL conversion values could be lower than the cases where water or methanol was used as the solvent. To verify those hypotheses, the residue D from the polymerized product of E5, PS-co-TMI4 and the product of PS-co-TMI4 that is subjected to reaction with an excess of CL in the absence of Cat were analyzed by FTIR, as shown in Figure 2.7. The FTIR spectrum of PS-co-TMI4 has a peak at 2255 cm^{-1} characteristic of the isocyanate group of TMI. That of residue D does not have it but has a new peak at 1641 cm^{-1} characteristic of PA6. This implies that residue D does not contain isocyanate moieties anymore. The FTIR spectrum of PS-co-TMI4-CL does not have the peak at 2255 cm^{-1} and is similar to that of residue D. These results infer that residue D likely does not contain PS-co-TMI but PS-g-PA6 whose PA6 content is low enough to be soluble in THF. This is further corroborated by the ^{13}C NMR spectra in Figure 2.8. Compared to PS-co-TMI4 or PS-co-TMI4-CL, residue D has new peaks characteristic of PA6 between 20 and 40 ppm.

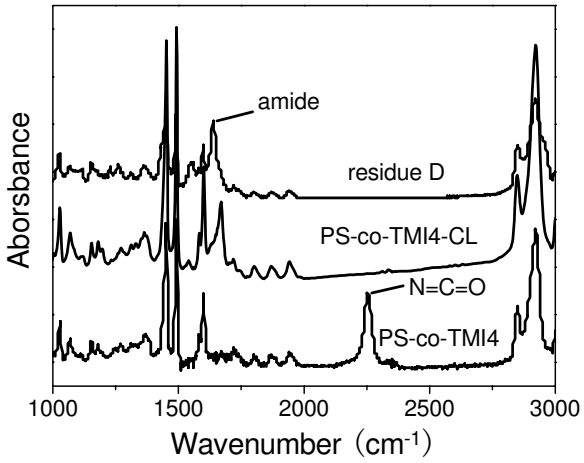


Figure 2.7 FTIR spectra of PS-co-TMI4, PS-co-TMI4-CL and residue D from the polymerized product of E5.

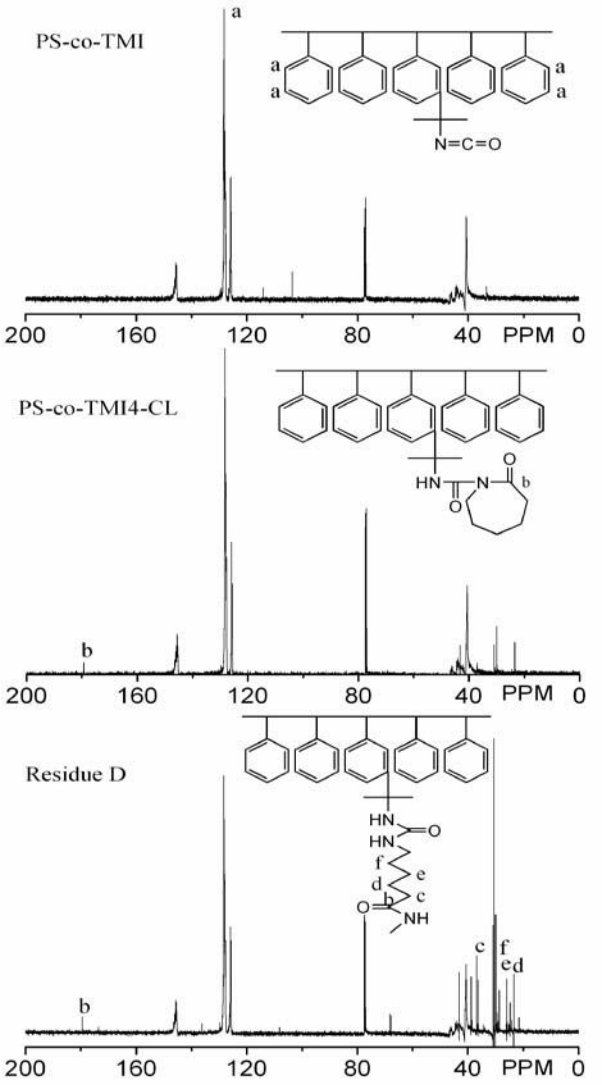


Figure 2.8 ^{13}C NMR spectra of PS-co-TMI, PS-co-TMI4-CL and residue D from the as-polymerized product of E5.

Figure 2.9 compares the UV spectrum of the PS-co-TMI in THF with that of solution C from the as-polymerized product of E5. Both had a characteristic peak of styrene at 259 nm. Nevertheless, they differed to a certain degree, suggesting that residue E was not the PS-co-TMI but likely PS-g-PA6 graft copolymer with very short PA6 grafts.

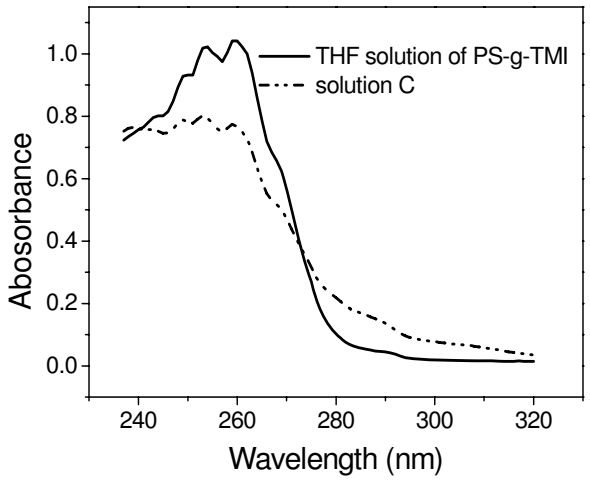


Figure 2.9 UV spectra of (a) PS-co-TMI in THF and (b) solution C from the as-polymerized product of E5. .

As shown in Table 2.4, the CL conversions from the methanol extraction were lower than those from the water extraction. A question then arose of which one to use. To answer it, the following experiment was done (Figure 2.10). The polymerized product E5 was first extracted in water under reflux for 1h. The resulting solute I was then vacuumed dried at 80 °C for 24 h. A known amount (0.5032 g) of the dried solute I was further extracted in boiling methanol for 1 h. After vacuum drying at 80 °C for 24 h, its mass became 0.4932 g. In other words, there was 0.01 g decrease in mass after the methanol extraction.

Figure 2.11 compares the UV spectra of three products: (a) the methanol solution of CL, (b) solution A and (c) solution L. They all had a peak at about 212 nm characteristic of CL. This suggests that water alone was unable to completely extract the CL residue from the polymerized product because further CL was extracted during the subsequent extraction with methanol. Therefore, methanol was better capable of extracting the CL residue from the polymerized product than water. Based on the respective mass decreases as a result of the water and methanol extraction steps, the CL conversion was recalculated to be 92.0 %, which was much closer to that obtained from the methanol extraction (90.9%).

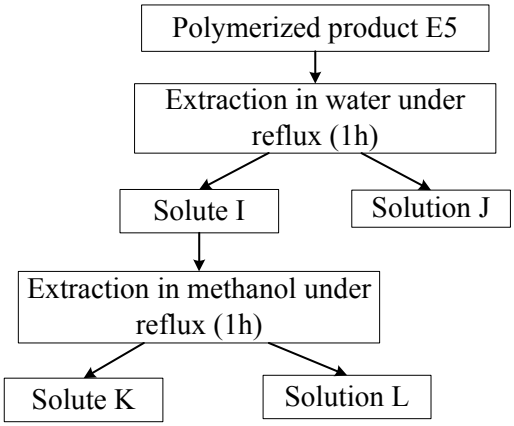


Figure 2.10 Procedure used for evaluating the performance of water and methanol as solvent for extraction.

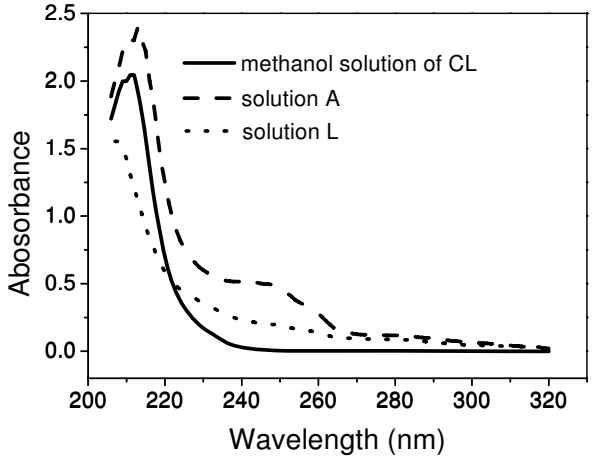


Figure 2.11 UV spectra of (a) the solution of CL, (b) solution A and (c) solution L.

Table 2.5 shows the minimum times necessary for the polymerized product E5 extracted in various solvents to reach a constant mass under vacuum drying at 80 °C. While 12 h was enough for water or methanol, above 36 h was needed for acetone or THF. Acetone and THF were good solvents of the PS part of the PS-g-PA6 graft copolymer. As such, longer times were needed for them to get out from the copolymer. On the other hand, water and methanol were neither good solvent for the PS part of the graft copolymer nor for its PA6 part. Thus they could be removed completely in a much shorter period of time. From this viewpoint, methanol and water were also better solvents for extraction than acetone and THF.

The results above suggest that a good solvent for extracting CL from a polymerized product like E5 should be one which should not have too strong or too weak affinity with either of the two parts of the PS-g-PA6 graft copolymer. Methanol seems to be the best compromise of the four solvents tested (methanol, water, THF

and acetone).

Table 2.5 Times necessary for complete solvent removal under vacuum drying at 80 °C.

Solvents extraction for product of experiment E5	Mass percentages after various drying times (%)			
	12 h	24 h	36 h	48 h
Water extraction	97.9	97.8	97.8	—
Methanol extraction	95.3	95.2	95.2	—
THF extraction	86.2	85.2	85.0	84.8
Acetone extraction	93.6	93.1	92.9	92.7

2.5.2.2 Method 2: Vacuum drying at 140 °C for 24 h

The performance of this method depends very much on how easy and the extent to which the CL residue is removed from polymerized products. In order to confirm that the CL residue was indeed removed thoroughly by vacuum drying at 140 ºC, the polymerized product E5 which had already been vacuum-dried at 140 ºC for 24 h was placed in boiling methanol and was keep there for 1 h. It was then vacuum-dried at 80 ºC for 24 h. It was found that its mass after the methanol extraction basically did not change with respect to its mass before the extraction, indicating that vacuum drying at 140 ºC for 24 h was enough to completely remove the CL residue from the polymerized product.

Table 2.6 shows the CL conversion of the experiments E12, E5 and E11 measured by vacuum drying at 140 ºC for 24 h. Comparison of the data in this table with those obtained by methanol extraction followed by vacuum drying at 80 °C for 24 h in Table 2.4 shows that they were almost the same, further confirming the conclusion that both the vacuum drying at 140 °C for 24 h and methanol extraction followed by vacuum drying at 80 °C for 24 h were good methods for determining the CL conversion of the PS-co-TMI/CL/Cat anionic polymerization system.

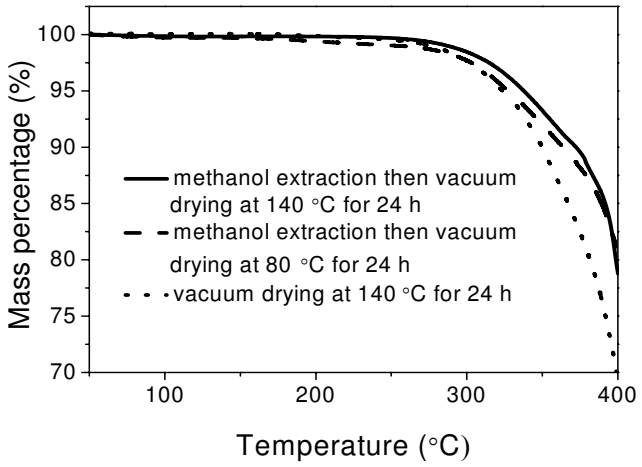
Table 2.6 CL conversions measured by vacuum drying at 140 ºC for 24 h

Polymerized product	CL conversion (%)
E12	87.3
E5	90.0
E11	92.3

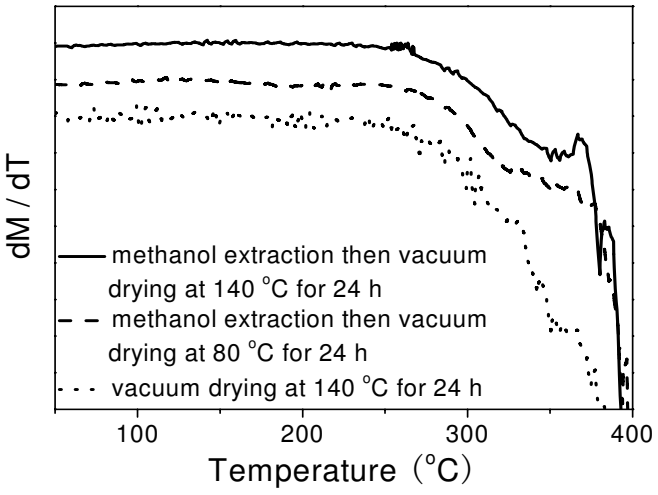
2.5.2.3 Method 3: TGA

TGA is based on mass balance and follows the instantaneous mass loss of a

product as temperature increases. Therefore, it can also be a good method to verify whether or not there are small molecules in polymers. Figure 2.12 shows the TGA traces of the polymerized product E5 which was subjected to one of the three different treatments: (1) methanol extraction and then vacuum drying at 140 ºC for 24 h; (2) methanol extraction and then vacuum drying at 80 °C for 24 h; and (3) vacuum drying at 140 °C for 24 h. It is seen that in all cases, the mass of the polymerized product E5 started to decrease only after 260 °C. This is another confirmation that the removal of the CL residue was indeed complete in all those three cases.



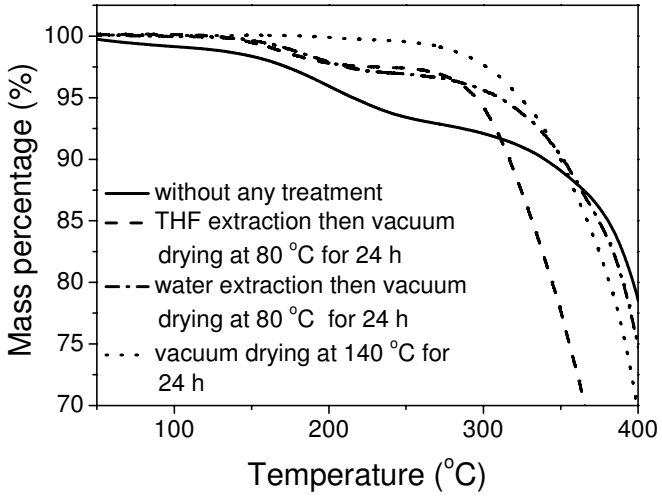
(a)



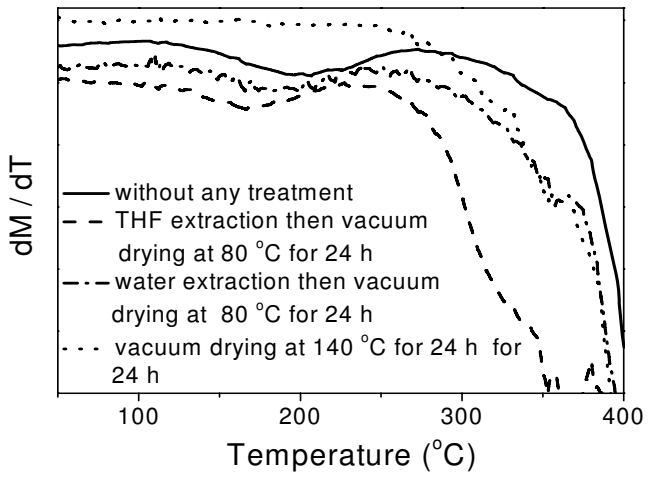
(b)

Figure 2.12 TGA traces of the polymerized product E5 subjected to one of the following treatments: (1) methanol extraction then vacuum drying at 140 ºC for 24 h; (2) methanol extraction then vacuum drying at 80 °C for 24 h and (3) vacuum drying at 140 ºC for 24 h. (a) remaining mass percentage; (b) instantaneous loss in the mass percentage.

Figure 2.13 shows the TGA traces of the polymerized product E5 which was subjected to: (1) no treatment; (2) THF extraction and then vacuum drying at 80 °C for 24 h; (3) water extraction and then vacuum drying at 80 °C for 24 h; and (4) vacuum drying at 140 °C for 24 h. It is seen that unlike the methanol extraction followed by vacuum drying at 80 °C for 24 h or the vacuum drying at 140 °C for 24 h, the polymerized product E5 treated by the water or THF extraction followed by vacuum drying at 80 °C for 24 h still lost its mass in the temperature range between 120 and 260 ºC. This indicates that either the CL residue or water (THF) or both were not completely removed. Those results were consistent with the aforementioned ones. The CL conversion could easily be determined from the TGA trace of the product without having been subjected to any treatment. The only difficulty was to fix up a temperature at which the CL residue could be considered being completely removed. It could be somewhere between 260 and 270 °C. The corresponding conversion would then be somewhere between 90.3 and 89.8. That value was close enough to that obtained by methanol extraction or vacuum drying at 140 ºC for 24 h. Thus, TGA could also be a suitable method for measuring the CL conversion.



(a)



(b)

Figure 2.13 TGA traces of the polymerized product E5 subjected to: (1) no treatment; (2) THF extraction and then vacuum drying at 80 °C for 24 h; (3) water extraction and then vacuum drying at 80 °C for 24 h and (4) vacuum drying at 140 °C for 24 h. (a) remaining mass percentage; (b) instantaneous loss in the mass percentage.

2.5.2.4 Method 4: Elemental analysis

Polymerized products contained nitrogen which came from the PS-co-TMI, CL and Cat. Thus in principle it was possible to determine the CL conversion by nitrogen analysis. Table 2.7 shows the CL conversion values for the experiments E11, E5, E12 and E14. They were much higher than those obtained by methanol extraction followed by vacuum drying at 80 °C for 24 h (Table 2.4), vacuum drying at 140 °C for 24 h (Table 2.6) and TGA. Thus, the nitrogen method was not suitable for measuring the CL conversion of the grafting anionic polymerization system. The reason remains unclear.

Table 2.7 CL conversions obtained by the nitrogen analysis

Experiment	CL conversion (%)
E12	89.0
E5	97.6
E11	98.0
E14	94.3

2.5.3 Suitability of the above methods for the anionic homopolymerization system

Table 2.8 compares the CL conversions of the polymerized product E19 obtained by

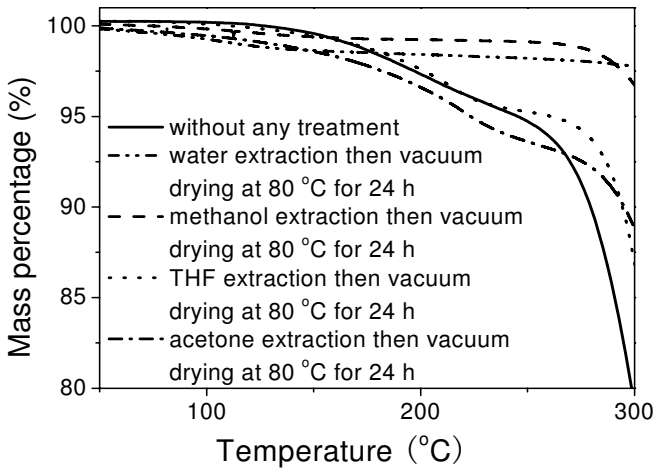
extraction in various solvents followed by vacuum drying at 80 °C for 36 h. From Table 2.8, it may be seen that the conversions of CL to PA6 by extraction in water and methanol were much lower than those by extraction in THF and acetone. In order to assess which solvents were suitable, the samples of the polymerized product E19 after extraction in those solvents were analyzed by the TGA. As shown in Figure 2.14, there was basically no mass loss till 260 °C for the sample subjected to extraction in methanol or water. This indicates that small molecules were successfully and thoroughly removed from the polymerized product during the extraction in methanol or water. On the other hand, the sample extracted in THF or acetone started to loss mass at a relatively low temperature, say, 120 °C. This implies that THF or acetone was unable to remove the small molecules from the polymerized product in a thorough manner.

Table 2.9 shows the CL conversions of the polymerized product E19 measured by the vacuum drying at 140 ºC for 24 h and TGA, respectively. Inspection of Table 2.8 and Table 2.9 shows that the vacuum drying at 140 °C for 24 h, the TGA and the extraction in methanol or water all yield very similar values for the CL conversion. Those results suggest that they were all good for measuring the conversion of the anionic homopolymerization of CL.

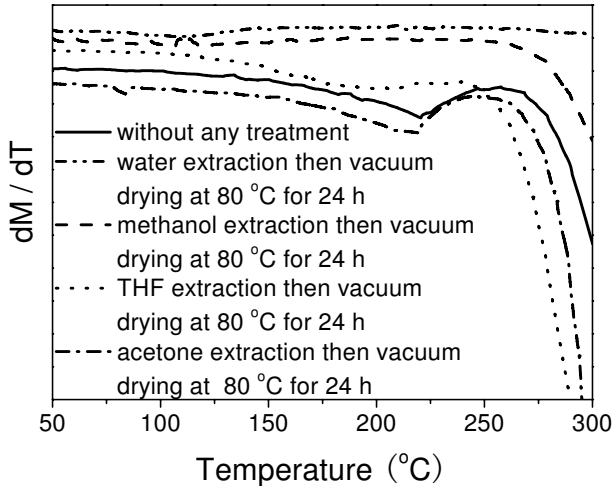
Table 2.8 CL conversions measured by extraction in various solvents

Solvent used for extraction of E19	Mass percentages after various times of vacuum drying (g)				CL conversion (%)[a]
	0 h	12 h	24 h	36 h	
Water	0.5312	0.4817	0.4782	0.4786	89.7
Methanol	0.4910	0.4464	0.4442	0.4437	90.0
THF	0.4940	0.4882	0.4845	0.4843	98.0
Acetone	0.5380	0.5265	0.5216	0.5213	96.8

(a) The conversions were calculated based on 36 h.



(a)



(b)

Figure 2.14 TGA traces of the polymerized product E19 subjected to one of the following treatments: (1) without any treatment; (2) water extraction then vacuum drying at 80 ºC for 24 h; (3) methanol extraction then vacuum drying at 80 ºC for 24 h; (4) THF extraction then vacuum drying at 80 ºC for 24 h and (5) acetone extraction then vacuum drying at 80 ºC for 24 h. (a) accumulated mass loss; (b) instantaneous mass loss.

Table 2.9 CL conversions of E19 obtained by vacuum drying at 140 ºC and TGA

Measuring method	CL conversion (%)
Vacuum drying at 140 ºC	89.7
TGA	90.5

2.5.4 Summary

The performance of four methods for measuring the conversion of CL to PA6 by activated anionic polymerization was compared. The resulting polyamide was either

Homo-PA6 or grafted onto polystyrene (PS-g-PA6 graft copolymer). Those four methods were: mass balance based on solvent extraction (methanol, water, THF or acetone), mass balance based on vacuum drying at 140 ºC, TGA and elemental analysis based on nitrogen. The mass balances based on methanol extraction and vacuum drying at 140 °C and TGA were all suitable for measuring the conversion of CL, whether the resulting polymer was the PA6 or PS-g-PA6. The mass balance based on water extraction was good for the Homo-PA6 and not good for the PS-g-PA6. The one based on THF or acetone extraction was good for none of the above two systems (PA6 and PS-g-PA6). The elemental analysis based on nitrogen was not applicable to the Homo-PA6 and was not suitable for the PS-g-PA6.

The CL conversions in following part were estimated by methanol extraction.

2.6 Characterization of PS-g-PA6 by SEC at room temperature

SEC is an important and routine technique for measuring the molar mass of polymers. It requires that polymers be soluble in a solvent suitable for SEC columns. The molar mass of polyamide (PA), an important family of polymers, can not be measured directly by SEC at room temperature because common eluents like THF, chloroform and dichloromethane (CH_2Cl_2) are not good solvents of PA [99]. On the other hand, it can be done by SEC using phenols and aliphatic fluorinated alcohols at high temperature such as *m*-cresol at 130 ºC [100], benzyl alcohol at 100 [101,102] or 130 ºC [103] and hexamethyphosphorotriamide at 85 ºC [104]. These conditions are not convenient enough. Moreover, PA may degrade under such conditions [105].

Schuttenberg and Schulz [99,106] developed a so-called *N*-trifluoroacetylation reaction for PA in order to get rid of the above problems. As shown in Figure 2.15, it consisted of reacting TFAA with hydrogen atoms of the amide groups of PA in dry CH_2Cl_2, leading to the corresponding *N*-trifluoroacetylated derivatives (PA-TFAA). The latter then became soluble in solvents suitable for SEC at room temperature, such as THF and CH_2Cl_2. The *N*-trifluoroacetylation reaction has been applied to many types of PA in order to use SEC or other techniques to determine their molar masses at room temperature [59,105,107,108].

In order to obtain the characterization of PS-g-PA6 by SEC, the above method must be extended to measurement of the molar mass of polyamide block/graft copolymers. It turned out that the extension was not trivial. Unlike a pure PA, the *N*-trifluoroacetylation reaction of PS-g-PA6 did not take place in dry CH_2Cl_2 alone because of the very poor solubility of PS-g-PA6. A co-solvent was thus needed to help dissolve the PS segments of PS-g-PA6. THF, toluene and chloroform, three common

good solvents of PS, were tested as co-solvents.

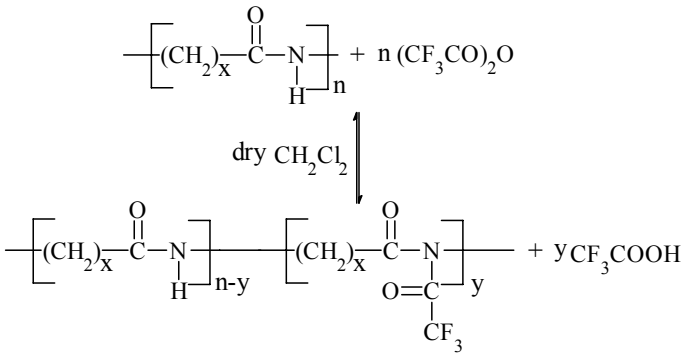


Figure 2.15 Schematic of the *N*-trifluoroacetylation reaction of polyamides with TFAA.

2.6.1 Choice of co-solvents for the *N*-trifluoracetylation reaction

Before the *N*-trifluoracetylation reaction, both the homo-PA6 (UBE Nylon Thailand Limited) and PS-g-PA6 (from E5) were in the form of pellets of about 1 mm in diameter. In the former case, the *N*-trifluoroacetylation reaction system (homo-PA6/CH_2Cl_2/TFAA = 0.05g/2ml/2ml) became homogeneous in about 2 h and the solution was clear and colourless. After 24 h of the *N*-trifluoroacetylation reaction, the *N*-trifluoroacetylated homo-PA6 was isolated and dried using a rotary evaporator at 30 ºC for subsequent SEC measurement.

Unlike the homo-PA6, the PS-g-PA6 was insoluble in the mixture of CH_2Cl_2 and TFAA (PS-g-PA6/CH_2Cl_2/TFAA = 0.1g/3ml/2ml). As a result, the *N*-trifluoracetylation reaction hardly occurred. In order to dissolve PS-g-PA6, a co-solvent capable of dissolving the PS segment was then used. THF, toluene and chloroform, three most common good solvents of PS, were tested as co-solvent candidates.

When THF was added to the PS-g-PA6/CH_2Cl_2/TFAA (0.1g/3ml/2ml) system, PS-g-PA6 became more soluble. PS-g-PA6 was completely dissolved in 4-6 h when the amount of THF was increased to 3 ml. It was also completely dissolved in approximately the same period of time when toluene or chloroform was used as a co-solvent and when the amount was above a threshold, say, 4 ml. The solutions were clear and slightly yellowish. After 24 h of the *N*-trifluoroacetylation reaction, the *N*-trifluoroacetylated PS-g-PA6 was isolated and dried under the same conditions as for the *N*-trifluoroacetylated homo-PA6 for subsequent SEC measurement. When chloroform was used as a co-solvent, the isolation and drying were easy. After 30 min

of the rotary evaporation, all liquid compounds were removed and the resulting polymer product was dry. This is easy to understand because CH_2Cl_2, TFAA, chloroform and trifluoroacetic acid (a product of the *N*-trifluoroacetylation reaction) were relatively volatile and their boiling points were about 40, 40, 61 and 72 ºC, respectively. The situation was different when toluene or THF was used as a co-solvent. After 30 min of the rotary evaporation, certain amounts of liquid compounds still remained in the rotary evaporator. The situation with toluene could be related to the fact that the boiling point of toluene is relatively high, 110 ºC. The situation with THF seemed to be surprising considering its low boiling point (66 ºC) and high volatility. Thus, it is likely that the liquid compounds that could not be removed by the rotary evaporation were not THF. Then what could they be?

It was suspected that the remaining liquid compounds resulted from chemical reactions between THF and TFAA. Unlike chloroform or toluene, when THF was added to the PS-g-PA6/CH_2Cl_2/TFAA (0.1g/3ml/2ml) *N*-trifluoroacetylation reaction system, the system became highly exothermic, implying chemical reactions occurring between THF and TFAA. The following experiment was done in order to check if chemical reactions did occur between them during the *N*-trifluoroacetylation reaction of PS-g-PA6. THF, toluene and chloroform were mixed with TFAA, respectively, and in the same proportions as those used for the *N*-trifluoroacetylation reaction of PS-g-PA6. When THF was mixed with TFAA, the system became highly exothermic. On the other hand, when toluene or chloroform was mixed with TFAA, the above-mentioned exothermic phenomenon did not occur. All these observations were similar to those observed with the PS-g-PA6/CH_2Cl_2/TFAA/co-solvent systems. 24 h later the above systems were subjected to the rotary evaporation under the same conditions as for the PS-g-PA6/CH_2Cl_2/TFAA/co-solvent *N*-trifluoroacetylation reaction systems. As expected, no liquid compounds were left for the mixture of chloroform and TFAA. Some residual liquid compounds were left for the mixture of toluene and TFAA and that of THF and TFAA.

Figure 2.16 shows the FTIR spectrum of the residual liquid compounds of the mixture of toluene and TFAA, and Figure 2.17 shows that of THF and TFAA. From Figure 2.16, the FTIR spectrum of the residual liquid compounds of the mixture of toluene and TFAA is the same as that of toluene, suggesting that the residual liquid was toluene that was not able to evaporate under the rotary evaporation conditions. On the other hand, the FTIR spectrum of the residual liquid compounds of the mixture of THF and TFAA matched neither that of THF nor that of TFAA (Figure 2.17). It was

more like a superposition of them, implying that the residual liquid compounds were likely a product of the reaction between THF and TFAA. This may be further confirmed by the fact that after 4 h of drying in a vacuum oven at 110 ºC, there were still residual liquid compounds left.

To sum up, the above results show that chloroform was a good co-solvent for the *N*-trifluoroacetylation reaction of the PS-g-PA6 and could easily be removed from the *N*-trifluoroacetylation reaction system by the rotary evaporation at 30 ºC. Toluene was also a good co-solvent for the *N*-trifluoroacetylation reaction of PS-g-PA6 but could not be removed easily by the rotary evaporation at 30 ºC because of its relatively high boiling point. THF was not a good co-solvent for the *N*-trifluoroacetylation reaction of PS-g-PA6 because it could chemically react with TFAA and the resulting products could not easily be removed by the rotary evaporation at 30 °C.

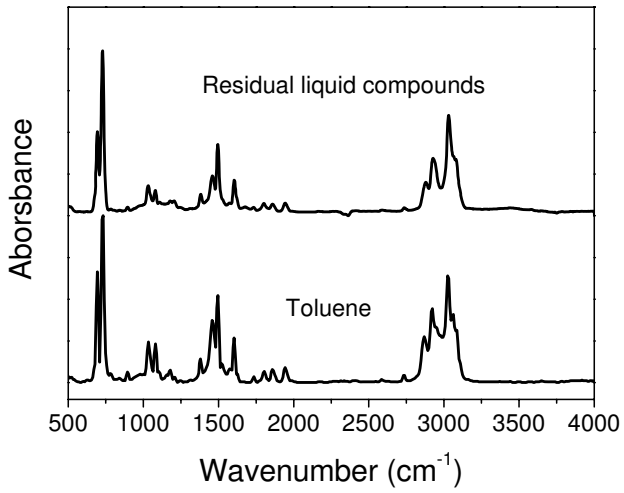


Figure 2.16 FTIR spectrum of the residual liquid compounds of a mixture of toluene/TFAA (8 ml/4 ml) after 30 min of rotary evaporation at 30 ºC. That of toluene is shown for comparison.

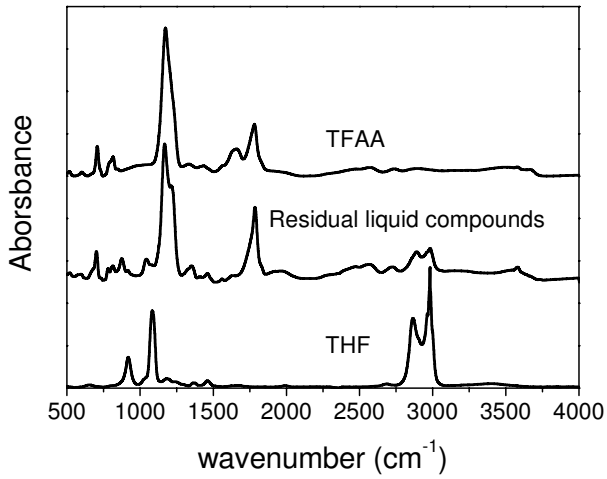


Figure 2.17 FTIR spectrum of the residual liquid compounds of a mixture of THF/TFAA (8 ml/4 ml) after 30 min of rotary evaporation at 30 ºC. Those of THF and TFAA alone are shown for comparison.

2.6.2 Characterization of the *N*-trifluoroacetylation reaction

In this section, reversibility, time and conversion of the *N*-trifluoroacetylation reaction will be addressed. One may wonder why the rotary evaporation was carried out at 30 ºC and not at a higher temperature. At a higher temperature toluene might be removed from the *N*-trifluoroacetylation reaction system as well. However, it was found that a temperature well above 30 ºC was prohibited because of the reversible nature of the *N*-trifluoroacetylation reaction. In fact, as temperature increased the *N*-trifluoroacetylation reaction would go back to the reactant side (see Figure 2.15). This will be shown below.

Note that the above *N*-trifluoroacetylated homo-PA6 and PS-g-PA6 obtained after the rotary evaporation at 30 °C were soluble in THF. However, when they were vacuum-dried at 80 °C for 2 h, they then became insoluble in THF. This is in line with the shift of the *N*-trifluoroacetylation reaction to the reactant side. Figure 2.18 compares the FTIR spectra of the homo-PA6 and the *N*-trifluoroacetylated homo-PA6 before and after the vacuum drying. Compared with the FTIR spectrum of the homo-PA6, that of the *N*-trifluoroacetylated homo-PA6 before the vacuum-drying exhibited two new intense peaks, one at 1719 cm^{-1} corresponding to  and another one at 1168 cm^{-1} corresponding to TFAA. This confirms that TFAA had reacted with the hydrogen atoms of the amide groups of the homo-PA6. After the vacuum drying, those two peaks disappeared and the corresponding FTIR spectrum was the same as that of the homo-PA6, implying that the *N*-trifluoroacetylation reaction had completely gone back to the reactant side during the vacuum-drying process. The *N*-trifluoroacetylated PS-g-PA6 behaved in a manner similar to that of the *N*-trifluoroacetylated homo-g-PA6 (see Figure 2.19).

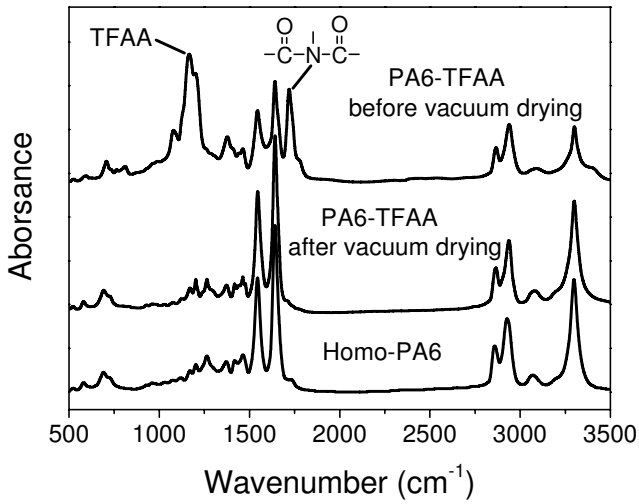


Figure 2.18 FTIR spectra of the homo-PA6 and the *N*-trifluoroacetylated homo-PA6 (PA6-TFAA) before and after the vacuum drying at 80 °C for 2 h.

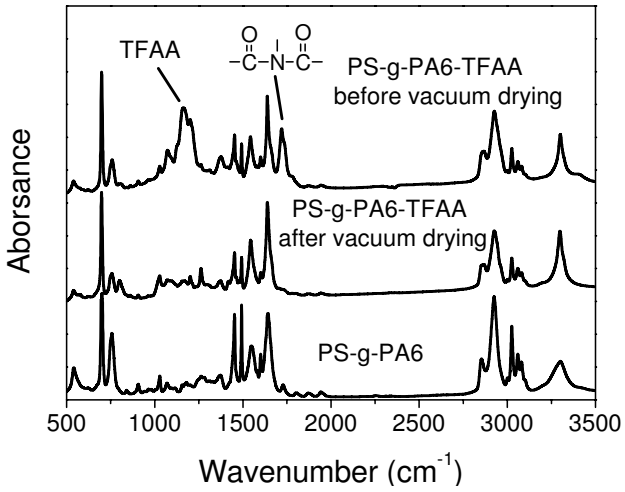


Figure 2.19 FTIR spectra of the PS-g-PA6 and the *N*-trifluoroacetylated PS-g-PA6 before and after the vacuum drying at 80 °C for 2 h.

In summary, the *N*-trifluoroacetylation reaction is a reversible one. Its equilibrium shifts to the reactant side upon increasing temperature. A good co-solvent for the *N*-trifluoroacetylation reaction should meet the following three criteria. First, it helps dissolve polyamide copolymers. Second, it is chemically inert. Third, it can easily be removed at a relatively low temperature (around room temperature). For PS-g-PA6, chloroform is a good co-solvent.

In all the above experiments, the time of the *N*-trifluoroacetylation reaction was 24 h. Was 24 h long enough for the *N*-trifluoroacetylation reaction to reach its equilibrium when chloroform was used as a solvent? In order to answer this question,

products obtained from the *N*-trifluoroacetylation reaction of PS-g-PA6 from E5 at two different times, 15 and 24 h, were analysed. Figure 2.20 compares the evolution of the mass fractions of the PA6 grafts and PS backbone of PS-g-PA6 as a function of the molar mass of PS-g-PA6 between those two *N*-trifluoroacetylated PS-g-PA6b products. Experimental and calculation methods of mass fraction of the PA6 grafts and PS backbone will be given in the subsequent sections. It shows that those two products yielded almost the same mass fractions of the PA6 grafts and PS backbone versus the molar mass of PS-g-PA6b, indicating that 15 or 24 h was long enough for the *N*-trifluoroacetylation reaction to reach its equilibrium.

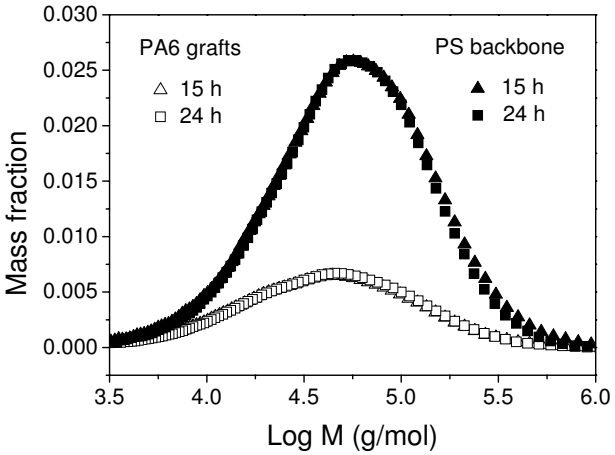


Figure 2.20 Mass fraction of the PS backbone and that of PA6 grafts and PS-g-PA6 from E5 after 15 or 24 h of *N*-trifluoroacetylation reaction using chloroform as a co-solvent as a function of the molar mass of PS-g-PA6b. Experimental and calculation methods will be given in the subsequent sections.

What were the conversions attained after 15 or 24 h of the *N*-trifluoroacetylation reaction? Based on Figure 2.15, the conversion of the *N*-trifluoroacetylation reaction may be defined as *y*/*n*, which was measured experimentally in the following manner. The product obtained after 15 or 24 h of the *N*-trifluoroacetylation reaction of PS-g-PA6b was first dried by the rotary evaporation at 30 ºC and then dried in an oven at 75 ºC in air for an hour in order to remove all solvents and other small molecules. The mass of the dried product was designated as M_1. The above dried product was then placed in a vacuum oven at 110 ºC for 4 h during which it would go back to pure PS-g-PA6. The corresponding mass was designated as M_2. The conversion of the *N*-trifluoroacetylation reaction could then calculated by the following equation:

$$\text{Conversion}\% = (M_1 - M_2)/[M_1 * \text{PA6}\% * (97-1)/113] \times 100 \qquad (2.5)$$

where ($M_1 - M_2$) is the gain in mass as a result of the *N*-trifluoroacetylation reaction,

PA6% is the percentage by mass of the PA6 grafts in the PS-g-PA6 and the coefficients 97 and 113 are the molar masses of the $OCCF_3$ moiety and CL, respectively. It was found that for PS-g-PA6, the conversions corresponding to 15 and 24 h of the *N*-trifluoroacetylation reaction under the specified conditions were 92 and 96%, respectively.

2.6.3 Measurement of the molar mass of PS-g-PA6 by SEC

After the *N*-trifluoroacetylation reaction, both the homo-PA6 and PS-g-PA6 became soluble in THF to be directly analyzed by SEC. Figure 2.21 shows the SEC traces of the *N*-trifluoroacetylated homo-PA6 and PS-g-PA6 from E12 using a refractive index detector (RI). Based on PS standards, the relative molar masses of the homo-PA6 and PS-g-PA6 from E12 are obtained and shown in Table 2.10.

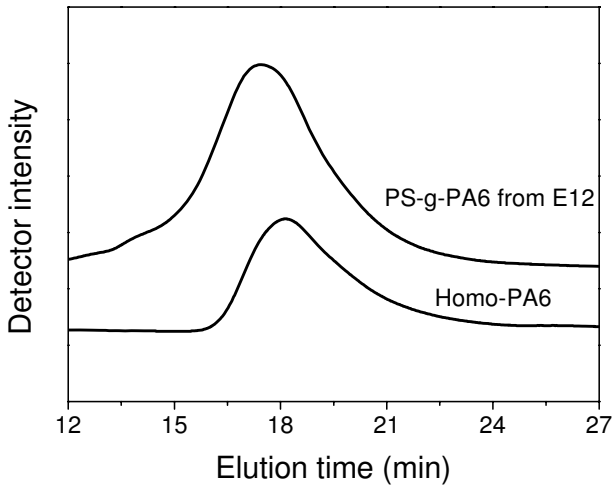


Figure 2.21 SEC traces of the homo-PA6 and PS-g-PA6 from E12 from the RI detector after *N*-trifluoroacetylation reaction using chloroform as a co-solvent.

Table 2.10 Molar masses of *N*-trifluoroacetylated homo-PA6 and PS-g-PA6 from E12 by SEC using a RI detector and based on the PS standards.

Sample	Mn (kg/mol)	Mw (kg/mol)	Polydispersity
Homo-PA6	29.5	54.4	1.8
PS-g-PA6 from E12	47.1	124.2	2.6

It should be noted that the molar mass values in Table 2.10 are not absolute ones but relative to the PS standards. Thus, in the case of a PS-g-PA6 graft copolymer they neither provide any information on the molar mass of the PS backbone nor that of each of the PA6 grafts. The molar mass of the PS backbone could be considered as

being equal to that of PS-co-TMI if it has not undergone any change in molar mass during the synthesis process of the PS-g-PA6. However, the molar mass of each of the PA6 grafts needs to be determined.

In addition to a RI detector, the use of a UV detector can also measure the relative molar masses of the *N*-trifluoroacetylated homo-PA6 and PS-g-PA6 because they are UV sensitive. Figure 2.22 shows the UV-absorption spectra of the PS-co-TMI, PA6-TFAA and PS-g-PA6-TFAA as a function of the wavelength. It is seen that the three products showed strong UV-absorption below 300 nm, confirming that SEC coupled with a UV detector is also expected to be able to measure the relative molar masses of the homo-PA6 and PS-g-PA6.

Figure 2.23 shows the SEC traces of the *N*-trifluoroacetylated homo-PA6 and PS-g-PA6c based on UV detection at 238 (UV-238) and 260 nm (UV-260). It is noted that for both polymers the detector signal at 238 nm was much stronger than that at 260 nm, as expected. Table 2.11 shows the molar masses calculated from the SEC curves in Figure 2.23. The molar masses of the homo-PA6 did not depend on the UV wavelength, whereas that of PS-g-PA6 from E12 did. This is because the homo-PA6 was a homopolymer and the PS-g-PA6 from E12 was a graft copolymer composed of a PS backbone and PA6 grafts. The molar mass of the PS-g-PA6 would not depend on the UV wavelength only if the mass ratio between PS and PA6 did not depend on the molar mass of PS-g-PA6. Inspection of Table 2.10 and Table 2.11 shows that for both the homo-PA6 and PS-g-PA6 from E12, the molar masses obtained from the RI detection were higher than those obtained from the UV detection. No explanations are available so far and are out of the scope of this work.

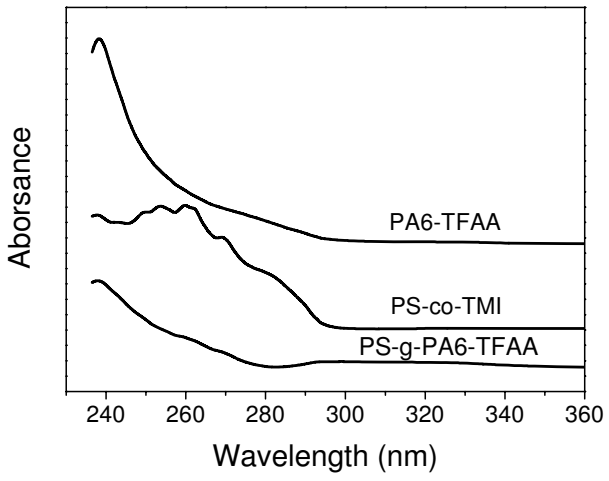


Figure 2.22 UV spectra of the PS-co-TMI, PA6-TFAA, PS-g-PA6-TFAA solutions in THF. The mass concentrations are 0.2, 0.05 and 0.04 mg/ml in the PS-co-TMI, homo-PA6 and PS-g-PA6,

respectively.

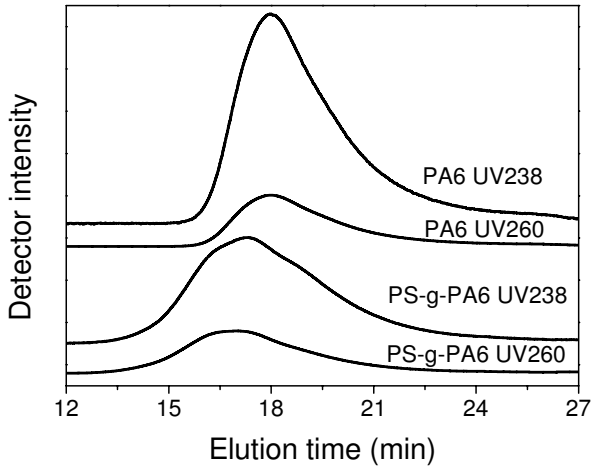


Figure 2.23 SEC traces of the *N*-trifluoroacetylated homo-PA6 and PS-g-PA6 from E12 from UV detection at 238 and 260 nm.

Table 2.11 Molar masses of the *N*-trifluoroacetylated homo-PA6 and PS-g-PA6 from E12 calculated from the UV detection at 238 and 260 nm and based on the PS standards.

Sample	Mn (kg/mol)		Mw (kg/mol)		Polydispersity	
	UV-238	UV-260	UV-238	UV-260	UV-238	UV-260
Homo-PA6	19.4	19.2	49.9	50.5	2.6	2.6
PS-g-PA6 from E12	28.1	33.9	110.8	124.0	3.9	3.7

Figure 2.24 shows the SEC traces of the PS-g-PA6 from E5 after *N*-trifluoroacetylation using THF as a co-solvent instead of chloroform. There are two main peaks on each of the SEC traces. The first one corresponds to the PS-g-PA6-TFAA and the second one to the THF-TFAA, a by-product that was formed between THF and TFAA and was unable to be removed by rotary evaporation at 30°C, as discussed in a preceding section. This is another indication that THF is not an appropriate co-solvent for the *N*-trifluoroacetylation reaction of the homo-PA6 or PS-g-PA6. Moreover, it was found that the THF-TFAA resulted in corrosion of the SEC column. Besides, the THF solution of the PS-g-PA6-TFAA or PA6-TFAA had to be freshly prepared prior to the SEC analysis because they could otherwise form gel in a few hours, as also pointed out by other authors [59,99].

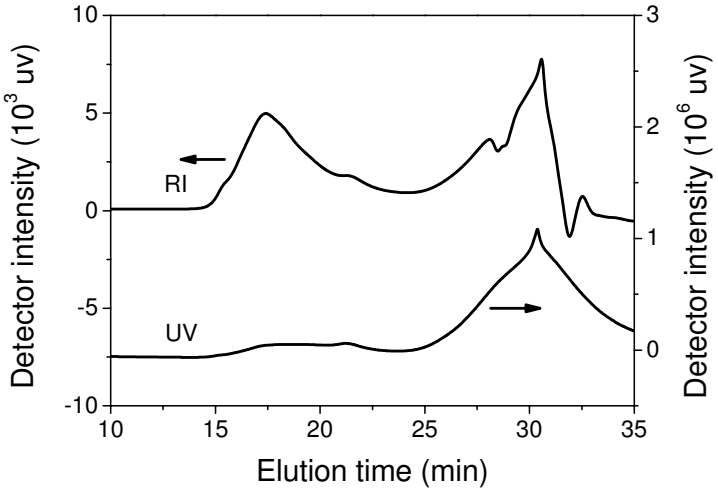


Figure 2.24 SEC traces of the *N*-trifluoroacetylated PS-g-PA6 from E5 detected by RI and UV-254 detectors. The *N*-trifluoroacetylation reaction was carried out with the use of THF as a co-solvent.

2.6.4 SEC measurement of the composition of PS-g-PA6

According to Figure 2.22, the *N*-trifluoroacetylated PS-g-PA6 and PS differ in UV absorbance over a relatively wide range of UV wavelength. Thus, it is expected that the use of a UV detector with a dual wavelength would allow determining quantitatively the mass fractions of the PS backbone and PA6 grafts of a PS-g-PA6 graft copolymer. In this work, the dual UV wavelengths chosen were 238 and 260 nm. Figure 2.25 shows the UV absorbance at 238 nm of PS-g-PA6 from E11 as a function of the elution time. The shaded area represents the integrated UV absorbance of PS-g-PA6. Figure 2.26 shows the integrated area of the PS-co-TMI and PA6 as a function of their concentration for the UV detection at two wavelengths: 238 and 260 nm. Based on the results, the following linear relationships are obtained:

$$Area_{PS-co-TMI-238} = 0.038 * 10^6 C_{PS-co-TMI} \tag{2.6}$$

$$Area_{PS-co-TMI-260} = 0.093 * 10^6 C_{PS-co-TMI} \tag{2.7}$$

$$Area_{PA6-260} = 0.25 * 10^6 C_{PA6} \tag{2.8}$$

$$Area_{PA6-238} = 1.05 * 10^6 C_{PA6} \tag{2.9}$$

where $Area_{PA6-238}$ and $Area_{PS-co-TMI-238}$ in uv·min are the integrated areas of the *N*-trifluoroacetylated homo-PA6 and PS-co-TMI at the UV wavelength of 238 nm, respectively; and $Area_{PA6-260}$ and $Area_{PS-co-TMI-260}$ in uv·min are their integrated areas at the UV wavelength of 260 nm, respectively. C_{PA6} and $C_{PS-co-TMI}$ in mg/ml are the

concentrations of the homo-PA6 and PS-co-TMI, respectively.

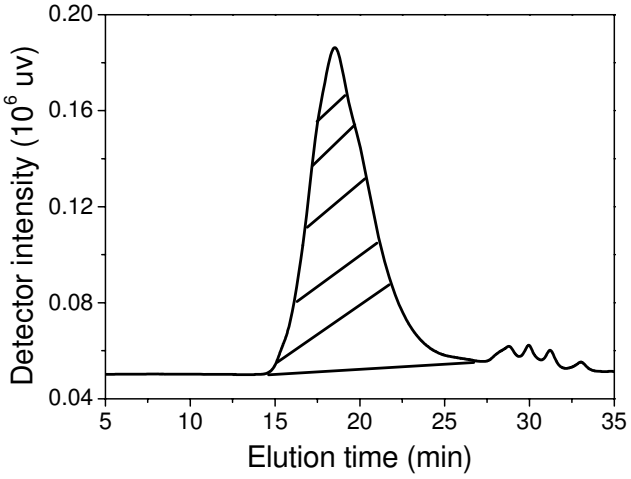


Figure 2.25 SEC trace of the *N*-trifluoroacetylated PS-g-PA6 from E11 corresponding to the UV detection at 238 nm. The shaded area represents the integrated UV absorbance.

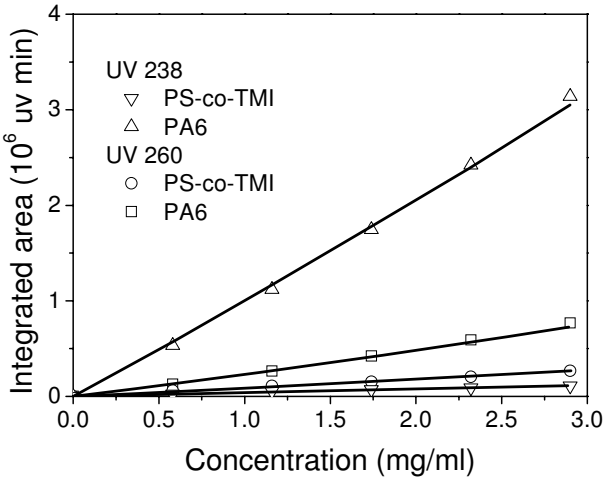


Figure 2.26 Integrated areas of the SEC traces of the PS-co-TMI or the N-trifluoroacetylated PA6 as a function of the polymer (PS-co-TMI or homo-PA6) concentration for the UV detection at two different wavelengths: 238 and 260 nm.

For a PS-g-PA6 graft copolymer, the mass fraction of the PA6 grafts is designated as *w*. That of the PS backbone is then (1-*w*). If SEC with a dual UV detection at 238 and 260 nm is used to analyze the PS-g-PA6 graft copolymer, Eqs. (2.10) and (2.11) can then express the integrated areas of the PS-g-PA6 at 238 and 260 nm as a function of the PS-g-PA6 concentration:

$$Area_{PS-g-PA6-UV\,238} = 1.05*10^6\, wC_{PS-g-PA6} + 0.038*10^6 (1-w) C_{PS-g-PA6} \qquad (2.10)$$

$$Area_{PS-g-PA6-UV\,260} = 0.25*10^6\, wC_{PS-g-PA6} + 0.093*10^6 (1-w) C_{PS-g-PA6} \qquad (2.11)$$

If the PS-g-PA6 concentration is known accurately, the PA6 mass fraction can be

calculated from Eq. (2.10) or (2.11). Otherwise, it can be calculated by solving Eqs. (2.10) and (2.11) simultaneously.

Table 2.12 shows the mass fractions of the PA6 grafts of PS-g-PA6 from E11 and from E12 obtained by SEC. The pertinence of the SEC for determining the composition of the PS-g-PA6 was confirmed by the elemental analysis based on the nitrogen content in purified PS-g-PA6. The PA6 content in PS-g-PA6 was calculated by the following equation:

$$PA6\% = \frac{N_4 - N_5 * N_6}{0.12} * 100\% \quad (2.12)$$

where N_4 is the nitrogen content in PS-g-PA6; N_5 is the initial PS-co-TMI content in the polymerizing system (%); N_6 is the nitrogen content in PS-co-TMI; 0.12 is the nitrogen content in CL. Both SEC and elemental led to similar results, supporting that SEC is indeed a reliable method for determining the mass fractions of the PS backbone and PA6 grafts of a PS-g-PA6 graft copolymer. Moreover, the concentrations of the PS-g-PA6a and PS-g-PA6c obtained by solving Eqs. (2.10) and (2.11) are 2.9 and 3.0 mg/ml, respectively. They are in excellent agreement with the real concentrations (3.0 mg/ml).

Table 2.12 Mass fractions of the PS backbone and PA6 grafts of PS-g-PA6 graft copolymers obtained by SEC and selective extraction.

Experimental designation	PA6 mass fraction	
	SEC	Elemental
PS-g-PA6 from E11	0.20	0.15
PS-g-PA6 from E12	0.44	0.43

Recall that the integrated areas in Eqs. (2.10) and (2.11) are products of the UV absorbance and elution time. Eqs. (2.10) and (2.11) can be rewritten as the integrated areas of the SEC curves corresponding to 238 and 260 nm, designated as $Area_{PS\text{-}g\text{-}PA6\text{-}UV238}$ and $Area_{PS\text{-}g\text{-}PA6\text{-}UV260}$ (uv·min), respectively, as a function of the grafts PA6 concentration (C_{PA6}, mg/ml) and the backbone PS concentration (C_{PS}, mg/ml):

$$Area_{PS-g-PA6-UV\,238} = 1.05 * 10^6 C_{PA6} + 0.038 * 10^6 C_{PS} \quad (2.13)$$

$$Area_{PS-g-PA6-UV\,260} = 0.25 * 10^6 C_{PA6} + 0.093 * 10^6 C_{PS} \quad (2.14)$$

Differentiation of Eqs. (2.13) and (2.14) with regard to the elution time t yields Eqs.(2.15) and (2.16), respectively:

$$\frac{dArea_{PS-g-PA6-UV\,238}}{dt} = 1.05*10^6 \frac{dC_{PA6}}{dt} + 0.038*10^6 \frac{dC_{PS}}{dt} \quad (2.15)$$

$$\frac{dArea_{PS-g-PA6-UV\,260}}{dt} = 0.25*10^6 \frac{dC_{PA6}}{dt} + 0.093*10^6 \frac{dC_{PS}}{dt} \quad (2.16)$$

Integration of the above two equations from t to $t+dt$ yields:

$$Area_{PS-g-PA6-UV\,238}\Big|_t^{t+dt} = 1.05*10^6 C_{PA6}\Big|_t^{t+dt} + 0.038*10^6 C_{PS}\Big|_t^{t+dt} \quad (2.17)$$

$$Area_{PS-g-PA6-UV\,260}\Big|_t^{t+dt} = 0.25*10^6 C_{PA6}\Big|_t^{t+dt} + 0.093*10^6 C_{PS}\Big|_t^{t+dt} \quad (2.18)$$

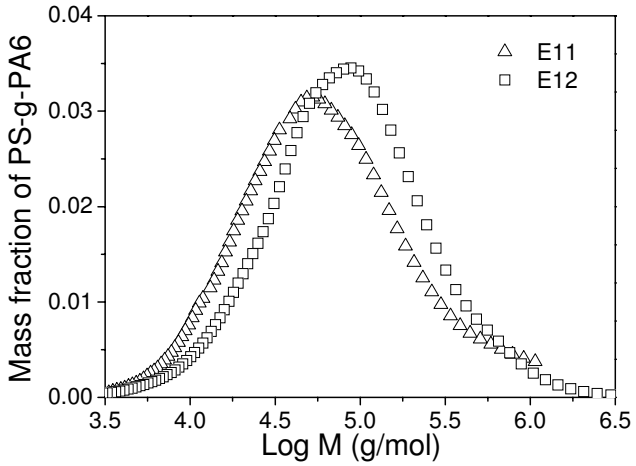
If w is designated as the mass fraction of the PA6 grafts between t and $t+dt$, then that of the PS backbone is (1-w). Then the above two equations can be rewritten as:

$$Area_{PS-g-PA6-UV\,238}\Big|_t^{t+dt} = 1.05*10^6 wC_{PS-g-PA6}\Big|_t^{t+dt} + 0.038*10^6 (1-w)C_{PS-g-PA6}\Big|_t^{t+dt} \quad (2.19)$$

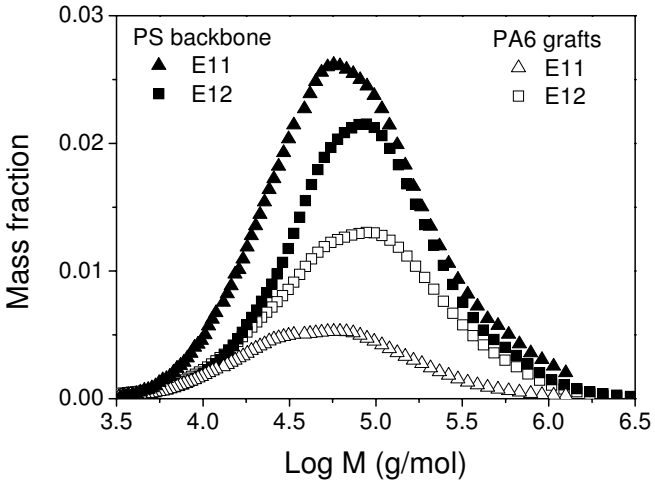
$$Area_{PS-g-PA6-UV\,260}\Big|_t^{t+dt} = 0.25*10^6 wC_{PS-g-PA6}\Big|_t^{t+dt} + 0.093*10^6 (1-w)C_{PS-g-PA6}\Big|_t^{t+dt} \quad (2.20)$$

in which, $C_{PS\text{-}g\text{-}PA6}$ (mg/ml) is the concentration of the PS-g-PA6 graft copolymer. The values of $Area_{PS-g-PA6-UV\,238}\Big|_t^{t+dt}$ and $Area_{PS-g-PA6-UV\,260}\Big|_t^{t+dt}$ can be obtained from the SEC curves at 238 and 260 nm, respectively. Thus, Eqs. (2.19) and (2.20) allow calculating w and the increment of the PS-g-PA6 concentration ($C_{PS-g-PA6}\Big|_t^{t+dt}$) between t and $t+dt$. Since the elution time corresponds to the molar mass of PS-g-PA6, the mass fractions of the PS backbone and PA6 grafts as a function of the molar mass of PS-g-PA6 can be obtained.

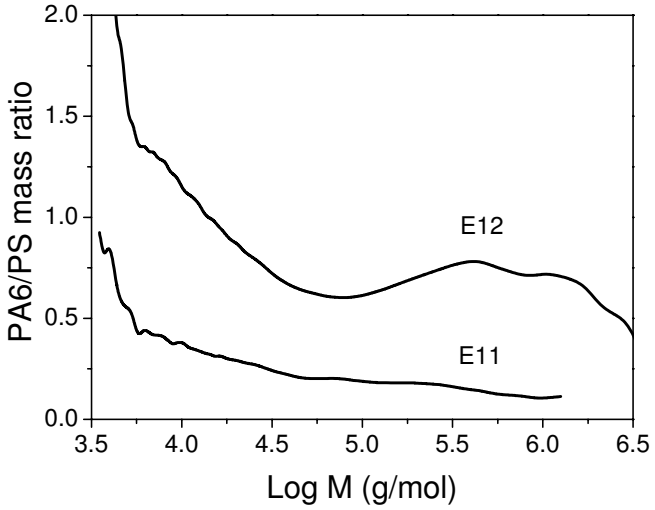
Figure 2.27a shows the mass fractions of PS-g-PA6 from E11 and E12 as a function of their respective molar masses. Figure 2.27b shows the mass fractions of the PS backbone and PA6 grafts of PS-g-PA6 from E11 and E12 as a function of their respective molar masses. It is seen from Figure 2.27b that the mass fraction of the PS backbone in PS-g-PA6 from E11 is higher than that of PS-g-PA6 from E12, and that of the PA6 grafts follows an opposite trend. This is expected because PS-g-PA6 from E11 and PS-g-PA6 from E12 are obtained from PS-co-TMI/CL = 42/18 and 18/42 by mass, respectively. Figure 2.27c shows the PS backbone/PA6 grafts mass ratio of as a function of the molar mass for PS-g-PA6 from E12 and E13 based on the results in Figure 2.27b. It is noted that, overall, the PS backbone/PA6 grafts mass ratio first decreases rapidly with increasing molar mass and then levels off with a further increase in the molar mass. This is true for both PS-g-PA6 graft copolymers. Detailed discussion will be found in a forthcoming sections..



(a)



(b)



(c)

Figure 2.27 Mass fractions of PS-g-PA6 from E11 and E12 (a), those of the PS backbone and PA6 grafts (b) and PS backbone/PA6 grafts mass ratios (c) as a function of the molar masses of

PS-g-PA6.

2.6.5 Summary

An SEC procedure was developed to measure the molar mass of polyamide block/graft copolymers and, more specifically, graft copolymers of PS and PA6 with PS as the backbone and PA6 as grafts. This procedure is an extension of one for PA. It consists of reacting TFAA with hydrogen atoms of the amide groups of PA in a mixture of dry CH_2Cl_2 and another solvent (co-solvent) that is capable of dissolving PS. Three co-solvents were tested: THF, toluene and chloroform, three common good solvents of PS. Results show that only chloroform is suitable for the *N*-trifluoroacetylation reaction of PS-g-PA6. THF reacts with TFAA. The boiling point of toluene is so high that it cannot be removed from the copolymer under vacuum at room temperature. A significantly higher temperature is forbidden because of the reversible nature of the *N*-trifluoroacetylation reaction. The use of UV detectors at different wavelengths, say 238 and 260 nm, allows determining both the molar mass and composition of PS-g-PA6.

2.7 PS-co-TMI characterization

The synthesis of PS-co-TMI is very important to control the structure of PS-g-PA6. On the one hand, PS-co-TMI is as the backbone of graft copolymer, which allows the control of the main chain parameters (such as molar mass); on the other hand, PS-co-TMI is as macro-initiator, which allows the control of the sites, number and distribution of active, and thus determines the graft sites and the graft density.

2.7.1 Molar mass

The molar mass of PS-co-TMI is measured by SEC using PS standards for the calibration and THF as the eluent. Table 2.13 shows the molar masses of the resulting PS-co-TMI. The synthesis conditions of PS-co-TMI see Table 2.1. From Table 2.1 and Table 2.13, it can be seen that both the increase of polymerization temperature and BPO concentration can decrease the molar mass. Therefore, it allows controlling the molar mass of PS-co-TMI by temperature and BPO concentration.

Table 2.13 The molar mass and TMI content of as-synthesized PS-co-TMI.

PS-co-TMI	*Mn*(kg/mol)	TMI content in PS-co-TMI (wt.%)
PS-co-TMI1	36.9	1
PS-co-TMI2	34.7	2
PS-co-TMI4	33.3	4
PS-co-TMI6	34.6	6
PS-co-TMI8	39.4	8
PS-co-TMI4L	19.6	4
PS-co-TMI4H	42.7	4

2.7.2 TMI content and distribution in PS-co-TMI

Figure 2.28 shows the infrared spectra of five PS-co-TMI. It was characterized by a peak at 2255 cm^{-1} corresponding to the isocyanate group of TMI and another one at 1944 cm^{-1} corresponding to St. The TMI contents in PS-co-TMI, which were calculated based on the infrared spectra according to a method reported in the literature [109], as shown in Table 2.13. From Table 2.1 and Table 2.13, it can be seen that TMI contents in PS-co-TMI4, PS-co-TMI4L and PS-co-TMI4H are uniform, which indicates that TMI content in PS-co-TMI has nothing with temperature and BPO concentration. Wu et al. [89] also has showed that the content of TMI in PS-co-TMI is independent of the reaction temperature. In addition, comparing PS-co-TMI1, PS-co-TMI2, PS-co-TMI4, PS-co-TMI6 and PS-co-TMI8, they are the same as molar mass but different in the TMI content, more specify, St/TMI ratio determines the TMI content in PS-co-TMI and has no effect on the molar mass of PS-co-TMI. These results suggest that two PS-co-TMI groups with different styles can be synthesized easily. One is with similar TMI content and different molar mass; the other is with different TMI content and similar molar mass. The former can be achieved by changing the polymerization temperature or BPO concentration in the condition of fixing St/TMI mass ratio (see PS-co-TMI4, PS-co-TMI4L, PS-co-TMI4H); the latter can be achieved by changing the St/TMI mass ratio in the condition of fixing temperature and BPO concentration (see PS-co-TMI1, PS-co-TMI2, PS-co-TMI4, PS-co-TMI6 and PS-co-TMI8).

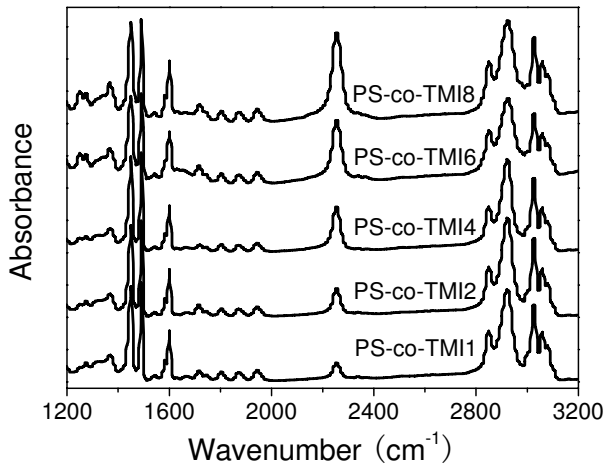


Figure 2.28 FTIR spectra of PS-co-TMI1, PS-co-TMI2, PS-co-TMI4, PS-co-TMI6 and PS-co-TMI8.

In the process of preparation of PS-g-PA6, the isocyanate moieties in PS-co-TMI initiate the polymerization of CL and more importantly, one isocyanate moiety will form one graft chain. Therefore, if all the isocyanate moieties in the PS-co-TMI participate in the activation of the polymerization of CL, the number of the PA6 grafts per PS chain was equal to that of the isocyanate moieties per PS-co-TMI chain. This will be discussed in detail in following sections. In addition, the graft chain distribution in backbone is also determined by the distribution of isocyanate distribution in PS-co-TMI chain. How do isocyanate distribute in PS-co-TMI chain? Is the number of iscoyanate moieties in a PS-co-TMI chain proportional to its chain length? To confirm this point, the isocyanate moieties of PS-co-TMI4 are reacted with an excess of 9-(methylamino-methyl)anthracene (MAMA) to form the corresponding PS-co-TMI-MAMA [87,110,111]. This is shown in Figure 2.29. Figure 2.30 shows the SEC traces of the PS-co-TMI-MAMA obtained with a dual UV detector at 254 and 367 nm. The former wavelength detects the PS while the latter one MAMA. The fact that both curves superimpose well indicates that the number of the isocyanate moieties in a PS-co-TMI is indeed proportional to its chain length.

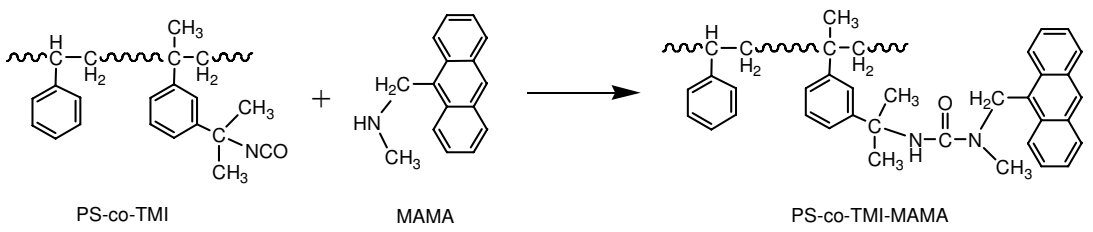


Figure 2.29 Schematic of the reaction of PS-co-TMI with MAMA.

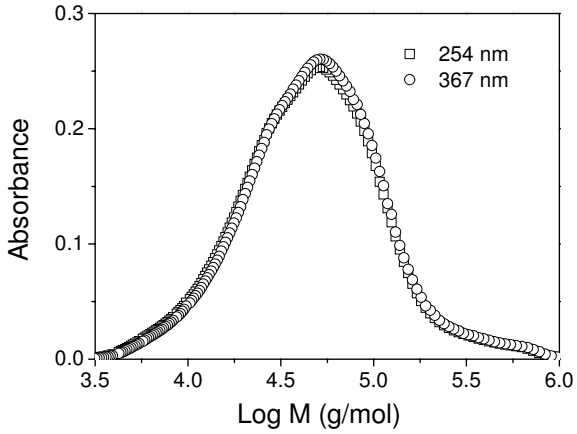


Figure 2.30 SEC traces of the PS-co-TMI-MAMA using a dual UV detector at 254 and 367 nm as a function of its molar mass.

2.8 Evaluation of as-synthesized graft copolymer

2.8.1 Composition of as-polymerized products

After the polymerization, a PS-co-TMI/CL/Cat system might be composed of the following components: pure PS-g-PA6 graft copolymer, Homo-PA6, un-reacted PS-co-TMI, un-reacted CL and possibly low molar mass derivatives of CL. Table 2.14 shows the mass percentages of the various fractions of four as-polymerized products obtained by successive extraction in various solvents according to the procedure outlined in Figure 2.5. Each extraction was repeated and the results showed good reproducibility.

From Table 2.14, both the TMI content in the PS-co-TMI and the composition of the PS-co-TMI/CL/Cat system strongly affect the composition of the as-polymerized product. An example is the fraction of the pure PS-g-PA6 graft copolymer, which corresponds to that of the as-polymerized product insoluble neither in methanol, THF nor formic acid. When the TMI content in PS-co-TMI is 1 wt.%, the fraction of the pure PS-g-PA6 is only about 18 wt.% (see E7). When it is 4 wt.%, the fraction of the pure PS-g-PA6 is increased to more than 50 wt.% (see E11, E5 and E12). Moreover, for a given TMI content, say 4.0 wt.%, the higher the PS-co-TMI/CL mass ratio, the higher the fraction of the pure PS-g-PA6 graft copolymer in the as-polymerized product.

Table 2.14 Mass percentages of the various fractions of four as-polymerized products obtained according to the procedure in Figure 2.5.

Experimental designation	E7		E11		E5		E12	
CL conversion, %	84.2	83.5	93.4	93.2	91.0	90.6	87.8	86.8
Fraction soluble in methanol (solution A), %	8.0	8.6	2.2	2.3	4.7	4.9	8.7	9.4
Fraction soluble in THF (residue D), %	33.0	35.2	13.6	14.3	9.3	8.6	6.6	6.0
Fraction soluble in formic acid (residue H), %	40.6	39.2	9.3	7.9	26.7	25.2	33.8	29.8
Fraction insoluble in methanol, THF and Formic acid (solute F), %	18.4	17.0	74.9	75.5	59.3	61.3	50.9	54.8

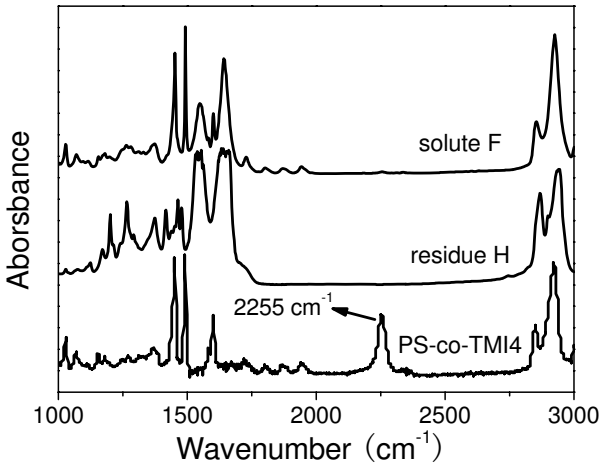


Figure 2.31 FTIR spectra of PS-co-TMI4, residue H and solute F. The latter two are from the polymerized product of E5.

It is worthy noting that the mass percentages of the products soluble in THF (residue D) and formic acid (residue H) are high. What is their chemical nature? The foregoing results have shown that the residue soluble in THF does not contain PS-co-TMI but PS-g-PA6 with very short PA6 grafts. Figure 2.31 compares the FTIR spectra among PS-co-TMI4, residue H and solute F from E5. From Figure 2.31, the FTIR spectrum of residue H does not have a peak at 1944 cm^{-1} characteristic of PS nor a peak at 2255 cm^{-1} characteristic of TMI but a peak at 1641 cm^{-1} characteristic of PA6. This indicates that residue H is most likely composed of pure homo-PA6 only and does not contain any PS-g-PA6. The FTIR spectrum of solute F exhibits both a

peak at 1944 cm^{-1} characteristic of PS and a peak at 1641 cm^{-1} characteristic of PA6. This further supports the fact that solute F is a pure PS-g-PA6 graft copolymer. It is also noted that none of the FTIR spectra of solute F and residue H has a peak at 2255 cm^{-1} characteristic of TMI, implying that none of them contains isocyanate moieties.

Does the fact that no single isocyanate moiety of PS-co-TMI has remained intact after the polymerization necessarily mean that all isocyanate moieties have participated in the activation of the polymerization of CL? One might argue that during the extraction in methanol, isocyanate moieties might have reacted with methanol. Figure 2.32 shows the FTIR spectra of PS-co-TMI4 and the insoluble product of PS-co-TMI4 after extraction in methanol under reflux for 1 h. These two FTIR spectra are similar in shape. Nevertheless, the ratios of the peak height between 2255 and 1944 cm^{-1} are slightly different. Based on these ratios, one can calculate the corresponding TMI contents. The TMI contents in PS-co-TMI4 before and after extraction in methanol are 4.0 and 3.5 wt.%, respectively. This indicates that methanol have reacted with isocyanate moieties but only to a relatively small extent under the specified conditions. Therefore, it is very likely that all isocyanate moieties have participated in the activation of the polymerization of CL. This is further confirmed by the FTIR spectrum of the as-polymerized product of E5 without any extraction, which does not have a peak at 2255 cm^{-1} characteristic of isocyanate moieties.

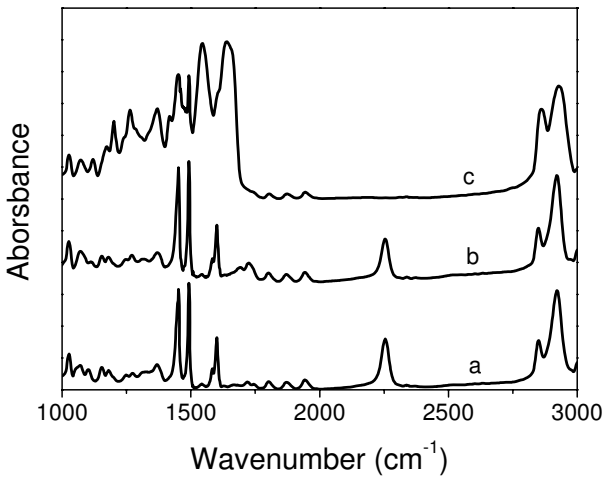


Figure 2.32 FTIR spectra of PS-co-TMI4 (a), the insoluble product of PS-co-TMI4 after extraction in methanol under reflux for 1 h (b) and the as-polymerized product from E5 without any extraction (c).

To sum up, the above results show that all isocyanate moieties of PS-co-TMI

have participated in the activation of the polymerization of CL, which indicates that the number and sites of iscocyanate moieties in PS-co-TMI indeed determine the graft number and density. In addition, the resulting as-polymerized product is very likely composed of a PS-g-PA6 graft copolymer, homo-PA6 and un-reacted CL.

It is worthy noted that the mass percentages of homo-PA6 soluble in formic acid are high obviously. Where is it come from? This may be answered from three aspects: (1) side reactions in the process of CL polymerization; (2) the degradation of PA6 graft chain in the process of formic acid extraction; (3) the degradation of PA6 graft chain in the polymerisation process due to the high temperature and high shear. Now the first reason is checked and other reasons will be discussed in following chapter.

The high rate of activated anionic polymerization is due to the fact that both reacting species are chemically activated and hence highly reactive: the lactam anion from the catalyst represents an activated monomer with increased nucleophilicity and then terminal *N*-acylated lactam unit from the activator presents an activated end group (growth centre) with increased acylating ability. However, in fact, an essential condition for starting the anionic polymerization of CL is the presence of an anionically activated monomer, i.e. ε-caprolacram anion, most often in the form of an alkaline salt. Some authors [112,113] had reported the catalyst itself may produce *N*-acylated lactam and thus initiate an anionic polymerization of lactam even without the addition of growth centres. Does this mean that the process mentioned above can result in the formation of Homo-PA6 in the process of PS-g-PA6 synthesis? In order to check up this point, a mixture of CL/Cat without PS-co-TMI was mixed in the Haake torque rheometer at 230 ºC. And then the raw product (about 2 g) was extracted by methanol or water under reflux for 8 h, finally filtrated and dried in the vacuum oven at 80 °C for 24 h. Table 2.15 shows the selected information on the experimental trials for CL/Cat mixing.

Table 2.15 Selected information on the experimental trials for CL/Cat mixing and the CL conversion

Ex. No.	CL/Cat (g/g)	Mixing time (min)	Screw speed (rpm)	CL conversion (%)	
				water	methanol
1	100/10	10	65	2.8	2.1
2	100/10	20	65	3.1	2.6
3	100/10	30	65	2.3	2.4
4	100/10	60	65	3.3	2.9
5	100/20	30	65	24.5	23.1

The FTIR spectra of the insoluble materials after methanol extraction from Ex.4 and Ex.5 are similar with Homo-PA6, as shown in Figure 2.33. This indicates that the insoluble material is Homo-PA6. The heating behaviors of insoluble materials are also shown in Figure 2.34. From Figure 2.34, it may be seen that the insoluble materials have the melting and crystallization peak corresponding to PA6, which further confirms that the insoluble material is Homo-PA6. The difference of peak position and area for these two residues perhaps results from the difference of the molar mass.

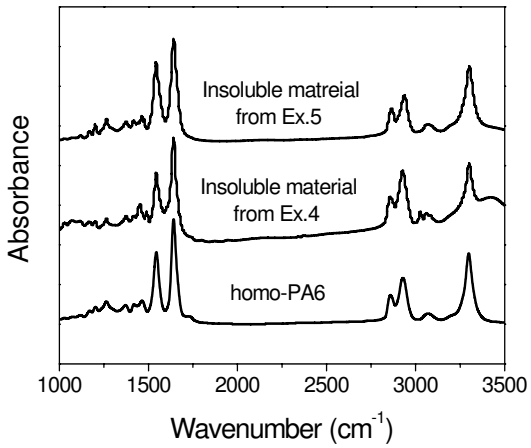


Figure 2.33 FTIR spectra of the insoluble material from Ex.4 and Ex.5 by methanol extraction and homo-PA6.

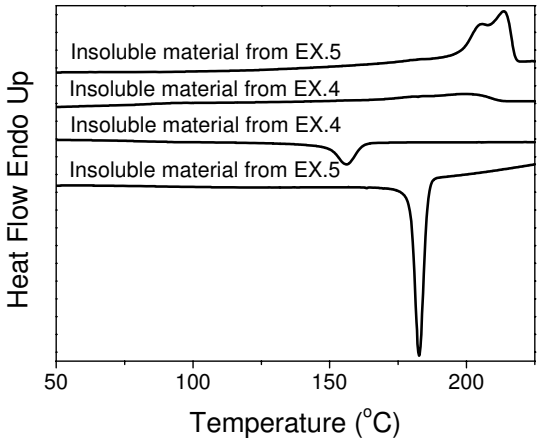


Figure 2.34 DSC thermograms of the insoluble material in methanol from EX.4 and EX.5 by methanol extraction. They were heated from 50 to 250 ºC at 10 ºC/min and maintained at 250 ºC for 2 min to erase their previous thermal history, and then cooled to 50 ºC at 10 ºC/min (recrystallization), finally heated up again to 250 ºC at 10 ºC/min (melting).

According to the mass before and after methanol or water extraction, CL conversion can be calculated, as shown in Table 2.15. From Table 2.15, it can be seen that for fixing CL/Cat ratio, CL conversion has almost not changed with the time

increasing in the range of researched mixing time, which indicates that the CL polymerization has reached balance in 10 min. In addition, for CL/Cat (100/10) system, the CL conversion is very low, but for CL/Cat (100/20), the CL conversion is overpass 20%, which indicates that the CL polymerization occurs easily with the higher Cat concentration.

The above results indicate that CL can polymerize in the presence of Cat without activator. However, for the researched polymerization systems in our work, the ratio of CL/Cat (100/10) is low so that the degree of CL converting into homo-PA6 is low. Therefore, it may be not the main factor for the contribution of homo-PA6 in the process of PS-g-PA6 synthesis.

In addition, some other reactions also can lead to the cleavage of polymer chains or the degradation of the polymer. For example, Havlice et al. [113] found that the viscosity-average degree of polymerization is first linear increase with polymer yield and then decrease after reaching a maximum value at about 80% polymer yield, which is an evidence of the participation of base-catalyzed in degradation reactions leading to the cleavage of polymer chains. Therefore, it is possible that some side reactions results in the cleavage of PA6 graft chains. However, the process is very complicated and it will not be discussed in detail.

2.8.2 Composition of pure PS-g-PA6

The composition of a pure PS-g-PA6 can be determined by the successive extractions of the as-polymerized product in methanol and formic acid. For example, Eq. (2.21) allows calculating the mass fraction of the PA6 grafts in PS-g-PA6:

$$PA6\% = \frac{W_1(W_{CL,0} + W_{cat,0} * 97.4\%) / W - W_5 - W_6}{W_1 - W_5 - W_6} * 100\% \qquad (2.21)$$

in which, W_5 (g) is the mass of the fraction that is soluble in methanol, and W_6 (g) is the mass of the fraction that is soluble in formic acid.

The molar mass of the pure PS-g-PA6 graft copolymer can be estimated based on the composition of the corresponding as-polymerized product and the fact that the number of the PA6 grafts in a PS-g-PA6 graft copolymer chain is equal to that of the isocyanate moieties in the corresponding PS-co-TMI chain because all isocyanate moieties of PS-co-TMI have participated in the activation of the anionic polymerization of CL. Thus the molar mass (*Mn*) of a PA6 graft can be obtained from Eq. (2.22).

$$M_n = \frac{w/(1-w)}{TMI\% / 201} \qquad (2.22)$$

in which TMI% is the TMI content in PS-co-TMI and 201 is the molar mass of TMI. Table 2.16 shows the mass percentages and the molar masses of the PS backbone and PA6 graft in PS-g-PA6 graft copolymers obtained from four PS-co-TMI/CL/Cat polymerization systems.

Table 2.16 Mass percentages and the molar masses of the PS backbone and a single PA6 graft of four pure PS-g-PA6 graft copolymers obtained by successive extraction.

Experimental designation	PS-g-PA6 graft copolymer			
	PS backbone		PA6 graft	
	Mass percentage (%)	*Mn* (kg/mol)	Mass percentage (%)	*Mn* (kg/mol)
E7	92.6	36.9	7.4	1.6
E11	75.3	33.3	24.7	1.7
E5	69.4	33.3	30.6	2.2
E12	49.7	33.3	50.3	5.1

The composition and molar mass of pure PS-g-PA6 also were measured using SEC. Table 2.17 shows the compositions and molar masses of various pure PS-g-PA6 graft copolymers. The results in Table 2.17 follow the same trend as those in Table 2.16. For a given TMI content in PS-co-TMI, say 4.0 wt.%, a higher PS-co-TMI/CL mass ratio leads to a lower molar mass and PA6 mass percentage in the pure PS-g-PA6 graft copolymer. Moreover, for a given PS-co-TMI/CL mass ratio, a higher TMI content in PS-co-TMI leads to a higher mass percentage of the PA6 grafts in the pure PS-g-PA6 graft copolymer. The molar mass of the pure PS-g-PA6 graft copolymer is also higher.

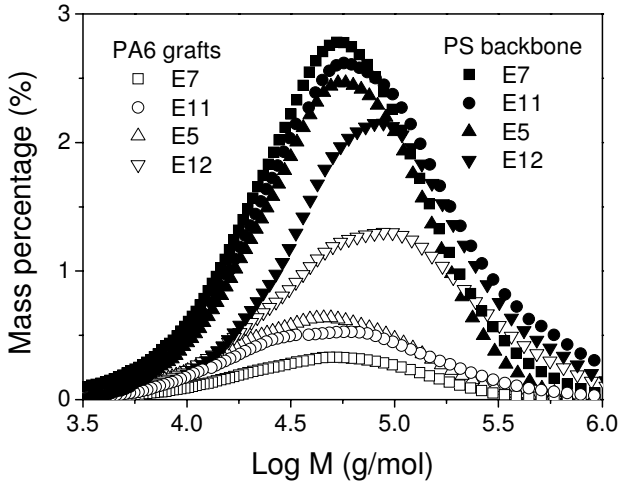
Table 2.17 Composition and relative molar mass of pure PS-g-PA6 obtained by SEC.

Experimental designation	PA6 mass percentage (%)[a]	M_n (kg/mol)[b]
PS-g-PA6 from E7	10.5	22.3
PS-g-PA6 from E11	20.2	34.9
PS-g-PA6 from E5	25.5	38.1
PS-g-PA6 from E12	44.0	47.1

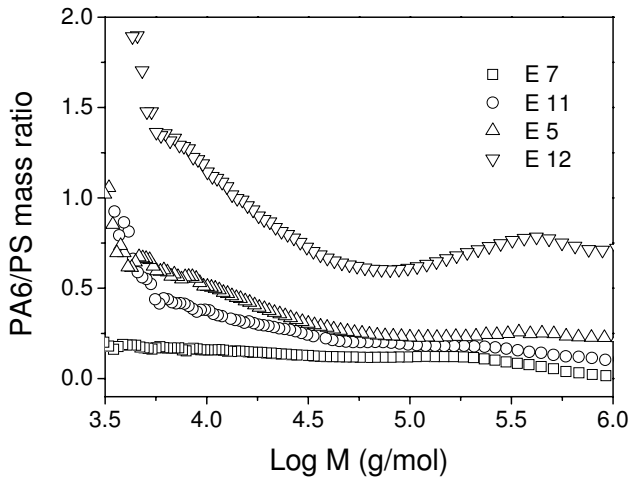
(a) Based on the dual channel curves of SEC at 238 nm and 260 nm.

(b) M_n based on the refractive index curves of SEC using PS standards for the calibration and THF as the eluent.

The mass percentages of the PA6 grafts in PS-g-PA6 shown in Table 2.17 are the average values with respect to the elution time or the molar mass of the PS-g-PA6. SEC also allows obtaining the mass percentage of a PS-g-PA6 graft copolymer and those of its PS backbone and PA6 grafts as a function of its molar mass. Figure 2.35a shows the mass percentages of the PS backbone and PA6 grafts of a pure PS-g-PA6 graft copolymer as a function of its molar mass. Figure 2.35b shows the mass ratio between the PS backbone and PA6 grafts of the pure PS-g-PA6 graft copolymer as a function of its molar mass for the four PS-g-PA6 graft copolymers. Within the experimental errors, for each of the graft copolymers this ratio is almost a constant over the entire molar mass range except for the low molar mass domain where experimental errors are much larger. The fact that this ratio is almost a constant for each of the graft copolymers and independent of the molar mass of the PS-g-PA6 graft copolymer infers two aspects: on the one hand, the number of isocyanate moieties in a PS-co-TMI chain would be proportional to its chain length which has been confirmed in foregoing sections; on the other hand, all isocyanate moieties, whatever the molar mass of the PS-co-TMI or their locations in a PS-co-TMI chain, would have participated in the activation of the polymerization of CL with the same reactivity. This may further support the above statement that the number of the PA6 grafts in a PS-g-PA6 graft copolymer chain is equal to that of the isocyanate moieties in the corresponding PS-co-TMI chain.



(a)

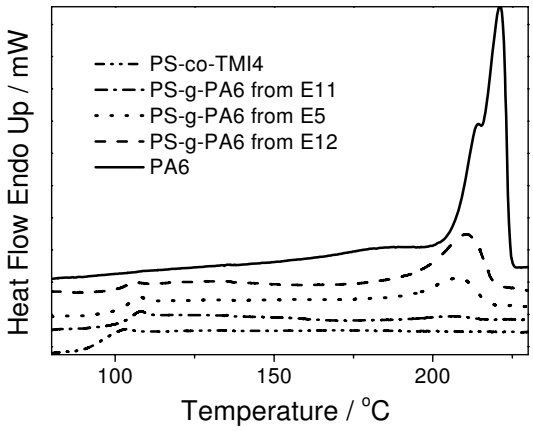


(b)

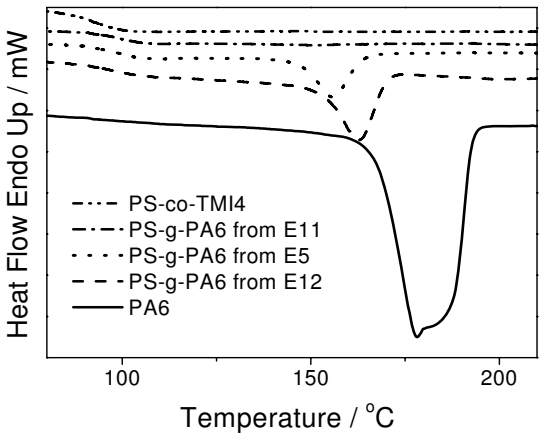
Figure 2.35 Mass percentages of the PS backbone and PA6 grafts of the four pure PS-g-PA6 graft copolymers from E7, E11, E5 and E12 (a) and the mass ratios between the PS backbone and PA6 grafts (b) as a function of their molar masses.

2.8.3 Melting and recrystallization behavior of pure PS-g-PA6

Figure 2.36 shows the DSC traces of the melting and recrystallization behaviour of the three PS-g-PA6 graft copolymers from E11, E5 and E12. Those of PS-co-TMI4 and a homo-PA6 obtained from TDI/CL/Cat (4ml/100g/10g) system (E19) by anionic polymerization of CL are also shown for comparison.



(a)



(b)

Figure 2.36 Melting and recrystallization DSC traces of PS-co-TMI4, PA6 and three pure PS-g-PA6 graft copolymers from the experiments E11, E5 and E12. (a) Melting at 10 ºC/min, (b) Recrystallization at -10 ºC/min.

Table 2.18 Heating behavior of the PA6 grafts of three PS-g-PA6 graft copolymers and homo-PA6

Experimental designation	M_n	$T_{melting}$ (ºC)	$T_{recrystallisation}$ (ºC)	Enthalpy of fusion (J/g)[a]	Enthalpy of recrystallisation (J/g)[a]
E11	1.7	206	—	5.94	—
E5	2.2	208	156	26.7	-25.5
E12	5.1	211	163	50.5	-39.5
Homo-PA6	18.3	221	178	57.4	-66.7

(a) The masses are based on those of the PA6 grafts in E11, E5 and E12.

Table 2.18 gathers selected data of these products. The melting and recrystallization temperatures of the PA6 grafts of PS-g-PA6 decrease with decreasing PA6 grafts chain length. The same is true for their enthalpies of fusion and recrystallization per unit mass of the PA6 grafts. These results suggest that PA6 grafts would no longer be able to crystallize when their length is below a certain threshold.

2.9 Kinetics of the anionic polymerization of CL from PS-co-TMI

2.9.1 Relationship between conversion and torque

Figure 2.37 shows the CL conversion as a function of time for experiments E14 and E5. The higher the Cat concentration, the more rapid the polymerization rate, as expected. Figure 2.38 shows the corresponding evolutions of temperature and torque of the polymerization system as a function of time. Overall, they were good signatures

of the CL conversion process. For example, as CL was converted to polymer, the torque increased. The higher the polymerization rate, the higher the rate with which the torque increased. Thus, the way the torque evolved was an approximate indication of the polymerization rate.

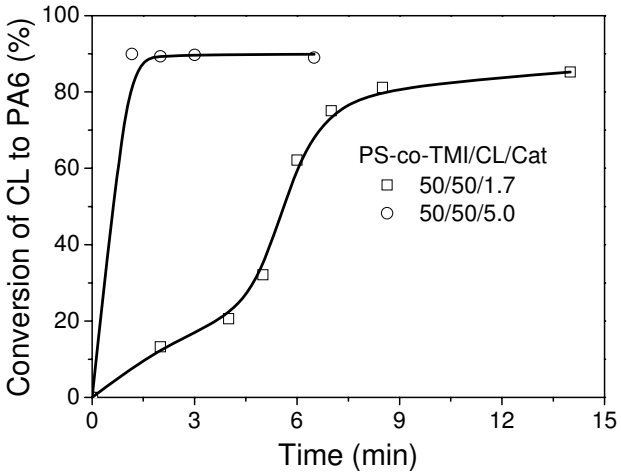


Figure 2.37 Conversion of CL to PA6 as a function of time for experiments E14 and E5.

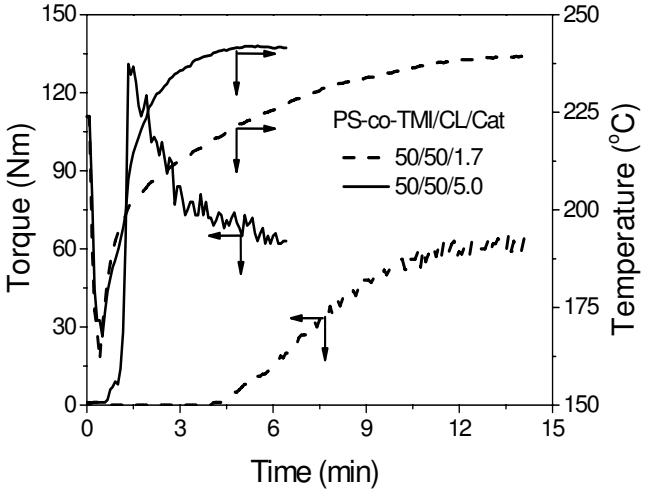


Figure 2.38 Torque values and melting temperature as a function of time for experiments E14 and E5.

2.9.2 Effect of the set temperature on the polymerization

The temperature of the mixing wall, called set temperature, was chosen to regulate the temperature of the polymerizing system. However, the latter did not necessarily match the former. As a matter of fact, differences were very often big between the two because of the viscous dissipation of the polymerizing system and the polymerization heat release, as shown in Figure 2.38. Figure 2.39 shows the effect

of the set temperature on the variation of the torque as a function of time for the PS-co-TMI4/CL/Cat system with a mass composition of 50/50/5. The set temperature ranged from 170 to 240 °C. When the set temperature was below 220 °C, the torque values were very low. When it was above that temperature, the torque started rapidly increasing after about 1 min of mixing and reached a plateau after about 2.5 min of mixing, indicating that the polymerization went to completion. It seemed that 220 °C was a critical temperature below which little polymerization occurred within the chosen polymerization time scale (10 min). Indeed, at 200 °C the conversion of CL obtained 10 min of mixing was less than 30%. Above 220 °C, when the torque reached a plateau, the conversion of CL was higher than 90 %.

However, it should be pointed out that thus far reasons for which there seemed to have a critical set temperature for the polymerization of CL are unclear. Nevertheless, the existence of a critical temperature could be justified at least by one of the following arguments. First, it could be that a certain temperature was necessary to activate the chemical process of the polymerising system. Second, considering the fact that the melting temperature of PA6 was about 210 °C, the polymerization temperature had to be above that value. Otherwise, the growing PA6 chains would crystallize [79]. The second argument was very likely.

From Figure 2.39, when the set temperature was above 220 °C, the torque first followed a very rapid increase and then a very rapid decrease before it levelled off. The ultimate torque value followed the expected order: 220 °C > 230 °C > 240 °C. An increase in the set temperature led to a decrease in the viscosity of the system and therefore a decrease in torque. Moreover, at higher temperatures PA6 chains would have subjected to more severe degradation resulting in a further decrease in torque.

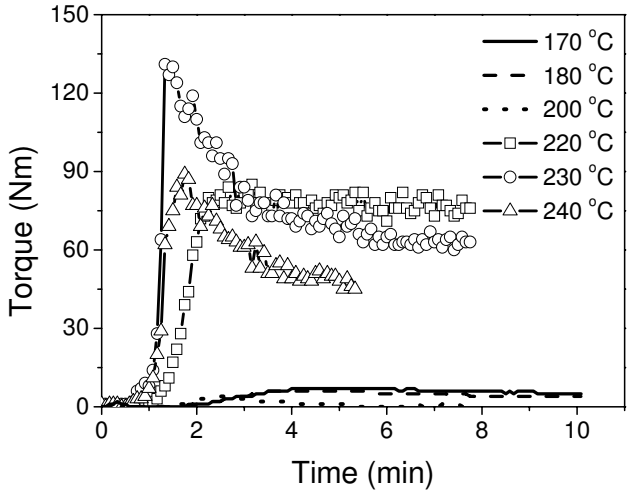


Figure 2.39 Effect of set temperature on the torque versus time of the PS-co-TMI4/CL/Cat (50/50/5 by mass) polymerization system corresponding to E1 to E6.

2.9.3 Effect of NaCL/CL

In fact, the effect of NaCL/CL molar ratio is proportional to that of Cat/CL mass ratio. Figure 2.40 shows the torque evolution as a function of time for the PS-co-TMI4/CL/Cat (50/50/Cat by mass) polymerized system with Cat being 1.7, 5.0 or 8.4%, respectively, with respect to the total amount of PS-co-TMI and CL. When the Cat concentration was at 1.7%, the time necessary for the torque to start significantly increasing was long, namely, about 4 min. On the other hand, when it was raised to 5.0 or 8.4%, the polymerization process started proceeding very rapidly, in about 40 s and ended in about 60 s. This implies that an increase in the NaCL/CL molar ratio led to an early start of the polymerization. This is further confirmed in Figure 2.41. Whatever the TMI content in the PS-co-TMI, the polymerization rate increased with increasing NaCL/CL molar ratio. This is in accordance with the result obtained from the PP-g-TMI/CL/Cat polymerization system [74].

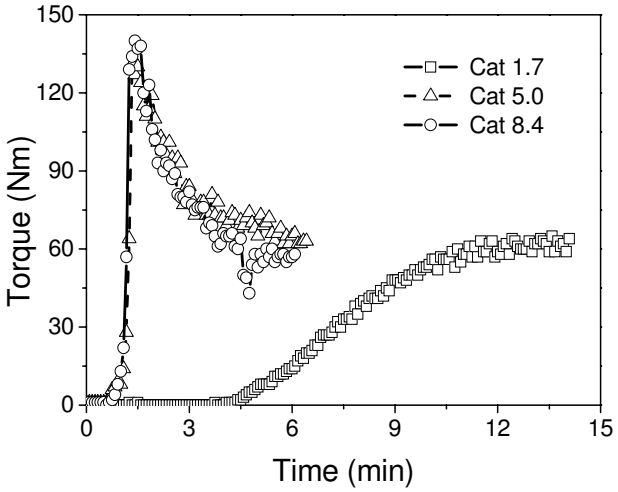


Figure 2.40 Effect of the NaCL/CL molar ratio on the polymerization rate characterised by the torque of the PS-co-TMI4/CL/Cat (50/50/Cat by mass) polymerization system. The percentage of the Cat was 1.7, 5.0 and 8.4 wt.%, corresponding to E14, E5 and E16, respectively.

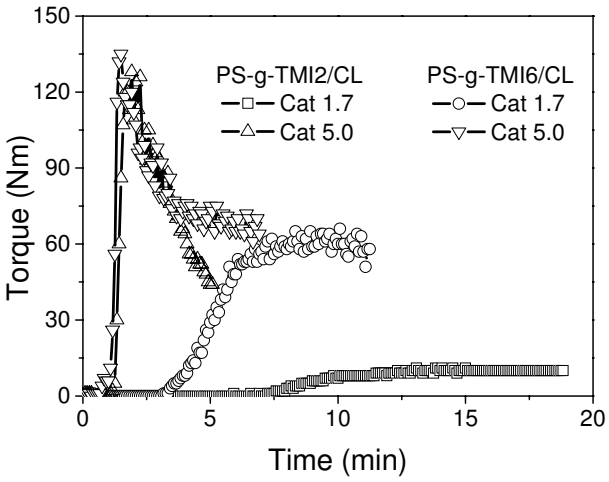
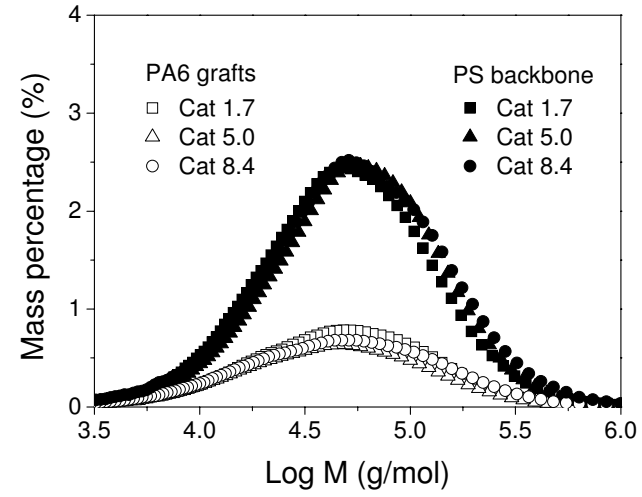
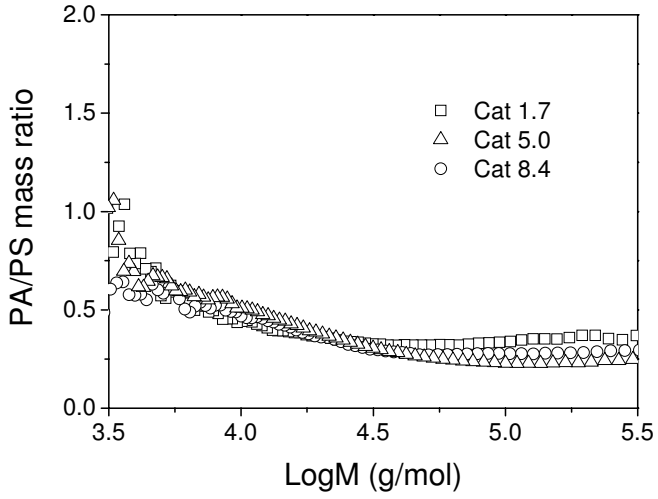


Figure 2.41 Effect of the NaCL/CL molar ratio on the polymerization torques of PS-co-TMI2/CL/Cat and PS-co-TMI4/CL/Cat (50/50/Cat by mass) polymerization systems with Cat being 1.7 and 5.0 wt.%, corresponding to E8, E13, E9 and E15.

From Figure 2.40, the final torque values were almost the same, whatever the Cat concentration. This is corroborated by the fact that the ultimate conversions of the PS-g-PA6 from the PS-co-TMI4/CL/Cat (50/50/Cat by mass) polymerized system with Cat being 1.7, 5.0 and 8.4% were very close, i.e., 89.1, 90.9 and 90.7%, respectively. Do these two points imply that for a given NCO/CL molar ratio, the NaCL/CL molar ratio had little effect on the composition of the PA6 grafts in PS-g-PA6 graft copolymers? In order to check it, SEC was used to analyze the polymerized products by successive extraction in methanol, THF and formic acid. Figure 2.42(a) shows the mass percentages of the PS backbone and PA6 grafts of various pure copolymers as a function of their respective molar mass. Indeed, all the three curves corresponding to the PA6 grafts superimposed relatively well, whatever the catalyst concentration. The same is true for the PS backbone. This confirms that within the catalyst concentration range, the catalyst concentration had little effect on the composition of the PA6 grafts in the PS-g-PA6. This is further corroborated by the curves of the mass ratio between the PS backbone and PA6 grafts versus molar mass in Figure 2.42(b).



(a)



(b)

Figure 2.42 Effect of the NaCL/CL molar ratio on the mass percentages of the PS backbone and PA6 grafts (a) and PS backbone/PA6 grafts mass ratios (b) of various PS-g-PA6 obtained from E14, E5 and E16 as a function of the respective molar masses of these pure graft copolymers. PS-co-TMI4/CL = 50/50 by mass.

2.9.4 Effect of the NCO/CL molar ratio

The NCO/CL molar ratio can be varied by varying either the TMI content in PS-co-TMI or the PS-co-TMI/CL mass ratio. Figure 2.43 shows the evolution of torque as a function of time for five different NCO/CL molar ratios corresponding to five different TMI contents in PS-co-TMI and a given PS-co-TMI/CL mass ratio (50/50). When it was 1 wt.%, it took about 2.5 min of mixing time for the polymerization to start proceeding. However, when it was above 2 wt.% the polymerization process started occurring only in about 1 min or less. In addition, from Figure 2.44 the composition of the PA6 grafts in the PS-g-PA6 obtained from

PS-co-TMI1 (1 wt.% TMI) was lower than that from PS-co-TMI whose TMI content was above 2 wt.%. This implies that when the TMI content in PS-co-TMI was below 2 wt.%, the polymerization induction time was long, and the polymerised rate and monomer conversion were low.

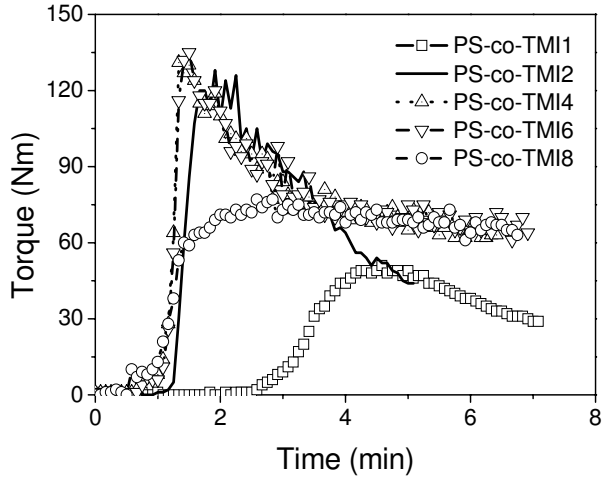


Figure 2.43 Effect of the TMI content in PS-co-TMI on the polymerization torque of the PS-co-TMI/CL/Cat (50/50/5 by mass) polymerization system with PS-co-TMI being PS-co-TMI1, PS-co-TMI2, PS-co-TMI4, PS-co-TMI6 and PS-co-TMI8, corresponding to E7, E8, E5, E9 and E10, respectively.

From Figure 2.43, when TMI content in PS-co-TMI was 8 wt.%, the torque evolved in a different manner. Moreover, it took about 3 min to reach the maximum instead of 1.5 min needed for the PS-co-TMI whose TMI contents were between 2 and 4 wt.%. This may imply that the polymerization rate and monomer conversions with PS-co-TMI8 could be even lower that with PS-co-TMI2 or PS-co-TMI4. This is in line with the results in Figure 2.44. The composition of the PA6 grafts in PS-g-PA6 with PS-co-TMI8 was lower than with PS-co-TMI2 or PS-co-TMI4.

The abnormal results with PS-co-TMI8 were surprising but not fully unexpected. When the PS-co-TMI/CL/Cat mass ratio was fixed, the higher the TMI content in PS-co-TMI, the faster the polymerization rate was expected to be. However, when the TMI content was very high, the molar ratio between the corresponding N-acyl-ε-caprolactam and NaCL was very high. Thus a so-called C-acylation reaction might have taken place, consuming lactam anions and consequently decreasing the polymerization rate [80]. In the case of PS-co-TMI8, the NCO/NaCL was 3.4. Hu et al. [74] also suggested that the NCO/NaCL ratio should be lower than 4.0 for PP-g-TMI/CL/Cat polymerization system. Šebenda et al. [83] reported that when the

acylcaprolactam/NaCL ratio was higher than 2.5, the lactam anions disappeared so quickly that the polymerization slowed down considerably even before attaining polymerization equilibrium.

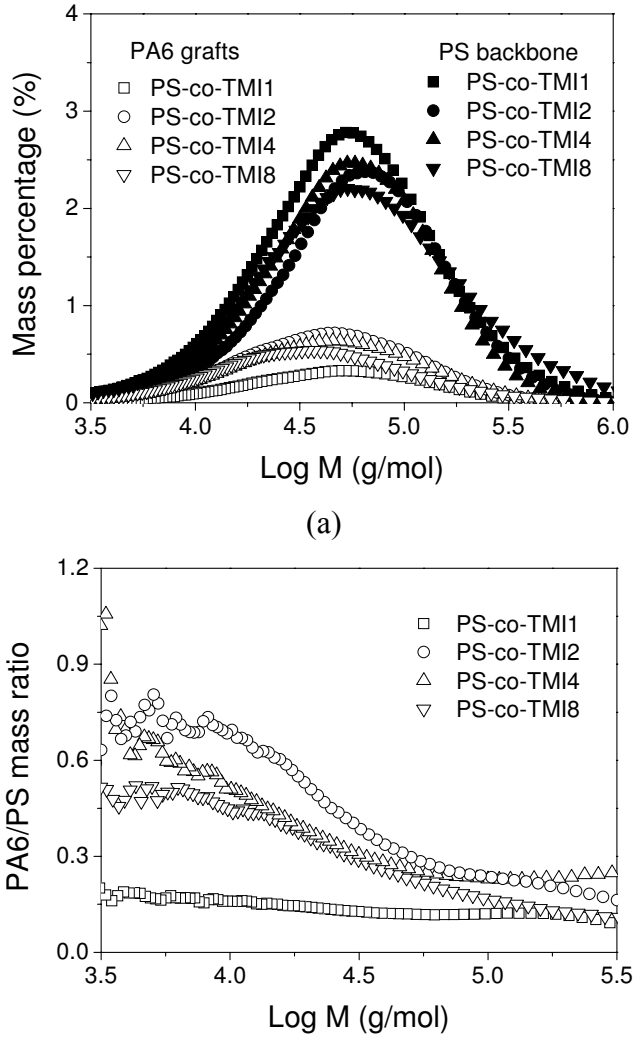


Figure 2.44 Mass percentages of the PS backbone and PA6 grafts (a) and PS backbone/PA6 grafts mass ratios (b) of various PS-g-PA6 from E7, E8, E5 and E10 as a function of the respective molar masses of these pure graft copolymers.

Figure 2.45 shows the torque evolution as a function of time for three different NCO/CL molar ratios, corresponding to three different PS-co-TMI4/CL mass ratios. The set temperature was 230 ºC. Whatever the PS-co-TMI4/CL mass ratio, the polymerization process started proceeding after about 1 min of mixing and almost went to completion after about 1.5 min of mixing. This implies that the NCO/CL molar ratio had little effect on the polymerization rate. The NCO/NaCL molar ratios of the above three different polymerization systems were 1.0, 1.7 and 2.4, respectively.

In that range, the above mentioned C-acylation reaction was expected to be unimportant. This is confirmed by the fact that the corresponding ultimate CL conversions were relatively high, 87.7, 90.9 and 93.2%, respectively. Hu et al. [74] also reported similar results: the polymerization rate and the ultimate monomer conversion were high for NCO/NaCL molar ratio being below 3.23; moreover, the ultimate monomer conversion increased slightly with increasing NCO/CL molar ratio till the latter exceeded 3.23.

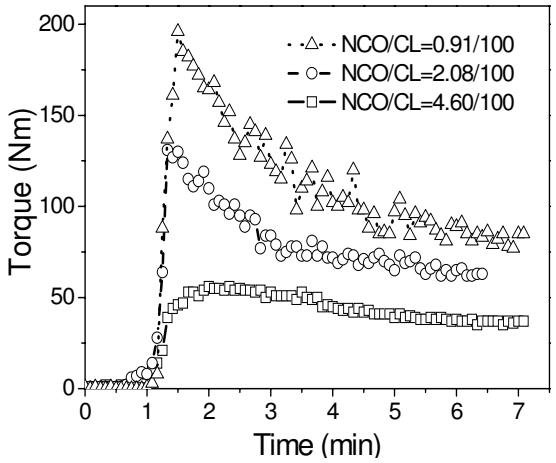
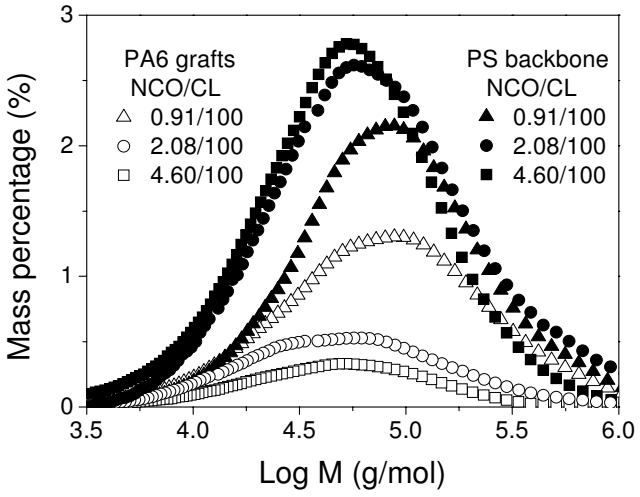
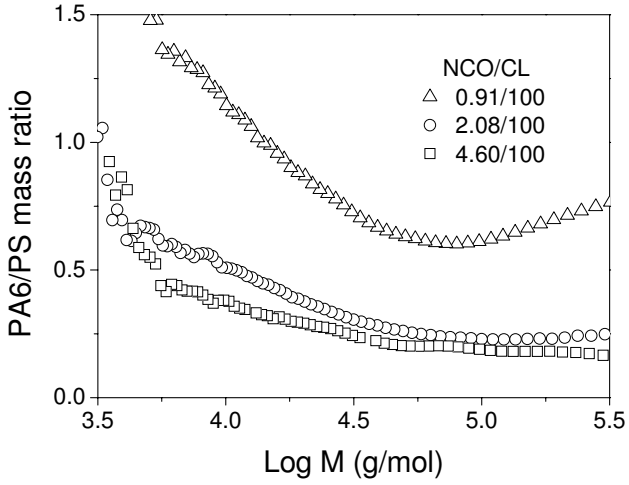


Figure 2.45 Effect of the NCO/CL molar ratio on the torque evolution as a function of time for the PS-g-TMI4/CL/Cat polymerization system corresponding to E12, E5 and E11, respectively.

The ultimate torque increased with decreasing PS-co-TMI4/CL mass ratio, as expected. This is because the lower the PS-co-TMI4/CL mass ratio, the longer the PA6 grafts in the corresponding PS-g-PA6 graft copolymer and consequently the higher the viscosity and torque of the polymerising system. This is further confirmed in Figure 2.46. Both the mass percentage of the PA6 grafts in the PS-g-PA6 copolymer and the PA6 graft/PS backbone mass ratio increased with decreasing PS-co-TMI/CL mass ratio.



(a)



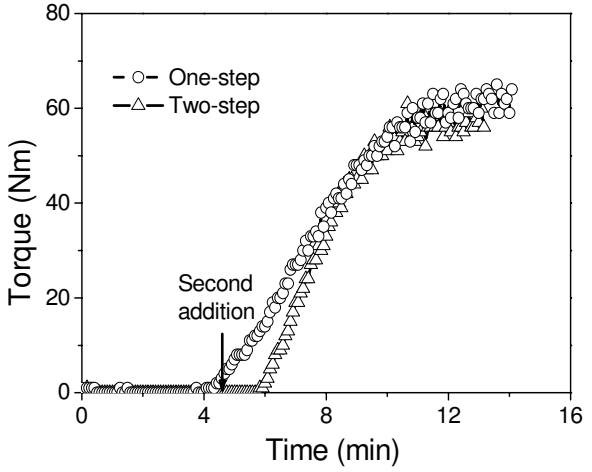
(b)

Figure 2.46 Effect of the NCO/CL molar ratio on the mass percentages of the PS backbone and PA6 grafts (a) and PS backbone/PA6 grafts mass ratio (b) of various PS-g-PA6 obtained from E11, E5 and E12 as a function of the their molar masses.

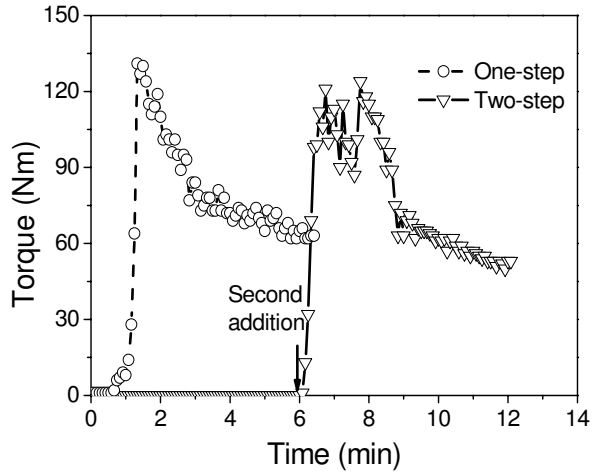
2.9.5 Effect of feeding mode

Figure 2.47 compares two feeding modes in terms of the torque evolution as a function of mixing time for the PS-co-TMI4/CL/Cat (50/50/Cat) with Cat being equal to 1.7 and 5.0, respectively. Figure 2.47(a) shows that when the Cat concentration was low (1.7 %), the time necessary for the torque to start increasing was 4 and 6 min for the one-step and two-step feeding modes, respectively. Since in the latter case the Cat was charged to the mixer 4.5 min later than PS-co-TMI4 and 80% of the total amount of CL, the real time necessary for the torque to start increasing was then 1.5 min, which was much shorter than that of the one-step feeding. The reason was that the first feeding step of the two-step feeding mode allowed mixing and heating up, to a

certain degree, the polymerizing system prior to the polymerization. During that step, the isocyanate groups of the PS-co-TMI could also have been converted to the corresponding acylcaprolactam, the real activating species of the anionic polymerization of CL. When the Cat concentration was high (5 wt.%), the difference in the effective time necessary for the torque to start increasing was much less smaller (Figure 2.47(b)).



(a)

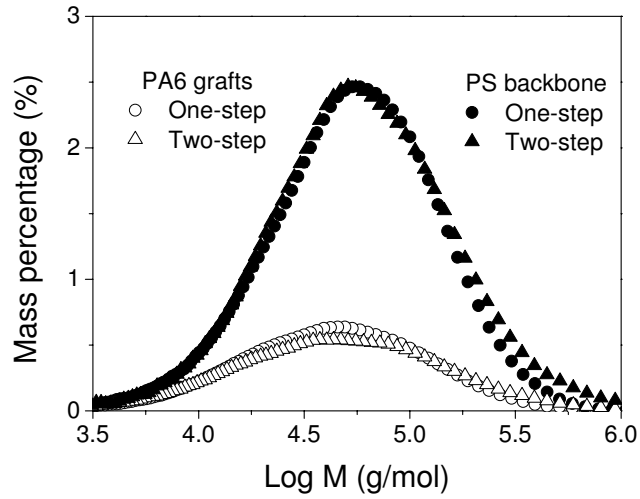


(b)

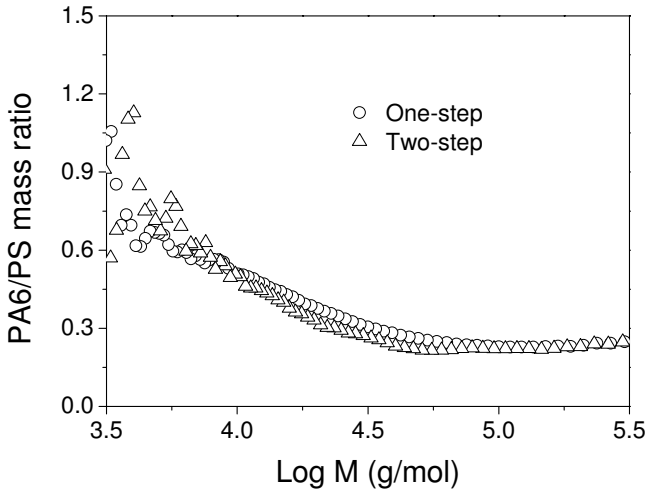
Figure 2.47 Comparison between the one-step and two-step feeding modes in terms of the torque evolution as a function of mixing time for the polymerising system: (a) PS-co-TMI4/CL/Cat=50/50/1.7 (E14 one-step versus E17 two-step); (b) PS-co-TMI4/CL/Cat=50/50/5.0 (E5 one-step versus E18 two-step).

It is also noted that the ultimate toque value did not depend on the feeding mode. This is consistent with the fact that the monomer conversion did not depend on the feeding mode. For example, the conversion of the PS-co-TMI4/CL/Cat (50/50/5)

polymerization system was 90.9 and 91.3% for the one-step feeding mode and two-step feeding mode, respectively. This is further confirmed by the fact that the mass percentages of the PA6 grafts and PS backbone, and the PA6 graft/PS backbone mass ratio in PS-g-PA6 between those two different feeding modes were similar (see Figure 2.48).



(a)



(b)

Figure 2.48 Mass percentages of the PS backbone and PA6 grafts (a) and PS backbone/PA6 grafts mass ratios (b) of various PS-g-PA6 graft copolymers obtained from one-step (E5) and two-step (E18) feeding modes as a function of the respective molar masses.

2.10 Conclusions

The controlled graft copolymers with PS as backbone and PA6 as grafts were synthesized by the anionic polymerization of CL onto a random copolymer

PS-co-TMI. The new measurement methods of CL conversion and the molar mass and composition of PS-g-PA6 also were developed, respectively.

The methanol extraction, vacuum drying at 140 ºC and TGA were all suitable for measuring the conversion of CL, whether the resulting polymer was the PA6 or PS-g-PA6. The molar mass and composition of PS-g-PA6 can be measured by SEC with dual UV detection at two different wavelengths after they are subjuected to the *N*-trifuloroacetylation reaction with TFAA, leading to the corresponding *N*-trifuoroacetylated derivative PS-g-PA6-TFAA.

In order to obtain relatively high monomer conversions and a polymerization kinetics that is compatible with the residence time of a typical reactive extrusion process, the polymerization temperature should be above the melting temperature of the resulting polyamide 6 grafts, i.e., 210 to 220 °C; the TMI content in the PS-co-TMI higher than 2 wt.%; and the isocyanate/NaCL molar ratio lower than 3. Moreover, the as-polymerized product is composed of the pure PS-g-PA6 graft copolymer, homo-PA6 and un-reacted CL and likely does not contain any PS-co-TMI.

The structural control of graft copolymer can be achieved by the control of following parameter:

(a) Length of backbone chain: both the increase of polymerization temperature and BPO concentration can decrease the molar mass. Therefore, it can control the length of backbone chain by the polymerization temperature or BPO concentration.

(b) Graft number per one backbone chain: It is very likely that all isocyanate moieties in the PS-co-TMI have participated in the activation of the polymerization of CL. This suggests that the number of the PA6 grafts in a PS-g-PA6 chain is likely equal to the number of the isocyanate moieties in the corresponding PS-co-TMI. Therefore, the graft number per one backbone can be controlled by St/TMI mass ratio for the synthesis of PS-co-TMI because the TMI content in PS-co-TMI is nearly proportional to the St/TMI mass ratio in the feed and has nothing with polymerization temperature and BPO concentration.

(c) Length of graft chain: for a given TMI content in the PS-co-TMI, the higher the PS-co-TMI/CL mass ratio, the lower the molar mass of and the PA6 mass percentage in the pure PS-g-PA6 graft copolymer; The Cat concentration and feeding mode has little effect on the conversion and the composition of the PS-g-PA6 graft copolymer. Therefore, the graft length of

the PS-g-PA6 graft copolymer is controlled primarily by the isocyanate/CL molar ratio.

Chapter 3 Degradation of PS-g-PA6 graft copolymer

3.1 Introduction

The foregoing studies have shown that the raw as-synthesized copolymer contained a remarkably amount of the Homo-PA6. The latter may result from the followings: (1) side reactions in the process of CL polymerization; (2) degradation of PA6 graft chain in the process of formic extraction; (3) degradation of PA6 graft chain in the polymerisation process due to the high temperature and the high shear. The first reason has discussed in the forgoing sections. Now, the other two reasons will be focused on.

In the purification process of PS-g-PA6, the Homo-PA6 was removed by extracted in formic acid. In fact, it is well known that the acid solution can lead to the degradation of polyamide [114- 119]. Shukla et al. [114] studied on the depolymerization of nylon 6 by dissolution and heating in formic acid and found that formic acid depolymerizes nylon 6 into low molecular weight compounds of various chain lengths and that even after 20 h, the depolymerization is incomplete. When PA66 in acid solution, at first water penetrates into polyamide and it is followed by acid. In this process, water does not affect the molecular weight at 50 ºC but proton (H^+) ion has contributed to the anion transport and degradation of polyamide by the hydrolytic reaction [115]. Hydrolysis of polyamide is often considered as a good example of a random chain scission process [117].

The polymerization of CL graft onto PS backbone is processed in the melting state at 230 ºC and the high shear ensuring the mixing. It is well-know that the polyamide can degrade in the high temperature [120,121]. An extensive overview of the degradation of polyamide in the melting process can be found in the literature [122- 124]. Most authors agree that oxygen first attacks methylene carbon adjacent to the amide NH, which is followed by the scission of alkyl-amide N-C. The polymerization reaction in our work is carried out in the condition of the high temperature and in the high shear, which may result in the degradation of the graft copolymer.

The above studies focused mainly on the degradation of Homo-PA6. The work reported in this section was aimed at studying resource of the Homo-PA6, especially interest in the degradation of graft copolymer in the different condition. The graft copolymer studied is PS-g-PA6g, as shown in Table A.2 of Applex section.

3.2 Experimental

3.2.1 Treatment in formic acid

The pure PS-g-PA6 films (about 2.0 g) were dipped into the formic acid (100 ml) for different time (3-24 h) at different temperature (30, 60 or 90 ºC) and then dried in vacuum oven at 80 ºC for 24 h. The masses of films before and after vacuum-dry were recorded. The residue soluble in formic acid was obtained by rotatory evaporation at 60 ºC.

3.2.2 Static annealing and mixing

In the process of polymerization, the high temperature and high shear may be two important factors for the degradation. However, the systems with polymerization reactions are complex so that it is difficult or even not to focus only on these two factors. Therefore, in order to research these two factors, the pure PS-g-PA6 was treated for different time at 230 ºC by two methods, one is annealing treatment (static pressed at a pressure of 10MPa) and the other is Haake mixing (mixed in haake torque rheometer). After treated, the samples were extracted in formic acid for 12 h at 30 ºC.

3.2.3 TEM microscopy

The morphology of PS-g-PA6 can be characterized by transmission electron microscopy (TEM) of type JEM-1200EX. Prior to the TEM analysis, specimens were stained in the following manner [125]. They were microtomed into films of less than 100 nm thick. They were then placed on a drop of 2% phosphotungstic acid solution for 30 min at 50 °C using a specimen grid. Thereafter they were rinsed three times with distilled water.

3.3 Results and discussion

3.3.1 Degradation in the process of formic acid extraction

In order to obtain the pure PS-g-PA6, the raw as-synthesized graft copolymer need be extracted in formic acid. In fact, polyamide can degrade in acid solution. Proton (H^+) in the acid contributes to the anion transport and degradation of polyamide by the hydrolytic reaction. Proton attacks the polyamide chain and scission of chain occurs, and then reacts with anion to form other material substances [115]. In general, metal halides were found to be most effective, while sulfates and acetates were less aggressive [118].

The mass percentage of soluble residue after PS-g-PA6 copolymer dipped in formic acid at 30 ºC as a function of time is shown in Figure 3.1. As expected, the graft copolymer PS-g-PA6 can indeed degrade in the formic acid. The curve of mass percentage of soluble residue versus time reveals the existence of two stages. In the first stage, the percentage of residue soluble in formic acid increased sharply with time prolonging before 4 h; after 4 h, it displayed a quasi linear increase and the increasing rate is much less than that of the first stage.

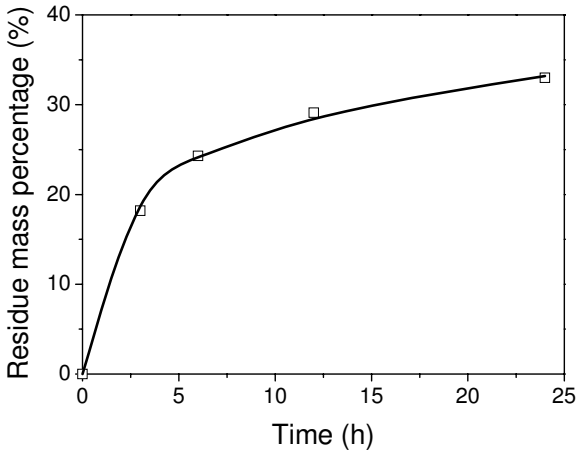


Figure 3.1 Mass percentage of the soluble residue after PS-g-PA6 dipped in formic acid at 30 ºC as a function of dipping time.

Figure 3.2 shows the FTIR spectra of PS-co-TMI, Homo-PA6, PS-g-PA6, the residue M. The latter are the soluble residue in formic acid after PS-g-PA6 dipped in formic acid at 30 °C for 12 h. By comparison of these four FTIR spectra, it can be seen that the soluble residue is similar with Homo-PA6 and has not appeared the PS characteristic peak at 1940 cm^{-1} and the TMI characteristic peak at 2255 cm^{-1}, which indicates that the soluble residue is Homo-PA6 without containing any PS or PS-co-TMI chain, that is, the degradation of graft copolymer results from the cleavage of PA6 grafts.

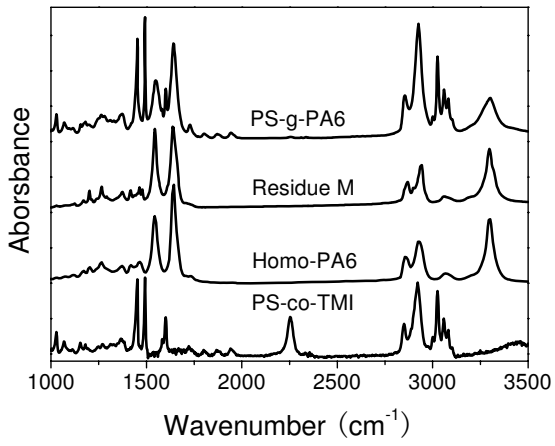
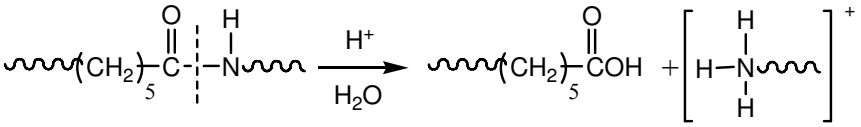


Figure 3.2 FTIR spectra of PS-co-TMI, Homo-PA6, PS-g-PA6 and the soluble residue M after PS-g-PA6 dipped in formic acid at 30 °C for 12 h.

It should be also noted that for residue M and PS-g-PA6, their ratios of the peak intensity of between 1640 and 1545 cm^{-1} are obviously different. The former attributes to the amide I, dominated by CO stretching vibrations; the latter corresponds to the amide II, dominated by N-H deformations. The decrease of the peak height of amide I may imply that the degradation of PA6 grafts chain results mainly from the hydrolytic scission of the peptide C(O)-NH bonds, as shown in Eq. (3.1) .



(3.1)

The above results show that PA6 grafts chain of copolymer PS-g-PA6 can degrade in formic acid, which implies that the PA6 content in PS-g-PA6 decreases after PS-g-PA6 dipped in formic acid. The PA6 content in PS-g-PA6 can be obtained by two methods: one is weight method and the other is SEC method. The former is based on the fact that the mass decrease before and after PS-g-PA6 dipped in formic acid results completely from the mass decrease of PA6 grafts. Consequently, the PA6 content in PS-g-PA6 after dipped in formic acid can be calculated by Eq. (3.2).

$$PA6\% = \frac{m_3 * w_1 - (m_3 - m_4)}{m_4} \tag{3.2}$$

in which, m_3 and m_4 (g) are the mass of PS-g-PA6 before and after dipped in formic acid; w_1 is the PA6 content in PS-g-PA6 before dipped formic acid. The latter method has reported in chapter 2. The PA6 contents in PS-g-PA6 obtained by these two methods are basically similar, as shown in Figure 3.3. This indicates that these two

methods can be used to calculate the PA6 content in PS-g-PA6. Form Figure 3.3, it also can be seen that the PA6 graft chain content in PS-g-PA6 copolymers decrease with the dipping time increasing, which further confirm that the degradation of copolymer results mainly from the scission of PA6 grafts chain.

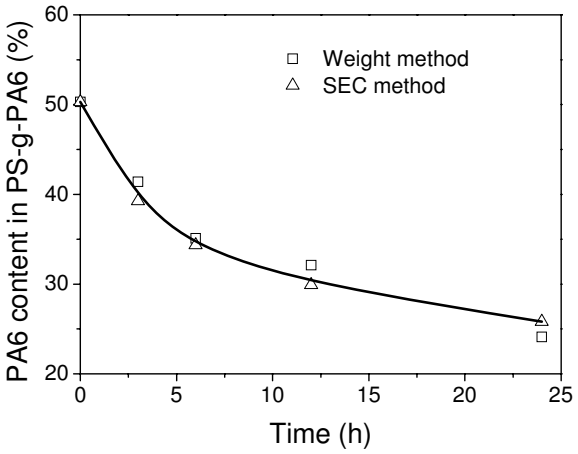
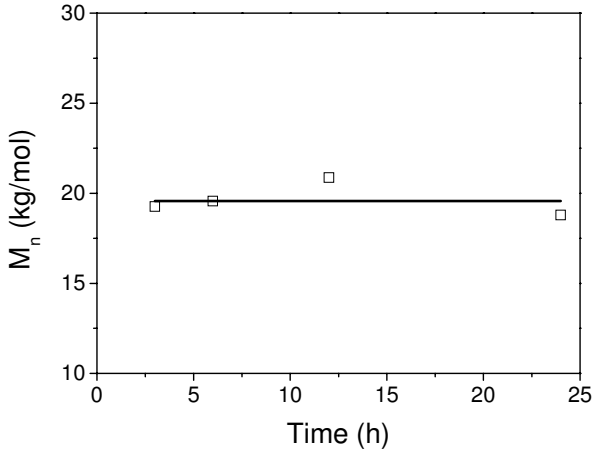


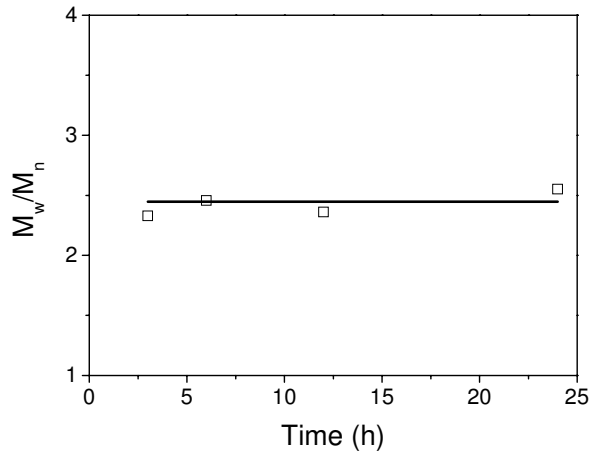
Figure 3.3 PA6 contents in PS-g-PA6 copolymers by dipped in formic acid at 30 °C for different times (0, 3, 6, 12 and 24 h). The PA6 content obtained by two methods: (1) Weighting; (2) SEC.

Hydrolyzed samples of polyamides may contain variable of monomer and oligomers depending on exposure conditions [117]. Can the PA6 grafts chain dipped in formic acid degrade into monomeric level or Homo-PA6 with certain molar mass? How do the composition and structure of the PS-g-PA6 copolymer change? In order to answer the above questions, SEC was used to analyze the residue soluble in formic acid and the PS-g-PA6 copolymer insoluble in formic acid.

Figure 3.4(a) and (b) show the molar mass and polydispersity index of the residue as a function of time for PS-g-PA6 dipped in formic acid at 30 °C, respectively. From Figure 3.4(a), it can be seen that the molar mass of residue is about 20 kg/mol and hardly changes with time for PS-g-PA6 dipped in formic acid. Moreover, the index of polydispersity of residue, the ratio of M_w/M_n, also is constant irrespective of dipping time, as shown in Figure 3.4(b). These two behaviours observed are interpreted as a homogeneous distribution of the length of scission chain. In addition, the constancy of polydispersity index of about 2.4, nearly 2.0, indicates apparently that the chain scission is random [117,126,127].



(a)

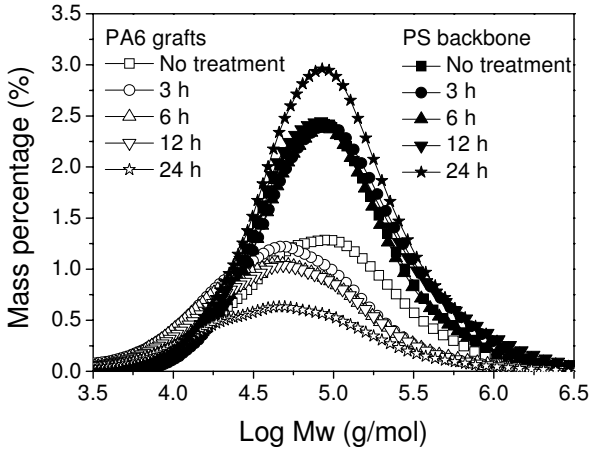


(b)

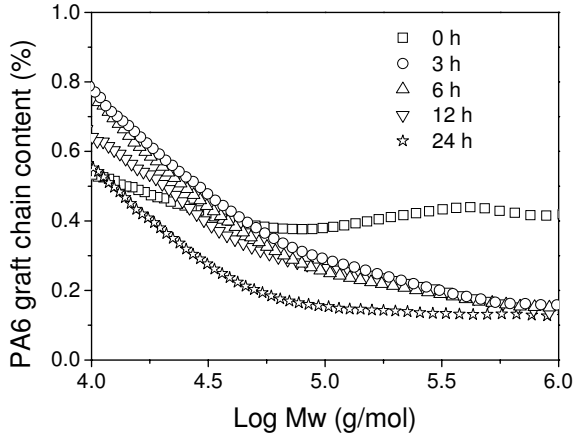
Figure 3.4 M_n (a) and M_w/M_n (b) of residue soluble in formic acid as a function of time for the extraction in formic acid at 30 °C.

Figure 3.5 shows the mass percentages of the PS backbone and PA6 grafts of various PS-g-PA6 copolymers by dipped in formic acid for different time at 30 °C and the PA6 content in PS-g-PA6 as a function of their respective molar mass. After PS-g-PA6 dipped in formic acid for different time, the curve of mass percentage of PS backbone as a function of their copolymer molar mass is similar but the peak height, which means that the PS backbone in formic acid has not changed, which further confirms that the PS backbone doesn't occur the scission of chain. While for PA6 grafts, two stages are shown clearly: before 3 h, the curves of mass percentage of PA6 grafts as a function of their copolymer molar mass shift toward the lower molar mass domain, which means that the PA6 grafts chain at higher molar mass domain of PS-g-PA6 copolymer degrades easily, that is, the proton (H^+) attacks the PA6 grafts chain of the copolymer with higher molar mass; after 3 h, the peak locations of the curves is similar but the peak heights still decrease, which may imply that homogeneous

distribution of chain scission in whole polymer volume.



(a)



(b)

Figure 3.5 Mass percentages of the PS backbone and PA6 grafts of the PS-g-PA6 graft copolymers after dipped in formic acid for different times at 30 ºC (a) and the PA6 grafts contents in PS-g-PA6 (b) as a function of their molar masses.

Recall that the foregoing curve of mass percentage of soluble residue versus time also reveals the existence of two stages: it increase sharply with time before 4 h, and then the increasing rate of mass percentage of soluble residue is much slower and moreover remains constant. The two results seem to be coincident and advise the rule about the degradation of PA6 graft chains in formic acid: at the early stage, the degradation of PA6 graft chain results mainly from the copolymer with high molecular weight, which leads to the mass percentage of residue soluble in formic acid increase sharply; and then, the PA6 graft chain occur to the homogenous scission in whole polymer volume and moreover the scission rate remain constant. This can also further be confirmed from the change of PA6 graft chain content with dipping

time (Figure 3.5b): at high molar mass domain, the PA6 graft contents is similar after 3 h, which imply that the degradation mainly locates on the higher molar mass domain; after 3 h, the curve shape is similar and move down with dipping time, which indicates the degradation exists in all polymer volume.

Figure 3.6 shows the mass percentage of soluble PA6 after PS-g-PA6 dipped in formic acid as a function of temperature. It can be seen obviously that the residue percentage increases with the increasing of dipping temperature. This implies that the degradation of PA6 grafts is more and more serious with the increase of dipping temperature. This may be further confirmed by the relation of PA6 grafts content in PS-g-PA6 and dipped temperature, as shown in Figure 3.7.

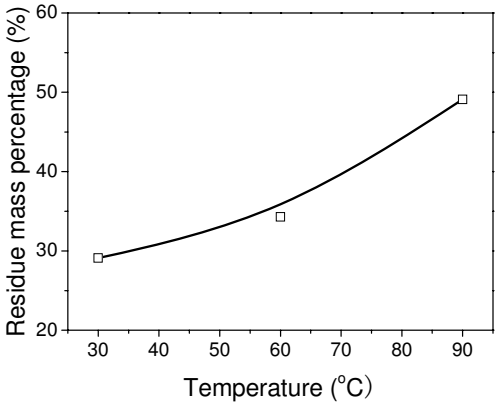


Figure 3.6 Percentage of the soluble residue after PS-g-PA6 being dipped in formic acid for 12 h as a function of temperature.

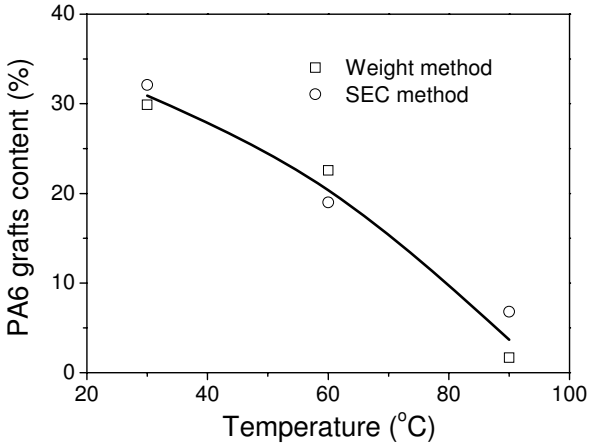
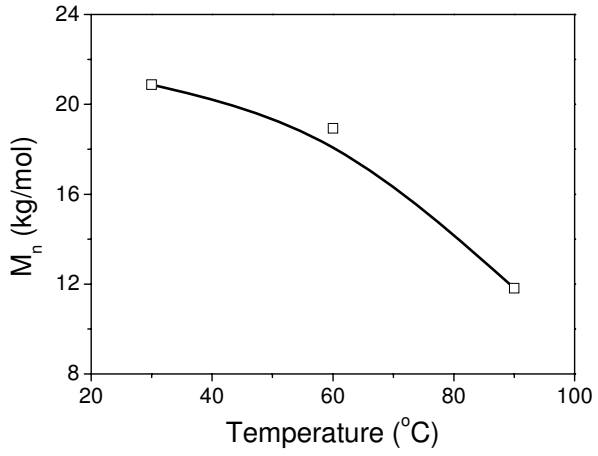


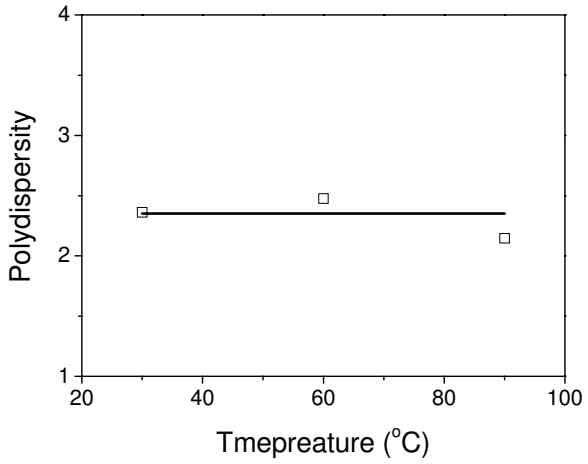
Figure 3.7 PA6 graft chain content of PS-g-PA6 copolymers after being by dipped in formic acid for 12 h at different temperature (30, 60 or 90 ºC). The PA6 graft chain content obtained by two methods: (1) Weighting; (2) SEC.

The molar mass and polydispersity index of the soluble residue after PS-g-PA6 dipped in formic acid at 30 °C for 12 h as a function of temperature are shown in

Figure 3.8. It can be seen that the higher the temperature is, the lower molar mass of the residue soluble in formic acid is, which indicates that the degradation is more and more serious with temperature increasing. However, the polydispersity index is close to 2 and remains constants, which may imply that the proton (H^+) attacked the PA6 grafts chain is random. From Figure 3.9, it also can be seen that increasing temperature leads to the more serious degradation of PA6 grafts chain of the copolymer. Moreover, for dipped in 60 or 90 ºC, PA6 graft content is almost a constant over the entire molar mass range except for the low molar mass domain, which is different from that for dipped in 30 ºC PA6 graft content still decreases with the molar mass. This may infer that the temperature raise will increase the range of molar mass that can degrade in the early stage. The above results show that the aggravation of the degradation of the PA6 grafts chain with temperature raise results mainly from two aspects: on the one hand, the proton (H^+) has more chance to attack the PA6 grafts chain leads to Homo-PA6 with lower molar mass; on the other hand, the molar mass of their copolymer will be not an important factor for the degradation in the early stage any more.

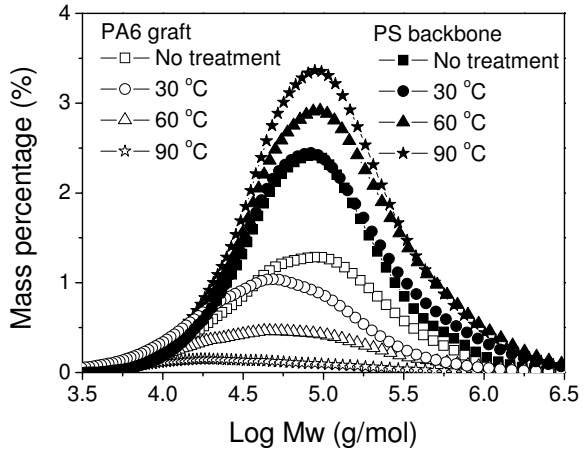


(a)

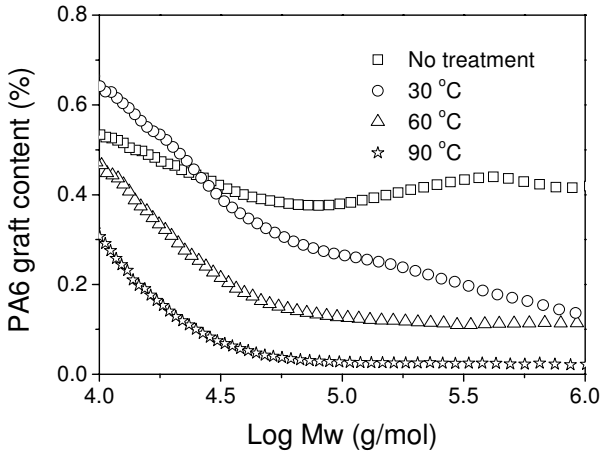


(b)

Figure 3.8 M_n (a) and M_w/M_n (b) of residue soluble in formic acid as a function of temperature for the extraction in formic acid for 12 h.



(a)



(b)

Figure 3.9 Mass percentages of the PS backbone and PA6 grafts of the PS-g-PA6 graft copolymers after dipped in formic acid for 12 h at different temperature (30, 60 and 90 ºC) (a) and the PA6 grafts content in PS-g-PA6 (b) as a function of their molar masses.

3.3.2 Degradation in high temperature and high shear

In the process of PS-g-PA6 synthesis, the typical evolutions of temperature and torque of the polymerization system as a function of time are shown in Figure 3.10. From Figure 3.10, it can be noted that the torque values decreased rapidly after reaching the maximum for the polymerization systems. This may results from two reasons: (1) the viscosities decrease of polymerisation systems with melting temperature increasing; (2) the degradation of copolymer in the process of polymerization process. The second argument was very likely. In order to confirm the second argument, the above polymerizing system was replaced to the CL/Cat/TDI one. The corresponding polymer after the polymerization was homo-PA6 instead of PS-g-PA6. Figure 3.11 shows both the evolution of the torque and the temperature of the polymerizing system as a function of mixing time for the CL/Cat/TDI (100/6/3.6) polymerizing system. Three samples were taken at 1 min 10 s corresponding to the maximum of the torque, 2 min and 3 min, respectively. It was found that the first sample taken at 1 min 10 s was insoluble in the solvent used for the molar mass measurement, in m-cresol. The second and the third samples were soluble therein without problems. Their molar masses obtained by an Ubbelohde viscometer method were 45.7 and 18.4 kg/mol, respectively. This indicates clearly that during the polymerization process, PA6 was subjected to the chain scission.

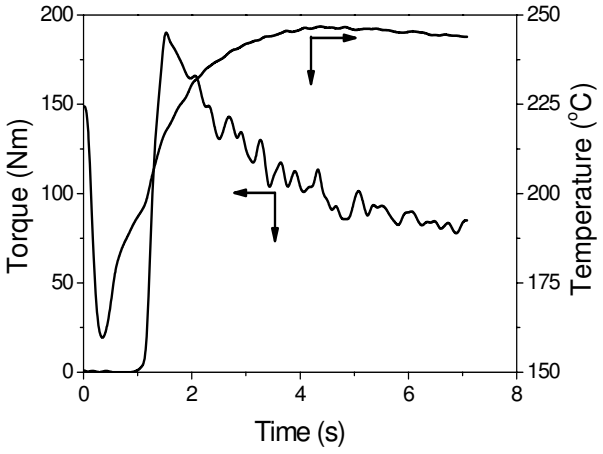


Figure 3.10 Torque and melting temperature versus time of PS-g-TMI/CL/Cat (30/70/5) polymerisation system. Rotate speed of screw: 65 rpm, temperature: 230 ºC.

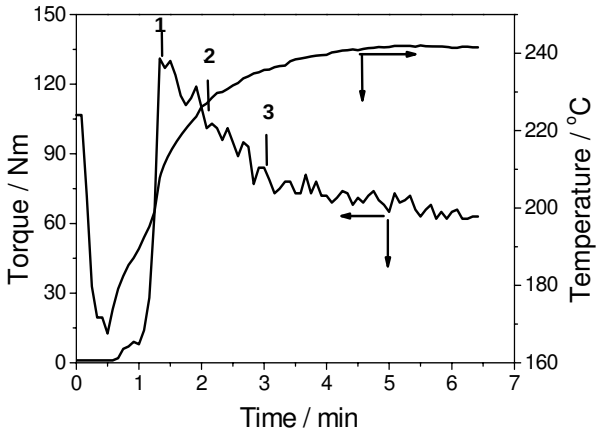


Figure 3.11 Torque and melting temperature versus time of the CL/Cat/TDI (100/6/3.6) polymerisation system. Rotate speed of screw: 65 rpm, temperature: 230 ºC.

In the process of polymerization, the high temperature and high shear may be two important factors for the degradation. However, the systems with polymerization reactions are complex so that it is difficult or even not to focus only on these two factors. In order to research these two factor, the pure PS-g-PA6 was treated for different time at 230 ºC by two methods, one is annealing treatment (static pressed at a pressure of 10 MPa) and the other is Haake mixing (mixed in Haake torque rheometer), and then was extracted in formic acid for 12 h at 30 ºC.

TEM micrographs of the phase morphologies of these above samples with various treatments were shown in Figure 3.12. From Figure 3.12 (A and B), it can be seen that whether the pure PS-g-PA6 graft copolymer was extracted in formic acid or not, their morphologies was similar and showed the behavior of typical pure copolymer. Once the pure PS-g-PA6 were treated by static annealing or haake mixing, their morphologies changed obviously into two phase structure, especially the one by Haake mixing, as shown in Figure 3.12 (C and E). It is useful to recall that for most polymers the degradation during processing is mainly due to temperature, but mechanical stress can have a synergistic effect making the thermal degradation easier and more severe. After the following extracted in formic acid, the most of the conglomeration phase is removed, as shown in Figure 3.12 (D and F). At the same time, it should also be noted their morphologies after formic treatment can't come back to the original morphology of pure PS-g-PA6. This indicates that in the condition of high temperature and high shear, PA6 grafts of PS-g-PA6 can be indeed degraded.

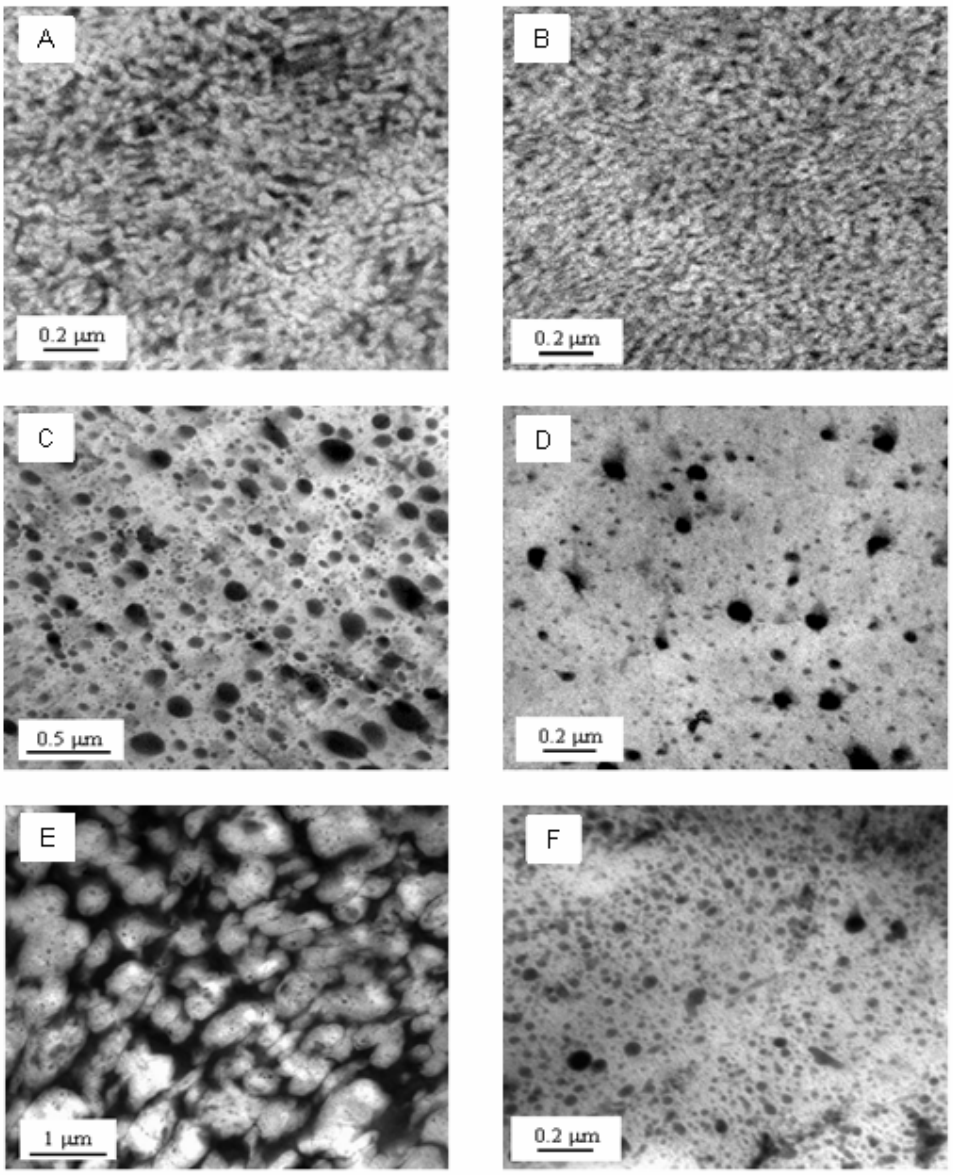


Figure 3.12 TEM micrographs of the phase morphology of various PS-g-PA6 by different treatment. A: Pure PS-g-PA6; B: Formic acid treatment 12 h at 30 ºC; C: Static annealing for 2 h at 230 ºC； D: Formic acid treatment 12 h at 30 ºC after static annealing for 2 h at 230 ºC; E: Haake mixing for 10 min at 230 ºC; F: Formic acid treatment 12 at 30 ºC after Haake mixing for 10 min at 230 ºC.

The mass percentages of soluble residue in formic acid after PS-g-PA6 treated by static annealing and Haake mixing as a function of time are shown in Figure 3.13. The treatment time being equals to zero means that the copolymer PS-g-PA6 has not any treatment but extracted in formic acid for 12 h at 30 ºC. From Figure 3.13, it can be seen that the mass percentage of residue soluble in formic acid by Haake mixing is increasing with mixing time, but the percentage of PA6 soluble in formic acid by annealing treatment has slightly increased with time, which may indicate that the

degradation of the PS-g-PA6 copolymer in the high shear at the high temperature is more prominent than that only at the high temperature. This can be further confirmed from two aspects: one is that the molar mass of residue in formic acid from the PS-g-PA6 by static annealing is lower than that by Haake mixing, as shown in Figure 3.14; the other is that the PA6 content in PS-g-PA6 by static annealing is higher than that by Haake mixing, as shown in Figure 3.15.

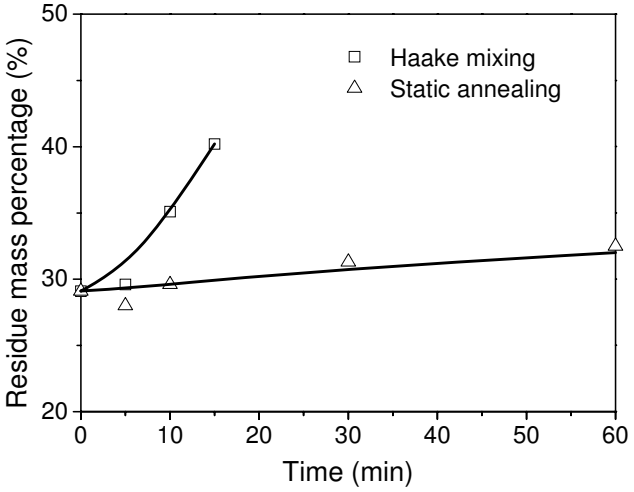


Figure 3.13 Percentage of soluble residue after PS-g-PA6 extracted in formic acid for static annealing and Haake mixing for different time at 230 ºC.

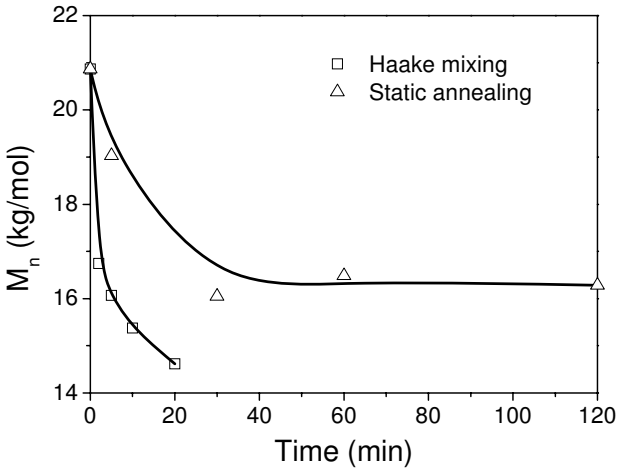


Figure 3.14 M_n of soluble residue after PS-g-PA6 extracted in formic acid for static annealing and Haake mixing for different time at 230 ºC.

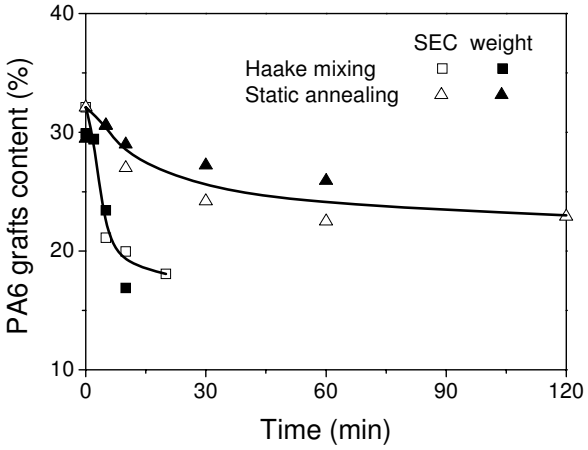


Figure 3.15 PA6 graft chain contents of PS-g-PA6 copolymers that were treated by static annealing and Haake mixing for different time at 230 ºC and then extracted in formic acid for 12 h at 30 ºC. The PA6 graft chain content obtained by two method: (1) Weight method; (2) SEC method.

The FTIR spectra of the soluble residues after PS-g-PA6 by static annealing and Haake mixing extracted in formic acid for 12 h at 30 ºC are shown in Figure 3.16. From Figure 3.16, it can be seen that two residues soluble in formic acid have not the PS characteristic peak. This implies that at static annealing or in Haake mixing, the degradation of PS-g-PA6 is mainly from the scission of PA6 grafts chain.

In addition, the FTIR spectrum of the soluble residue M after PS-g-PA6 extracted in formic acid for 12 h at 30 ºC was shown for comparison. All spectra are very similar without the appearance of new absorption peak. However, it should be noted their ratios of the peak intensity between the amide I dominated by CO stretching vibrations (1640 cm^{-1}) and amide II dominated by N-H deformation (1545 cm^{-1}) is different, which may result from that the disappearance of C(O)-NH. The ratio of residue M is the highest, and then residue N, lastly residue O, which implies the degradation is most serious in the process of Haake mixing. The aggravation of degradation can be further confirmed from that the absorption peak of C=O in -COOH (approximately 1723 cm^{-1}) is more and more obvious with PS-g-PA6 by static annealing and Haake mixing.

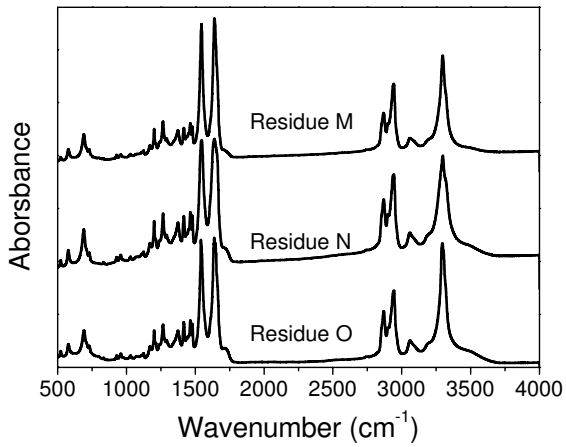


Figure 3.16 FTIR spectra of the soluble residue after PS-g-PA6 dipped in formic acid for 12 h at 30 °C. Residue M, N and O came from the PS-g-PA6 without treatment, by static annealing for 2 h at 230 ºC and Haake mixing for 10 min at 230 ºC, respectively.

In the condition of static annealing and Haake mixing, there is no proton (H^+) to attack the C(O)-NH chain like in formic acid. Therefore, the decrease of C(O)-NH may result from different mechanism. In fact, it is a well-documented phenomenon that the thermal-oxidation during processing of a polymer is the primary initiating process resulting in formation of hydroperoxides, causing subsequent degradation [122, 127,128]. The mechanism is shown in Figure 3.17. In polyamides, the hydroperoxidation of amides expected to occur mainly on the methylene carbon adjacent to the amide NH (step I, II and III). The release of a hydroxyl radical from the hydroperoxide formed in step III leads to the alkoxy radical (Step IV) either thermally or in a process catalyzed by other species in the polymer, and then formed the hydroxylated amide (step V). Once formed, the hydroxylated amide can eventually be cleaved to form an amide (step VI) and a carboxylic acid (step VI~VV). When dipped in formic acid, the amide will convert into a carboxylic acid (step VVI). This mechanism appears to be more adequate to support the results obtained from FTIR, namely, the carboxylic acid formation and C(O)NH chain decrease.

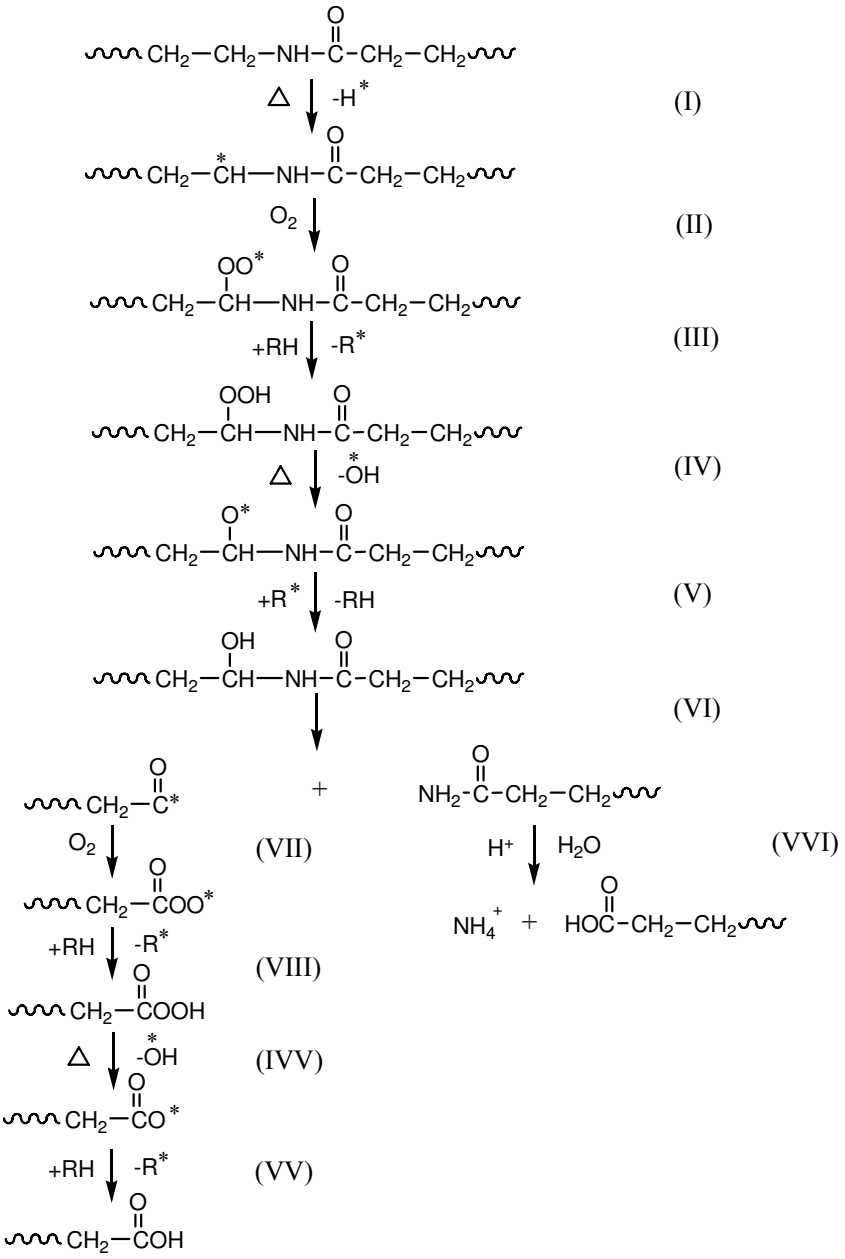
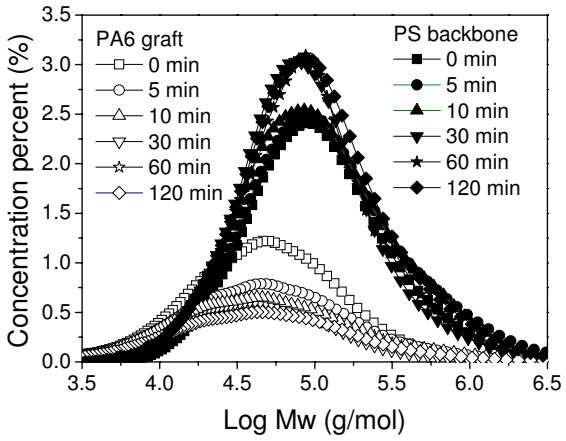
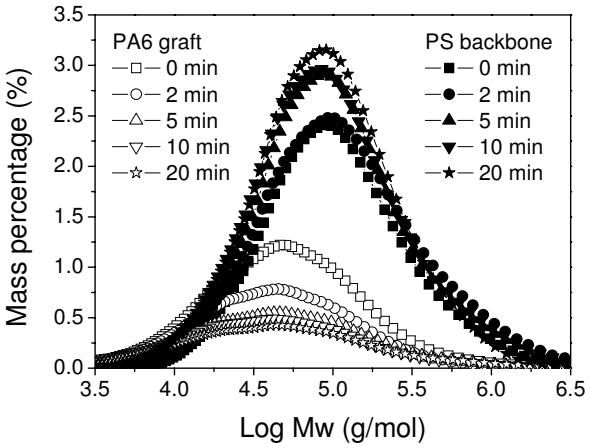


Figure 3.17 Degradation mechanism of the PA6 graft in Haake mixing or static annealing.

Figure 3.18 shows the mass percentages of the PS backbone and PA6 grafts of various PS-g-PA6 treated by static annealing and Haake mixing as a function of their molar mass. From Figure 3.18, it can be seen that the curve of mass percentage of PS backbone as a function of their copolymer molar mass is similar to that of PS-g-PA6 by only extracted in formic acid but the peak height. This may imply that PS backbone in PS-g-PA6 hasn't occurred any degradation. In addition, the mass percentage of PA6 grafts chain decreases with the increase of treatment time at static annealing or in Haake mixing, which indicates that the degradation is more and more serious with the prolong of treated time.



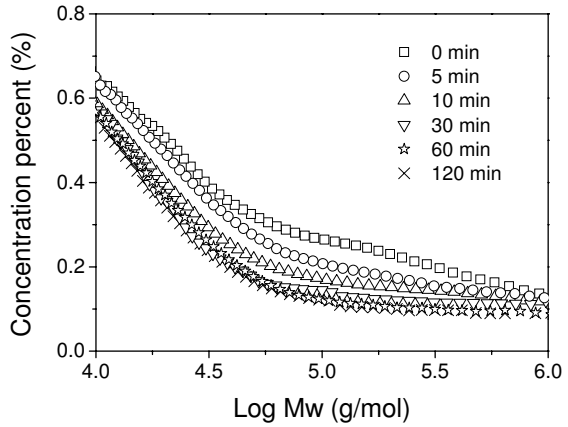
(a)



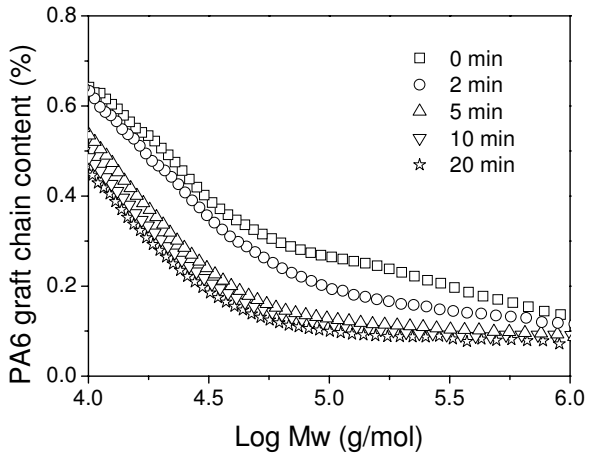
(b)

Figure 3.18 Mass percentages of the PS backbone and PA6 grafts of the PS-g-PA6 graft copolymers after dipped in formic acid for different time at 30 ºC (a) static annealing at 230 ºC for different time (0, 5, 10, 30, 60 and 120 min); (b) Haake mixing at 230 ºC for different time (0, 2, 5, 10 and 20 min)

Figure 3.19 shows that the PA6 content in PS-g-PA6 that were treated by static annealing and Haake mixing for different time at 230 ºC and then extracted in formic acid for 12 h at 30 ºC. The molar mass of PS-g-PA6 is the higher; the PA6 content is the lower. It can be concluded that PS-g-PA6 with higher molar mass will degrade more seriously. In addition, it should be noted that the polydispersity index of residue soluble in formic acid are still about 2.4 for all systems, which imply that the chains scission of PA6 grafts chain is random.



(a)



(b)

Figure 3.19 PA6 graft chain content in PS-g-PA6 graft copolymers after dipped in formic acid for different time at 30 ºC. (a) static annealing at 230 ºC for different time (0, 5, 10, 30, 60 and 120 min); (b) Haake mixing at 230 ºC for different time (0, 2, 5, 10 and 20 min)

3.4 Conclusions

The graft copolymers of PS as the backbone and PA6 as the grafts was synthesized by CL polymerized onto PS backbone via the initiation of TMI bearing PS using NaCL as catalyst. The components of raw polymerized product were investigated by various solvents extraction and found that the residue soluble in formic acid is remarkable and has not any PS or PS-co-TMI chain but Homo-PA6. The Homo-PA6 results mainly from the degradation due to the high temperature and high shear in the synthesis process of PS-g-PA6 and the acid solution in purified process. Therefore, the degradations of pure graft copolymer in the formic acid and in the high temperature and high shear were studied. The results are as following:

(1) The graft copolymer PS-g-PA6 can degrade in formic acid, which comes mainly from the cleavage of the CO-NH chain in PA6 grafts. The process of

degradation includes two stages: firstly, the degradation of PA6 graft chain occurs mainly in the copolymer with high molecular weight, which results in the mass percentage of residue soluble in formic acid increase sharply; and then, the PA6 graft chain degrade as the homogenous scission in whole polymer volume and moreover the scission rate remain constant. In addition, the degradation of PA6 grafts is more and more serious with the increase of temperature.

(2) The degradation of PS-g-PA6 in the condition of high temperature and high shear was studied by two treatments, one is static annealing and the other is Haake mixing. The TEM micrograph and mass of residue soluble in formic acid indicate the degradation of PA6 chain of PS-g-PA6 is obvious, especially in Haake mixing. The degradation of PA6 grafts results mainly from that the methylene carbon adjacent to the amide NH by thermal-oxidation forms the hydroxylated amide, and then cleaves into an amide (step VI) and a carboxylic acid.

Chapter 4 Compatibilization efficiency of graft copolymers for immiscible polymer blends

4.1 Introduction

Emulsification curves, essentially follows the evolution of the dispersed phase size with the copolymer concentration, have used to evaluate the efficiency of copolymers as emulsifiers [4-6,11-13]. It is often characterized by an initial significant decrease in the size of the dispersed phase domains with the addition of the copolymer followed by a leveling-off at higher copolymer concentrations. The shape of the emulsification curve depends both on the molar mass and molecular architecture of the copolymer and on the processing conditions.

The effect of the molecular architecture of the copolymers on the compatibilization of immiscible polymer blends has focused mainly on block copolymer. Table 4.1 gathers some literature results on the effects of the molar mass and molecular architecture of a block copolymer on its emulsification efficiency for polymer blends. The emulsification efficiency followed the order: tapered diblock > conventional diblock > triblock; a smaller molar mass > a higher molar mass.

Table 4.1 Literature results on the emulsification efficiency of copolymers.

Blend	Type of copolymer	Emulsifying effect of the copolymer
PS/EPR (90/10) [11]	SEBS (50 to 174 kg/mol; 28.6~33.3%PS); SBu (66 to 176 kg/ml; 30.0 to 45.4%PS)	Molar mass: little effect Chemical composition: big effect. SEBS (without unsaturation) was more efficient than SBu (with unstruration) because the saturated EB middle block of the SEBS had higher affinity with EPR than the unsaturated Bu.
SPS/EPR [12,13]	SEB (85 to 130kg/mol; 31%PS) for SPS/EPR (75/25); SEBS (50 to 74 kg/mol; 30 to 33%PS) for SPS/EPR (80/20)	The smaller the molar mass, the higher the emulsification efficiency because of higher diffusivity.

PS/EPR (80/20) [4]	SBu (symmetrical: 63 kg/mol, 53%PS; asymmetrical: 67 kg/mol, 30%PS)	The symmetrical one was more efficient than the asymmetrical one because the latter had higher tendency to form micelles.
PS/EPR [5]	Diblock: SEB (67 kg/mol; 30%PS); Triblock: SEBS (70 kg/mol; 29%PS)	Diblock was more efficient than triblock for PS/EPR (80/20) and less efficient for PS/EPR (90/10) because the latter had higher tendency to form micelles.
LDPE/PS (80/20)[6]	Diblock: PS-b-PB (35-35 kg/mol); Tapered diblock: PS-b-P(S-co-B)-b-PB (23-19-28 kg/mol); Triblock: PS-b-P(S-co-B)-b-PB (75-35-75 kg/mol)	The tapered diblock copolymer was the most efficient. Unlike the tapered diblock, the diblock was partly located in the PS and the triblock micellized in the LDPE.

However, the aforementioned block copolymer is mainly those based on styrene-butadiene or –isoprene block copolymers because many important polymer blends are constituted by components, whose corresponding block copolymers are difficult to prepare. In addition, the prevailing method of in-situ compatibilization results mainly from the formation of graft copolymer. Therefore, it is very important to investigate the compatiblized efficiency of the graft copolymer with different molecular architecture and/or molecular weight. Using Monte Carlo computer simulations, Gerasppe et al. [129] and Zhu et al. [130] varied the number and length of the graft chain and found that the graft copolymer with fewer and longer grafts chain can more readily localize at the interface than that with multiple and shorter grafts. Lyatskaya et al. [17,18] and Israels et al. [20] using self-consistent mean field theory also found that the graft copolymer with the longest graft chain are most efficient. However, there have been few experimental studies comparing compatibilized efficiency of graft copolymer because the control of the copolymer structure is not as easy as in the case of block copolymer. Asaletha [131] et al. studied the effect of the compatibilization of natural rubber-graft-polystyrene in natural rubber/polystyrene blends and observed a better interfacial action when graft copolymers with a higher molecular weight of PS grafted segments were employed. Soares et al. [15] prepared the graft copolymer of poly(ethylene-co-vinyl acetate) (EVA) grafted with polystyrene (PS) with different molecular weight and different EVA/PS ratio by coupling reaction

between acyl chloride functionalized PS and hydrolyzed EVA and investigated the effect of EVA-g-PS on the compatiblization of PS/EVA blends. They found that substantial improvement in the elongation at break and ductility using the graft copolymer with PS segments with molecular weight as high as 66000 g/mol and with a PS proportion equal to higher than EVA. Kvist and Bertilsson [21] studied the interfacial activity of the poly(styrene-g-ethylene oxide) (PS-g-EO) copolymer in binary incompatible mixtures of polymers having different degree of miscibility toward the graft copolymer components. They found the effect of the graft copolymer PS-g-EO is moderate in the PS/PEO blends while the structure of PS-g-EO is very importance for the PS/PMMA blend system where a negative heat of mixing between the graft copolymer and one of the blend components. Feng et al. [132] found the effect of linear low density polyethylene-g-polystyrene (LLDPE-g-PS) on the supermolecular structure of LLDPE in the LLDPE/SBS blends obviously depends on the composition of the blends, but has little dependence on the PS grafting yields of LLDPE-g-PS. Lyatskaya et al. [18] adapted the formalism derived by Leibler for the interfacial activity of diblocks and applied the theory to graft copolymer. They concluded that the symmetric graft are the most efficient when ratio of the homopolymer A and homopolymer B is 1; when the ratio is not 1, the optimal composition of the graft copolymer is shifted from symmetry. Thus the optimal copolymer composition depends on the relative volume fraction of homopolymers in the blend. In addition, the graft copolymer is different with the block copolymer in that the former has the difference of backbone and grafts. For example, Zhu et al. [130] found by using Monte Carlo simulation that A-g-B (A was backbone) copolymer was more effective to compatibilize the blend if homopolymer A formed the dispersed phase than that formed the matrix. Therefore, the effect of copolymer as compatibilizer is directly related with backbone homopolymer as the matrix or graft homopolymer as the matrix.

In order to investigate the efficiency of graft copolymer PS-g-PA6 as compatibilizer in PS/PA6 blend with Homopolymer PS as the matrix or Homopolymer PA6 as the matrix, two composition of PS/PA6 blend systems (80/20) and (20/80) was studied. The former is PS as the matrix and PA6 as the dispersed phase, the latter is PA6 as matrix and PS as the dispersed phase. A series of graft copolymers of PS and PA6, denoted as PS-g-PA6, with different molecular structures and/or molar masses were used as compatibilizers. The characteristics of these graft copolymers, PS, and PA6 were shown in Applex section.

4.2 Experimental

4.2.1 Blending process

Polymer blends were prepared by mixing the components in a Haake torque rheometer (HBI systems 90) equipped with a mixing chamber and two rotors inside the mixing chamber. Two blend compositions of PS/PA6 are studied: one is 80/20, which PA6 is the dispersed phase; the other is 20/80, which PS is the dispersed phase. For the compatibilized blend systems, the concentration of the PS-g-PA6 graft copolymer in the blends was 2.5, 5, 7.5, 10, 15% and 20% (only for PS/PA6 (20/80) blend systems) with respect to the dispersed phase. Prior to mixing, the PS, PA6 and PS-g-PA6 were dried in a vacuum oven at 80 ºC for 12 h. The dried blend components were charged simultaneously to the mixing chamber and were mixed at 65 rpm and 230 °C for 8 min. Samples were taken from the mixing chamber and then quenched in liquid nitrogen to freeze-in their morphologies.

4.2.2 Rheological characterization

The rheological behaviors of the PS, PA6 and their blends were carried out using a parallel plate rheometer of type RDA3 (Rheometric scientific, USA). A dynamic mode was used to measure the complex viscosity as a function of frequency. The samples were disks of 25 mm in diameter and about 0.8 mm in thickness. The strain amplitude was set 10%, which is in the range of the linear viscoelastic shear oscillation. The test was performed within the frequency range from 100 to 0.1 rad/s.

4.2.3 Characterization of blend morphologies

A scanning electron microscopy (SEM) of type JEOL JSM-T330A was used to characterize the blend morphologies. Before the SEM observations, samples were first fractured in liquid nitrogen. The fractured surfaces were then immersed in formic acid to remove the dispersed phase PA6 for PS/PA6 (80/20) blends or in THF remove the dispersed phase PS for PS/PA6 (20/80) blends at room temperature for 12 h. They were dried for 12 h in the vacuum oven at 80 ºC and then gold sputtered for measurement.

The diameter of the dispersed phase domains was measured using a semi-automatic image analysis method. It was characterized by two quantities: volume average particle diameters, d_v, and volume-to-surface area average particle diameters, d_{vs}, defined as:

$$d_v = \frac{\sum n_i d_i^4}{\sum n_i d_i^3} \tag{4.1}$$

$$d_{vs} = \frac{\sum n_i d_i^3}{\sum n_i d_i^2} \tag{4.2}$$

For each blend at least 500 particles were counted for statistically meaningful values of d_v and d_{vs}.

4.3 Results and discussion

4.3.1 Rheology

Figure 4.1 shows the complex viscosity (η^*) at 230 ºC of PS, PA6 and their blends with a mass composition of 80/20 and 20/80 as a function of frequency. At low frequency, the complex viscosity of PA6 was lower than that of PS. Those of the PS/PA6 blends were in between those of PS and PA6, as expected. At high frequency, the complex viscosities of PS, PA6 and their blend became close.

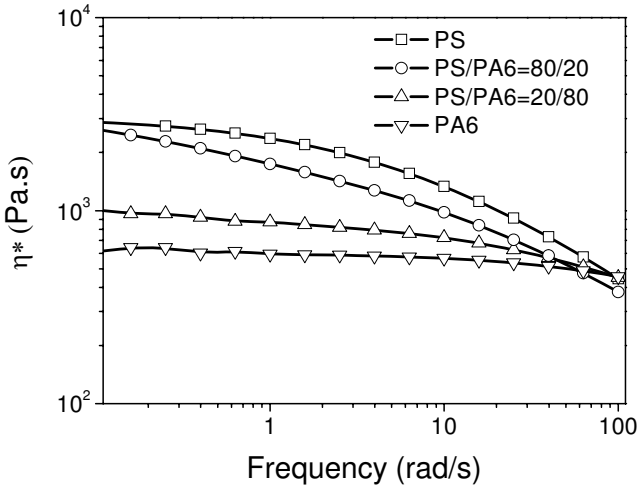


Figure 4.1 Complex viscosity vs. frequency for the PS, PA6 and PS/PA6 blends (80/20, 20/80) blend at 230 ºC.

4.3.2 Effect of PS-g-PA6 graft copolymer for PS/PA6 (20/80) blend system

Figure 4.2 and Figure 4.3 compare, respectively, the SEM micrographs and emulsification curves of PS/PA6 (80/20) blend systems without and with PS-g-PA6a,

PS-g-PA6b, PS-g-PA6c and PS-g-PA6d as the compatibilizers. The addition of compatibilizers can decrease obviously the size of dispersed phase. More interestingly, the size of dispersed phase followed the order: PS-g-PA6d < PS-g-PA6c < PS-g-PA6b < PS-g-PA6a, which indicates that the structure and composition of PS-g-PA6 has a significant effect on the dispersed phase size. PS-g-PA6b and PS-g-PA6c were similar in the PS backbone length and same in number of PA6 but different in the PA6 graft length (see Table A.2). The number-average molar mass of each PA6 graft was 1.5 and 2.4 kg/mol for PS-g-PA6b and PS-g-PA6c, respectively. It is obvious that the longer the PA6 grafts, the smaller the final PA6 particle, thus higher the compatibilization efficiency. PS-g-PA6a and PS-g-PA6b have similar PS backbone and backbone/grafts composition ratio but different in the length and number of PA6 graft. More specifically, the number of the PA6 grafts per PS backbone of PS-g-PA6a was about two times of the PS-g-PA6b but the length of the PA6 grafts of PS-g-PA6a was only about half of PS-g-PA6b. From the SEM micrographs (Figure 4.2) and emulsification curves (Figure 4.3), it can be seen that the dispersed phase size of the blends with PS-g-PA6a as the compatibilizer is higher than that of PS-g-PA6b, which indicates that graft copolymers having fewer and longer grafts were more efficient at compatibilizing the immiscible polymers. It can be further supported by the comparison of the compatibilization efficiency of PS-g-PA6c and PS-g-PA6d. Although the number of the PA6 grafts per PS backbone of PS-g-PA6d was about half of that of PS-g-PA6c and the length of the PA6 of the former was only about one and half of that of the latter, the dispersed phasesize of the blends with the former as compatibilizer is lower than that of the latter. Lyatskaya et al. [17, 18] and Israels et al. [20] using self-consistent mean field theory also found that the graft copolymer with the fewer and longer graft chain are more efficient.

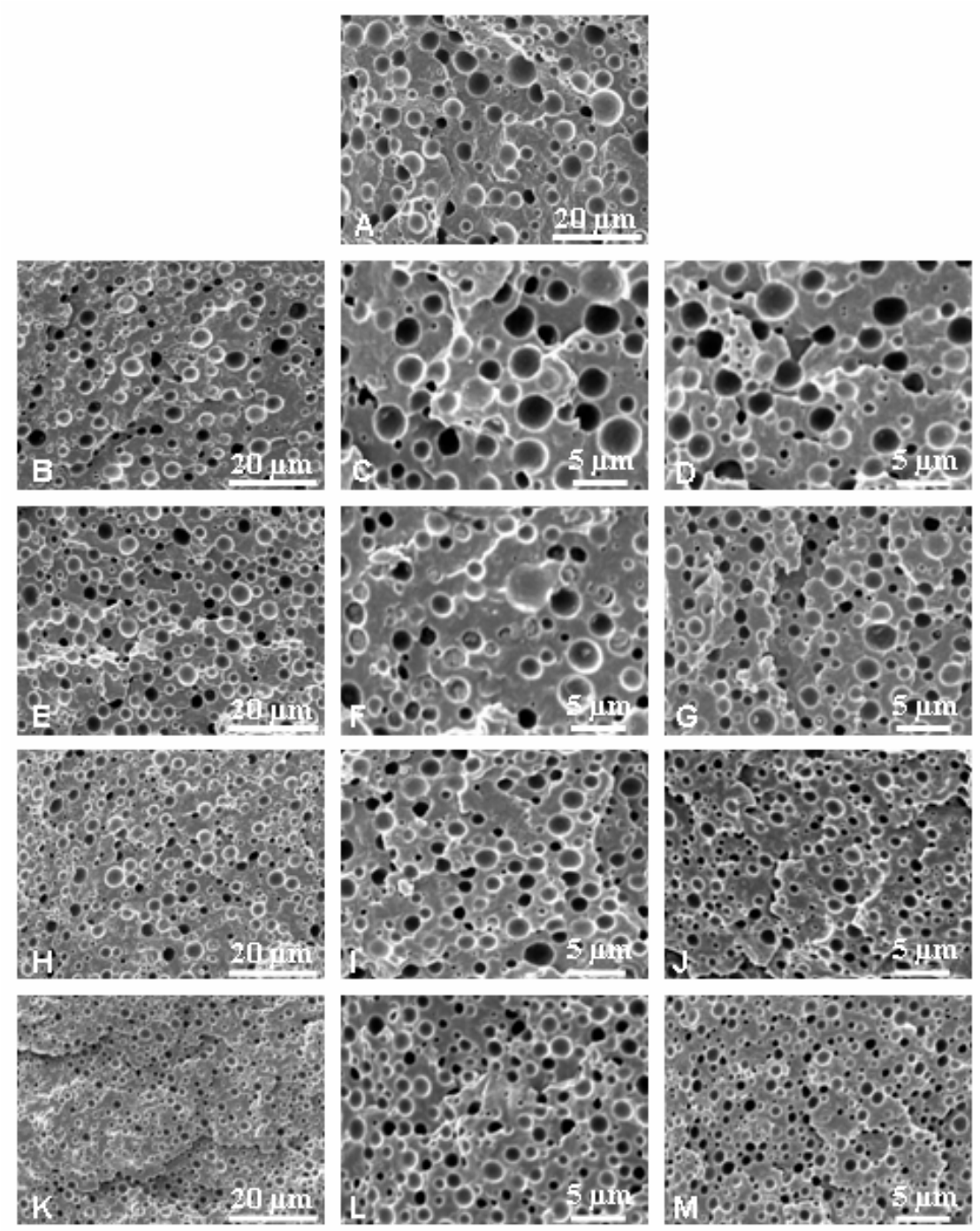


Figure 4.2 SEM micrographs of microtomed surface for the various PS/PA6 (20/80) blends: (A) without PS-g-PA6, (B) PS-g-PA6a (5%), (C) PS-g-PA6a (10%), (D) PS-g-PA6a (15%), (E) PS-g-PA6b (5%), (F) PS-g-PA6b (10%), (G) PS-g-PA6b (15%), (H) PS-g-PA6c (5%), (I) PS-g-PA6c (10%), (J) PS-g-PA6c (15%), (K) PS-g-PA6d (5%), (L) PS-g-PA6d (10%) and (M) PS-g-PA6d (15%). The compatibilizer concentration was based on the dispersed phase concentration. Mixing temperature: 230 ºC; mixing time: 8 min and rotation speed: 65 rpm.

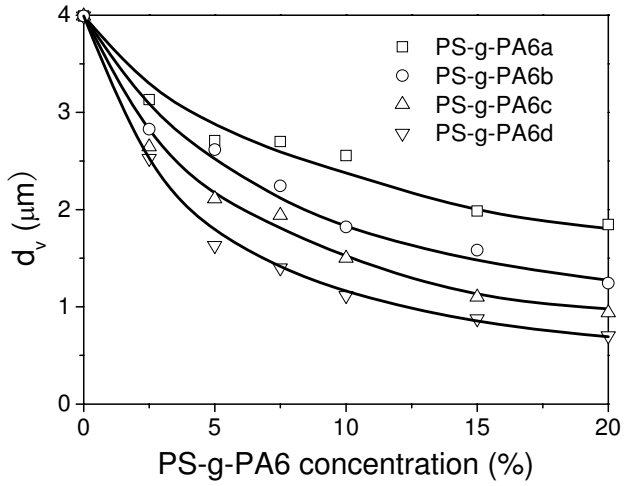


Figure 4.3 Effect of PS-g-PA6 structure and composition as the compatibilizer on emulsification curves of the PS/PA6 (20/80) blend. The PS-g-PA6 concentration bases on the mass of the dispersed phase. Mixing temperature: 230 ºC, mixing time: 8 min; rotation speed: 65 rpm. Symbols: experimental data; lines: trend line.

4.3.3 Effect of PS-g-PA6 graft copolymer for PS/PA6 (80/20) blend system

Figure 4.4 and Figure 4.5 compare, respectively, the SEM micrographs and emulsification curves of PS/PA6 (80/20) blends without and with PS-g-PA6a, PS-g-PA6b, PS-g-PA6c and PS-g-PA6d as the compatibilizers. It can be seen that the dispersed phase size followed the order: PS-g-PA6d < PS-g-PA6c < PS-g-PA6b ≈ PS-g-PA6a. Therefore, it can be concluded that for a given PS backbone and number of PA6 grafts per PS backbone, the copolymer with the longer PA6 grafts was more efficient, which can be seen from the comparison of PS-g-PA6b and PS-g-PA6c as compatibilizers; for a given backbone/graft composition, graft copolymers having fewer and longer grafts were more efficient as compatibilization, which can be seen from the comparison PS-g-PA6c and PS-g-PA6d as compatibilizers. However, it should be noted that it is different with the results obtained from the comparison of PS-g-PA6a and PS-g-PA6b as compatibilizers. This may imply that at a given lower grafts/backbone composition ratio, the structure and composition of the graft copolymers have less effect on the compatibilization efficiency; when the grafts/backbone composition ratio is higher, the graft copolymers having fewer and longer grafts were more efficient as compatibilizer.

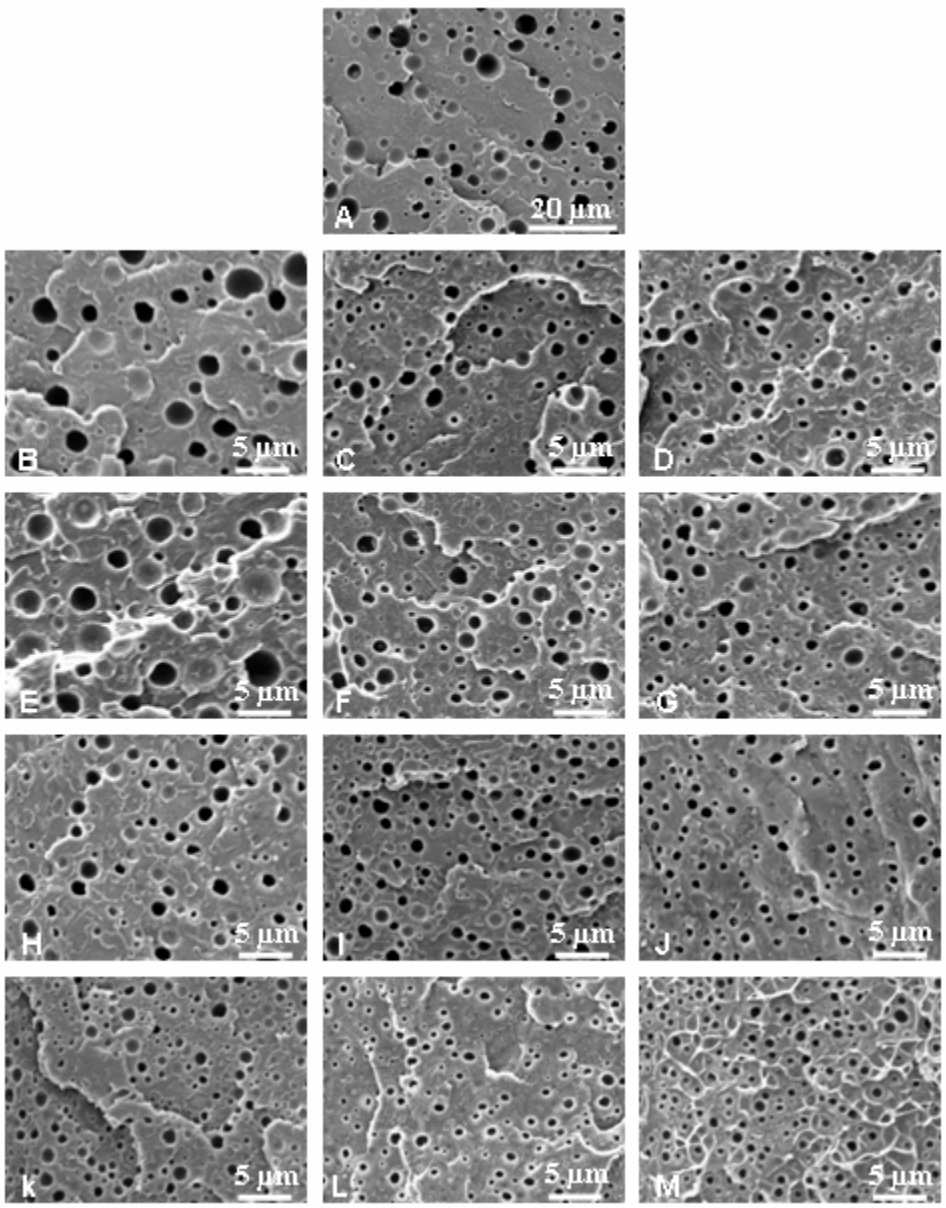


Figure 4.4 SEM micrographs of microtomed surface for the various PS/PA6 (80/20) blends: (A) without PS-g-PA6, (B) PS-g-PA6a (5%), (C) PS-g-PA6a (10%), (D) PS-g-PA6a (15%), (E) PS-g-PA6b (5%), (F) PS-g-PA6b (10%), (G) PS-g-PA6b (15%), (H) PS-g-PA6c (5%), (I) PS-g-PA6c (10%), (J) PS-g-PA6c (15%), (K) PS-g-PA6d (5%), (L) PS-g-PA6d (10%) and (M) PS-g-PA6d (15%). The compatibilizer concentration was based on the dispersed phase concentration. Mixing temperature: 230 ºC; mixing time: 8 min and rotation speed: 65 rpm.

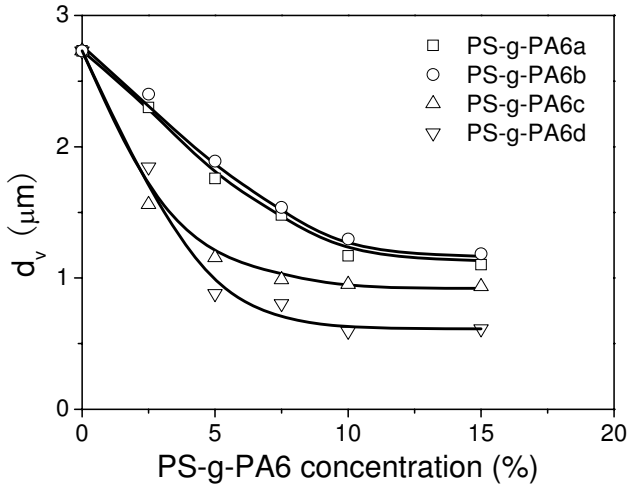


Figure 4.5 Effect of PS-g-PA6 structure and composition as the compatibilizer on emulsification curves of the PS/PA6 (80/20) blend. The PS-g-PA6 concentration bases on the mass of the dispersed phase. Mixing temperature: 230 ºC, mixing time: 8 min; rotation speed: 65 rpm. Symbols: experimental data; lines: trend line.

4.3.4 Comparison of two blend systems

The above results have shown the efficiency of graft copolymer as compatibilizer: for PS/PA6 (20/80) blend systems: PS-g-PA6d > PS-g-PA6c > PS-g-PA6b > PS-g-PA6a; for PS/PA6 (80/20) blend systems: PS-g-PA6d > PS-g-PA6c > PS-g-PA6b ≈ PS-g-PA6a. It can be seen that the PS/PA6 blend composition has less effect on the compatibilization efficiency of PS-g-PA6 with different composition and structure but the graft copolymer with lower grafts/backbone ratio and more number of PA6 grafts per PS backbone (PS-g-PA6a). This may result from PS-g-PA6a being highly soluble in PS phase and will be discussed in the following part. In addition, two obviously differences can be seen irrespective of the structure of composition of PS-g-PA6: one is the critical concentration of graft copolymer; the other is the dispersed phase size.

Firstly, let us focus on that the first difference. Contrasting Figure 4.3 to Figure 4.5, it can be seen that for PS/PA6 (80/20) blend systems, the critical concentration of PS-g-PA6, was defined as the concentration when the dispersed phase size reached constant in emulsification curves, is about 10% irrespective of the composition and structure of PS-g-PA6; while for PS/PA6 (20/80) blend systems, the critical concentration of PS-g-PA6 is higher than 20%. The difference of critical concentration may mainly result from the difference of copolymer reaching the interface of immiscible polymer blend.

The interface coverage (Σ) of copolymer, which is defined as the number of

copolymer chains per unit area, has been used to understand the interface characterization of the compatibilization polymer blend. Σ can be estimated by:

$$\Sigma = \frac{w_{gcp}\rho_d N_{av} d_{vs}}{6\phi_d M_n} \tag{4.3}$$

where w_{gcp} is the mass fraction of the graft copolymer in the blends, ρ_d is the density of dispersed phase, N_{av} is Avogadro's number, ϕ_d is the mass fraction of the dispersed phase and M_n is the number average molar mass of the graft copolymer. The values of ρ_d of PS and PA6 at 230 ºC are 0.93 and 0.97 g/cm^3, respectively [133]. The values of M_n of PS-g-PA6 graft copolymers was estimated by SEC based on PS standards and are shown in Table A.2. Eq. (4.3) was used to calculate Σ with the following assumptions. First, all the graft copolymers added to the blends resided at the interface between PS and PA6. Second, no micelles were formed in the blend systems. The maximum interfacial coverage (Σ_{max}) can be estimated by using a scalling relation $\Sigma_{max} \sim M^{-1/3}$ [22, 23]. Jeon et al. [59] had estimated Σ_{max} values of 0.21 chain/nm^2 for a block copolymer of PS and polyamide 66 (PS-b-PA66) with *Mn* of 44.0 kg/mol based on PS standards. Assuming that for a given *Mn*, PS-g-PA6 and PS-b-PA66 have the same Σ_{max} valued, the Σ_{max} values estimated are 0.25, 0.25, 0.24 and 0.23 chain/nm^2 for PS-g-PA6a, PS-g-PA6b, PS-g-PA6c and PS-g-PA6d, respectively. Table 4.2 shows the normalized interfacial coverage (Σ/Σ_{max}). The ratio of Σ/Σ_{max} being above unity implies generally that a portion of copolymer existed in the matrix or dispersed phase. Moreover, the value of Σ/Σ_{max} is the higher, the more copolymers are not in the interface. For the blend with PS-g-PA6, the values of Σ/Σ_{max} obtained from PS/PA6 (20/80) blend system are still higher than that from PS/PA6 (80/20) blend system, which indicates that PS-g-PA6 is more difficult to reach the interface of PS and PA6. Those results were not fully expected and remain poorly understood.

Table 4.2 Normalized interfacial coverage (Σ/Σ_{max}) for PS/PA6/PS-g-PA6 blends.

PS-g-PA6	Σ/Σ_{max}											
	PS/PA6/PS-g-PA6=80/20/x[a]						PS/PA6/PS-g-PA6=20/80/x[a]					
	2.5	5	7.5	10	15	20[b]	2.5	5	7.5	10	15	20
PS-g-PA6a	0.8	1.1	1.5	1.6	2.2	2.9	1.0	1.7	2.6	3.5	3.8	4.7
PS-g-PA6b	0.8	1.2	1.5	1.7	2.2	2.9	0.9	1.7	2.2	2.3	3.0	3.2
PS-g-PA6c	0.5	0.8	1.0	1.3	1.9	2.5	0.8	1.3	1.8	1.9	2.1	2.4
PS-gPA6d	0.5	0.5	0.7	0.7	1.1	1.5	0.7	0.9	1.2	1.3	1.5	1.6

(a) x is the PS-g-PA6 mass concentration based on the mass of the dispersed phase.

(b) The size of dispersed phase equals to the equilibrium size.

In the case of PS/PA6 (80/20) blend systems, PS (matrix), PA6 (dispersed phase) and PS-g-PA6 (compatibilizer) were charged to and mixed in the mixer at the same time. In the blend process, PS started to be molten first, followed by PS-g-PA6 and then PA6. After PS and PS-g-PA6 are molten and before PA6 was molten, the PS-g-PA6 was dispersed in PS Phase. As PA6 gradually melted, the molten fraction was concomitantly dispersed in the molten mixture of PS and PS-g-PA6. PA6 droplets can move to PS-g-PA6 and contact with PS-g-PA6 or PS-g-PA6 can move to and wrap the PS-g-PA6 droplets. Lastly, PA6 droplets were then stabilized by PS-g-PA6. For PS/PA6 (20/80) blend system, the molten process of PS, PA6 and PS-g-PA6 is uniform with that for PS/PA6 (80/20) blend system. The dispersed phase PS first was molten and acted as the matrix at this stage. As PS-g-PA6 gradually melted, PS-g-PA6 was dispersed in the temporary matrix PS. Once PA6 start to be molten, the temporary matrix PS will give place to PA6 and become the dispersed phase. However, PS-g-PA6 may still be dispersed in the PS phase. Thus, at this time, the polymer blends form three phase structure: the PS phase was dispersed in the PA6 matrix, on the one hand; the copolymer PS-g-PA6 formed micelles in the PS disperse phase, on the other hand. And then, PS-g-PA6 will move to the interface and lastly stabilized the morphology. The schematic diagrams of morphology formation mechanism of two blend systems are shown in Figure 4.6.

From Figure 4.6, it can be noted that two importance differences for these two blend systems. One is the way of PS-g-PA6 reaching the interface: for PS/PA6 (80/20) blend system, the dispersed phase PA6 can move toward to the copolymer and the copolymer also can move toward to the PA6 particle, moreover, the mechanics mixing can accelerate the movement; while for PS/PA6 (20/80) blend system, the copolymer can reach the interface of PS and PA6 only by its diffusion in the PS dispersed phase. This indicates that the copolymer is easier to reach the interface for PS/PA6 (80/20) blend systems. The other is the behavior of copolymer warping the dispersed droplet after reaching the interface. As above mechanism shown, before PA6 molten, PS-g-PA6 copolymer dispersed in PS phase is in the form of backbone PS embracing the grafts PA6. When PS-g-PA6 is close to the interface, for PS/PA6 (80/20) blend system, the dispersed droplet can directly move into the grafts embraced by backbone and the curvature of the backbone decrease and become more and more plat; while for PS/PA6 (20/80) blend system, grafts first must break the encirclement of backbone before inserting into the PA6 matrix, that is, the structure of the copolymer must reserve to make PA6 outward. This can be the second reason that the critical

concentration of graft copolymer for PS/PA6 (20/80) is higher than that for PS/PA6 (80/20).

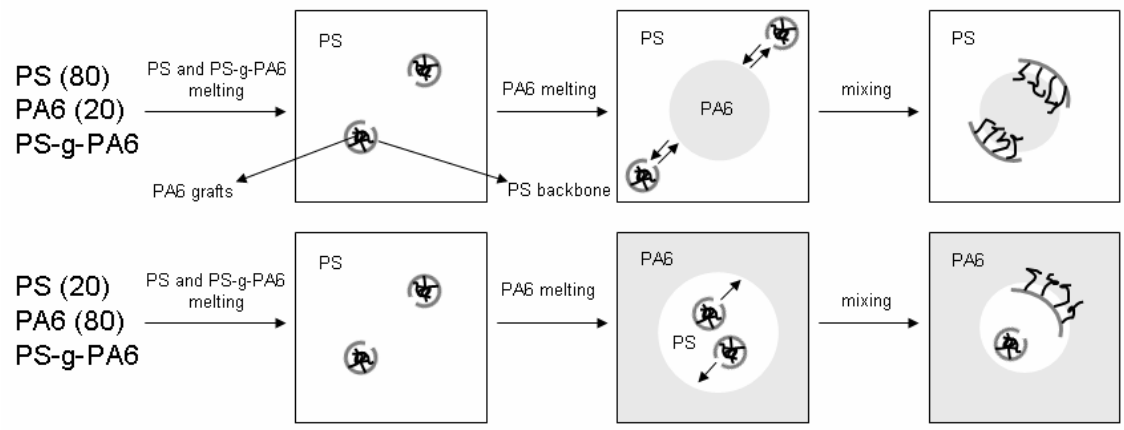


Figure 4.6 Schematic diagrams of the morphology formation process for PS/PA6 (80/20) and (20/80) blend systems with PS-g-PA6 as the compatibilizer.

The second difference is the dispersed phase size. For the blend systems without PS-g-PA6, the dispersed phase sizes of PS/PA6 (20/80) blend systems are bigger than that of PS/PA6 (80/20) blend systems. To quantify the asymmetry effect of PS/PA6 blend composition on the dispersed phase size, an asymmetry index, φ, may be defined as

$$\varphi = (d_v)_{PS} / (d_v)_{PA6} \tag{4.4}$$

where $(d_v)_{PS}$ and $(d_v)_{PA6}$ are the average size of dispersed phase PS and PA6 for the blends whose compositions are just reverse. More specific, $(d_v)_{PS}$ and $(d_v)_{PA6}$ is the dispersed phase size of PS/PA6 (20/80) and PS/PA6 (80/20) blend systems, respectively. Table 4.3 shows the value of φ. The value of φ is 1.5, which means that the size of PS as dispersed phase is bigger than that of PA6 as dispersed phase. This may be result from the viscosity difference of PS and PA6. Wu proposed the following equation to predict the particle size for polyamide and polyester blends contain 15% ethylene-propylene rubber as a dispersed phase. The positive exponent is for $\eta_r > 1$, while the negative exponent is for $\eta_r < 1$.

$$\overline{d} = 4\gamma\eta_r^{\pm 0.84} / G\eta_m \tag{4.5}$$

where $\overline{d}$ is the diameter of the droplet, G is the shear rate, γ is the interfacial tension and η_r is the viscosity ratio, equals to η_d/η_m (η_d is the dispersed phase viscosity and η_m is the matrix phase viscosity). For our two blend systems, the size of dispersed phase

depends on the viscosity of the matrix since $4\gamma\eta_r^{\pm 0.84}/G$ is same. The PA6 phase was likely less viscous than the PS phase under the blending conditions, so the size of dispersed phase for PS/PA6 (80/20) blend systems is lower than that for PS/PA6 (20/80) blend systems. The addition of PS-g-PA6 into PS/PA6 blend systems will lead to change the value of φ. When the sizes of dispersed phase both two PS/PA6 (80/20; 20/80) blend systems with PS-g-PA6b, PS-g-PA6c and PS-g-PA6d as compatibibilizers reach a platform, the values of φ were about 1.l as shown in Table 4.3, which indicates that the dispersed phase PS size in PA6 matrix is near or similar to the dispersed phase PA6 size in PS matrix. This may imply that the addition of compatibilizer into the immiscible polymer blends can decrease or eliminate the effect of viscosity of the matrix and dispersed phase on the dispersed phase size. However, it also should be noted that for PS-g-PA6a as the compatibilizer, the values of φ is high. This may be because PS-g-PA6a has short grafts so that it is more highly soluble in PS phase than that in PA6 phase. Therefore, for the PS/PA6 (20/80) blend systems, after PS-g-PA6a was dispersed in the dispersed phase PS, it is very difficult to diffuse into the interface and make PA6 graft outward; while for the PS/PA6 (80/20) blend systems, PS-g-PA6a reaching the interface is much easier and more effective to decrease the dispersed phase size.

Table 4.3 Asymmetry index obtained from the PS/PA6 blends without and with PS-g-PA6.

PS-g-PA6	$(d_v)_{PS}$ (μm) PS/PA6/PS-g-PA6		$(d_v)_{PS}/(d_v)_{PA6}$
	20/80/20	80/20/15	
Without	3.99	2.73	1.5
PS-g-PA6a	1.81	1.13	1.6
PS-g-PA6b	1.27	1.17	1.1
PS-g-PA6c	0.98	0.92	1.1
PS-g-PA6d	0.69	0.61	1.1

4.4 Conclusions

This section focused on the emulsification efficiency of graft copolymers with different compositions and structures. The blends were composed of PS and PA6. The two PS/PA6 blend systems were studied: one is 20/80 with PS as PS the dispersed phase and the other is 80/20 with PA6 as the dispersed phase. A series of PS-g-PA6

with different molecular structures were used as compatibilizers.

The addition of PS-g-PA6 can decrease the size of the dispersed phase and the structure and composition of PS-g-PA6 have big effect on compatibilization efficiency. Irrespective of the blend composition, for graft copolymers with the same backbone and the number of grafts per backbone, the longer the grafts, the higher their compatibilizing and stabilizing efficiency; for a given backbone/graft mass ratio, the longer the grafts and concomitantly the smaller the number of grafts per backbone, the higher the compatibilizing and stabilizing efficiency of the PS-g-PA6 graft copolymer, especially for PS-g-PA6 with higher PA6 content.

By the comparison of the emulsification curve of two PS/PA6 (20/80 and 80/20) blend systems with PS-g-PA6 as compatibilizers, it can be seen that both the critical concentration and dispersed phase size for the two blend systems are obviously different. Firstly, the critical concentration for PS/PA6 (20/80) blend systems is also higher than that for PS/PA6 (80/20) blend systems. For this two blends system, their molten processes of PS, PA6 and PS-g-PA6 are uniform, PS firstly molten, followed by PS-g-PA6 and then PA6. However, for the PS/PA6 (80/20) blend systems, PS still is the matrix and PS-g-PA6 easier to reached the interface; while for the PS/PA6 (20/80) blend systems, PS-g-PA6 is dispersed in the PS phase firstly, and after PA6 molten, the PS phase containing PS-g-PA6 become dispersed phase, the PS-g-PA6 must diffuse into the interface and moreover make PA6 outward. Thus PS-g-PA6 as the compatiblilizer is more effective for PS/PA6 (80/20) blend systems. Secondly, the dispersed phase size for PS/PA6 (20/80) blend systems for a given PS-g-PA6 concentration is higher than that for PS/PA6 (80/20) blend systems, which may result from the different viscosity of PS and PA6. For the two phase blend without compatibilizer, the dispersed phase size of blend systems with higher viscosity polymer as the matrix is lower than that of blend systems with the other lower viscosity polymer as the matrix. However, the addition of compatibilizer can decrease or eliminate the effect of viscosity of the matrix and dispersed phase on the dispersed phase size.

Chapter 5 Efficiency of graft copolymers at stabilizing co-continuous polymer blends during quiescent annealing

5.1 Introduction

It is common practice to create new polymer materials with desirable properties by blending different polymers. In a two phase polymer blend, two types of morphologies can be encountered: disperse/matrix and co-continuous morphology. In general, at low concentration of one phase, the morphology is the former; increasing the concentration of the minor phase leads to the latter; at higher concentrations phase inversion leads once again to disperse/matrix morphology. The type of morphology depends not only on their volume fractions but also on the nature of the polymers (interfacial tension [134], viscosity ratio [135,136] and interface type [137]), and processing conditions [138]. Due to their interconnected nature, co-continuous morphologies have the potential to significantly widen the application range of polymer blends [139-141]. Therefore, recently there has been significant interest in polymer blends with co-continuous morphology [1-3,14,142-153].

Many studies [144-148] have focused on the stability of co-continuous morphologies under quiescent annealing conditions. On the one hand, below a critical volume fraction of the minor component, the co-continuous morphology may evolve into a dispersed morphology at isothermal annealing, implying a narrowing of the co-continuous range [144-146]. On the other hand, co-continuous morphologies can undergo significant coarsening effects under quiescent annealing condition. Yuan and Favis [147,148] found that the domain diameter increased linearly with annealing time at all annealing temperatures and for all the co-continuous polystyrene (PS)/polyethylene (PE) blends.

Block or graft copolymers whose segments are chemically identical to or have affinity with the polymer components are often used as compatibilizers to reduce the interfacial tension, promote the dispersion of one phase in another and stabilize resulting blends [1-3]. Several studies have investigated the effect of block copolymer on the boundaries of the region of co-continuity [14,149,150] and the morphologies stability of co-continuous polymer blends during quiescent annealing [148,151-153]. In each case, the addition of block copolymer narrowed down the composition range of co-continuity. Table 5.1 gathers some literature results on the effects of the molar mass and molecular architecture of a block copolymer on its efficiency at stabilizing

the co-continuous morphology of polymer blends during quiescent annealing. The efficiency of block copolymer followed the order: tapered diblock > conventional diblock > triblock; an intermediate molar mass was most efficient.

Table 5.1 Literature results on the efficiency of copolymers to stabilize co-continuous morphology.

Blend	Type of copolymer	Effect of the copolymer
PS/PE (80/20) [152,153]	Diblock: PS-b-PB (35-35 kg/mol; 50% PS); Tapered diblock: PS-b-P(S-co-B)-b-PB (23-19-28 kg/mol, 50% PS); Triblock: PS-b-P(S-co-B)-b-PS (7.5-35-7.5 kg/mol, 30% PS)	The tapered diblock copolymer was the most efficient. The superiority of the tapered diblock over the diblock and triblock might be due to its ability to quantitatively locate at the interface.
PS/PE (50/50) [148]	Diblock: SEB (33.4-29.6 kg/mol; 53% PS) Triblock: SEBS (7.5-35-7.5 kg/mol, 30% PS)	The diblock copolymer was more efficient in the suppression of the coarsening effect. The triblock had higher tendency to form micelles.
PS/PE (50/50) [14]	Four symmetric PS-PE diblock with molar masses of 6, 40, 100 and 200 kg/mol.	An intermediate molar mass PS-PE, 40 kg/mol, was most efficient. The existence of a copolymer with an optimal molar mass was due to a balance between the ability of copolymer to reach the interface and its relative stabilization effect at the interface.

The aforementioned studies are mainly focused on the efficiency of block copolymers. The work reported in this section was aimed at studying the efficiency of graft copolymers with different molecular structures and compositions at stabilizing co-continuous morphology under quiescent annealing with emphasis on the length and density of grafts. The blend system was composed of PS and polyamide 6 (PA6). A series of the graft copolymer PS-g-PA6 with different molecular structures and/or molar masses were used as compatibilizers. The characteristics of PS, PA6, and these graft copolymers were shown in the Applex section.

5.2 Experimental

5.2.1 Blend preparation

Polymer blends were prepared by mixing the components in a Haake torque rheometer (HBI system 90) equipped with a mixing chamber and two rotors inside the mixing chamber. For the compatibilized blend systems, the concentration of the as-synthesized PS-g-PA6 graft copolymer in the blends was 1% with respect to the PS/PA6 blends. Prior to the blending, the PS, PA6 and PS-g-PA6 were dried in a vacuum oven at 80 ºC for 12 h. The dried blend components were charged simultaneously to the mixing chamber and were mixed at 100 rpm and 230 °C for 10 min. Samples were taken from the mixing chamber and then quenched in liquid nitrogen to freeze-in their morphologies.

5.2.2 Quiescent annealing

Pieces of blend samples of about 20 mm thick were warped with coppery netting and then annealed in a silicon oil-bath that was preheated to 230, 235 or 240 ºC. After various annealing times (from 2 to 20 min), they were taken out from the oil-bath and then quenched immediately in liquid nitrogen to freeze-in the morphologies.

5.2.3 Solvent extraction

Solvent extraction was used to check if the PS/PA6 blends had a co-continuous structure or not. THF was used to dissolve out the PS or formic acid the PA6 at room temperature for 15 days, respectively. If the remaining phases, i.e., the PA6 phase after the THF extraction and PS phase after the formic acid extraction, were self-supporting without disintegration, they were considered as having a co-continuous morphology. The percentage of PS continuity was calculated based on the mass loss measurements before and after THF extraction:

$$\%Continuity = \frac{(MassPS_{init} - MassPS_{final})}{MassPS_{init}} * 100 \quad (5.1)$$

5.2.4 Mercury intrusion porosimetry

Mercury intrusion porosimetry techniques were used to characterize the microstructure of etched co-continuous blends and provided the pore diameter (*d*) [147,148]. It is based on the capillary law governing liquid penetration into small pores. This law, in the case of a non-wetting liquid like mercury and cylindrical pores, is expressed by the Washburn equation:

$$d = -(\frac{1}{P})4\gamma\cos\varphi \tag{5.2}$$

where P the applied pressure, γ the surface tension, and φ the contact angle, all in consistent units. The volume of mercury (V) penetrating the pores is measured directly as a function of applied pressure. This P-V information serves as a unique characterization of pore structure. The surface tension of mercury used here is 0.485 N/m. The contact angle between mercury and the solid is 130 degrees.

Pores are rarely cylindrical. Hence the above equation constitutes a special model. Such a model may not best represent pores in actual materials, but its use is generally accepted as the practical means for treating what, otherwise, would be a most complex problem.

5.3 Results and Discussion

5.3.1 Rheology

Figure 5.1 shows the complex viscosity (η^*) at 230 ºC of the PS, PA6 and their blends with a mass composition of 50/50 as a function of frequency. At low frequency, the complex viscosity of the PA6 was lower than that of the PS. That of the PS/PA6 blend was in between those of the PS and PA6, as expected. At high frequency, the complex viscosities of the PS, PA6 and their blend became close.

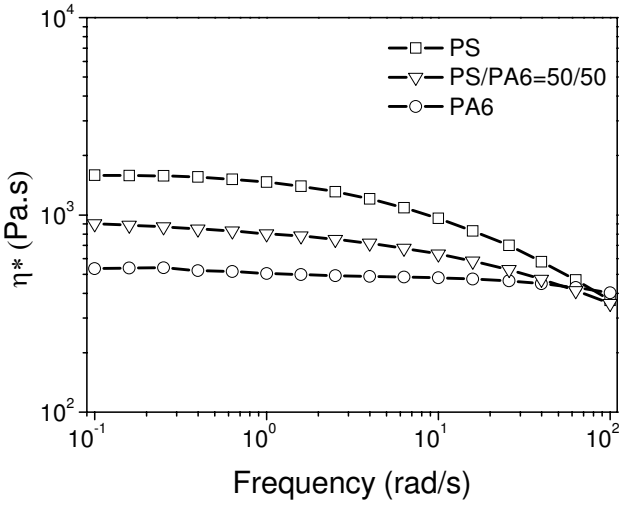


Figure 5.1 Complex viscosity vs. frequency for the PS, PA6 and PS/PA6 blends (50/50) at 230 ºC.

5.3.2 Annealing of blend systems without PS-g-PA6

Figure 5.2 shows the SEM micrographs of the PS/PA6 (50/50) blend without

PS-g-PA6 graft copolymer after quiescent annealing at different times (0, 5, 10 and 15 min) and different temperature (230, 235 and 240 ºC). Before the annealing the blend was a co-continuous structure (Figure 5.2a). After the annealing, whatever the annealing time and/or temperature, the co-continuous morphology remained. This was also confirmed by the solvent extraction results. The latter showed that for all the samples before and after the annealing, the percentage of the PS continuity defined in Eq. (5.1) reached 100%. Moreover, after one phase was extracted out, the other phase was still self-supported. However, the pore size drastically increased with increasing annealing time and/or annealing temperature, indicating that a significant coarsening process had taken place. The fact that the pore size drastically increased while the co-continuous morphology remained is very interesting.

Figure 5.3 shows the pore diameter *(d*) after the PS extracted in THF as a function of the annealing time for three different annealing temperatures. Both the annealing time and annealing temperatures had a big effect on the coarsening process. At 230 ºC, *d* increased from 23 to 62 μm in 15 min; at 240 ºC, it increased from 23 to 201 μm in 10 min. It is also noted that the pore size increased linearly with annealing time, whatever the annealing temperature. This is in agreement with the following two theories. The first one is an extension of a theory describing the disintegration of a cylinder thread immerged in another fluid, developed by Tomotika, to immiscible co-continuous blends. It was assumed that the coarsening rate *dr/dt* be directly related to the rate of growth of the distortion amplitude, $d\alpha/dt$ [147]. The growth of the average phase domain upon annealing was therefore governed by a capillary breakup process driven by interfacial tension, and a relation between phase size (*d* or *r*, the average pore diameter or radius) and annealing time (*t*) was finally obtained and expressed as:

$$\frac{d}{2} = r \sim kt \tag{5.3}$$

where *k* is the coarsening rate and is expressed as

$$k = (\alpha_0 / r_0)\frac{\sigma\Omega(\lambda, p)}{2\eta_c} \tag{5.4}$$

α_0/r_0 is the ratio of the original amplitude to the thread radius, σ is the interfacial tension, η_c is the viscosity of the continuous phase, and $\Omega(\lambda, p)$ is the Tomotika function related to the dominant wavelength, λ, and the viscosity ratio p ($p = \eta_d/\eta_c$, where η_d the viscosity of the dispersed phase).

The second theory is an extension of the Doi-Ohta theory for complex interfaces to the annealing of co-continuous polymer blends [154]. The coarsening rate of

co-continuous blends under quiescent annealing was expressed by:

$$\frac{1}{Q} = \frac{1}{Q_0} + c_1 \frac{\sigma}{\eta} t \tag{5.5}$$

where Q_0 is the specific interfacial area at zero annealing time, c_1 is a kinetic constant for size relaxation, η is the viscosity of the polymer blend. The term $c_1\sigma/\eta$ represents the coarsening rate and $1/Q$ is proportional to r. Thus, these two theories indicate that at a given temperature, the coarsening rate is constant.

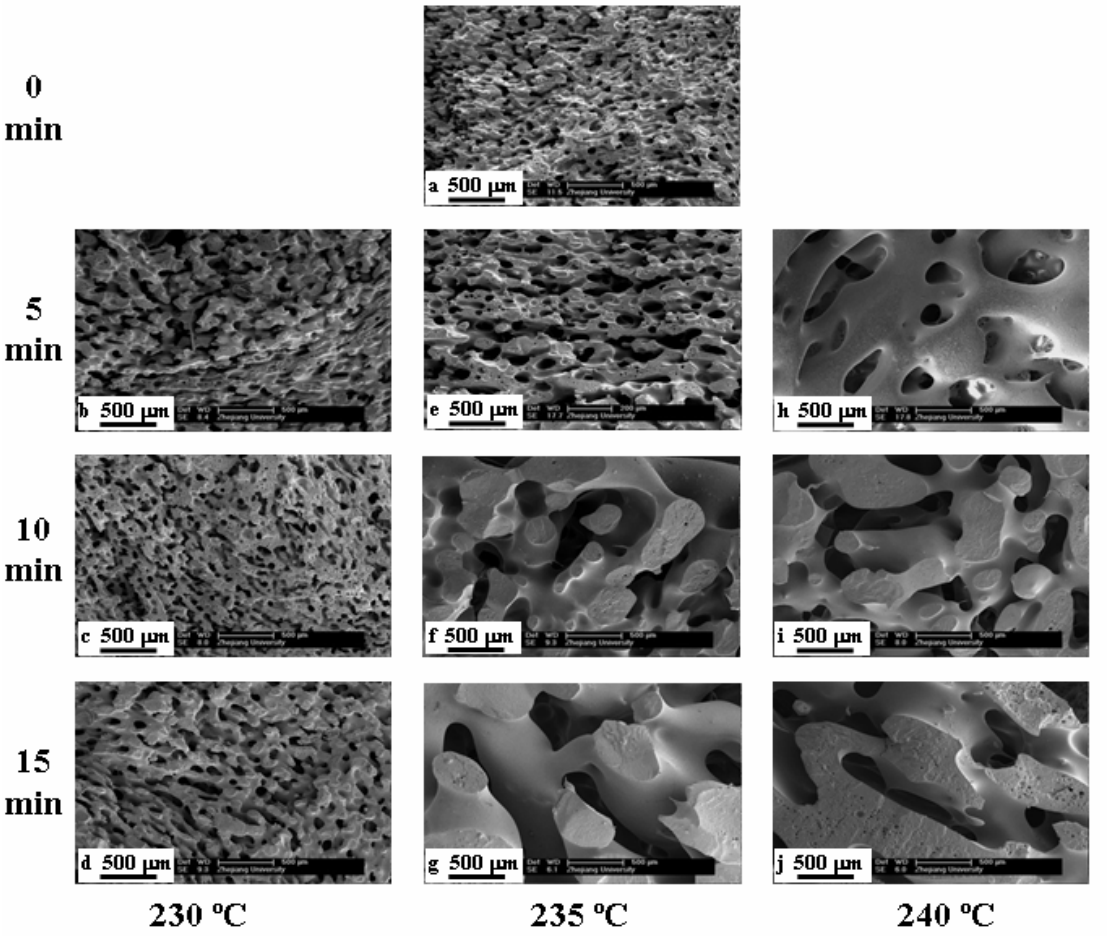


Figure 5.2 Effect of the quiescent annealing on the morphology of the PS/PA6 (50/50) blend obtained after mixing at 100 rpm at 230 ºC for 10 min. Without annealing (a); annealing at 230 ºC for 5 min (b), 10 min (c) and 15 min (d); annealing at 235 ºC for 5 min (e); 10 min (f) and 15 min (g); annealing at 240 ºC for 5 min (h), 10 min (i) and 15 min (j).

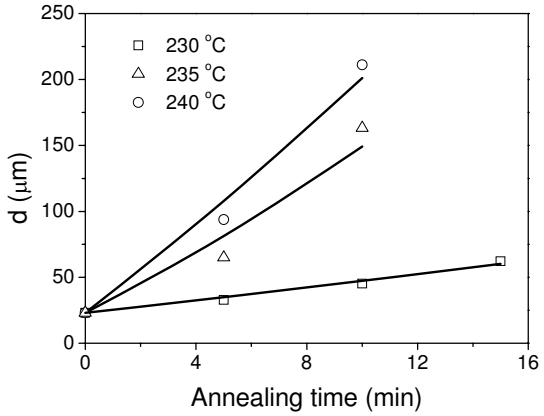


Figure 5.3 Pore diameter (*d*) vs. annealing time for the PS/PA6 (50/50) blend at different annealing temperatures (230, 235 and 240 ºC).

5.3.3 Annealing of polymer blends with PS-g-PA6

Figure 5.4 compares the efficiency of three PS-g-PA6 graft copolymers (PS-g-PA6e, PS-g-PA6f and PS-g-PA6g) at stabilizing the morphology of the PS/PA6 (50/50) blend during annealing at 240 ºC. Surprisingly, those blends did not have a co-continuous structure anymore. This is very different from the PS/PA6 (50/50) blend without PS-g-PA6. The solvent extraction showed that the region of co-continuity without and with 1 wt% of PS-g-PA6 was from 40/60 to 65/35 (PS/PA6) and from 55/45 to 65/35, respectively, indicating that the addition of the PS-g-PA6 narrowed down the composition region of co-continuity. This is consistent with the literature results using block copolymers as compatilizers [14,149,150]. It is also noted that the addition of PS-g-PA6 shifted the lower limit of the composition region of co-continuity to a higher PS/PA6 composition. However, it did not have a significant effect on its upper limit. This implies that in the presence of PS-g-PA6, the PA6 phase might have greater tendency to form the matrix than the PS phase. This could be explained as follows. First, the PA6 was likely less viscous than the PS under the blending conditions. The less viscous component has greater tendency to be the matrix [144,155,156]. Second, co-continuous structures of immiscible polymer blends are developed by droplet-droplet coalescence [137]. The presence of a copolymer reduces coalescence, stabilizes droplet morphologies and consequently disfavors the formation of co-continuous morphologies. In short, the above results seem to advise a rule that the addition of a compatibilizer tends to shift the lower limit of the co-continuity of the more viscous component to a higher value.

The size of dispersed phase of these three polymer blends before the annealing followed the order: PS-g-PA6e (Figure 5.4a) > PS-g-PA6f (Figure 5.4e) > PS-g-PA6g

(Figure 5.4i). After the annealing at 240 ºC, the dispersed phase morphology with PS-g-PA6e as the compatiblizer tended to evolve into a co-continuous morphology and the domain size increased greatly. In the case of PS-g-PA6f, the dispersed phase morphology partly evolved into a co-continuous phase morphology and the domain size increased slightly. When PS-g-PA6g was used as the compatibilizer, the dispersed phase morphology was not subjected to any noticeable change. From the above results, the efficiency of PS-g-PA6 at suppressing coarsening followed the order: PS-g-PA6e < PS-g-PA6f < PS-g-PA6g. This implies that a PS-g-PA6 with longer grafts has higher compatibilizing and stabilizing efficiency. This is in line with their emulsifying efficiency for dispersed phase blends in chapter 4.

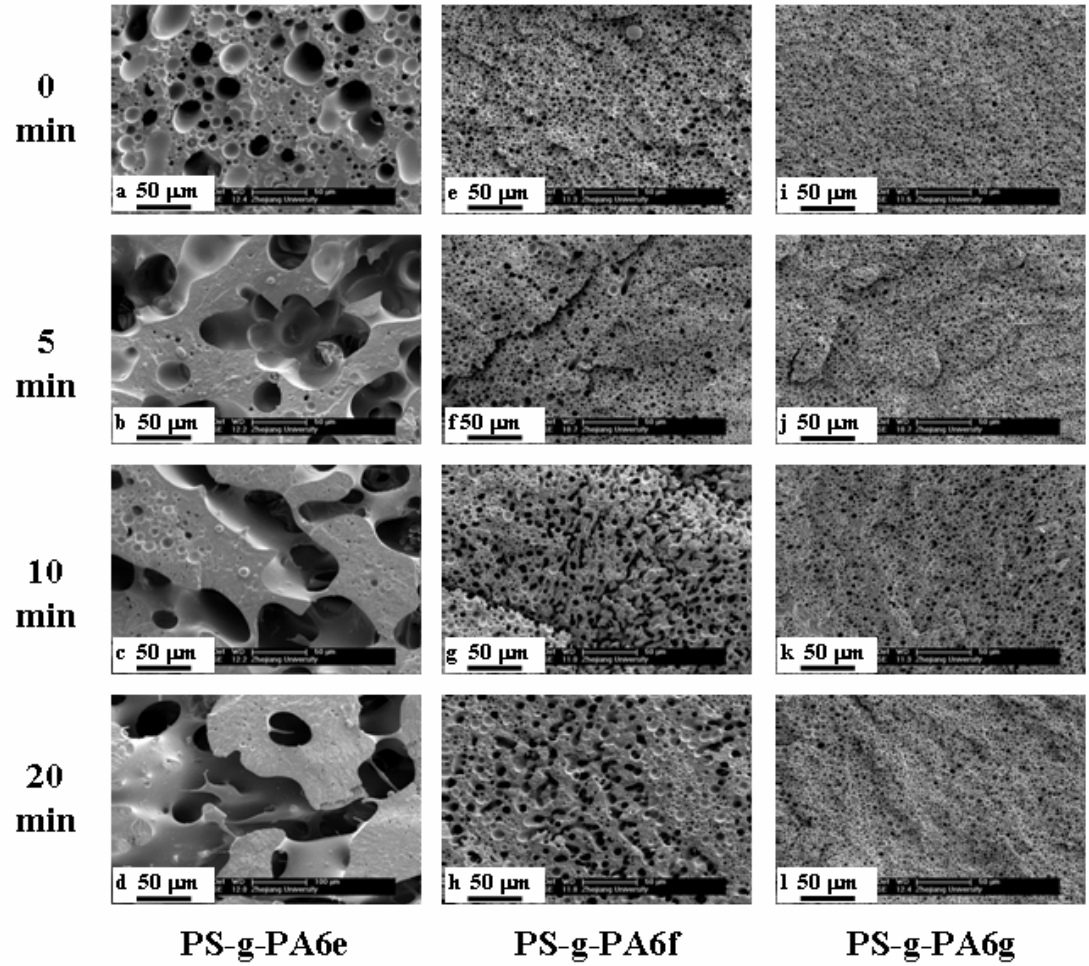


Figure 5.4 SEM micrographs of PS/PA6/PS-g-PA6 (50/50/1) blends after mixing at 100 rpm for 10 min at 230 ºC followed by annealing at 240 ºC. The blend with PS-g-PA6e as the compatibilizer was annealed for 0 (a), 5 (b), 10 (c) and 20 min (d), respectively; the blend with PS-g-PA6f as the compatibilizer was annealed for 0 (e), 5 (f), 10 (g) and 20 min (h), respectively; the blend with PS-g-PA6g as the compatibilizer was annealed for 0 (i), 5 (j), 10 (k) and 20 min (l), respectively.

Figure 5.5 shows the SEM micrographs of the PS/PA6 (60/40) blends before and after annealing at 240 ºC and without PS-g-PA6 or with 1 wt.% of PS-g-PA6e, PS-g-PA6f, PS-g-PA6g or PS-g-PA6h as the compatibilizer. The compatibilizing and stabilizing efficiency followed the order: PS-g-PA6e << PS-g-PA6f < PS-g-PA6h < PS-g-PA6g. Figure 5.6 shows the pore diameter (*d*) of the above blends as a function of the annealing time. For the blends that contained 1 wt.% of PS-g-PA6e, *d* increased linearly with annealing time. In the case of PS-g-PA6f, *d* increased in size for the first two minutes and stopped increasing in size thereafter. As for PS-g-PA6g and PS-g-PA6h, *d* did not increase at all over the entire annealing time (20 min).

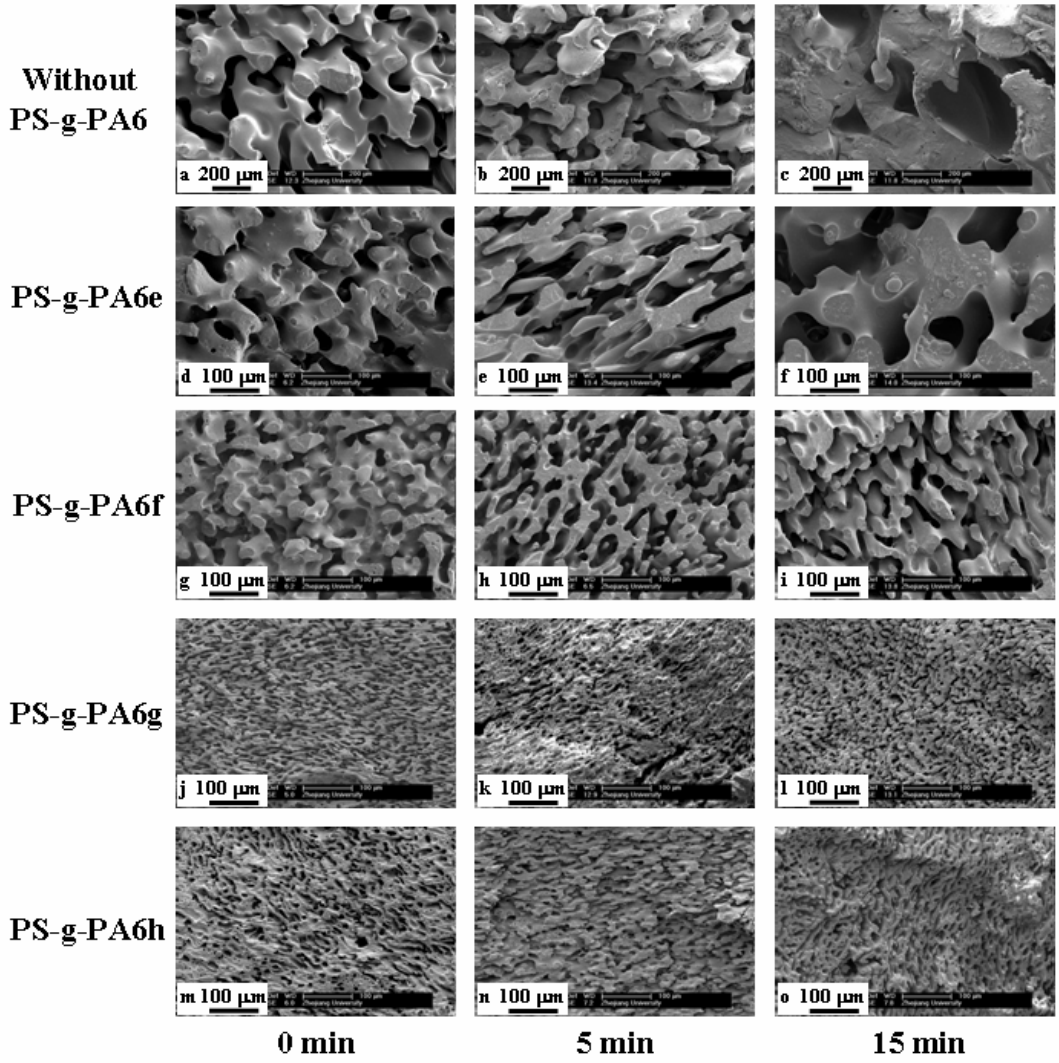


Figure 5.5 Effect of adding 1 wt.% of PS-g-PA6 graft copolymer on the morphology of the PS/PA6 (60/40) blend after mixing at 100 rpm for 10 min at 230 ºC followed by annealing at 240 ºC. Without PS-g-PA6 and annealing for 0 (a), 5 (b) and 15 min (c), respectively; with PS-g-PA6e and annealing for 0 (d), 5 (e) and 15 min (f), respectively; with PS-g-PA6f and annealing for 0 (g), 5 (h) and 15 min (i), respectively; with PS-g-PA6g and annealing for 0 (j), 5 (k) and 15 min (l), respectively; with PS-g-PA6h and annealing for 0 (m), 5 (n) and 15 min (o).

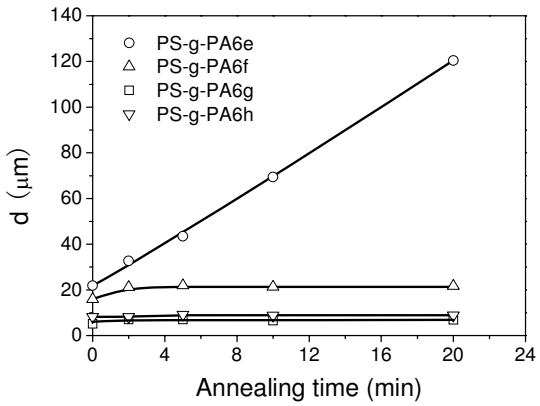


Figure 5.6 Pore diameters of the PS/PA6/PS-g-PA6 (60/40/1) blends versus annealing time at 240 ºC. The compatibilizer was PS-g-PA6e, PS-g-PA6f, PS-g-PA6g and PS-g-PA6h, respectively.

Figure 5.7 is the schematic of the molecular architectures of the four PS-g-PA6 graft copolymers. Their PS backbones were almost the same in length and their PA6 grafts were different in length and/or in number of grafts per PS backbone. More specifically, PS-g-PA6e, PS-g-PA6f and PS-g-PA6g had the same PS backbone and number of grafts per PS backbone but differed in the PA6 graft length. As for PS-g-PA6h, both its PS backbone and PS/PA6 ratio was similar to that of PS-g-PA6f. However, the number of the PA6 grafts per PS backbone of the former was only half of the latter. Based on the above results, it can be concluded that for graft copolymers with similar backbone and graft chain number, the longer the grafts, the higher their compatibilizing and stabilizing efficiency. For a given backbone/graft composition, graft copolymers having fewer and longer grafts were more efficient at compatibilizing and stabilizing the co-continuous morphology.

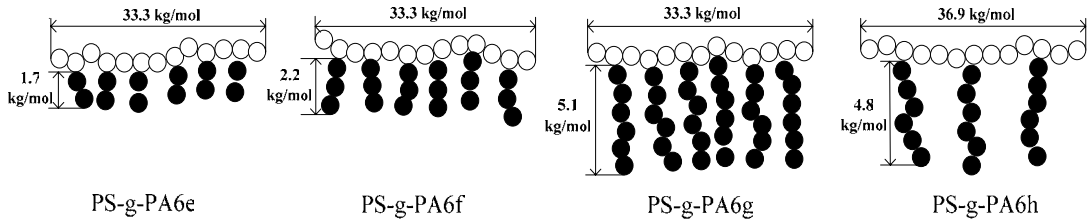


Figure 5.7 Schematic of the molecular architectures and molar masses of the four PS-g-PA6 graft copolymers used in this work.

The interface coverage (Σ) of copolymer, which is defined as the number of copolymer chains per unit area, has been used to understand the compatibilization efficiency of copolymers in immiscible polymer blends. For co-continuous blends it can be estimated by [58]:

$$\Sigma = \frac{w_{gcp}\rho_{PS}N_{av}d_{VS}}{6\phi_{PS}M_n} \tag{5.6}$$

where ϕ_{PS} the mass fraction of the PS phase and ρ_{PS} the density of homopolymer PS (0.934 g/cm^3 at 240 ºC [133]). The values of M_n of PS-g-PA6 graft copolymers was estimated by SEC based on PS standards and are shown in Table A.2. Eq. (5.6) was used to calculate Σ with the following assumptions. First, all the graft copolymers added to the blends resided at the interface between PS and PA6. Second, no micelles were formed in the blend systems. Third, the values of d_{vs} were equal to those of d obtained by the mercury intrusion porosimetry mentioned above. Table 5.2 shows the values of Σ.

The maximum interfacial coverage (Σ_{max}) can be estimated by the method in chapter 4. The Σ_{max} values are 0.23, 0.23, 0.21 and 0.23 chain/nm^2 for PS-g-PA6e, PS-g-PA6f, PS-g-PA6g and PS-g-PA6h, respectively. Table 5.2 shows the normalized interfacial coverage (Σ/Σ_{max}).

The ratio of Σ/Σ_{max} being above unity implies generally that a portion of copolymer existed in the bulk phases. For the blend with PS-g-PA6e, Σ/Σ_{max} increased from 6.50 to 35.65 during the annealing from 0 to 20 min. This indicates that a large portion of PS-g-PA6e was not at the interfaces before the annealing and that that portion increased during the annealing. The short PA6 grafts might have favored the formation of PS-g-PA6 micelles in the PS phase. In the case of PS-g-PA6f, the Σ/Σ_{max} value was 4.34 before the annealing and reached about 6 after 2 min of annealing. It did not increase anymore with further annealing. As for PS-g-PA6g and PS-g-PA6h, the Σ/Σ_{max} values increased only slightly during the annealing, indicating that the graft copolymer chains that were located in the interfaces prior to the annealing remained there during the annealing.

Table 5.2 Apparent interfacial coverage (Σ) and normalized interfacial coverage (Σ/Σ_{max}) for PS/PA6/PS-g-PA6 (60/40/1) blends before and after the annealing at 240 ºC.

Compatibilizer	Σ (chains/nm^2)		Σ/Σ_{max}	
	Before annealing	After 20 min's annealing	Before annealing	After 20 min's annealing
PS-g-PA6e	1.50	8.20	6.50	35.65
PS-g-PA6f	1.00	1.36	4.34	5.90
PS-g-PA6g	0.30	0.35	1.43	1.66
PS-g-PA6h	0.54	0.59	2.42	2.64

The interfacial thickness is also an important parameter for retarding coarsening during annealing. Noolandi et al. [157,158] predicted that longer chains of copolymer would increase the thickness of the interface, which would decrease the enthalpy of the system. Therefore, for graft copolymers with similar PS backbone and graft chain number, the longer the grafts of PS-g-PA6, the higher their compatibilizing and stabilizing efficiency. Kim et al. [159] investigated the effect of the chain architecture of graft copolymers on the characteristic of an adsorbed layer on a surface using an off-lattice Monte Carlo simulation method. They found that when the mass ratio between the backbone and grafts is fixed, the layer thickness of a graft copolymer adsorbed onto the surface decreases with increasing the number of side chains. In other words, the chain conformation of the adsorbed polymer becomes more flattened as the length of the side chain becomes shorter. This implies that the graft chain length is more important for increasing the interfacial thickness than the graft chain density. This is may explain the fact while PS-g-PA6f and PS-g-PA6h had almost the same PS/PA6 mass ratio, the latter exhibited much higher compatibilizing and stabilizing efficiency.

5.4 Conclusions

This work focused on the effect of adding a graft copolymer on the co-continuity of polymer blends, on the one hand; and their stability during quiescent annealing, on the other hand. The blends were composed of PS and PA6. A series of graft copolymers PS-g-PA6 with different molecular structures were used as compatibilizers.

The addition of PS-g-PA6 narrowed the composition range of co-continuity of the PS/PA6 blend, from 40/60 - 65/35 (without PS-g-PA6) to 55/45 - 65/35 (with PS-g-PA6). In other words, it shifted the lower composition limit of co-continuity of the more viscous polymer component to a higher value.

Be compatibilized or not, a polymer blend with a co-continuous structure before annealing remained to be co-continuous after annealing. The presence of PS-g-PA6 reduced or stopped completely the coarsening of the co-continuous morphologies of the polymer blends, depending strongly on the molecular architecture (graft length and graft density) of the PS-g-PA6 graft copolymer. For graft copolymers with the same backbone and the number of grafts per backbone, the longer the grafts, the higher their compatibilizing and stabilizing efficiency. For a given backbone/graft mass ratio, the longer the grafts and concomitantly the smaller the number of grafts

per backbone, the higher the compatibilizing and stabilizing efficiency of the PS-g-PA6 graft copolymer.

Chapter 6 Effect of feeding mode on the morphologies of immiscible polymer blends

6.1 Introduction

Table 6.1 gathers some literature results on the effect of feeding mode on the morphology of polymer blends. It is seen that the effect of feeding mode could also be very important but appeared to be blend specific. In other words, a feeding mode that was most efficient for a blend might not necessarily be so for another one, even for the same blend of a different composition. Therefore, the sections will focus on four feeding modes on the morphologies of PS/PA6 blend with PS-g-PA6f as compatibilizer. The selected characteristics of the PS and PA6 used in this work are PS-2 and PA6-2 shown in Table A.1 of Applex section. The PS-g-PA6f in Table A.2 of Applex section is used as the compatibilizer

Table 6.1 Literature results on the effects of feeding mode on the morphology of reactive blends.

Blend system	Feeding mode	Morphology
PA6/EPR/EPR-g-MA (80/15/5) [160]	One-step: all the blend components were charged to the mixer at the same time; two-step: EPR and EPR-g-MA charged first and PA6 10 min later.	Two-step much better than one-step.
PA6/PE/PE-co-acid [161]	One-step: all the blend components were charged to the mixer at the same time; two-step: PE-g-acid mixed first with the dispersed phase and then the matrix.	Two-step was better than one-step for PA6/PE/PE-g-acid (90/10/0.5) and opposite result for PA6/PE/PE-g-acid (10/90/0.5).
PA6/PP/PP-g-MA [162]	One step: all the blend components were charged to the mixer at the same time; two-step1: PP and	Similar morphologies for the one step and two-step1 and finest morphology for the

	PP-g-MA charged first and then PA6; two-step2: PA6 and PP-g-MA charged first and then PP.	two-step2.
PA6/PP/PP-g-MA [53]	Two step: PP was first functionalized with MA in an extruder (first step), and PA6, PP and the resulting PP-g-MA were blended in a separate extrusion step; one-step: PP was functionalized with MA in the first part of the extruder and PA6 and PP were charged to the extruder downstream.	Both two-step and one-step processes yielded similar morphologies and mechanical properties provided that in the one-step process monomer residues were removed in an efficient manner.
PBT/PP/PP-g-GMA [163,164]	Two step: PP was first functionalized with GMA (glycidyl mthacrylate) in an extruder (first step), and PBT, PP and the resulting PP-g-GMA were blended in a separate extrusion step; one-step: PP was functionalized with GMA in the first part of the extruder and PBT and PP were charged to the extruder downstream.	Both two-step and one-step processes yielded similar morphologies and mechanical properties provided that in the one-step process monomer residues were removed in an efficient manner.

6.2 Experimental

6.2.1 Blending process

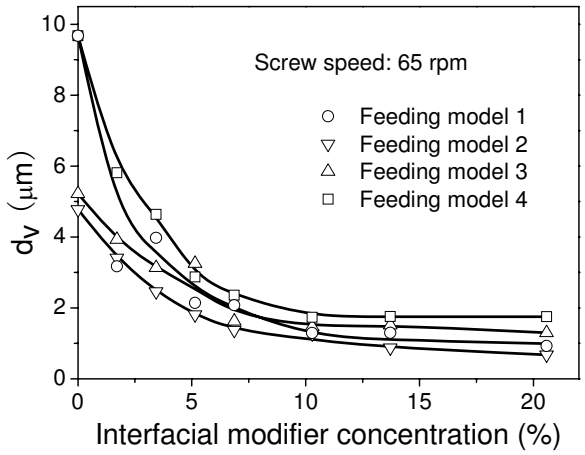
Table 6.2 shows four different feeding modes that were designed to study the effect of feeding mode on the morphology. Feeding mode 1 was one-step feeding and the other three two-step feeding. Two different rotation speeds of the rotor used were 65 rpm and 130 rpm.

Table 6.2 Description of four feeding modes for the PS/PA6/PS-g-PA6f blends.

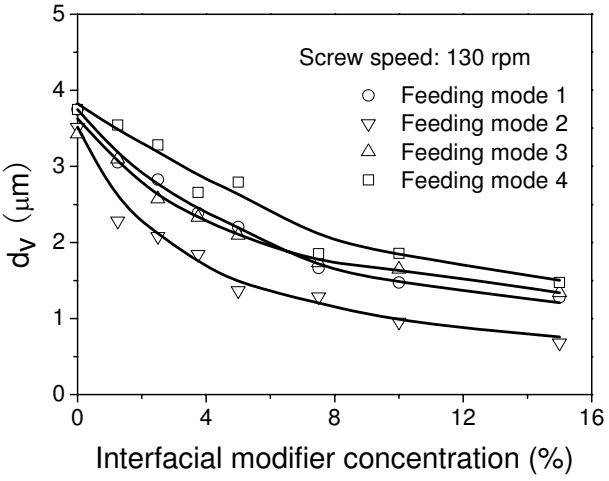
Feeding mode designation	Description
Feeding mode 1 (one-step)	All the components (PS, PA6 and PS-g-PA6f) were charged to the mixer at the same time and were mixed for 8 min.
Feeding mode 2 (two-step)	The PS and PS-g-PA6f were charged to the mixer first and then the PA6 4 min later. The blend was mixed for another 4 min.
Feeding mode 3 (two-step)	The PA6 and PS-g-PA6f were charged to the mixer first and then the PS 4 min later. The blend was mixed for another 4 min.
Feeding mode 4 (two-step)	The PS and PA6 were charged to the mixer first and then the PS-g-PA6f 4 min later. The blend was mixed for another 4 min.

6.3 Results and discussion

Figure 6.1 compares the four feeding modes in terms of the evolution of the dispersed phase domain size as a function of the equivalent pure PS-g-PA6f concentration - emulsification curve for the PS/PA6 (80/20) blend for two different rotation speeds of the rotors. For both rotation speeds, when the PS-g-PA6 concentration was higher than 10% of PA6, the PA6 particle size followed the order: feeding mode 2 < feeding mode 1 < feeding mode 3 < feeding mode 4, which may further be seen from the SEM micrographs of the PS/PA6/PS-g-PA6(/80/20/20.6) blends from these four feeding modes (Figure 6.2). When the PS-g-PA6 concentration was below 10%, the above order was not fully expected. Nevertheless, for both rotation speeds and over the entire PS-g-PA6 concentration range studied, feeding modes 2 and 4 were clearly the most and least efficient, respectively.



(a)



(b)

Figure 6.1 Emulsification curves of the PS/PA6 (80/20) blend for four different feeding modes. The PS-g-PA6f concentration was based on the mass of the dispersed phase. (a) rotation speed at 65 rpm, (b) rotation speed at 130 rpm. Mixing time: 8 min for the one-step feeding and 4 min for the two-step feeding after the last component of the blend was charged; temperature = 230 ºC. Symbols: experimental data; lines: trend lines.

For a given PS/PA6 blend and a given rotation speed, the above differences in the emulsification curve among the four different feeding modes had to result mainly from differences in conditions under which the PS-g-PA6f compatibilizer reached the PS/PA6 interfaces. From the thermodynamic viewpoint, whatever the feeding mode the final PA6 particle size would have been the same if the copolymer added to the blend had all reached the interfaces. That the PA6 particle size depended on the feeding mode implies that the amount of the PS-g-PA6f copolymer chains that had reached the PS/PA6 interfaces depended on the feeding mode. The fact that feeding modes 2 and 4 were the most efficient and most inefficient, respectively, implies that

the former and latter feeding modes provided, respectively, the most favorable and most unfavorable conditions for the mass transfer (migration) of the PS-g-PA6f graft copolymer to the PS/PA6 (80/20) blend. Those results were not fully expected and remain poorly understood.

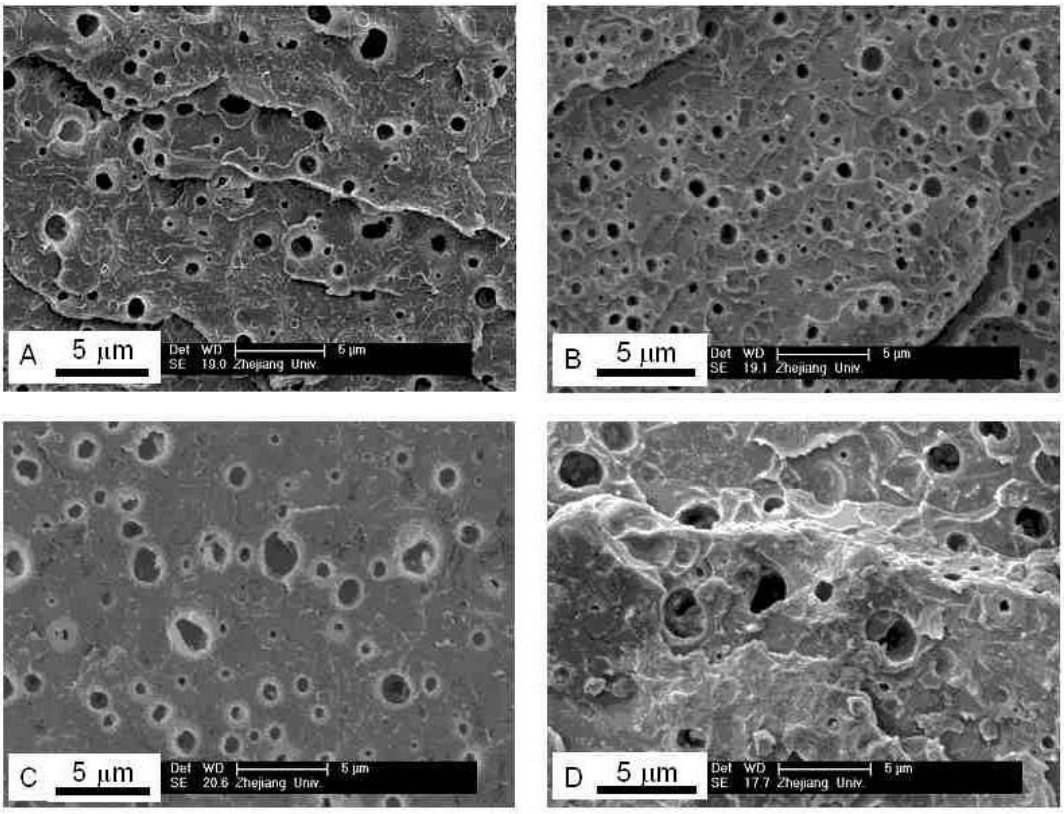


Figure 6.2 SEM micrographs of microtomed surface of the PS/PA6/PS-g-PA6f (80/20/20.6) blend for four different feeding modes. (A) Feeding mode 1, (B) Feeding mode 2, (C) Feeding mode 3 and (D) Feeding mode 4. Mixing time: 8 min for the one-step feeding and 4 min for the two-step feeding after the last component of the blend was charged; temperature = 230 ºC.

In the case of feeding mode 2, the PS (major phase) and PS-g-PA6 (compatibilizer) charged to and mixed in the mixer first. The PA6 (minor phase) was added later when the PS and PS-g-PA6 were completely molten. As the PA6 gradually melted, the molten fraction was concomitantly dispersed in the molten mixture of the PS and PS-g-PA6. PA6 droplets were then stabilized by the PS-g-PA6 that was already present in the medium. In feeding mode 1, all the components of the blend were charged to the mixer at the same time. However they did not melt at the same time. The PS started to melt first, followed by the PS-g-PA6 and then the PA6. From this viewpoint, feeding mode 1 was similar to feeding mode 2.

In feeding mode 3, the PA6 and PS-g-PA6 were charged to the mixer first and the

PS later. To some extent, it was the opposite of feeding mode 2 in terms of the feeding sequence. Since PA6 was the minor phase, the addition of the PS, the major phase, necessarily led to phase inversion. The results in Figure 6.1 infer that the phase inversion process might not have been good for the migration of the compatibilizer to the PS/PA6 interfaces. In feeding mode 4, the PS and PA6 were mixed first and the PS-g-PA6 compatibilizer was added later. The results in Figure 6.1 show that it was the worst feeding mode. The biggest difference between feeding mode 4 and the other three feeding modes was that in feeding mode 4, the PS-g-PA6 compatibilizer was added the latest after the PS and PA6 were already mixed.

Although detailed mechanisms that govern the morphology development of the PS/PA6/PS-g-PA6 blends are unclear, the above results seem to advise two rules. First, the compatibilizer should be present as soon as the blending process starts (the minor phase begins to melt). Second, phase inversion should be avoided. The first rule is in line with a conclusion drawn in the literature [165]. To the authors' knowledge, the second one has not been mentioned in the literature. It should be pointed out that these two rules may not necessarily be valid for all blend systems or process conditions. This is because many important parameters (such as the viscosity ratio of the matrix and dispersed phase, the interface tension and so on) that may affect the morphology development of polymer blends are not studied.

As pointed out above, based on the thermodynamic arguments, the final size of the dispersed phase domain should be independent of the feeding mode provided that all the copolymer chains reach the interfaces. In order that all the copolymer chains reach the interfaces, a certain amount of time was necessary, which may be confirmed from the fact that the size of the dispersed phase decreased with the blending time, as shown in Figure 6.3. Figure 6.4 compares the four feeding modes in terms of the evolution of the PA6 particle size as a function of time for the PS/PA6/PS-g-PA6f (80/20/13.7) blend. It is seen that the difference was very big at short mixing time. As the mixing time increased, the difference narrowed and possibly disappeared at longer times. In other words, when the mixing time was long enough, the feeding mode itself had little effect on the final morphology. This confirms that the differences in the emulsification curve among the four different feeding modes were mostly related to differences in the speed at which the copolymer migrated to the interfaces. Since polymer blending is often carried out in a screw extruder whose residence time is normally very short, an appropriate feeding mode can be crucial for the morphology.

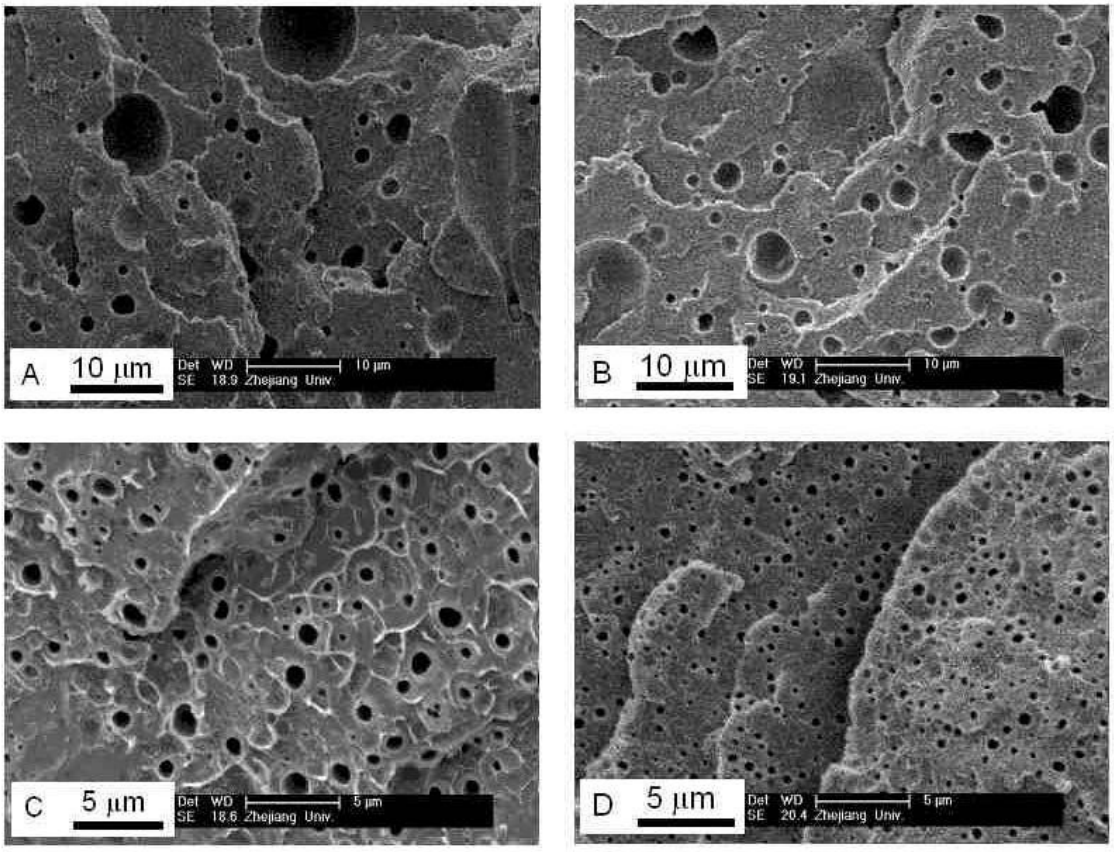


Figure 6.3 SEM micrographs of microtomed surface of the PS/PA6/PS-g-PA6f (80/20/13.7) blend change with mixing time for feeding mode 1. Mixing temperature = 230ºC and rotation speed = 65 rpm. Mixing time: (A) 2 min, (B) 4 min, (C) 6 min, (D) 10 min.

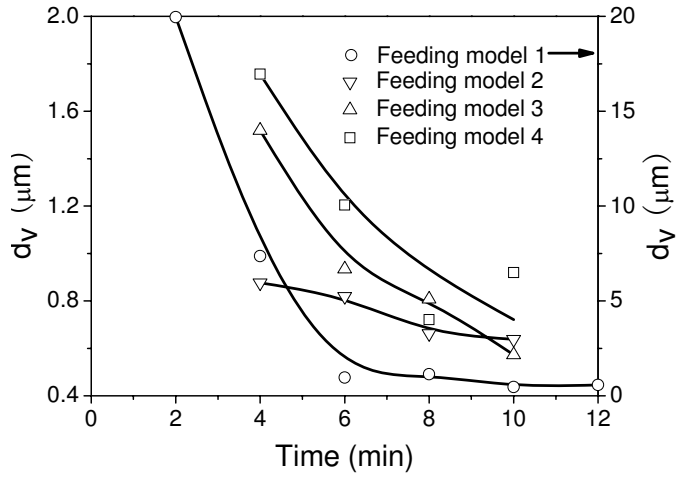


Figure 6.4 Change in the size of the dispersed phase of the PS/PA6/PS-g-PA6f (80/20/13.7) blend with mixing time for different feeding modes. Mixing temperature = 230ºC and rotation speed = 65 rpm. For feeding mode 1 time "0" corresponds to the moment when all the components were fed to the mixer. In the other feeding modes it corresponds to the moment when the last component was fed to the mixer, i.e., 4 min after the first two components were fed to the mixer. Symbols: experimental data; lines: trend lines.

6.4 Conclusions

Feeding mode had a very significant effect on the size of the dispersed phase domains at short mixing time and its effect decreased or became negligible at long mixing time. At short mixing time the efficiency of four feeding modes followed the order: feeding mode 2 (PS and PS-g-PA6 were fed to the mixer first and PA6 later) > feeding mode 1 (PS, PA6 and PS-g-PA6 were fed altogether) > feeding mode 3 (PA6 and PS-g-PA6 were fed first and PS later) > feeding mode 4 (PS and PA6 were fed first and PS-g-PA6 later). This indicates that feeding mode affected mostly the time necessary for the PS-g-PA6 compatibilizer to reach and emulsify the PS/PA6 interfaces.

Chapter 7 Preparation of tracer-emulsifier and comparison of RTD and DSD in TSE

7.1 Introduction

Polymer blending processes use mainly batch mixers and continuous mixers of type screw extruder especially twin-screw extruder (TSE). The former are mainly used in the laboratory and the latter in the laboratory and for production purposes. The foregoing chapters have reported that the emulsification curve is good method to evaluate the efficiency of the compatiblizer. An emulsification curve in a batch mixer can be built up in the following manner. Given compositions of the polymer components of the blend as well as the copolymer are charged to the mixer. After a certain elapse of time, the process reaches a steady state and samples are then taken from the mixer. The size of the dispersed phase domains of the corresponding blend is measured. This makes up a point on the emulsification curve. The above process is repeated upon varying the copolymer concentration. An emulsification curve is then build-up for the said composition of the blend. In the case of a screw extruder, the so-called steady-state experiments are carried out. They are similar to what is followed for a batch mixer. Given compositions of the polymer components of the blend as well as the copolymer are charged to the hopper of the extruder. After a certain elapse of time, the process reaches a steady state and samples are then taken from the die exit for measurement.

However, studies reported in the literature concerning emulsification curves often use batch mixers and not screw extruders. The main reason is that batch mixers are often more accessible in a laboratory than twin-screw extruders and that they are easier to operate too. More importantly, the amount of the copolymer required for building up an emulsification curve in a batch mixer is often much smaller than in a twin-screw extruder. This is especially true for a pilot or industrial-scale screw extruder of which the production rate can reach from a few dozens of kilograms to a few tones per hour. In such a case, the amount of the copolymer required may be too large to build up an emulsification curve.

The residence time distribution (RTD) is a key parameter for characterizing the performance of an extruder [166,167]. Typically, RTD is measured by a pulse injecting the tracer into the flow stream at a chosen location of the extruder, and then its concentration at another location downstream is determined by an analytical

instrument [168]. A tracer is a substance that is either radioactive (MnO_2, La_2O_3, etc.) [166], electrically conductive (KNO_3, $NaNO_3$, KCL, etc.) [169], optical reflective (TiO_2) [170], UV or fluorescent (anthracene) [87,111,171-173]. The fluorescence emission has developed as high sensitive and performable method.

RTD can be measured offline, online, inline while emulsification curve can be only measured by offline. Offline method is done in a discrete manner, which is tedious and time-consuming; on-line and in-line measurement can analyze continuously the flow material and have no need to collect samples the way off-line one. Obviously, on-line and in-line measurements have many advantages over the off-line measurement.

This sections aims at extending RTD, an old concept in chemical engineering, to polymer blending in order that a very small amount of copolymer still allows building up an emulsification curve in a pilot or industrial screw extruder. The idea is based on RTD transient experiments. Unlike a steady-state experiment in which given compositions of the polymer components of the blend and the copolymer are charged to the hopper of the extruder altogether, in a transit experiment the polymer components are first charged to the hopper of the extruder. When the process reaches its steady state, a given amount of the copolymer is then introduced to the hopper of the extruder as a pulse. Samples are taken at the die exit as a function of time. Both the evolution of the copolymer concentration and that of the morphology as a function of time can be obtained. The former provides the RTD and the latter the morphology distribution (MD) or the dispersed phase domain size distribution (DSD) for dispersed type polymer blends. From both distributions, the emulsification curve can be easily deduced.

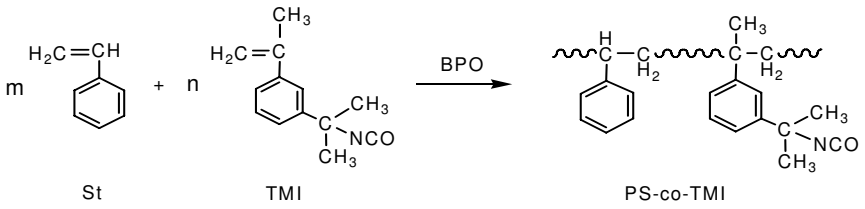
In order to achieve the connection of RTD and DSD, a route must be developed to prepare a tracer-emulsifier with both tracer and emulsification characteristic. A polymer with desired trace characteristic had developed by incorporating anthracene moieties to polymer backbones using the reaction of the amino-group of the 9-(methylamino-methyl)anthrancene (MAMA) and the isoyanate moieties of backbone [87,111]; a copolymer with emulsification characteristic has also developed in forgoing chapter using the similar polymer backbone containing isoyanate moieties to initiate the polymerization of interesting monomer to form the graft copolymer. This work combines the two above routes to prepare the tracer-emulsifier and compares the RTD and SDS using the trace-emulsifier injected into the TSE as a pulse in order to identify which a measured RTD may or may not accurately reflect the SDS

of polymer blends.

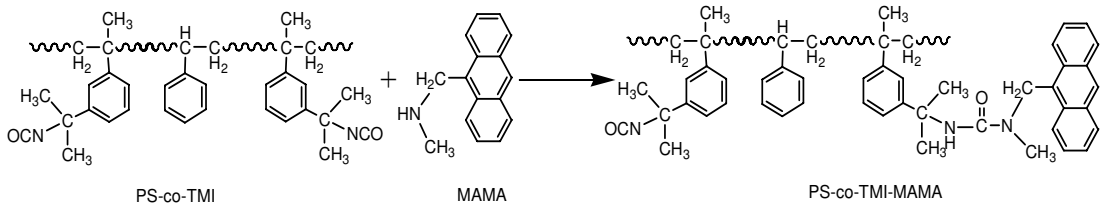
7.2 Basic principles of the preparation of tracer-emulsifier

Basically, the route to be developed to synthesize the tracer-emulsifier consists of three steps. The first one is to prepare the tracer-emulsifier precursor, PS-co-TMI. The second step is to make some isocyanate moieties contained in the tracer-emulsifier precursor react with MAMA. The anthracene moieties incorporated to the polymer backbone make it detectable by an ultraviolet or fluorescent spectrophotometer. The last step is to use remained intact isocyanate moieties acted as initiating centers from which polyamide grafts grow in the presence of a catalyst like NaCL, which form the desired graft copolymer used as emulsifier. Figure 7.1 illustrates the route to synthesize the desired tracer-emulsifier in this study.

Step 1. Preparation of the tracer-emulsifier precursor (PS-co-TMI) by free radical polymerisation of styrene and TMI:



Step 2. Reaction between the some isoyanate moieties bearing polymer and anthracene bearing amine moieties leading to the desired tracer characteristic:



Step 3. Remained intact isoyanate moieties bearing polymer initiates interest monomer to form the copolymer leading to the desired tracer-emulsifier:

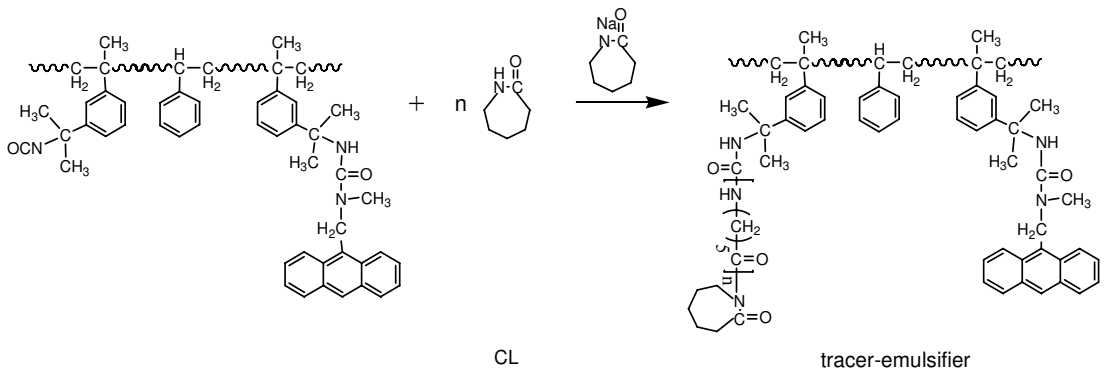


Figure 7.1 Underlying chemistry used for the preparation of tracer-emulsifier

7.3 Experimental

7.3.1 Synthesis of the tracer-emulsifier

The tracer-emulsifier was synthesized according to the basic principle shown in Figure 7.1. The detail synthesized processes are as follows:

Firstly, the copolymer PS-co-TMI of St and TMI was obtained by the solution polymerization from toluene/styrene/TMI/benzoyl peroxide (BPO) (60 ml/40 ml/1.6 ml/0.2 g) systems. The TMI content in PS-co-TMI is 4 wt.% and the number average molar mass of PS-co-TMI is 33.3 kg/mol.

Secondly, the isocyanate moieties in PS-co-TMI reacted with MAMA to form PS-co-TMI-MAMA in THF at 40 ºC. The mass ratio of MAMA and PS-co-TMI is about 0.4%. After reaction for about 2 h, the reacted products were precipitated in methanol and dried in the vacuum oven at 80 ºC for 24 h. In fact, MAMA is not enough to react completely with all isocyanate moieties in PS-co-TMI and there are still intact isocyanate moieties in PS-co-TMI-MAMA.

Thirdly, the intact isocyanate moieties in PS-co-TMI-MAMA are used as an activator to initiate the anionic polymerization of ε-caprolactam (CL) in the presence of catalyst at 230 ºC in a Haake torque rheometer (HBI systems 90). During the polymerisation, those two screws rotated in the opposite directions with a speed of 65 rpm (revolutions per minute) to ensure mixing two polymerization systems were chosen: 1. PS-co-TMI-MAMA/CL/Cat (30/70/5); 2. PS-co-TMI-MAMA/CL/Cat (70/30/5). Two above polymerization products were purified by successive extraction with methanol under reflux for 1 h, THF under reflux for 1 h and formic acid at room temperature for 12 h, and then dried in vacuum oven at 80 ºC. The purified products were denoted as tracer-emulsifier A (from the first polymerization system) and tracer-emulsifier B (from the second polymerization system).

Before used, the tracer-emulsifiers were extruded into pellets whose dimensions were similar to those of PS and PA6 in Melt Flow Speed Indicator with a type of CEΛST.

7.3.2 Extruder, screw configurations and instrumentation

Experiments were carried out on a corotating twin-screw extruder with a diameter of 35 mm and a length to diameter ratio of 48.

The screw configurations used in this study were shown in Figure 7.2. The screw configurations basically are consisted of right-handed screw elements and kneading blocks. The latter is used in order to ensure mixing of polymer blend. The head of the extruder was equipped with strip die that was 30 mm in length and 5 mm in width.

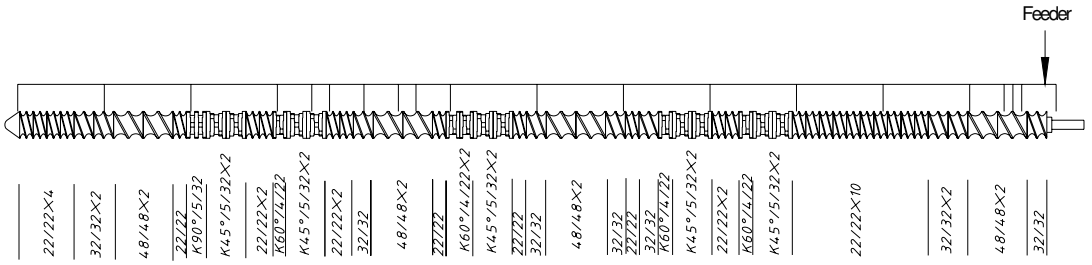


Figure 7.2 Screw configurations of the twin screw extruder

An in-line RTD measuring system developed by our research group was mainly composed of the following three parts: fluorescent light generation, fluorescent light detection, and signal processing. The fluorescent light source was ultraviolet high-pressure mercury lamp (125w) and was split into two beams. Each of them successively passed through a coupler and a bifurcated optical fiber before it irradiated the tracer containing polymer flow stream in the extruder. The light with a specific wavelength emitted from the provocative tracer was subsequently transmitted to a fluorescent detector (a photomultiplier) through the bifurcated optical fiber probe and was then amplified through an amplifier. Finally, the amplified optical signals coming from the two fluorescent detectors reached the signal processing unit. The latter converted them to two analogs. They were then collected by the computer system and were displayed in real time on the screen. The sensitivity of the measuring system could be regulated by a knob with respect to different amounts of tracer. Signals were collected once every second. The reliable of this in-line RTD intruments had been evaluated by Zhang et al. [172].

The measured probe was placed in the die and measured the overall RTD density function of the extruder between the feeder and the die.

7.3.3 Measurement Procedure

In this study, PS and PA6 used as immiscible polymer blends were PS-2 and PA6-2 shown in Table A.1 of Applex section. The feed rate of the polymer blend was typically about 13 kg/h and the screw speed was 100 and 150 rpm. The barrel temperature was set at 230 ºC. When the extruder was in a steady state, the

tracer-emulsifier was injected to the hopper as a pulse. At the same time, the RTD signals started to be collected. Before the signals increasing, one sample was taken out from the die. And then other samples were taken out once every ten seconds until the signals reached original value. Every sample taken out from the die was quenched immediately in liquid nitrogen to freeze-in its morphologies.

With the assumption that the value of the analog fluorescence signal (voltage) was proportional to the concentration of tracer-emulsifier, the normalized RTD function was calculated according to the following expression:

$$E(t_i) = \frac{V(t_i)}{\sum_{i=1}^{n} V(t_i)(t_i - t_{i-1})} \tag{7.1}$$

where $V(t)_i$ is the signal value of the processed material corresponding to time t_i (i= 1, 2, ..., n).

7.3.4 SEC measurements

A foregoing work has successfully applied the *N*-trifluoroacetylation reaction to PS-g-PA6 graft copolymers so that they could be characterised by SEC using THF as eluent. The treatment procedure of *N*-trifluoroacetylation of the tracer-emulsifier is same with that PS-g-PA6 graft copoloymers. The SEC measurement was done with an apparatus of type Waters 1525/2414 equipped with a refractometer and a dual UV-detector at 238 and 260 nm or 260 nm and 367 nm. THF was the mobile phase and PS standard for the calibration.

7.4 Results and discussion

7.4.1 PS-co-TMI-MAMA

The trace characteristic of tracer-emulsifier results basically from the content of anthracene moieties. Figure 7.3 shows the infrared spectra of PS-co-TMI before and after reaction with MAMA. PS-co-TMI is characterized by two characteristic peaks of St at 1944 cm^{-1} and the isocyanate moieties of TMI at 2255 cm^{-1}. After reaction, a new peak has appeared at 1658 cm^{-1}, indicative of the formation of a urea as a result of the reaction between the isocyanate moieties of TMI and the amine moieties of MAMA. Moreover, the ratios of the peak height between 2255 and 1944 cm^{-1} after reaction is lower than that before reaction, which further confirms that MAMA has reacted with isoyanate moieties in PS-co-TMI.

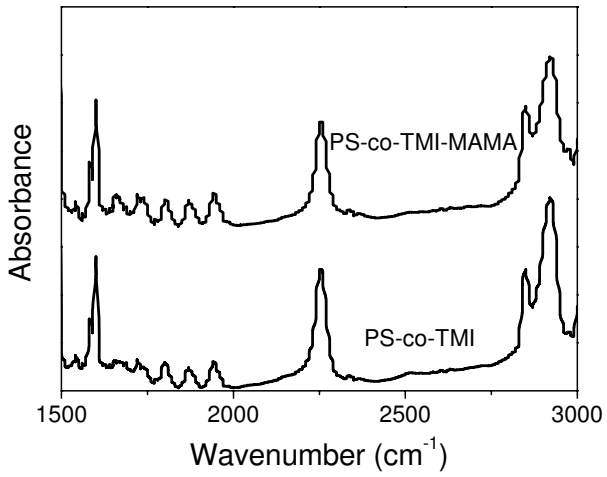


Figure 7.3 Infrared spectra of PS-co-TMI before and after reaction with MAMA.

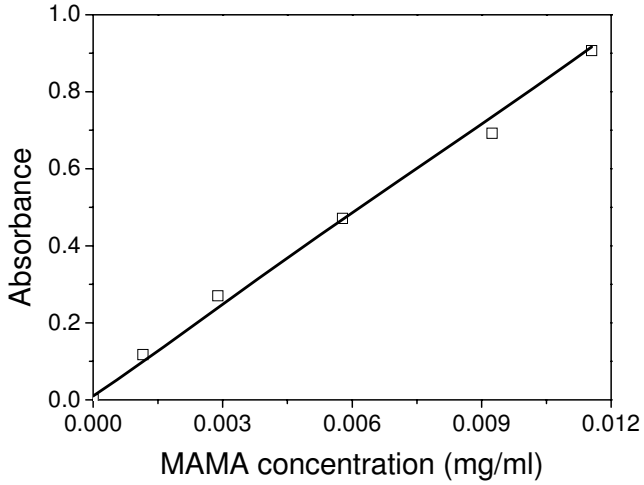


Figure 7.4 Linear relationships between the intensity of UV absorption of MAMA and its concentration in THF at room temperature. The UV wavelength is located at 367 nm.

The UV absorption spectrum of PS-tracer, the product of PS-co-TMI that was subjected to reaction with an excess of MAMA in THF, is in quantitative agreement with those of MAMA [87]. Therefore, the MAMA content in PS-co-TMI-MAMA can be calculated based on the linear relationship between the intensity of UV absorption of MAMA and its concentration in THF at 367 nm, as shown in Figure 7.4. The MAMA content in PS-co-TMI-MAMA is 0.26%, that is, there are still 3.75% intact isocyanate moieties in PS-co-TMI-MAMA.

7.4.2 Tracer-emulsifier

Figure 7.5 shows the evolutions of the torque of the polymerization systems as a function of time. From Figure 7.5, it can be seen that the lower the PS-co-TMI-MAMA/CL mass ratio, the higher the final torque value; the ratio of PS-co-TMI-MAMA/CL has little effect on the induction time. This is accord with that

of the foregoing PS-co-TMI/CL/Cat polymerization systems. This may indicate that MAMA has hardly effect on the polymerization reaction.

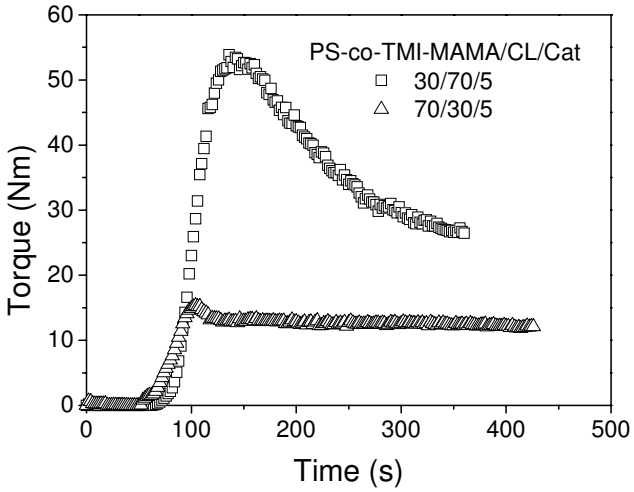


Figure 7.5 Torque value as a function of time for the polymerization system of PS-co-TMI-MAMA/CL/Cat: (a) 30/70/5; (b) 70/30/5. Temperature: 230 ºC; screw speed: 65 rpm.

For tracer-emulsifier, two importance parameters must be determined: one is the anthracene moieties content in polymer, that is, the MAMA content in polymer, which is primary for tracer characteristic; the other is the molecular composition and structure of polymer, which is related intimately with the emulsifier characteristic.

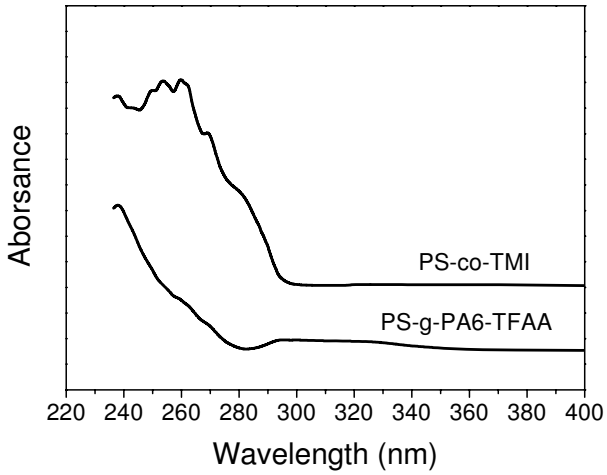


Figure 7.6 UV spectra of the solutions of PS-co-TMI and PS-g-PA6-TFAA in THF. The mass concentrations of polymers are 0.2 and 0.04 mg/ml (excluding the mass of TFAA in PA6-TFAA and PS-g-PA6-TFAA), respectively.

Firstly, we focus on the former. By the *N*-trifluoroacetylation reaction of PS-g-PA6 graft copolymers, it can achieve PS-g-PA6 soluble in THF. Both

PS-co-TMI and PS-g-PA6-TFAA have not UV absorbance at 367 nm, which can be seen from Figure 7.6. This indicates that the MAMA content in polymer can also be measured by the foregoing methods of UV absorbance. The MAMA content in tracer-emulsifier A and tracer-emulsifier B is 0.10 and 0.23%, respectively.

The compositions and molecular masses of two tracer-emulsifiers obtained by SEC method were shown in Table 7.1. It can be seen that the PA6 content in tracer-emulsifier A is higher than that in tracer-emulsifier B, that is, the length of graft chain of the former is longer than that of the latter.

Table 7.1 Molar mass, the PA6 content and the MAMA content of two tracer-emulsifiers

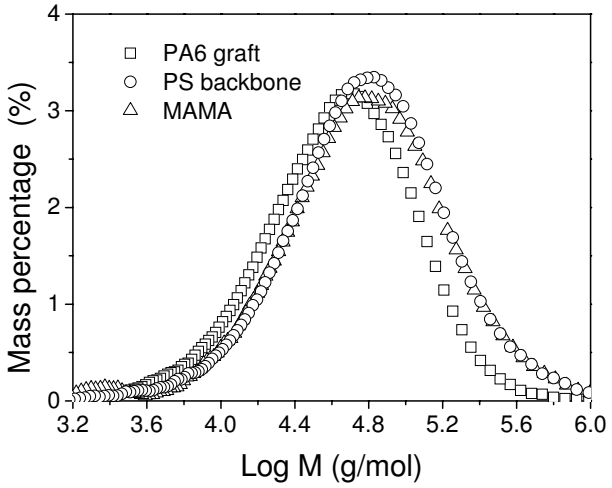
Sample	Mn[a] (kg/mol)	Mw[a] (kg/mol)	The PA6 content[b] (%)	The MAMA content[c] (%)
Tracer-emulsifier A	37.8	137.0	35.3	0.10
Tracer-emulsifier B	32.3	88.2	13.2	0.23

(a) Molar masses of *N*-trifluoroacetylated PS-g-PA6 by SEC using a refractometer detector and based on the PS standards.

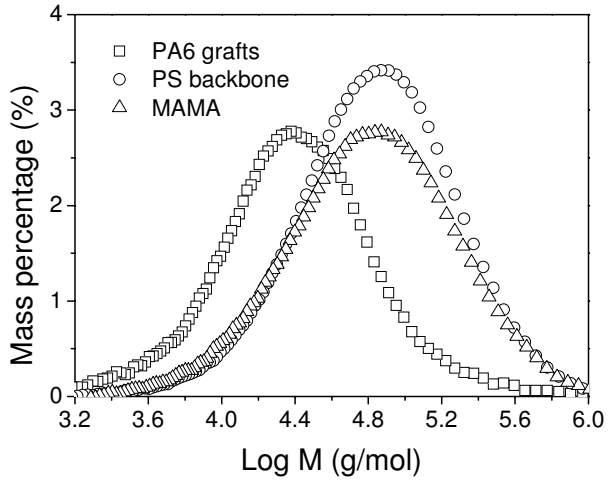
(b) From SEC using dual UV detection at 238 and 260 nm

(c) From UV absorbance method at 367 nm.

The mass percentages of the PA6 grafts, PS backbone and MAMA of the tracer-emulsifier A and tracer-emulsifier B as a function of its molar mass were shown in Figure 7.7(a) and (b), respectively. It should be noted that the mass percentages is not corresponding to the mass of tracer-emulsifier but their respective mass of PA6 grafts, PS backbone and MAMA. From Figure 7.7, it can be seen that the mass percentage curve of PS backbone and MAMA are fell approximately on a curve, which indicates that MAMA is distributed symmetrically in PS backbone. However, the mass percentage curve of PA6 grafts is lean to the low mass molar domain of tracer-emulsifier, especially for the tracer-emulsifier B. This may imply that the PA6 content in tracer-emulsifier is higher at low mass molar of tracer-emulsifier.



(a)



(b)

Figure 7.7 Mass percentages of the PA6 grafts, PS backbone and MAMA of the tracer-emulsifier A and tracer-emulsifier B as a function of their molar mass.

To sum up, the MAMA content in the tracer-emulsifier A is lower than that in tracer-emulsifier B, while the PA6 content in the former is higher than that in the latter. Moreover, the PA6 grafts of the tracer-emulsifier A are more uniformly distributed in PS backbone than that of the tracer-emulsifier B.

7.4.3 Mass of tracer-emulsifier for one experiment in twin screw extruder

The emulsification curves of polymer blends and RTD have mainly resulted from the difference concentration of the emulsifier and the tracer, respectively. Therefore, in order to achieve the comparability of DSD of polymer blend and RTD in TSE, the tracer-emulsifier concentration must firstly be determined. In fact, the in-line RTD measuring system allows measured at the big range of tracer concentration by adjusting the sensitivity. Therefore, the mass of tracer-emulsifier for one experiment is

mainly depending on the emulsification characteristic.

Figure 7.8 shows a typical RTD curve in TSE. The feed rate was 13 kg/h, that is, 3.6 g/s, and the screw speed was 100 rpm, which were uniform with the operated conditions in our study. With the assumption that the signal intensity for RTD measurement is directly ratio with the tracer-emulsifier concentration, the RTD curves can been convert into the mass distribution curves of tracer-emulsifier. For example, if the content of tracer-emulsifier in polymer blend was 10% when E(t) reached the maximum, that is, the mass of tracer-emulsifier is 0.36 g at this time, the corresponding mass distribution of tracer-emulsifier is shown in Figure 7.9. It may be obtained that the mass of all tracer-emulsifier for one experiment is 24 g by the integral of the distribution curves of tracer-emulsifier mass.

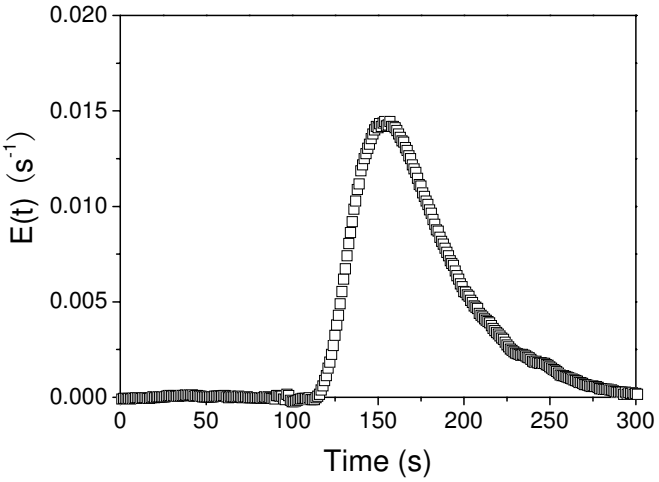


Figure 7.8 A typical residence time distribution curve. Screw speed: 100 rpm; Feed rate: 13 kg/h.

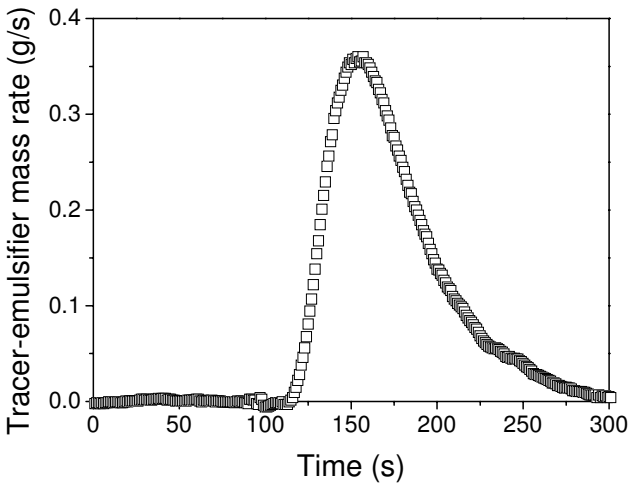


Figure 7.9 Mass distribution of tracer-emulsifier corresponding to the RTD curve in Figure 7.8.

In foregoing study in Haake torque rheometry, it had been shown that for the

PS/PA6 polymer blends, the critical concentration of PS-g-PA6 was about 8% based on the dispersed phase. For PS/PA6 (80/20) blend systems, the content of tracer-emulsifier should be about 1.6%. Therefore, for one experiment, the tracer-emulsifier mass should be about 3.8 g. In our study, 1.6 g, 3.2 g and 4.8 g was chosen as the tracer-emulsifier mass for one experiment.

7.4.4 Comparability of RTD and DSD in different conditions

7.4.4.1 Tracer-emulsifier with different composition and structure

The two different as-synthesized tracer-emulsifiers were used to measure RTD of the blend system of PS/PA6 (80/20) in TSE, as shown in Figure 7.10. PS-tracer was used as tracer for comparison. From Figure 7.10, it can be seen that the RTD curves obtained with tracer-emulsifier B and PS-tracer are wider than that with tracer-emulsifier A. This may imply that the axial mixing quality of tracer-emulsifier A is less than that of tracer-emulsifier B. This result is not unexpected. Recall that the composition and structure of tracer-emulsifier A and tracer-emulsifier B shown in Table 7.1 and Figure 7.7, it can be known that the emulsification ability of tracer-emulsifier A is better than that tracer-emulsifier B according to the foregoing studies about the emulsification ability of emulsifier with different structure and composition. This may imply that tracer-emulsifier A prefers to stay the interface of PS and PA6 while tracer-emulsifier B is easier to disperse in matrix. Therefore, the diffusion of tracer-emulsifier B is more intensity over the length scales than that of tracer-emulsifier A, which leads to the wider RTD curve. This is also valid for PS-tracer dispersed in PS matrix. As for the difference of RTD with tracer-emulsifier B and PS-tracer, it may result from the difference of their mass, 4.8 g tracer-emulsifier B and 0.16 g PS-tracer, which will be discussed in following sections.

The SDS curve of polymer blend is also shown in Figure 7.10. The size of dispersed phase with tracer-emulsifier A is lower than that with tracer-emulsifier B at the range of studied time, which further confirms that the emulsification ability of tracer-emulsifier A is better than that of tracer-emulsifier B. In addition, by comparison of the RTD and DSD curves in Figure 7.10, the latter with tracer-emulsifier A is similar to the former but the direct of two curves. However, it is not real for tracer-emulsifier B, as DSD curve is narrower and shifts toward the longer time domain than RTD curve. The above results may suggest that the DSD curve can be good combined with the RTD curve when the tracer-emulsifier has good emulsification ability.

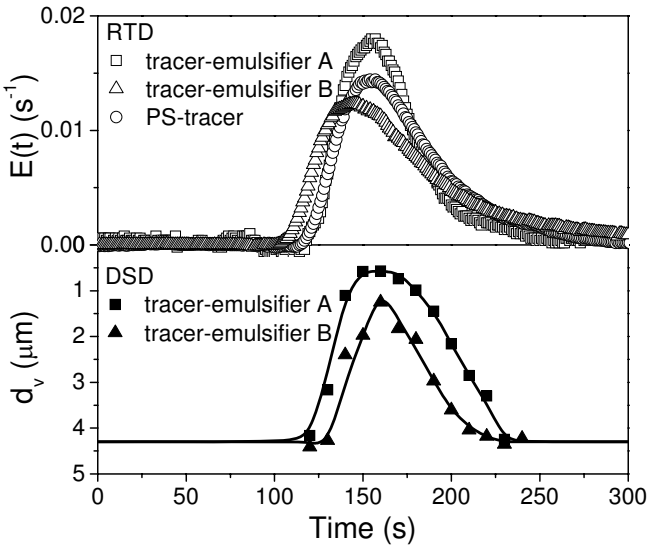


Figure 7.10 Comparison of the RTD and DSD curves obtained using two different tracer-emulsifiers and PS-tracer (only RTD). Their masses are 4.8, 4.8 and 0.16 g, respectively. Feed rate: 13 kg/mol; Screw speed: 100 rpm.

7.4.4.2 Tracer-emulsifier mass for one experiment

Many investigators had reported that the tracer concentration has less effect on the RTD [111,173]. However, it should be noted that the tracer concentration or mass of tracer for one experiment is much lower that in our studied.

Figure 7.11 shows the effect of the mass of the tracer-emulsifier A for one experiment on the RTD curve. Increasing the mass of tracer-emulsifier A, the RTD curve widens and shifts toward the shorter time domain, which can further be confirmed from tracer-emulsifier B as shown in Figure 7.12. From the Figure 11 in the reference 88, it also be seen that when the mass of tracer is 0.2401 g, the RTD curve is slightly shifted to the shorter time domain than that when the mass of tracer is lower 0.2401 g. On the one hand, the mass of tracer-emulsifier for one experiment (1.6~4.8 g) can not be neglected relative to the feed rate (3.6 g/s). The addition of tracer-emulsifier may increase the local feed rate, which lead to the RTD curve shift to the shorter time domain as that the feed rate shifted the RTD curve to the shorter time domain reported in the literature [111,173]. This may be the main reason for the RTD curve with the tracer-emulsifier B shift to the shorter time domain than that with PS-tracer (Figure 7.10). On the other hand, the mass increasing of tracer-emulsifier will increase the probability of the axial diffusion, which results in that the RTD curve widens.

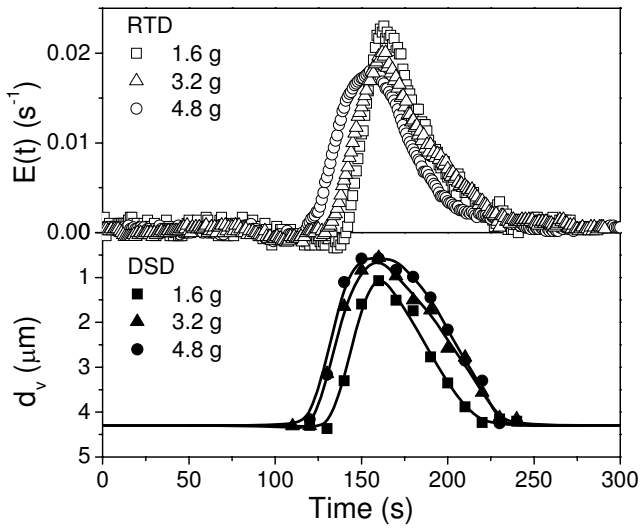


Figure 7.11 Effect of the mass of the tracer-emulsifier A for an experiment on the RTD and DSD curves. Feed rate: 13 kg/h; screw speed: 100 rpm.

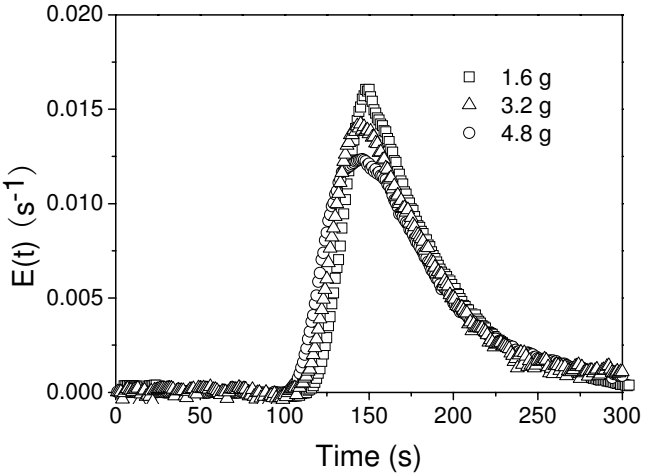


Figure 7.12 Effect of the mass of the tracer-emulsifier B for an experiment on the RTD curves. Feed rate: 13 kg/h; screw speed: 100 rpm.

Figure 7.11 compares DSD of the PS/PA6 (80/20) blend systems for three different mass of tracer-emulsifier for one experiment (1.6~4.8 g). The PA6 particle size followed the mass order of the tracer-emulsifier: 4.8 g < 3.2 g < 1.6 g, which may further be seen from the SEM micrographs of the PS/PA6 polymer blends extruded in TSE with these three different mass of tracer-emulsifier for one experiment (Figure 7.13). In addition, it should be noted that the SDS curve for the system with 4.8 g tracer-emulsifier has a platform between 150 s and 165 s, which is not real for other two systems with 1.6 g and 3.2 g tracer-emulsifier, which imply the maximum concentration of tracer-emulsifier in polymer blend can reach the critical concentration using 4.8 g tracer-emulsifier for one experiment. This further indicates

that the foregoing method of calculating tracer-emulsifier for one experiment is valid.

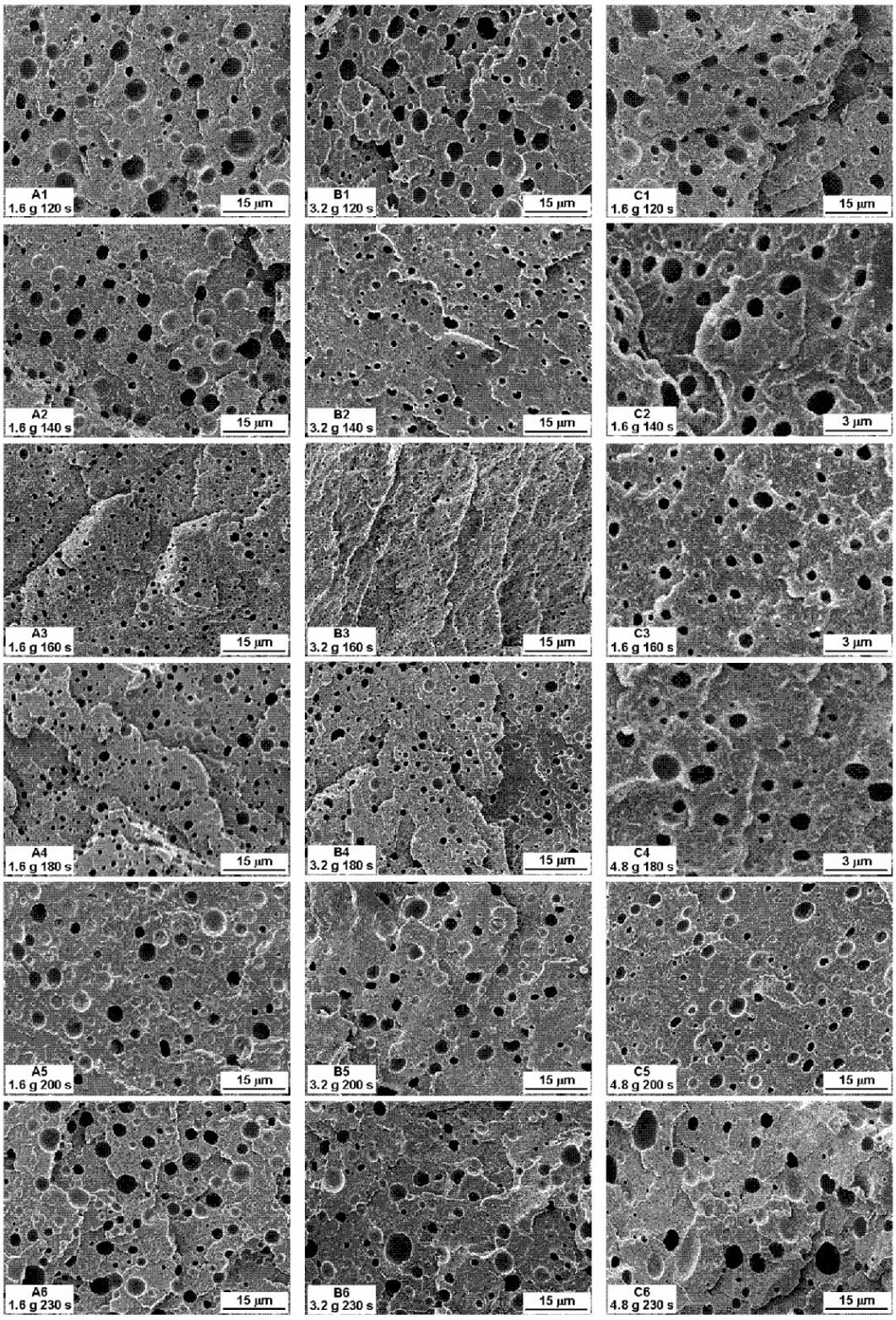


Figure 7.13 SEM micrographs of microtomed surface for PS/PA6 (80/20) blends collected at different extruder die exit at different times. In the extrusion process, the tracer-emulsifier A was injected to the hopper as a pulse at zero time. The mass of tracer-emulsifier A for an experiment is 1.6 g (A), 3.2 g (B) and 4.8 (C).

At the first glance, the DSD curves from tracer-emulsifiers A with three different mass can be not good match with the RTD curves from Figure 7.11. In fact, the size of the dispersed phase is mainly rest with the mass of emulsifier. After the data in Figure 7.14 were treated by multiplying the mass of tracer-emulsifiers, the mass distribution curve of tracer-emulsifier (Figure 7.14) is good match with the DSD curve. This further indicates the RTD function can be used to evaluate the DSD function.

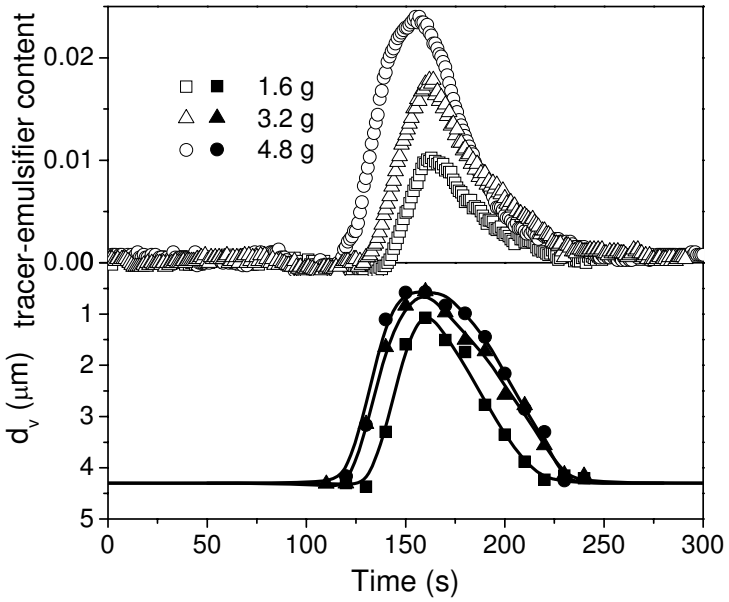


Figure 7.14 Comparison of DSD curves and mass distribution of tracer-emulsifier of PS/PA6 (80/20) blend systems extruded in TSE with different amounts of tracer-emulsifier A for an experiment. The mass distribution of tracer-emulsifier obtained from the data in Figure 11. The mass indicated in the figures corresponds to the amounts of tracer-emulsifier A injected to the extruder.

7.4.4.3 Screw speed

Figure 7.15 shows the effect of the screw speed on RTD at a given feed rates. An increase in the screw speed shifts the RTD curve toward the shorter time domain, which is agreement with all the works reported in the literature [111,173]. This implies that the tracer behavior of the as-synthesized tracer-emulsifier is similar to that of the micro-tracer or macro-tracer.

The corresponding DSD curves at 100 rpm and 150 rpm are shown in Figure 7.15. It also can be found that an increase in the screw speed shifts the DSD curve toward the shorter time domain, which is uniform with RTD. In addition, the shape and position of RTD and DSD are similar but the curve directions, the former upward while the latter downward. This further indicates that the DSD curve is able to be reflected by the RTD curve under a relatively large processing window.

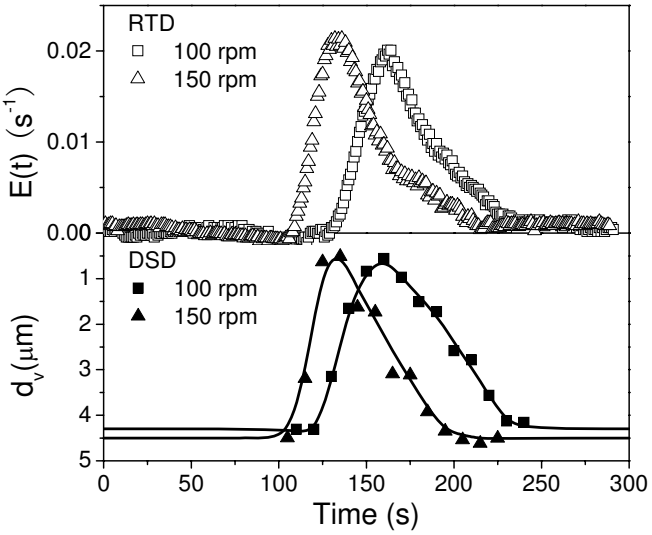


Figure 7.15 Effect of the screw speed on the RTD and DSD curves. The mass of tracer-emulsifier A injected to the extruder is 3.2 g; feed rate is 13 kg/h.

7.4.4.4 Effect of PS/PA6 ratio

A comparison of the RTD curves of two different PS/PA6 ratio systems (90/10 and 80/20) was made, as shown in Figure 7.16. From Figure 7.16, it can be seen that their RTD curves coincide into a single RTD curve. This may infer that the PS/PA6 ratio has hardly effect on the RTD curve in the studied range.

The shape of DSD curve from these two systems is similar, as shown in Figure 7.16. Moreover, the size of dispersed of the PS/PA6 (90/10) systems is lower than that of the PS/PA6 (80/20), as expected.

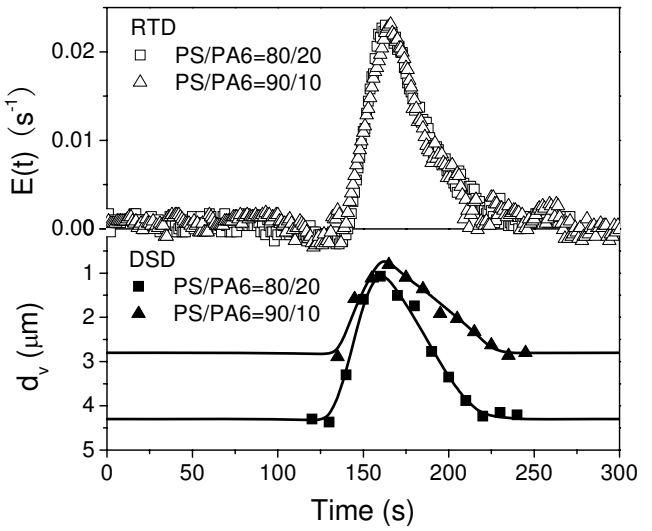


Figure 7.16 Effect of the PS/PA6 ratio on RTD and DSD curves. PS/PA6 mass ratio is 90/10 (a) and 80/20 (b); the mass of tracer-emulsifier A injected to the extruder is 1.6 g; feed rate is 13 kg/h; screw speed is 100 rpm.

Contrast these two curves in Figure 7.16, it can be seen that the RTD curve and SDS are in good agreement.

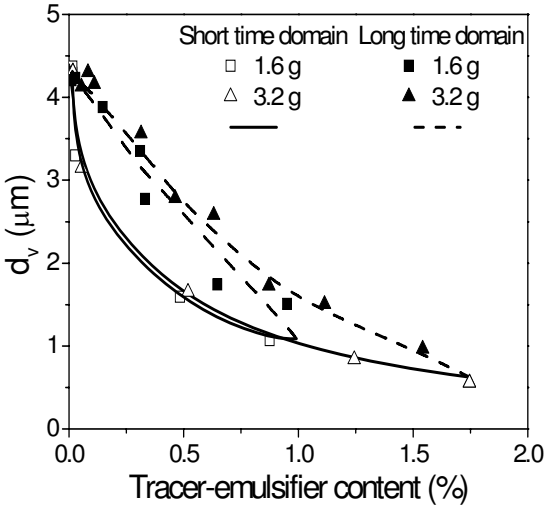
To sum up, the above study on the effect of tracer-emulsifier concentration, feed rate and PS/PA6 ratio is a direct way to evaluate that the performance of the compatibility of RTD and DSD. The results show that RTD can be well combined with SDS, that is, RTD can be used to evaluate the emulsification performance of polymer blend in TSE.

7.4.5 DSD in different time domains

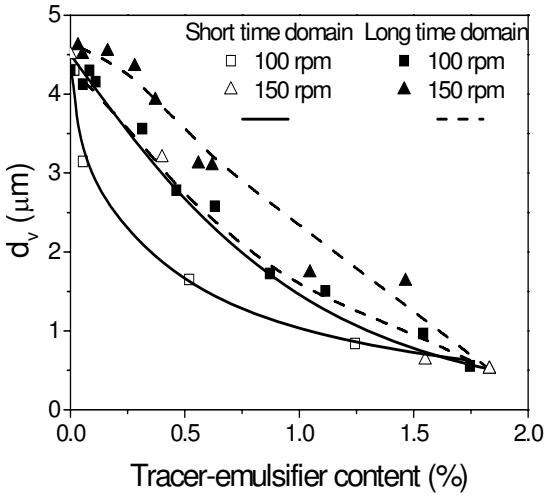
Figure 7.17 shows the emulsification curves in the different conditions.The emulsification curve from batch mixing in Haake torque rheometry is also shown for comparison in Figure 7.17c. The structure of emulsifier used for batch mixing is similar to that of the tracer-emulsifier, the PA6 contents and the number of the PA6 grafts per PS backbone of the former was 30.3% and 6.6, respectively. As expected, d_v decreases rapidly with increasing tracer-emulsifier concentration. The most striking feature of these emulsification curves from twin-screw extruder is that they are not single curves but loops, regardless of the amount of the tracer-emulsifier, the screw speed or the PS/PA6 mass ratio used. These loops result from the fact that a RTD curve can be divided into short and long time domains which are demarcated by the maximum of the residence time distribution density function E(t). In the short time domain, the tracer-emulsifier concentration increases with increasing residence time and in the long time domain it decreases with increasing residence time. In other words, a steady experiment leads to a single emulsification curve, a transient experiment results in two distinct emulsification curves.

The fact that the two curves of an emulsification loop do not superimpose implies that the emulsification curve of a polymer blend is controlled not only by the tracer-emulsifier concentration but also by other parameters such as the type of mixer, as indicated in Figure 3c, and processing conditions. This is expected. However, the literature has not yet paid enough attention to them. Closer inspection of Figure 7.17 reveals a second unique feature of the emulsification loops: the curves corresponding to the short time domain are all systematically below those corresponding to the long time domain. However, mechanisms responsible for this phenomenon remain poorly understood. Nevertheless, coalescence of the dispersed phase domains of the polymer blend could be one. For a given tracer-emulsifier concentration, coalescence is supposed to be more important at longer time or higher PS/PA6 ratio. This is consistent with the results in Figure 7.17b and especially those in Figure 7.17c. The

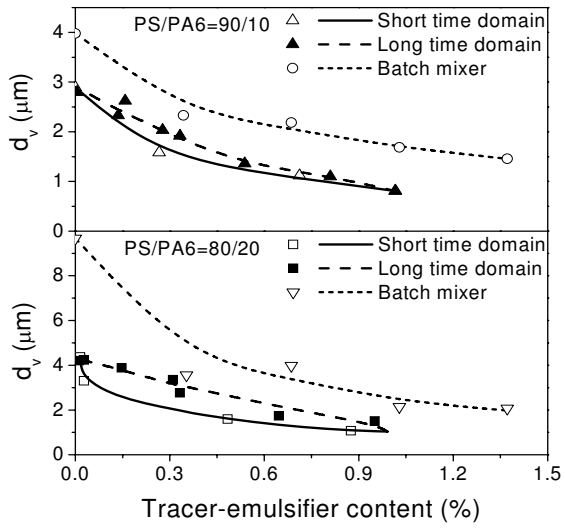
differences between the curves at the short and long time domains are indeed much more pronounced at the higher PS/PA6 mass ratio.



(a)



(b)



(c)

Figure 7.17 Effects of the amount of the tracer-emulsifier (a), the screw speed (b) and the PS/PA6 mass ratio (c) on the emulsification curve of the PS/PA6 blend. The emulsification curve from a Haake torque rheometer (a batch mixer) is shown in c. The structure of the emulsifier used is similar to that of the tracer-emulsifier. The PA6 content and the number of the PA6 grafts per PS backbone of the emulsifier were 30.3% and 6.6, respectively.

7.5 Conclusions

In this study, a route has been developed to prepare a polymer with tracer and emulsification characteristic which was denoted as tracer-emulsifier. It consists of three steps. The first one is to prepare the precursor of the polymer of interest by copolymerizing the monomer of the polymer with TMI. The second one is to make the precursor detectable by an ultraviolet or fluorescent spectrophotometer trace characteristic by reaction between some isocyante moieties with MAMA. The last one is to use the remained intact isocyanate moieties to initiate the polymerization of the monomer of polyamide in the presence of catalyst. Thus, the anthracene moieties and polyamide graft chain incorporated to polymer backbone.

The use of a very small amount of a tracer-emulsifier allows obtaining at the same time the tracer-emulsifier concentration distribution (i.e. the residence time distribution) and the corresponding dispersed phase domain size distribution of the blend system. From these two distributions, an emulsification curve can be easily obtained. More importantly, it reveals two unique features that have yet been reported in the literature. First, a transient experiment leads to two distinct emulsification curves that form a loop. They correspond to the short and long residence time

domains, respectively. Secondly, under the conditions studied in this work, the one corresponding to the higher time domain is always above the one corresponding to the long time domain. Coalescence could be an important mechanism responsible for this phenomenon.

Chapter 8 General conclusion and future work

8.1 General conclusion

Graft copolymer as an important compatibilizer has been applied widely in the immiscible polymer blend. However, there is no clear picture of how copolymer architecture and composition affects the compatibilization of a polymer blend. An important challenge in the study of the compatiblizing efficiency of graft copolymer is accurate to control the graft copolymer structure in the process of its synthesis. To address challenge, a significant portion of this thesis was dedicated to the synthesis of graft copolymer and the methods for the structure analysis.

The graft copolymer with PS as backbone and PA6 as grafts was synthesized by the anionic polymerization of CL onto a random copolymer of St and TMI. The conversion of CL to PA6 was evaluated by four methods: mass balance based on solvent extraction (methanol, water, THF, or acetone), mass balance based on vacuum drying at 140 ºC, TGA, and elemental analysis based on nitrogen. The mass balances based on methanol extraction and vacuum drying at 140 ºC and TGA were all suitable for measuring the conversion of CL. In addition, a method has been developed to allow using SEC to measure the molar mass and composition of PS-g-PA6. This method is an extension of the one for PA. It consists of reacting TFAA with hydrogen atoms of the amide groups of PA6 grafts chain in a mixture of dry CH_2Cl_2 and co-solvent chloroform. The use of the different intensity of UV absorbance at 238 nm and 260 nm allows determining structure and composition of PS-g-PA6.

In order to obtain relatively high monomer conversions and a polymerization kinetics that is compatible with the residence time of a typical reactive extrusion process, the polymerization temperature should be above the melting temperature of the resulting polyamide 6 grafts, i.e., 210 to 220 °C; the TMI content in the PS-co-TMI higher than 2 wt.%; and the isocyanate/NaCL molar ratio lower than 3. Moreover, the as-polymerized product is composed of the pure PS-g-PA6 graft copolymer, Homo-PA6 and un-reacted CL and likely does not contain any PS-co-TMI. The unreacted CL can be removed by methanol extraction under reflux for 1 h; the Homo-PA6, results mainly from the degradation of PA6 graft chains in high temperature and shear of synthesis process, can be removed by formic acid extraction at room temperature for 12 h.

The structure of graft copolymer is mainly determined by three parameters,

backbone length, graft density, and graft chain length. The control of these parameters can be achieved by the following methods:

(a) The length of backbone chain can be controlled by the polymerization temperature or the peroxide concentration in the process of PS-co-TMI systhesis. This backbone is directly determined by PS-co-TMI becaue there no evidence to show the degradation of PS-co-TMI in the process of PS-g-PA6 synthesis. In addition, the increase of polymerization temperature or BPO concentration can decrease the molar mass.

(b) Graft number per one backbone chain can be determined by the St/TMI ratio in the process of PS-co-TMI. It is very likely that all isocyanate moieties in the PS-co-TMI have participated in the activation of the polymerization of CL. This suggests that the number of the PA6 grafts in a PS-g-PA6 chain is likely equal to the number of the isocyanate moieties in the corresponding PS-co-TMI. Therefore, the graft number per one backbone can be controlled by St/TMI mass ratio for the synthesis of PS-co-TMI because the TMI content in PS-co-TMI is nearly proportional to the St/TMI mass ratio in the feed and has nothing with polymerization temperature and BPO concentration.

(c) The length of graft chain is controlled primarily by the iscoyante/CL molar ratio. For a given TMI content in the PS-co-TMI, the higher the PS-co-TMI/CL mass ratio, the lower the molar mass of and the PA6 mass percentage in the pure PS-g-PA6 graft copolymer; the Cat concentration and feeding mode have little effect on the conversion and the composition of the PS-g-PA6 graft copolymer. Therefore, the graft length of the PS-g-PA6 graft copolymer is controlled primarily by the isocyanate/CL molar ratio.

The polymer blends with two types of morphologies, disperse/matrix and co-continuous morphology, were evaluated to determine the effect of graft copolymer structure and composition on the compatibilization of polymer blends. The disperse/matrix polymer blends focus mainly on the compatibilizing efficiency in the process of mixing, while the co-continuous blends investigates basically the ability of stabilizing polymer blends during quiescent annealing. Whether disperse/matrix blends or co-continuous blends, results show that the efficiency of PS-g-PA6 depends very much on its molecular structure and/or composition: for graft copolymers with similar backbone and graft chain number, the longer the grafts, the higher their compatibilizing and stabilizing efficiency; for a given backbone/graft composition, graft copolymer having fewer and longer grafts are more efficient at compatibilizing

and stabilizing the morphology. This is helpful to design a graft copolymer as the high efficient compatibilizer of the immiscible polymer blend.

By the comparison of the emulsification curves of two PS/PA6 (20/80 and 80/20) blend systems, it can be noted that the dispersed phase size and critical concentration for two blend systems are different although they have uniform dispersed phase/matrix mass ratio. The difference of dispersed phase size may result from the viscosity difference of dispersed phase and matrix. Without compatibilizer, the dispersed phase size for the systems with the lower viscosity polymer act as dispersed phase (such as PS/PA6 (20/80)) is obviously higher than that with the higher viscosity polymer act as matrix (such as PS/PA6 (80/20)). However, the addition of compatibilizer can decrease or eliminate the difference of dispersed phase size for the two blend systems. The difference of critical concentration results mainly from the mode of compatiblizer migration into the interface and wrapping the dispersed phase. In the melting process, PS-g-PA6 first dispersed in PS phase and then diffuse into the interface followed by making PA6 grafts outward for PS/PA6 (20/80), while for PS/PA6 (80/20), PS-g-PA6 can move to PA6 or PA6 can move to PS-g-PA6 and moreover PS-g-PA6 can wrap directly PA6 phase. Therefore, it needs less compatibilizer for PS/PA6 (80/20) than that for PS/PA6 (20/80). The above results seem to advise one rule: the copolymer phase inversion should be avoided.

Feeding mode has a very significant effect on the size of the dispersed phase domains at short mixing time. It is suggested two rules to choose the better feeding mode: first, the compatibilizers should be present as soon as the blending process starts (the minor phase begins to melt); second, the phase inversion of matrix and dispersed phase should be avoided.

The emulsification curves of a polymer blend in a continuous mixer such twin screw extruders be constructed by the extension of RTD to polymer blending. It is based on the incorporation of a tracer molecule in an emulsifier of the polymer blend in a low content, on the one hand; and on the injection of the resulting tracer-emulsifier to the continuous mixer as a pulse, on the other hand. In this manner, for the first time the use of a very small amount of a tracer-emulsifier allows obtaining at the same time the tracer-emulsifier concentration distribution (i.e. the residence time distribution) and the corresponding dispersed phase domain size distribution of the blend system. From these two distributions, an emulsification curve can be easily obtained.

8.2 Future work

In fact, the synthesis method of graft copolymer was separately from the process of the in-situ compatibilization and in-situ polymerization. The latter is an effective method to prepare polymer blends. As shown in Chapter 2, Hu et al. [62-64] have obtained nanoblend by this method. However, the process and mechanism of the nanoblend formation need further investigating. This is a possible study direction. In the process of in-situ compatibilication and in-situ polymerization, two polymerization processes are contained: one is the CL homopolymerization to form the homopolymer act as a phase of polymer blend by the initiation of the micro-initiator and the other is the copolymerization of CL to form copolymer act as compatibilizer by the initiation of macro-initiator. Therefore, it is very indispensable to compare the kinetics of these two polymerization reactions. In addition, in chapter 2, it has shown that the PS-co-TMI characteristic not only has effect on the kinetic of copolymerization and but also determine the structure of graft copolymer which directly determines the compatibilizing efficiency. Therefore, the choice of macro-initiator characteristic may be vital to prepare nanoblend with high performance.

In order to more fully understand the compatibilization of graft copolymers, further experiments will be beneficial. Our study mainly focus on the middle molar mass range so that the rules of compatibilizing efficiency of graft copolymer may be not suitable to all molar mass range. It would be interesting to see if the same trend would occur at higher or lower molar mass range. Therefore, one possible study would be to compare the rules in the different molar mass range. Another possible study is to understand the behavior of the graft copolymer diffusion to the interface in polymer blends. This is because the success of a copolymer to compatibilize and improve the interfacial adhesion relies on the ability of that copolymer to get to the interface and strengthen it, as shown in chapter 4 that the reversal of dispersed phase/matrix leads to the different compatibility effect.

The optimum compatibilization of immiscible polymer blends may not occur with a single type of copolymer, but rather a combination of copolymers with varying architectures or compositions. By using a combination of copolymers rather than a single structure type, the limitations of some types of structure could be overcome by the strength of another type. For example, at fixing the graft chains/backbone mass ratio, the combination of graft copolymers with high molar mass and low molar mass is used as compatibilizer.

Finally, the emulsification curves in twin screw extruder were obtained by the corresponding RTD and DSD. It shows two unique and very interesting features that have not been reported in the literature. First, a single pulse experiment leads to distinct emulsification curves that form a loop, corresponding to the short and long residence time domains, respectively. Secondly, under the conditions studied in this work, the one corresponding to the higher time domain is always above the one corresponding to the long time domain. Coalescence could be an important mechanism responsible for this phenomenon. The method should open up a new research field related to polymer blending.

Appendix

Characteristics of PS, PA6 and PS-g-PA6

This appendix deals with the characteristics of PS, PA6 and PS-g-PA6 that were used to study the compatibilizing efficiency of graft copolymers for immiscible polymer blends, as shown in Table A.1 and Table A.2. Their molar masses measured by SEC using PS standards for the calibration and THF as the eluent. The PA6 and PS-g-PA6 were first *N*-trifluoroacetylated before the SEC measurement.

Table A.1 Selected characteristics of PS and PA6.

	Number average molar mass (*Mn*)[a]	Mass average molar mass *(Mw)*[a]	Supplier
PS-1	151 kg/mol	308 kg/mol	Dow chemical company
PA6-1	30 kg/mol	51 kg/mol	Domo company
PS-2	101 kg/mol	229kg/mol	Yangzi-BASF Styrenics Co. Nanjing, China
PA6-2	19 kg/mol	49 kg/mol	UBE Nylon Ltd., Thailand

Table A.2 Selective characteristics of PS backbone and PA6 grafts of various PS-g-PA6

Copolymer designation	Composition of PS-g-PA6		Number of PA6 grafts per PS backbone	*Mn* (kg/mol)[a]		
	PS backbone	PA6 grafts		PS backbone	Each PA6 graft	PS-g-PA6
PS-g-PA6a	78.4	21.6	15.3	34.3	0.6	26.8
PS-g-PA6b	76.5	23.5	7.1	33.9	1.5	27.3
PS-g-PA6c	66.9	33.1	7.1	33.9	2.4	28.3
PS-g-PA6d	71.2	28.8	3.8	32.0	3.4	33.1
PS-g-PA6e	75.3	24.7	6.6	33.3	1.7	34.9
PS-g-PA6f	69.4	30.6	6.6	33.3	2.2	38.1
PS-g-PA6g	49.7	50.3	6.6	33.3	5.1	47.1
PS-g-PA6h	69.2	30.8	3.4	36.9	4.8	36.0

For the study about compatibilizing the dispersed/matrix phase (Chapter 4), PS-1 and PA6-1 were used as the two immiscible polymers and PS-g-PA6a, PS-g-PA6b, PS-g-PA6c and PS-g-PA6d were used as the compatibilizers. PS-g-PA6a has the same composition with PS-g-PA6b but differed in that the number of the PA6 grafts per PS backbone was not 7.1 but 15.3. PS-g-PA6b and PS-g-PA6c have the same PS backbone and the same number of the PA6 grafts per PS backbone with different lengths. PS-g-PA6d differed from the PS-g-PA6c in that the number of the PA6 grafts per PS backbone was not 7.1 but 3.8.

For the study about efficiency of graft copolymers at stabilizing co-continuous polymer blends during quiescent annealing (Chapter 5), PS-2 and PA6-2 were used as the two immiscible polymers and PS-g-PA6e, PS-g-PA6f, PS-g-PA6g and PS-g-PA6h were used as the compatibilizers. The first three graft copolymers had the same PS backbone and the same number of PA6 grafts with different lengths. The fourth graft copolymer, PS-g-PA6h, differed from the first three in that the number of the PA6 grafts per PS backbone was not 6.6 but 3.4. Its graft length was almost the same as that of PS-g-PA6g and almost twice that of PS-g-PA6f.

For the investigation about effect of feeding mode on the morphologies of immiscible polymer blends (Chapter 6), PS-2 and PA6-2 were used as the two immiscible polymers and PS-g-PA6f was used as the compatibilizers.

References

1. Baker, W.; Scott, C.; Hu, G. H. *Reactive polymer blending*, Hanser publisher, Munich, 2001.
2. Li, T.; Topolkaraev, V. A.; Hiltner, A.; Baer, E.; Ji, X. Z.; Qurik, R. P. Block copolymers as compatibilizers for blends of linear low density polyethylene and polystyrene. *Journal of Polymer Science Part B: Polymer Physics* 1995, 33: 667-683.
3. Li, H.; Hu, G. H.; Sousa, J. A. Morphology development of immiscible polymer blends during melt blending: Effects of interfacial agents on the liquid-solid interfacial heat transfer. *Journal of Polymer Science Part B: Polymer Physics* 1999, 37: 3368-3384.
4. Cigana, P.; Favis, B. D.; Jerome, R.; Diblock copolymers as emulsifying agents in polymer blends: Influence of molecular weight, architecture, and chemical composition. *Journal of Polymer Science Part B: Polymer Physics* 1996, 34: 1691-1700.
5. Cigana, P.; Favis, B. D. The relative efficacy of diblock and triblock copolymers for a polystyrene/ethylene-propylene rubber interface. *Polymer* 1998; 39: 3373-3378.
6. Harrats, C.; Fayt, R.; Jérôme R. Effect of block copolymers of various molecular architecture on the phase morphology and tensile properties of LDPE rich (LDPE/PS) blends. *Polymer* 2002; 43: 863-873.
7. Jannasch, P.; Hassander, H.; Wesslén, B. On the macro- and microphase separation of compatibilizers in immiscible polymer blends. *Journal of Polymer Science Part B: Polymer Physics* 1996, 34: 1289.
8. Edgecombe, B. D.; Stein, J. A.; Fréchet, J. M. J.; Xu, Z.; Kramer, E. J. The role of polymer architecture in strengthening polymer-polymer interfaces: A comparison of graft, block, and random copolymers containing hydrogen-bonding moieties. *Macromolecules* 1998, 31: 1292-1304.
9. Starý, Z.; Fortelný, I.; Kruliš, Z.; Šlouf, M. Effect of molecular structure of ethane-propene and styrene-butadiene copolymers on their compatibilization efficiency in low-density polyethylene/polystyrene blends. *Journal of applied polymer science* 2008, 107: 174-186.
10. Vranješ, N.; Lednický, F.; Kotek, J.; Baldrian, J.; Rek, V.; Fortelný, I.

Compatibilization efficiency of styrene-butadiene block copolymers as a function of their block number. *Journal of Applied Polymer Science* 2008, 108: 466-472.

11. Matos, M.; Favis, B. D.; Lomellini, P. Interfacial modification of polymer blends-the emulsification curve: 1. Influence of molecular weight and chemical composition of the interfacial modifier. *Polymer* 1995, 36: 3899-3907.
12. Chio, W. M.; Park, O. O.; Lim, J. G. Effect of diblock copolymer on morphology and mechanical properties for syndiotactic polystyrene/ethylene-propylene copolymer blends. *Journal of Applied Polymer Science* 2004, 91: 3618-3626
13. Hong, B. K.; Jo, W. H. Effects of molecular weight of SEBS triblock copolymer on the morphology, impact strength, and rheological property of syndiotactic polystyrene/ethylene-propylene rubber blends. *Polymer* 2004, 41: 2069-2079.
14. Bourry, D.; Favis, B. D. Cocontinuity and Phase inversion in HDPE/PS blends: Influence of interfacial modification and elasticity. *Journal of Polymer Science Part B: Polymer Physics* 1998, 36: 1889-1899.
15. Soares, B. G.; Moreira, A. C. F.; Sirqueira, A. S.; Barbosa, R. V.; Simão, R. A. Effect of the molecular architecture of graft copolymers on the phase morphology and tensile properties of PS/EVA blends. *Journal of Applied Polymer Science* 2008, 107: 930-938.
16. Retsos, H.; Anastasiadis, S. H.; Pispas, S.; Mays, J. W.; Hadjichristidis, N. Interfacial tension in binary polymer blends in the presence of block copolymers. 2. Effects of additive architecture and composition. *Macromolecules* 2004, 37: 524-537.
17. Lyatskaya, Y.; Gersappe, D.; Gross, N. A.; Balazs, A. C. Designing compatibilizers to reduce interfacial tension in polymer blends. *Journal of Physical Chemistry* 1996, 100: 1449-1458.
18. Lyatskaya, Y.; Jacobson, S. H.; Balazs, A. C. Effect of composition on the compatibilizing activity of comb copolymers. *Macromolecules* 1996, 29: 1059-1061.
19. Gersappe, D.; Irvine, D.; Balazs, A. C.; Liu, Y.; Sokolov, J.; Rafailovich, M.; Schwarz, S.; Peiffer, D. G. The use of graft copolymers to bind immiscible blends. *Science* 1994, 265: 1072-1074.
20. Israels, R.; Foster D. P.; Balazs, A. C. Designing optimal comb compatibilizers: AC and BC combs at an A/B interface. *Macromolecules* 1995, 28: 218-224.
21. Kvist, L.; Bertilsson, H.; Meuller, P. Poly(styrene-g-ethylene oxide) copolymers

as interfacial agents in immiscible polymer blends. *Polymer Engineering and Science* 1998, 38: 1303-1312.

22. Adedeji, A.; Hudson, S. D.; Jamieson, A. M. Effect of exothermic interfacial mixing on interfacial activity of a block copolymer. Macromolecules 1996, 29: 2449-2456.
23. Kim, S.; Kim, J. K.; Park, C. E. Effect of molecular architecture of in situ reactive compatibilizer on the morphology and interfacial activity of an immiscible polyolefin/polystyrene blend. *Polymer* 1997, 38: 1809-1815.
24. Kitayama, N.; Keskkula, H.; Paul, D. R. Reactive compatibilization of nylon 6/styrene-acrylonitrile copolymer blends. Part 2. Dispersed phase particle size. *Polymer* 2000, 41: 8053-8060.
25. Zhang, M. F.; Müller, H. E. Cylindrical polymer brushes. *Journal of Polymer Science Part A: Polymer Chemistry* 2005, 43: 3461-3481.
26. Bhattacharya, A.; Misra, B. N. Grafting: a versatile means to modify polymers techniques, factors and applications. *Progress in Polymer Science* 2004, 29: 767-814.
27. Pitsikalis, M.; Pispas, S.; Mays, J. W.; Hadjichristidis, N. Nonlinear block copolymer architectures. *Advances in Polymer Science* 1998, 135: 1-137.
28. Börner, H.G.; Matyjasewski, K. Graft copolymer by atom transfer polymerization. *Macromolecular Symposium* 2002, 177: 1-15.
29. Vivek, A. V.; Dhamodharan, R. Grafting of methacrylates and styrene on to polystyrene backbone via a “grafting from” ATRP process at ambient temperature. *Journal of Polymer Science Part A: Polymer Chemistry* 2007, 45: 3818-3832.
30. Li, Z.; Li, P.; Huang J. Synthesis of amphiphilic copolymer brushes: poly(ethyleneoxide)-graft-polystyrene. *Journal of Polymer Science Part A: Polymer Chemistry* 2006, 44: 4361-4371.
31. Ruokolainen, J.; Tanner, J.; Ikkala, O.; Brinke, G. T.; Thomas, E. L. Direct imaging of self-organized comb copolymer-like systems obtained by hydrogen bonding: poly(4-vinylpyridine)-4-nonadecylphenol. *Macromolecules* 1998, 31: 3532-3536.
32. Bazuin, C. G.; Tork, A. Generation of liquid crystalline polymeric materials from non liquid crystalline components via ionic complexation. *Macromolecules* 1995, 28: 8877-8880.
33. Matyjaszewski, K.; Xia, J. Atom transfer radical polymerization. *Chemical*

reviews 2001, 101: 2921-2990.

34. Tsukahara, Y.; Mizuno, K.; Segawa, A.; Yamashita, Y. Study on the radical polymerization behavior of macromonomers. Macromolecules 1989, 22: 1546-1552.
35. Al-muallem, H. A.; Knauss, D. M. Graft copolymers from star-shaped and hyperbranced polystyrene macromonomers. *Journal of Polymer Science Part A: Polymer Chemistry* 2001, 29: 3547-3555.
36. Matyjaszewski, K.; Beers, K. L.; Kern, A.; Gaynor, S. G. Hydrogels by atom transfer radical polymerization. I. Poly(*N*-vinylpyrrolidinone-g-styrene) via the macromonomer method. *Journal of Polymer Science Part A: Polymer Chemistry* 1998, 36: 823-830.
37. Edgecombe, B. D.; Stein, J. A.; Fréchet, J. M. J.; Xu, Z.; Kramer, E. J. The role of polymer architecture in strengthening polymer-polymer interfaces: a comparision of graft, block and random copolymers containing hydrogen-bonding moieties. *Macromolecules* 1998, 31: 1292-1304.
38. Shinoda, H.; Miller, P. J.; Matyjaszewski, K. Improving the structural control of graft copolymers by combining ATRP with the macromonomer method. *Macromolecules* 2001, 34: 3186-3194.
39. Rieger, J.; Dubois, P.; Jérôme, C. Controlled synthesis and interface properties of new amphiphilic PCL-g-PEO copolymers. *Langmuir* 2006, 22: 7471-7479.
40. Roos, S. G.; Müller, A. H. E.; Matyjaszewski, K. Copolymerization of *n*-butyl acrylate with methyl methacrylate and PMMA macromonomers: comparison of reactivity ratios in conventional and atom transfer radical copolymerization. *Macromolecules* 1999, 32: 8331-8335.
41. You, Y. Z.; Hong, C. Y.; Wang, W. P.; Wang, P. H.; Lu, W. Q.; Pan, C. Y. A novel strategy to synthesize graft copolymers with controlled branch spacing length and defined grafting sites. *Macromolecules* 2004, 37: 7140-7145.
42. Roovers, J.; Toporowski, P. Synthesis and characterization of multiarm star polybutadienes. *Macromolecules* 1989, 22: 1897-1903.
43. Beers, K. L.; Gaynor, S. G.; Matyjaszewski, K.; Sheiko, S. S.; Möller, M. The synthesis of densely grafted copolymers by atom transfer radical polymerization. *Macromolecules* 1998, 31: 9413-9415.
44. Zhang M.; Breiner, T.; Mori, H.; Müller, A. H. E. Amphiphilic cylindrical brushes with poly(acrylic acid) core and poly(*n*-butyl acrylate) shell and narrow length distribution. *Polymer* 2003, 44: 1449-1458.

45. Venkatesh, R.; Yajjou, L.; Koning, C. E.; Klumperman, B. Novel brush copolymers via controlled radical polymerization. *Macromolecular chemistry and physics* 2004, 205: 2161-2168.
46. Wang, X. S.; Luo, N.; Ying, S. K. Synthesis of EPDM-g-PMMA through atom transfer radical polymerization. *Polymer* 1999, 40: 4515-4520.
47. Cao, C.; Dong, J. Y.; Hu, Y.; Chung, T. C. Synthesis of polypropylene graft copolymers by the combination of a polypropylene copolymer containing pendant vinylbenzene groups and atom transfer radical polymerization. *Journal of Polymer Science Part A: Polymer Chemistry* 2005, 43: 429-437.
48. Inoue, Y.; Matsugi, T.; Kashiwa, N.; Matyjaszewski, K. Graft copolymers from linear polyethylene via atom transfer radical polymerization. *Macromolecules* 2004, 37: 3651-3658.
49. Liu, S.; Sen, A. Synthesis of novel linear polyethene-based graft copolymers by atom transfer radical polymerization. *Macromolecules* 2001, 34: 1529-1532.
50. Matyjaszewski, K.; Teodorescu, M.; Miller, P. J. ; Peterson, M. L. Graft copolymers of poyethylene by atom transfer radical polymerization. *Journal of Polymer Science Part A: Polymer Chemistry* 2000, 38: 2440-2448.
51. Pae, Y. Preparation of polyimide/nylon 6 graft copolymers from polyimides containing ester moieties: synthesis and characterization. *Journal of Applied Polymer Science* 2006, 99: 309-318.
52. Koutalas, G.; Lohse, D. J.; Hadjichristidis, N. Novel block-comb/graft copolymers with macromonomer strategy and anionic polymerization. *Journal of Polymer Science Part A: Polymer Chemistry* 2005, 43: 4040-4049.
53. Cartier, H.; Hu, G. H. Morphology development of in situ compatibilized semicrytalline polymer blends in a co-rotating twin-screw extruder. *Polymer Engineering and Science* 1999, 39: 996-1013.
54. Su, W. Y.; Wang, Y.; Min, K.; Quirk, R. P. In situ copolymerization and compatibilization of polyester and polystyrene blends. I. Synthesis of functionalized polystyrenes and the reactions with polyester. *Polymer* 2001, 42: 5107-5119.
55. Maric, M.; Ashurov, N.; Macosko, C. W. Reactive blending of poly(dimethylsiloxane) with nylon 6 and poly(styrene): effect of reactivity on morphology. *Polymer Engineering and Science* 2001, 41: 631-642.
56. Seo, Y.; Ninh, T. H. Enhanced interfacial adhesion between polypropylene and nylon 6 by in situ reactive compatibilization. *Polymer* 2004, 45: 8573-8581.

57. Jose, S.; Francis, B.; Thomas, S.; Karger-kocsis, J. Morphology and mechanical properties of polyamide 12/polypropylene blends in presence and absence of reactive compatibiliser. *Polymer* 2006, 47: 3874-3888.
58. Jeon, H. K.; Zhang, J.; Macosko, C. W. Premade vs. reactively formed compatibilizers for PMMA/PS melt blends. *Polymer* 2005, 46: 12422-12429.
59. Jeon, H. K.; Feist, B. J.; Koh, S. B.; Chang, K.; Macosko, C. W.; Dion, R. P. Reactively formed block and graft copolymers as compatibilizers for polyamide 66/PS blends. *Polymer* 2004, 45: 197-206.
60. Yu, X.; Wu, Y.; Li, B.; Han, Y. Studies on interfacial reaction kinetics and properties at a reactive compatibilization interface. *Polymer* 2005, 46: 3337-3342.
61. Moad, G. The synthesis of polyolefin graft copolymers by reactive extrusion. *Progress in Polymer Science*1999, 24: 81~142.
62. Hu, G. H.; Cartier H. Reactive extrusion: toward nanoblends. *Macromolecules*, (1999), 32, 4713~4718.
63. Cartier, H.; Hu G. H. A novel reactive extrusion process for compatibilizing immiscible polymer blends. *Polymer* 2001, 42: 8807~8816.
64. Hu G. H.; Feng, L. F. Extrusion processing for nanoblends and nanocomposites. *Macromolecular symposia* 2003, 195: 303~308
65. Teng, J.; Otaigbe, J. U.; Taylor, E. P. Reactive blending of functionalized polypropylene and polyamide 6: in situ polymerization and in situ compatibilization. *Polymer Engineering and Science* 2004, 44: 648-659.
66. Datta, S.; Lohse, D. J. *Polymeric compatibilizers: uses and benefits in polymer blends*, Hanser; New York, 1996.
67. Macosko, C. W.; Jeon, H. K.; Hoye, T. R. Reactions at polymer-polymer interfaces for blend compatibilization. *Progress in polymer science* 2005, 30: 939-947.
68. Tan, N. C. B.; Tai, S. K.; Briber, R. M. Morphology control and interfacial reinforcement in reactive polystyrene/amorphous polyamide blends. *Polymer* 1996, 37: 3509-3519.
69. Jeon, H. K.; Kim, J. K. Effect of reaction rate on morphological change of reactive blends. *Macromolecules* 2000; 33: 8200-8210.
70. Dedecker, K.; Groeninckx, G. Interfacial graft copolymer formation during reactive melt blending of polyamide 6 and styrene-maleic anhydride copolymers. *Macromolecules* 1999, 2472-2479.

71. Moon, B.; Hoye, T. R.; Macrosko, C. W. Synthesis and application of fluorescently labeled phthalic anhydride (PA) functionalized polymers by ATRP. *Polymer* 2002, 43: 5501-5509.
72. Moon, B.; Hoye, T. R.; Macosko, C. W. Anionic synthesis and detection of fluorescence-labeled polymers with a terminal anhydride group. *Journal of Polymer Science Part A: Polymer Chemistry* 2000, 38: 2177-2185.
73. Hu, G. H.; Li, H.; Feng, L. F. A two-step reactive extrusion process for the synthesis of graft copolymers with polyamides as grafts. *Macromolecules* 2002, 35: 8247-8250.
74. Hu, G. H.; Li, H.; Feng, L. F. Rate of the activated anionic polymerization of ε-caprolactam onto an isocyanate bearing polypropylene in the melt. *Polymer* 2005, 46: 4562-4570.
75. Ji, Y.; Li, W.; Ma, J.; Liang, B. A novel approach to the preparation of nanoblends of poly(2,6-dimethyl-1,4-phenylene oxide)/polyamide 6. *Macromolecular rapid communications* 2005, 26: 116-120.
76. Matzer, M.; Schober, D. L.; Mcgrath, J. E. Polystyrene-nylon 6 graft copolymers. *European Polymer Journal* 1973, 9: 469-480.
77. Petit, D.; Jerome, R.; Teyssie, Ph. Anionic block copolymerization of ε-caprolactam. *Journal of Polymer Science: Polymer Chemistry Edition* 1979, 17: 2903-2916.
78. Yamashita, Y.; Matsui, H.; Ito, K. Block copolymerization. V. block anionic polymerization of lactams. *Journal of Polymer Science: Polymer Chemistry Edition* 1972, 10: 3577-3587.
79. Hu, G. H.; Li, H.; Feng, L. F. Follow-up of the course of the anionic ring-opening polymerization of lactams onto an isocyanate-bearing polymer backbone in the melt. Journal of Applied Polymer Science 2006, 102: 4394-4403.
80. Šebenda, J. Lactam Polymerization. *Journal of Macromolecular Science, Part A* 1972, 6: 1145-1199.
81. Udipi, K.; Davé, R. S.; Kruse, R. L.; Stebbins, L. R. Polyamides from lactams via anionic ring-opening polymerization: 1. chemistry and some recent findings. *Polymer* 1997, 38:927-938.
82. Šebenda, J.; Kouřil, V. Anionic polymerization of carprolactam-XL. Estimation of the content of active base from the rate of polymerization and from the increase of the number of polymer molecules in activated polymerization.

European Polymer Journal 1972, 8: 437-447.

83. Šebenda, J.; Kouřil, V. Anionic polymerization of caprolactam-XXXIX. Number of polymer molecules formed per molecule of acyl caprolactam in high-temperature polymerization. *European Polymer Journal* 1971, 7: 1637-1648.
84. Davé, R. S.; Robert, L. K.; Linonel, R. S. Udipi, K. Polyamides from lactams via anionic ring-opening polymerization: 2. Kinetics. *Polymer* 1997, 38: 939-947.
85. Marelová, J.; Roda, J.; Stehlíček, J. Anionic polymerization of ε-caprolactam in the presence of symmetrically substituted ureas. *European Polymer Journal* 1999, 35: 145-155.
86. Mateva, R.; Ishtinakova, O.; Nikolov, R. N.; Djambova, Ch. Kinetics of polymerization of ε-caprolactam in the presence of inorganic dispersed additives. *European Polymer Journal* 1998, 34: 1061-1067.
87. Hu, G. H.; Kadri, I. Preparation of macromolecular tracers and their use for studying the residence time distribution of polymeric systems. *Polymer Engineering and Science* 1999, 39: 299-311.
88. Mohammed, S.; Daniels, E. S.; Klein, A.; El-Aasser, M. S. Bulk copolymerization of dimethyl meta-isopropenyl benzyl isocyanate (TMI): Determination of reactivity ratios. *Journal of Applied Polymer Science* 1998, 67: 559~568
89. Wu, H. S.; Chuang, M. H.; Hwang, J. W. Kinetics and thermal analysis of copolymerization of *m*-isopropenyl-**α,α´**-dimethylbenzyl isocyanate with styrene. *Journal of applied polymer science* 1999, 73: 2763~2770.
90. Barner, L.; Barner-kowollik, C.; Davis, T. P. Free-radical copolymerization of styrene and *m*-isopropenyl-α,α´-dimethylbenzyl isocyanate studied by 1H NMR kinetic experiments. *Journal of Polymer Science Part A: Polymer Science* 2002, 40: 1064~1074
91. Hu, G. H.; Li, H.; Feng, L. F.; Pessan, L. A. Strategies for maximizing free-radical grafting reaction yields. *Journal of applied polymer science* 2003, 88: 1799-1807.
92. Ricco, L.; Russo, S.; Orefice, G.; Riva, F. Anionic poly(ε-caprolactam): Relationships among conditions of synthesis, chain regularity, reticular order, and polymorphism. *Macromolecules* 1999, 32: 7726-7731.
93. Mateva, R.; Petrov, P.; Rousseva, S.; Dimitrov, R.; Zolova, G. On the structure

of poly-ε-caprolactams, obtained with bifunctional *N*-carbamyl derivatives of lactams. *European Polymer Journal* 2000, 36: 813-821.

94. Rusu, G.; Ueda, K.; Rusu, E.; Rusu, M. Polyamides from lactams by centrifugal molding via anionic ring-opening polymerization. *Polymer* 2001, 42: 5669-5678.
95. Ongemach, G. C.; Moody, A. C. Determination of caprolactam monomer content in nylon 6 extractables by gas chromatography. *Analytical chemistry* 1967, 39: 1005-1006.
96. Zilio-Grandi, F.; Sassu, G. M.; Callegaro, P. Direct determination or residual caprolactam in nylon 6 by gas chromatography. *Analytical chemistry* 1969, 41: 1847-1849.
97. Kotelnikov, V. A.; Persits, I. E.; Surin, N. N.; Danilevskaya, L. B.; Sekiguchi, H.; Bui, Ch. *European Polymer Journal* 1996, 32: 767-771.
98. Heberstroh, E.; Jakisch, L.; Henßge, E.; Schwarz, P. Real-time monitoring of reactive extrusion processes by means of in-line infrared spectroscopy and infrared temperature measurement. *Macromolecular Materials and Engineering* 2002, 287: 203-208.
99. Jacobi, E.; Schuttenberg, R. C. Schulz, R. C. A new method for gel permeation chromatography of polyamides. *Die Makromolekulare Chemie, Rapid Communications* 1980, 1: 397.
100. Dudley, M. A. Characterization of nylon 66 by gel permeation chromatography. *Journal of Applied Polymer Science* 1972, 16: 493-504.
101. Pastuska, G.; Just, U. Gelpermeationschromatographie von polyamiden. *Angewandte Makromolekulare chemie* 1979, 81: 11-18.
102. Pastuska, G.; Just, U.; August, H. Zur analyse von polyamiden. Bestimmung der molekülmassen und ihre verteilung. *Angewandte Makromolekulare chemie* 1982, 107: 173-184.
103. Marot, G.; Lesec, J. Size exclusion chromatography of polyamides. *Journal of Liquid Chromatography & Related Technologies* 1988, 11: 3305-3319.
104. Panaris, R.; Pallas, G. Caracterisation des polyamides par chromatographie sur gel (GPC) en milieu hexamethylphosphorotriamide. *Journal of Polymer Science Part B : Polymer letters* 1970, 8: 441.
105. Girardon, V.; Tessier, M.; Maréchal, E. Characterization of functional aliphatic oligoamides using *N*-trifluoroacetylation-II. Size exclusion chromatography. *European Polymer Journal* 1998, 34: 1325-1330.

106. Schuttenberg, H.; Schulz, R. C. Trifluoracetylierung von aminen mit *N*-trifluoracetyl-Nylon 66. *Angewandte Chemie* 1976, 88: 848-849.
107. Weisskopf, K.; Meyerhoff, G. Molecular weight determinations of polyamides by *N*-trifuoroacetylation. *Polymer* 1983, 24: 72-76.
108. Biagini, E.; Costa, G.; Gattiglia, E.; Imperato, A.; Russo, S. Gel permeation chromatographic analysis of *N*-trifluoroacetylated poly(ε-caprolactam): calibration procedures. *Polymer* 1987, 28:114-118.
109. Li, G. Z.; Feng, L. F.; Gu, X. P.; Xu, Z. B.; Hu, G. H.; Liu, J. H. Synthesis of PSt-TMI copolymer and studies of the copolymerization kinetics. *Journal of Functional Polymers* 2005, 18: 127-133.
110. Hu, G. H.; Kadri, I. Modeling reactive blending: an experimental approach. *Journal of Polymer Science Part B: Polymer Physics* 1998, 36: 2153-2163.
111. Hu, G. H.; Kadri, I.; Picot, C. On-line measurement of the residence time distribution in screw extruders. *Polymer Engineering and Science* 1999, 39: 930-939.
112. Šebenda, J. Comprehesive lactams kinetics. *Elevies* 1976, 115: 379.
113. Havlice, J.; Brožek, J.; Šáchová, M.; Nováková, V.; Roda, J. Non-activated anionic polymerization of ε-caprolactam initiated with the sodium salt of ε-caprolactam. *Macromolecular Chemistry and Physics* 1999, 200: 1200-1207.
114. Shukla, S. R.; Harad, A. M.; Mahato, D. Depolymerization of nylon 6 waste fibers. *Journal of Applied Polymer Science* 2006, 100: 186-190.
115. Abastari; Sakai, T.; Sembokuya, H.; Kubouchi, M.; Tsuda, K. The reciprocal influence between ion transport and degradation of PA66 in acid solution. *Polymer Degradation and Stability* 2006, 91: 2595-2604.
116. Abastari; Sakai, T.; Sembokuya, H.; Kubouchi, M.; Tsuda, K. Study on permeation behavior and chemical degradation of PA66 in acid solution. *Polymer Degradation and Stability* 2007, 92: 379-388.
117. Chaupart, N.;Serpe, G.; Verdu, J. Molecular weight distribution and mass changes during polyamide hydrolysis. *Polymer* 1998, 39 : 1375-1380.
118. Klun, U.; Kržan, A. Degradation of polyamide-6 by using metal salts as catalyst. *Polymers for Advanced Technologies* 2002, 13: 817-822.
119. Serpe, G.; Chaupart, N. Ageing of polyamide 11 in acid solutions. *Polymer* 1997, 38: 1911-1917.
120. Lehrle, R. S.; Parsons, I. W.; Rollinson, M. P. Thermal degradation mechanisms of Nylon 6 deduced from kinetic studies by pyrolysis-g.c. *Polymer Degradation*

and Stability 2000, 67: 21-33.

121. Zhang, Y. Cheng, K.; Xu, J. Thermal stability studies of polyamides and their block copolymers. *Thermochimica Acta* 2005, 425: 137-141.
122. Oliveira, M. J.; Botelho, G. Degradation of polyamide 11 in rotational moulding. *Polymer Degradation and Stability* 2008, 93: 139-146.
123. Fornes, T. D.; Yoon, P. J.; Paul, D. R. Polymer matrix degradation and color formation in melt processed nylon 6/clay nanocomposites. *Polymer* 2003, 44: 7545-7556.
124. Russo, G. M.; Nicolais, V.; Maio, L. D.; Montesano, S.; Incarnato, L. Rheological and mechanical properties of nylon 6 nanocomposites submitted to reprocessing with single and twin screw extruders. *Polymer Degradation and Stability* 2007, 92: 1925-1933.
125. Martinez-Salazar, J.; Cannon, C. G. Transmission electron microscopy of polyamides. *Journal of Materials Science Letters* 1984, 3: 693-694
126. Forsström, D.; Terselius, B. Thermo oxidative stability of polyamide 6 films I. Mechanical and chemical characterization. *Polymer Degradation and stability* 2000, 67: 69-78.
127. Guaita, M.; Chiantore, O.; Luda, M. P. Monte carlo simulations of polymer degradations. 1. Degradations with volatilization. *Macromolecules* 1990, 23: 2087-2092.
128. Gonçalves, E. S.; Poulsen, L.; Ogilby, P. R. Mechanism of the temperature-dependent degradation of polyamide 66 films exposed to water. *Polymer Degradation and Stability* 2007, 93: 1977-1985.
129. Gersappe, D.; Harm, P. K.; Irvine, D.; Balazs, A. C. Contrasting the compatibilizing activity of comb and linear copolymers. *Macromolecules* 1994, 27: 720-724.
130. Zhu, Y.; Ma, Z.; Li, Y.; Cui, J.; Jiang, W. Monte carlo simulation of the compatibility of graft copolymer compatibilized two incompatible homopolymer blends: Effect of graft structure. *Journal of Applied Polymer Science* 2007, 105: 1591-1596.
131. Asaletha, R.; Thomas, S.; Kumaran, M. The technological compatibilization of natural rubber/polystyrene blends by the addition of natural rubber-graft-polystyrene. *Rubber Chemistry and Technology Journal* 1995, 68: 671.
132. Feng, H.; Ye, C.; Tian, J.; Feng, Z.; Huang, B. Compatibilization effect of graft

copolymer on immiscible polymer blends: 1. LLDPE/SBS/LLDPE-g-PS systems. *Polymer* 1998, 39: 1787-1792.

133. Brandrup, J.; Immergut, E. H, editors. Polymer Hanndbook. 4 th ed.; 1998.
134. Willemse, R. C.; Boer, A. P.; Dam, J. V.; Gotsis, A. D. Co-continuous morphologies in polymer blends: the influence of the interfacial tension. *Polymer* 1999, 40: 827.
135. Bhadane, P. A.; Champagne, M. F.; Huneault, M. A.; Tofan, F. ; Favis, B. D. Erosion-dependant continuity development in high viscosity ratio blends of very low interfacial tension. *Journal of Polymer Science Part B: Polymer Physics* 2006, 44: 1919-1929.
136. Bhadane, P. A.; Champagne, M. F.; Huneault, M. A.; Tofan, F.; Favis, B. D. Continuity development in polymer blends of very low interfacial tension. *Polymer* 2006, 47: 2760-2771.
137. Li, J.; Ma, P. L.; Favis, B. D. The role of the blend interface type on morphology in cocontinuous polymer blends. *Macromolecules* 2002, 35: 2005-2016.
138. Sarazin, P.; Favis, B. D. Influence of temperature-induced coalescence effects on co-continuous morphology in poly(ε-caprolactone)/polystyrene blends. *Polymer* 2005, 46: 5966-5978.
139. Pernot, H.; Baumert, M.; Court, F.; Leibler, L. Design and properties of co-continuous nanostructured polymers by reactive blending. *Nature Materials* 2002, 1: 54-58.
140. Bhanu, N.; Kandpal, L. D.; Mathur, G. N. Poly(ether ether Ketone)/poly(aryl ether sulfone) blends: Relationships between morphology and mechanical properties. *Journal of Applied Polymer Science* 2003, 90: 2887-2905.
141. Arns, C. H.; Knackstedt, M. A.; Roberts, A. P.; Pinczewski, V. W. Morphology, cocontinuity, and conductive properties of anisotropic polymer blends. *Macromolecules* 1999, 32: 5964.
142. Meincke, O.; Kaempfer, D.; Weickmann, H.; Friedrich, C.; Vathauer, M.; Warth, H. Mechanical properties and electrical conductivity of carbon-nanotube filled polyamide-6 and its blends with acrylonitrile/butadiene/styrene. *Polymer* 2004, 45: 739-748.
143. Li, Y.; Hiroshi, S. Co-continuous polyamide 6 (PA6)/acrylonitrile -butadiene-styrene (ABS) nanocomposites. *Macromolecular Rapid Communications* 2005, 26: 710-715.
144. Lee, J. K.; Han, C. D. Evolution of a dispersed morphology from a

co-continuous morphology in immiscible polymer blends. *Polymer* 1999, 40: 2521-2536.

145. Willemse, R. C. Co-continuous morphologies in polymer blends: stability. *Polymer* 1999, 40: 2175-2178.
146. Mekhilef, N.; Favis, B. D.; Carreau, P. J. Morphological stability, interfacial tension, and dual-phase continuity in polystyrene-polyethylene blends. *Journal of Polymer Science Part B: Polymer Physics* 1997, 35: 293-308.
147. Yuan, Z.; Favis, B. D. Coarsening of immiscible co-continuous blends during quiescent annealing. *AIChE Journal* 2005, 51: 271-280.
148. Yuan, Z.; Favis, B. D. Influence of the efficacy of interfacial modification on the coarsening of cocontinuous PS/HDPE blends during quiescent annealing. *Journal of Polymer Science Part B: Polymer Physics* 2006, 44: 711-721.
149. Dedecher, K.; Groeninchx, G. Reactive compatibilisation of A/(B/C) polymer blends. Part 2. Analysis of the phase inversion region and the co-continuous phase morphology. *Polymer* 1998, 39: 4993-5000.
150. Chuai, C. Z.; Almdal, K. Lyngaae-Jørgensen, J. Phase continuity and inversion in polystyrene/poly(methyl methacrylate) blends. *Polymer* 2003, 44: 481-493.
151. Galloway, J. A.; Jeon, H. K.; Bell, J. R.; Macosko, C. W. Block copolymer compatibilization of cocontinuous polymer blends. *Polymer* 2005; 46: 183-191.
152. Harrats, C.; Blacher, S.; Fayt, R.; Jérôme, R.; Teyssié, Ph. Molecular design of multicomponent polymer systems XIX: Stability of cocontinuous phase morphologies in low-density polyethylene-polystyrene blends emulsified by block copolymers. *Journal of Polymer Science Part B: Polymer Physics* 1995, 33: 801-811.
153. Harrats, C.; Fayt, R.; Jérôme, R.; Blacher, S. Stabilization of a cocontinuous phase morphology by a tapered diblock or triblock copolymer in polystyrene-rich low-density polyethylene/polystyrene blends. *Journal of Polymer Science Part B: Polymer Physics* 2003, 41: 202-216.
154. Vinckier, I.; Laun, H. M. Assessment of the Doi-Ohta theory for co-continuous blends under oscillatory flow. *Journal of Rheology* 2001, 45: 1373-1385.
155. Jafari, S. H.; Pötschke, P.; Stephan, M.; Warth, H.; Alberts, H. Multicomponent blends based on polyamide 6 and styrenic polymers: morphology and melt rheology. *Polymer* 2002, 43: 6985-6992.
156. Willemse, R. C.; Boer, A. P.; Dam, J. V.; Gotsis, A. D. Co-continuous morphologies in polymer blends: a new model. *Polymer* 1998, 39: 5879-5887.

157. Noolandi, J.; Hong, M. K. Interfacial properties of immiscible homopolymer blends in the presence of block copolymers. *Macromolecules* 1982, 15: 482-492.
158. Noolandi, J.; Hong, K. M. Effect of block copolymers at a demixed homopolymer interface. *Macromolecules* 1984, 17: 1531-1537.
159. Kim, K. H.; Jo, W. H. Effect of chain architecture of graft copolymer on the structure of adsorbed layer: a Monte Carlo simulation approach. *Polymer* 2001, 42: 3205-3211.
160. Cimmino, S.; Coppola, F.; D'Orazio, L.; Greco, R.; Maglio, G.; Malinconico, M.; Mancarella, C.; Martuscelli, E.; Ragosta, G. Ternary nylon-6/rubber/modified rubber blends: Effect of the mixing procedure on morphology, mechanical and impact properties. *Polymer* 1986, 27: 1874-1884.
161. Willis, J. M.; Favis, B. D. Processing-morphology relationships of compatibilized polyolefin/polyamide blends. Part I: The effect of an ionomer compatibilizer on blend morphology. *Polymer Engineering and Science* 1988, 28: 1416-1426.
162. Lee, J. D.; Yang, S. M. Effects of mixing procedures on properties of compatibilized polypropylene/nylon 6 blends. *Polymer Engineering and Science* 1995, 35: 1821-1833.
163. Hu, G. H.; Sun, Y. J.; Lambla, M. Devolatilization: A critical sequential operation for in situ compatibilization of immiscible polymer blends by one-step reactive extrusion. *Polymer Engineering and Science* 1996, 36: 676-684.
164. Sun, Y. J.; Hu, G.. H.; Lambla, M.; Kotlar, H. K. In situ compatibilization of polypropylene and poly(butylene terephthalate) polymer blends by one-step reactive extrusion. *Polymer* 1996, 37: 4119-4127.
165. Li, H.; Hu, G. H. The early stage of the morphology development of immiscible polymer blends during melt blending: Compatibilized vs.uncompatibilized blends. *Journal of Polymer Science Part B: Polymer Physics* 2001, 39: 601-610.
166. Wolf, D.; White, D. Experimental study of the residence time distribution in plasticating screw extruders. *AIChE Journal* 1976, 22: 122-131.
167. Chen, L.; Pan, Z.; Hu, G. H. Residence time distribution in screw extruders. *AIChE Journal* 1993, 39: 1455-1464.
168. Nauman, E. B.; Buffham, B. A. *Mixing in continuous flow system*, Wiley, New York, 1983.
169. Unlu, E.; Faller, J. F. Geometric mean vs. arithmetic mean in extrusion residence time studies. *Polymer Engineering and Science* 2001, 41: 743-751.

170. Gao, J.; Walsh, G. C.; Bigio, D.; Briber, R. M.; Wetzel, M. D. Residence-time distribution model for twin-screw extruders. AIChE Journal 1999, 45: 2541-2549.
171. Carneiro, O. S.; Covas, J. A.; Ferreira, J. A.; Cerqueira, M. F. On-line monitoring of the residence time distribution along a kneading block of a twin-screw extruder. *Polymer Testing* 2004, 23: 925-937.
172. Zhang, X. M.; Xu, Z. B.; Feng, L. F.; Song, X. B.; Hu, G. H. Assessing local residence time distributions in screw extruders through a new in-line measurement instrument. *Polymer Engineering and Science* 2006, 46: 510-519.
173. Zhang, X. M.; Feng, L. F.; Hoppe, S.; Hu, G. H. Local residence time, residence revolution, and residence volume distributions in twin-screw extruders. *Polymer Engineering and Science* 2008, 48: 19-28.

INSTITUT NATIONAL
POLYTECHNIQUE
DE LORRAINE

AUTORISATION DE SOUTENANCE DE THESE
DU DOCTORAT DE L'INSTITUT NATIONAL
POLYTECHNIQUE DE LORRAINE

o0o

VU LES RAPPORTS ETABLIS PAR :
Monsieur Luc AVEROUS, Professeur, LIPHT-ECPM, Strasbourg

Monsieur Ming-Qiang ZHONG, Professeur, Zhejiang University of Technology, Chine

Le Président de l'Institut National Polytechnique de Lorraine, autorise :

Monsieur ZHANG Cai-Liang

NANCY BRABOIS
2, AVENUE DE LA
FORET-DE-HAYE
BOITE POSTALE 3
F - 54501
VANDŒUVRE CEDEX

à soutenir devant un jury de l'INSTITUT NATIONAL POLYTECHNIQUE DE LORRAINE, une thèse intitulée :

"Procédés d'extrusion réactive et de mélange de polymères : synthèse contrôlée de copolymères greffés à base de polystyrène et de polyamide ; et étude de l'efficacité de compatibilisation de ces copolymères"

en vue de l'obtention du titre de :

DOCTEUR DE L'INSTITUT NATIONAL POLYTECHNIQUE DE LORRAINE

Spécialité : « **Génie des Procédés et des Produits** »

Fait à Vandoeuvre, le 16 octobre 2008
Le Président de l'I.N.P.L.,
F. LAURENT

TEL. 33/03.83.59.59.59

TITRE

Procédés d'extrusion réactive et de mélange de polymères : Synthèse contrôlée de copolymères greffés à base de polystyrène et de polyamide ; et étude de l'efficacité de compatibilisation de ces copolymères.

RESUME

Les mélanges de polymères ouvrent une importante voie à l'obtention de nouveaux matériaux dont les propriétés peuvent être très différentes de celles de chacun des constituants des mélanges. La plupart des polymères sont immiscibles. Ainsi leurs mélanges constituent des phases distinctes et les propriétés de ces mélanges sont souvent médiocres. Afin de relever ce défi, copolymères à bloc ou greffés synthétisés séparément ou générés in-situ lors du procédé de mélanges sont souvent utilisés en tant que agents compatibilisants. Beaucoup d'études ont porté sur l'efficacité de compatibilisation de copolymères à bloc et peu d'études sur celle de copolymères greffés, en partie en raison des difficultés dans le contrôle de leurs structures moléculaires. Cette thèse porte sur l'étude de l'efficacité d'émulsification de copolymères greffés. Elle est composée de trois parties : (1) développement d'un nouveau procédé d'extrusion réactive pour la synthèse de copolymères greffés avec polystyrène (PS) comme squelette et polyamide 6 (PA6) comme greffons ; (2) efficacité d'émulsification du copolymère greffé, PS-g-PA6 pour les mélanges à base de PS et PA6 ; et (3) développement d'un nouveau concept dit d'agent émulsifiant – traceur.

MOTS-CLES

Procédé d'extrusion réactive ; copolymère greffé ; mélange de polymères ; compatibilisation.

TITLE

Reactive and polymer blending processes: Controlled synthesis of polystyrene and polyamide graft copolymers and compatibilizing efficiency of these copolymers.

ABSTRACT

Polymer blending offers an important route to new materials with combinations of properties not available in constituent polymers. Most polymer pairs are immiscible, leading to phase separation at equilibrium and yield a material with poor properties. To address this challenge, block or graft copolymers pre-made or generated in-situ by reactive blending are often used as compatibilizers. Most studies are focused on the compatibilizing efficiency of block copolymers and few studies address that of graft copolymers, partly because of difficulties of controlling their molecular structures.This thesis is devoted to the study of the emulsification efficiency of graft copolymers. It is composed of three parts: (1) development of a novel reactive extrusion process for synthesizing graft copolymers with polystyrene (PS) as backbone and polyamide 6 (PA6) as grafts; (2) emulsification efficiency of PS-g-PA6 graft copolymers for PS/PA6 blends; and (3) concept of emulsifier- tracer.

KEY WORDS

Reactive extrusion process; polymer blends; compatibisation.